# Neutrophil biomechanical properties and immune function in health and inflammatory disease

**Kathleen Rose Bashant**

This thesis is submitted for the degree of Doctor of Philosophy

University of Cambridge

Clare Hall

September 2020

Department of Medicine

# Declaration

This thesis is the result of my own work and includes nothing which is the outcome of work done in collaboration except as declared in the Preface and specified in the text. I thank Dr. Arlette Vassallo and Dr. Nicole Toepfner for their assistance in generating data presented in this thesis. Their specific contributions have been acknowledged in the relevant results sections and figure legends. I have published sections of Chapter I as a first-author review article in the Biology of the Cell. I have published sections of Chapter VI as a first-author research article in the Journal of Leukocyte Biology. I have published sections of Chapters V and VI as a first-author research article at the Annals of Rheumatic Disease. The citations for all manuscripts associated with this thesis can be found in the appendices.

This thesis is not substantially the same as any that I have submitted, or, is being concurrently submitted for a degree or diploma or other qualification at the University of Cambridge or any other University or similar institution except as declared in the Preface and specified in the text. I further state that no substantial part of my thesis has already been submitted, or, is being concurrently submitted for any such degree, diploma or other qualification at the University of Cambridge or any other University or similar institution except as declared in the Preface and specified in the text. It does not exceed the prescribed word limit set by the Degree Committee of the Department of Medicine.

Kathleen Bashant
September 30th, 2020

# Neutrophil biomechanical properties and immune function in health and inflammatory disease

Low density granulocytes (LDGs) are a poorly understood class of immune cells found in patients with chronic inflammatory diseases including psoriasis and systemic lupus erythematosus (SLE). Research completed at the National Institutes of Health (NIH) revealed that in the context of SLE, LDGs release higher levels of type 1 interferons, undergo increased NETosis, and accordingly drive inflammation. Meanwhile, advances in mechanical phenotyping at the University of Cambridge have driven hypotheses of neutrophil trafficking and immune function being intimately linked to cellular biomechanical properties (*e.g.* density, stiffness, morphology). This thesis analyses the intersection of immune cellular biomechanical phenotypes and their function. Specifically, it focuses on the role of neutrophils and LDGs in inflammatory diseases.

In this thesis, real-time deformability cytometry (RT-DC) was optimised as a high-throughput mechanical phenotyping technique for the analysis of neutrophils. This enabled development of a protocol to recover purified neutrophils to their whole blood mechanical phenotype. Neutrophil biomechanical properties were analysed by RT-DC, lattice light-sheet microscopy, confocal microscopy and scanning electron microscopy. Neutrophil immunologic functions (*e.g.* NETosis, macropinocytosis) were imaged using florescence microscopy. To analyse the contribution of biomechanical properties to neutrophil trafficking, a novel microfluidic microvasculature mimetic was developed. An endothelial flow assay was used to image neutrophils interacting with endothelial cells. Finally, the complete proteomes and phosphoproteomes of LDGs and normal dense neutrophils (NDNs) were obtained from five healthy donors and five SLE patients.

Several key insights were gained. Firstly, hypotonic lysis and magnetic column-based isolation techniques are damaging to neutrophil biomechanical properties, but purification of neutrophils retaining their biomechanical properties can be achieved by using gradients and column-free magnetic systems followed by recovery at 37 degrees Celsius. Secondly, the biphasic biomechanical kinetics of neutrophil priming were described; cells contract briefly before immediately expanding. The expansion phase was determined to be macropinocytosis dependent. Thirdly, SLE LDGs are phenotypically rougher than autologous SLE NDNs or healthy LDGs. This appears to impact their microvasculature trafficking abilities, as SLE LDGs were increasingly trapped in the narrow channels of a three-dimensional microvasculature mimetic. These results suggest a role for biomechanical properties in modulation of neutrophil trafficking, indicating that SLE LDGs may be increasingly retained in microvasculature networks, similar to what has been described for primed neutrophils. Finally, unbiased proteomics quantified 4109 proteins and 875 phosphoproteins in four neutrophil subsets (healthy unstimulated NDNs, healthy primed NDNs, SLE NDNs, and SLE LDG). This shed new light

into neutrophil heterogeneity at the protein level and to my knowledge, is the first proteomic profile of the SLE LDG. In addition to findings pertaining to SLE LDG biology and function, differential phosphorylation of proteins associated with cytoskeletal organisation were identified in SLE LDGs relative to SLE NDNs, suggesting a phosphoproteomic explanation for the SLE LDGs' distinct biomechanical phenotype. When taken together, this work could have important pathogenic implications in the context of SLE manifestations in various organs and the development of small vessel vasculopathy.

Kathleen Bashant

# Acknowledgements

I arrived at Cambridge a hugely enthusiastic, but young and raw scientist. Prof Edwin Chilvers taught me to lay a solid foundation by careful reading, thought, and planning. My scientific career and my personal life have both benefited from this lesson. Edwin has struck the perfect balance of supporting me, while also pushing me to grow as an independent scientist and making it clear that he believes me capable; because of him, I leave Cambridge both a better scientist and a wiser person. In addition, I am beyond grateful to Dr. Charlotte Summers for her support and for her example. I will be a better supervisor and mentor because of her.

Dr. Mariana Kaplan, Dr. Nehal Mehta, Dr. Carmelo Carmona-Rivera, Dr. Davide Randazzo, Angel Aponte, Dr. Christopher Bleck, and Dr. Yvonne Baumer at the National Institutes of Health have all taught some truly valuable lessons and supported my growth into an independent scientist. Paniz Sangsari and Dr. Nicole Morgan were critical to the design of the microvasculature mimetic. Similarly, I thank Angel Aponte, Dr. Alex Wood, and Dr. Andrew Conway-Morris for their extensive support in completing the proteomics and phosphoproteomics analyses. Dr. Christopher Bleck and Dr. Yvonne Baumer assisted considerably with my training in scanning electron microscopy. Dr. Davide Randazzo has spent hours with me in the light imaging section of NIAMS helping with confocal microscopy, lattice light-sheet microscopy, and imaging of the microvasculature mimetic and endothelial flow assay. I am grateful for his advice and for his support during long imaging sessions.

Moving around the world during a PhD creates for some unique challenges and some unique opportunities. I will forever be grateful to the International Biomedical Research Alliance and the NIH-Cambridge program for affording me this opportunity. I will miss my friends from Cambridge and Washington DC, who are now scattered across the globe, but I have benefited enormously from meeting people who do not think exactly as I do. And of course, thank you to Chris, my favourite. For donating blood, for moving around the world for this PhD, and for pushing me to be better in a way that no one else does.

# Table of Contents

# List of Figures

# List of Tables

# Abbreviations

| Abbreviation | Definition |
|---|---|
| ADAMxx | A disintegrin and metalloproteinase-xx |
| AFM | Atomic force microscopy |
| ALI | Acute lung injury |
| AQP-x | Aquaporin x |
| ARDS | Acute respiratory distress syndrome |
| ARFGEFx | Brefeldin A-inhibited guanine nucleotide-exchange protein x |
| AS | Autologous serum |
| AU | Arbitrary units |
| BMI | Body mass index |
| bRP | Basic pH reversed-phase |
| BSA | Bovine serum albumin |
| Cxx | Complement component xx |
| C5a | Complement component C5a |
| CD-xx | Cluster of differentiation xx |
| CEBPD | CCAAT enhancer binding protein delta |
| CIBxx | Calcium-binding protein-xx |
| COPD | Chronic obstructive pulmonary disease |
| COROxx | Coronin-xx |
| CXCLxx | C-X-C motif chemokine ligand xx |
| CXCRxx | C-X-C motif chemokine receptor xx |
| CytoD | Cytochalasin D |
| DAPI | 4',6-diamidino-2-phenylindole |
| dH2O | Deionized water |
| DMSO | Dimethyl sulfoxide |
| DOCKx | Dedicator of cytokinesis x |
| EDTA | Ethylenediaminetetraacetic acid |
| ELISA | Enzyme-linked immunosorbent assay |
| FBC | Full blood count |
| FBS | Foetal bovine serum |
| FDR | False discovery rate |
| fMLF | N-formyl methionyl-leucyl-phenylalanine |
| GO | Gene ontology |
| GP-xx | Glycoprotein |

| | |
|---|---|
| G-CSF | Granulocyte-colony stimulating factor |
| GM-CSF | Granulocyte-macrophage colony stimulating factor |
| HC | Healthy control |
| HEPES | N-(2-Hydroxyethyl)piperazine-N'-(2-ethanesulfonic acid) |
| HMVEC-P | Human pulmonary microvascular endothelial cells |
| HLA-DR | Human leukocyte antigen D-related |
| HISTxx | Histone protein xx |
| HRG | Histidine rich glycoprotein |
| IC | Immune complex |
| ICAMxx | Intercellular adhesion molecule xx |
| IFIxx | Gamma-interferon-inducible protein |
| IFITxx | Interferon induced proteins with tetratricopeptide repeats |
| IFN | Interferon |
| IFNGRxx | Interferon-gamma receptor xx |
| IgG | Immunoglobin G |
| IL-xx | Interleukin-xx |
| ISG | Interferon stimulated gene |
| ITGA-xx | Integrin-xx |
| LC-MS/MS | Liquid chromatography and tandem mass spectrometry |
| LCP-x | Lymphocyte cytosolic protein x |
| LDG | Low density granulocyte |
| LPS | Lipopolysaccharide |
| MACS | Magnet-associated cell sorting |
| MMM | Microfluidic microcirculation mimetic |
| MMP-x | Matrix metalloproteinase x |
| MORE | Morpho-rheological |
| MPO | Myeloperoxidase |
| mL | Millilitre |
| MX | MX dynamin like GTPase |
| NIH | National Institutes of Health |
| NDN | Normal dense neutrophil |
| NET | Neutrophil extracellular trap |
| OASxx | 2'-5'-oligoadenylate synthetase xx |
| PAD | Peptidylarginine deiminase |
| PAF | Platelet activating factor |

| | |
|---|---|
| PBMC | Peripheral blood mononuclear cell |
| PBS | Dulbecco's phosphate buffered saline |
| PDMS | Polydimethylsiloxane |
| PECAM-x | Platelet endothelial cell adhesion molecule x |
| PFN1 | Profilin 1 |
| PIEZO | Pore-forming subunits of mechanically activated channels |
| PLSCRxx | Phospholipid scramblase xx |
| PMN | Polymorphonuclear cells (neutrophils) |
| PMA | Phorbol myristate acetate |
| PPBP | Pro-platelet basic protein |
| PROS | Protein S |
| RMDN1 | Regulator of microtubule dynamics 1 |
| RNA-SEQ | RNA sequencing |
| RNP | Ribonucleoprotein |
| RPxx | Ribosomal protein xx |
| RT-DC | Real-time deformability cytometry |
| ROCK | Rho-associated coiled-coil-containing protein kinase 1 |
| ROS | Reactive oxygen species |
| RTI | Respiratory tract infection |
| SDS | Sodium dodecyl sulphate |
| SDS-PAGE | Sodium dodecyl sulphate-polyacrylamide gel electrophoresis |
| SEM | Standard error of the mean |
| SELL | L-selectin |
| SELP | P-selectin |
| SELPLG | Selectin P ligand |
| SLE | Systemic lupus erythematosus |
| SLEDAI | Systemic lupus erythematosus disease activity index |
| Sm | Smith protein |
| SPI1 | Transcription factor PU.1 |
| TCEP | Tris(2-carboxyethyl)phosphine |
| TEAB | Triethylammonium bicarbonate |
| TF | Tissue factor |
| THBS1 | Thrombospondin 1 |
| TICAMx | TIR domain-containing adapter molecule x |
| TLR-x | Toll-like receptor-x |

| | |
|---|---|
| TNF-x | Tumour necrosis factor-x |
| TUBBx | Tubulin-x |
| VWF | von Willebrand factor |
| βME | 2-mercaptoethanol |

## Structure of the thesis

This thesis is structured into seven chapters. Bookmarks for ease of navigation are accessible by enabling the 'Navigation pane' in both Word and Adobe Acrobat Reader. Chapter I, the introduction, outlines the relevant literature pertaining to this thesis, identifies areas for further exploration, and highlights gaps to be addressed by this thesis. The central research questions and core research aims are found at the end of Chapter I. The second chapter (Methods) details the experimental and statistical protocols used to generate and analyse data presented in this thesis. The methods discussed in Chapter II are supplemented by full-length protocols for key experimental strategies provided in the Appendices.

Chapters III-VI describe the results generated during this thesis. Each is structured identically, beginning with a brief introduction and summary of relevant literature, followed by statement of the key chapter hypotheses and aims. Chapter-specific notes on the relevant methods are provided and this is followed by the experimental results. Each chapter concludes with a detailed discussion of the experimental results in the context of the thesis and the wider literature. The final chapter summarises the key findings, discusses the results of the entire thesis at a broader level, and suggests avenues of potential research to be conducted in the future.

# Chapter I: Introduction

## 1. Autoimmune Disease

Although the immune system is well prepared to defend against a variety of pathogens, dysregulation can lead to pathology. Immune deficiency syndromes are an inability of the immune system to respond to a pathogen. Autoimmune diseases are a failure of self-tolerance, *i.e.* the immune system's failure to avoid targeting components of self. Approximately 3-5 per cent of the general population has some sort of autoimmunity disorder but understanding of the events leading to clinical pathology remains limited. All ages and sexes can be affected, although different diseases typically emerge at different ages [1]. There is also a significant sex bias, with conservative estimates indicating 78.8 per cent of people affected by autoimmune diseases are women [2]. This higher frequency of autoimmune diseases in women has been attributed to differences in sex hormones, which can interact with receptors on immune cells [2], and to modulation of the immune system that occurs during pregnancy.

With respect to sex hormones, it was recently demonstrated that immune cells (neutrophils) from healthy young adult females are more activated than neutrophils from age-matched males. Specifically, female neutrophils display an increased proinflammatory response and type 1 interferon (IFN) production, likely driven by sex hormones [3].

With respect to pregnancy, to protect the foetus from maternal immunity, and to simultaneously protect the mother and foetus from infection, the composition and function of the maternal immune system changes. Tolerance of foetal cells and paternal antigens is promoted. Long-term, a state of microchimerism is created as foetal cells remain in the mother for decades after birth. Accordingly, after delivery, the maternal immune system cannot return to exactly the state it was in pre-conception. These immune system changes introduce the potential for immune system dysregulation, and development of autoimmunity [4].

Development of autoimmunity has both genetic and environmental components. Inheritance of a single mutated gene or, more commonly, of multiple susceptibility sequence variants play a major role in the development of many autoimmune disorders [1]. Infection can also initiate autoimmune disease. Molecular mimicry refers to the process by which the immune system responds to a foreign antigen sharing structural or sequence similarities to self-antigens. After foreign antigens have been cleared, host immune cells may continue to react against self-antigens [5].

### 1.1 Systemic lupus erythematosus (SLE)

Systemic lupus erythematosus (SLE) is a systemic, immune complex-mediated disease in which autoantibodies are generated against cellular nuclear components. It is predominantly observed in

women of child-bearing age [6], and certain racial groups are more likely to develop the condition. SLE is the result of a polygenic genetic predisposition in combination with environmental triggers. Ultra-violet (UV) light exposure, hormonal factors, and infections may initiate immune dysregulation. Diagnosis remains challenging due to the disease's diverse clinical manifestations which can affect many organs including the joints, central nervous system, kidneys, lungs and skin to varying degrees. SLE treatment typically involves immune suppression, increasing patients' risk of infection, and this disease also confers an increased risk of premature cardiovascular disease [7].

### 1.2. Immune dysregulation in SLE

SLE is caused by an innate and adaptive immune response to nucleic acids or to proteins binding to nucleic acids. Auto-antibodies most specific to SLE are anti-Smith (Sm) antibodies, against a component of the spliceosome, and anti-double-stranded DNA (dsDNA) antibodies [5]. In addition, over 100 mostly small effect genetic loci have been identified as being associated with SLE development. A smaller number of low-frequency single-gene mutations with a considerable effect on susceptibility have also been identified [8].

SLE is a multi-faceted disease in which innate immune system dysregulation as well as T cell, B cell, and cytokine defects lead to autoantibody production, complement activation, and tissue damage (Figure I-1) [5]. Secretion of type 1 interferons (IFNs) and dendritic cell activation are hallmarks of SLE pathogenesis [9] but historically this disease has been considered to primarily involve the adaptive immune system. However, the contribution of the neutrophils to SLE pathogenesis is an emerging area of research [10].

## 2. Neutrophils

Neutrophils are the most abundant white blood cell in humans and are a key component of the innate immune system. Also known as polymorphonuclear cells (PMNs) for their distinctive multilobulated nucleus [11], neutrophils are produced in the bone marrow in response to granulocyte-colony stimulating factor (G-CSF), granulocyte-macrophage colony stimulating factor (GM-CSF), and interleukin (IL)-6. Neutrophil trafficking from bone marrow to blood is regulated by bone marrow stromal cell C-X-C chemokine ligand (CXCL) interactions with neutrophil C-X-C chemokine receptors (CXCR), principally through CXCR4. Immature neutrophils are retained by expressing CXCR4, which binds CXCL12 expressed by bone marrow stromal cells [12]. Downregulation of CXCR4/CXCL12, along with upregulation of CXCL1/2 and CXCR2, shifts neutrophils into the circulatory system where they can patrol and respond to infection at sites throughout the body [13]. Although estimates in the literature vary, most studies point to a circulating neutrophil half-life in peripheral blood of less than 20 hours [14, 15]. In humans, 50-70 percent of circulating leukocytes are neutrophils, which at maturity have an average diameter of 7-10μm [16].

As neutrophils mature within the bone marrow, they form granules and secretory vesicles. Granules are filled with antimicrobial peptides including lysozyme, cathelicidins, defensins, and proteases that contribute to neutrophil effector function. Azurophilic, or primary granules, contain myeloperoxidase (MPO) and develop first, during the promyelocyte stage. Specific (secondary granules) develop when neutrophils are myelocytes, and gelatinase (tertiary granules), develop in band cells [11]. The antibacterial proteins within these granules can be quickly transported to the cell surface for extracellular release by secretory vesicle, which develop in segmented neutrophils [16].

Beyond proteins found in granules, neutrophils constitutively express Ca2+ binding proteins S100A8 and S100A9, which together make up approximately 45% of neutrophil cytosolic proteins and may be involved in cytoskeletal rearrangements. During the inflammatory process, S100A8 and S100A9 are released to modulate inflammatory cytokines and production of reactive oxygen species (ROS). These proteins also bind zinc ions, which may assist with bacterial clearance [17]. In patients with active SLE, an increase in serum levels of S100A8 and S100A9 is driven by neutrophils. These levels of S100A8/A9 may be used to monitor the level of disease activity for patients with SLE [18].

### 2.1. Transmigration and chemotaxis

Neutrophils are the first cells to localize to the site of injury or infection, responding to pro-inflammatory cytokines (*e.g.* IL-1β, IL-6, and TNF-α), chemokines (*e.g.* IL-8), or chemoattractants including bacterial product fMLF, complement C5a produced by tissue-resident cells or microbial molecules [11]. Circulating neutrophils roll along the endothelial surface of blood vessels, where geometry allows, and shed CD162 and CD62 (L-selectin) as they become activated. Activated endothelial cells express intracellular adhesion molecule (ICAM-1) or vascular cell adhesion molecule (VCAM-1), which are recognized by lymphocyte function-associated antigen-1 (LFA-1) and CD11b (MAC1) on neutrophils [16]. This interaction facilitates extravasation of neutrophils into tissues. Extravasation can occur in a paracellular (between endothelial cell) or transcellular (through endothelial cell) manner [19].

### 2.2. Functional capabilities

As the first line of defence against invading pathogens, neutrophils are an essential part of the innate immune system, eliminating pathogens through multiple intracellular and extracellular mechanisms. Neutrophils are phagocytes, engulfing pathogens and killing them via reactive oxygen species (ROS) or antibacterial proteins (e.g. cathepsins, defensins, lactoferrin, and lysozyme). These antibacterial proteins can also be released from neutrophil granules via secretory vesicles to eliminate extracellular pathogens, in a process known as degranulation [16].

Highly activated neutrophils are also capable of releasing neutrophil extracellular traps (NETs) through a process called NETosis. These NETs consist of chromatin bound to histones and granule proteins, and effectively trap pathogens, allowing for subsequent phagocytosis. Many knowledge gaps exist around this process, but it is generally agreed that NETosis promotes clearance of pathogens but externalizes intracellular autoantigens and other immune-stimulatory molecules in the process. Certain NETosis processes appear to be oxidant dependent, while others are not. There are at least two different mechanisms which drive NETosis, including both a cell-death pathway considered a suicide lytic NETosis and a live cell NETosis termed "vital NETosis" [20].

Although the scientific field currently lacks a thorough understanding of NETosis, it can be stated that neutrophil effector responses, including NETosis, are intended to mitigate infectious threats, dysregulation of neutrophil biology can result in tissue damage and, in susceptible hosts, may promote development of autoimmunity and targeted organ damage [21]. An overactive NETosis response has been reported to promote thrombosis, accelerated atherosclerosis, and ultimately an increased risk of premature cardiovascular disease (CVD)-related mortality and morbidity [22].

Specifically, in the context of SLE, NETosis is linked to increased production of type 1 interferons (IFNs) [23]. This phenomenon may be driven by the innate immune sensor cyclic GMP-AMP synthase (cGAS). It was recently demonstrated that macrophages and other myeloid cells phagocytose NETs and translocate them to the cytosol, where NET DNA leads to cGAS activation and subsequently production of type 1 IFN. This was specifically studied in the context of a model of autoimmune hepatitis [24]. Stimulation of the phagocytic plasmacytoid dendritic cells by NETs induced by SLE-specific autoantibodies was also previously established to drive type 1 IFN production. The antimicrobial peptide LL-37 is extruded in NETs, facilitates uptake of extracellular DNA by plasmacytoid dendritic cells, and has been identified in the NETs of SLE patients, but not the NETs from healthy individuals [23]. Such robust production of type I IFNs primes neutrophils for further NETosis and induces higher levels of inflammation [25].

Neutrophils express Fc receptors, which bind the constant (Fc) region of immunoglobulins (Ig) produced by B cells. This interaction with the adaptive immune system has also been reported to induce NETosis [22].

### 2.3. Priming and de-priming

Exposure of neutrophils to pro-inflammatory cytokines or chemokines (*e.g.* tumour necrosis factor, fMLF, or GM-CSF) induces transition to a 'primed' state. This primed state enhances their response to activating stimuli such as bacterial products. Priming is characterised by increased responsiveness to

agonist stimulations and a ‘polarized’ morphology [26-28]. Although neutrophil priming was originally identified *in vitro* [29], it has been reported *in vivo*, including in the context of systemic infection [30].

Neutrophil priming delays apoptosis, increasing the time viable cells spend at sites of inflammation or tissue injury [31-33]. Following a second exposure to stimuli, primed neutrophils become maximally activated, producing increased superoxide anions and employing a range of effector functions including phagocytosis, degranulation of antibacterial proteins, release of neutrophil extracellular traps (NETs) and other immunologic defence mechanisms [34, 35]. Neutrophil priming can increase a neutrophil’s lifespan via anti-apoptotic signalling [36]. Although research studies involving *ex*-vivo labelling of neutrophils suggested the half-life of a circulating neutrophil to be 8-10 hours, more robust studies which avoided *ex-vivo* manipulation suggest the average lifespan to be closer to 5.4 days [37]. Early research studies showed inflammatory signals prolonged neutrophil survival [38]. More recent studies have also recorded longer neutrophil lifespans within inflamed tissues, suggesting that having been primed, neutrophils remain alive for a sufficient amount of time to mediate their effector functions [39, 40].

In some instances, neutrophils can return to their un-primed functional state, via a mechanism known as ‘de-priming’ [41, 42]. Although several mechanisms of neutrophil de-priming have been advanced, this process remains poorly understood. First, neutrophils appear to spontaneously de-prime if they do not receive ongoing or repeated stimulation [42, 43]. Second, neutrophils can be mechanically de-primed. Ekpenyong *et. al*. [41] reported that as neutrophils are directed through a “microfluidic microcirculation mimetic” (MMM) made up of channels with lung capillary-sized constrictions or, as in separate experiments, repeatedly stretched with optical lasers, both processes rapidly recovered the neutrophils to an un-primed state.

## 2.4. Accumulation in lungs during ARDS

Neutrophils are recognised as key players in the development of acute inflammatory diseases. For example, neutrophil accumulation in the lungs, as well as neutrophil priming and activation, are recognized as hallmarks of many lung pathologies including acute respiratory distress syndrome (ARDS) [44], with the pulmonary vasculature being an important site of pathological neutrophil margination [45]. Recent evidence suggests only primed neutrophils pool in the lungs, prompting the hypothesis that failure of neutrophil de-priming is at least partially responsible for ARDS development [44]. Similarly, it has been established that neutrophils play a vital role in sepsis pathogenesis. Increased sepsis morbidity and mortality are directly correlated with dysregulation in neutrophil effector functions, but this relationship remains incompletely understood [46].

## 2.5. Role in SLE

As previously described, neutrophils can cause tissue damage and immune dysregulation via the release of a meshwork of chromatin bound to granular proteins known as NETosis [21]. NETosis is now considered a potentially important pro-inflammatory mechanism of immune system activation in SLE and other rheumatic diseases, specifically via the type 1 IFN pathway and activation of the inflammasome. Increased levels of apoptosis in neutrophils are also associated with SLE activity, and a considerable number of SLE patients exhibit neutropenia [6]. This increase in both NETosis and apoptosis in the context of SLE is interesting in light of recent studies completed in the context of cystic fibrosis, where delayed neutrophil apoptosis appeared to allow neutrophils from patients with cystic fibrosis to survive longer and go on to produce NETs [47]. Perhaps this suggests fundamental differences between the disease states driven by SLE and cystic fibrosis. Indeed, in the context of SLE, microparticles derived from apoptosis were shown to drive inflammation and enhanced NETosis; perhaps in the context of SLE, both apoptosis and NETosis ultimately contribute to the development of inflammation and neutropenia [48]. Alternatively, and/or additionally, this may be a testament to the many knowledge gaps that exist in our understanding of NETosis.

Despite these lower levels of neutrophils found in patients with SLE, neutrophil-synthesised antibacterial proteins including defensins and lactoferrins are increased in the serum of patients with SLE [6]. Neutrophils are also key contributors to antibody-mediated lupus nephritis, based on neutrophil depletion studies in mice [49]. Granule proteins including myeloperoxidase (MPO) and neutrophil elastase can damage glomerular structures, and SLE-related skin disease is associated with neutrophil infiltration [6]. In addition, overactive NETosis or impaired clearance of NET material leads to thrombosis and endothelial cell damage [22] while promoting externalisation of modified nucleic acids that, in predisposed hosts, can lead to immune dysregulation [50]. Hence, neutrophils are potentially vital players in the development of the immune dysregulation, tissue inflammation, atherosclerosis and cardiovascular disease associated with chronic inflammatory diseases including SLE [51].

**Figure I-1: Immune dysfunction in systemic lupus erythematosus.** *Reproduced from Kaul, A., et al., Systemic lupus erythematosus. 2016.* ***2****: p. 16039.*

## 2.6. Low density granulocytes

Density gradients, created using substances such as Percoll (Figure I-2) or Ficoll (Figure I-3), are frequently used to isolate neutrophils from peripheral blood. Neutrophils typically separate at the interface of the 42 per cent and 51 per cent Percoll layers [52] or below the Ficoll layer [29]. However, peripheral blood obtained from patients with psoriasis [53] or SLE [6] additionally contains neutrophils that separate with the peripheral blood mononuclear cell (PBMC) layer, the layer which typically contains primarily monocytes and lymphocytes. These neutrophils are known as low density granulocytes (LDG) and some scientists consider them to be a recently identified subset of neutrophil [6]. However, it is not yet clear how unique SLE LDGs are within the neutrophil family. Indeed, LDGs of various phenotypes have been identified in a variety of disease states (Table I-1) as well as in healthy individuals. LDGs found in healthy individuals were recently demonstrated to have little functional differences to normal dense neutrophils (NDNs)[54] .

In the context of SLE, it has been reported that LDGs have a striking predisposition to form NETs in the absence of any additional stimulus, unlike SLE NDNs. Furthermore, NETs generated by LDGs are more proinflammatory and vasculopathic than NETs generated by other neutrophil subsets [50]. This cell type has been studied more extensively in SLE than in other autoimmune diseases; it has been determined that SLE LDGs produce higher levels of type 1 IFN than NDNs and can induce endothelial cell apoptosis [6]. As such, LDGs may play an important role in SLE pathogenesis and specifically in the SLE-associated predisposition to accelerated vascular damage [51].

Phenotypically, SLE LDGs (referred to in this chapter hereafter as “LDGs”) resemble immature neutrophils in that their hetero- and euchromatin are clearly delineated. Genetic data suggest an immature phenotype as well; mRNA encoding proteases typically upregulated during early neutrophil differentiation are high in LDGs [55]. In addition, LDGs display various granules, indicating they are not fully activated, degranulated neutrophils [55]. However, LDG surface markers suggest a mature granulocyte. As a subset of neutrophils, LDGs are CD14-hi and CD15-low. Similar to mature neutrophils, LDGs are CD10-hi, CD16-hi, CD33-low, and CD34-low. While it is unclear exactly how this cell surface marker analysis should be reconciled with nuclear morphology and genetic analyses, LDGs do appear to be a heterogeneous population of neutrophils that may need to be further sub-divided for more accurate analysis [55]. This analysis may also be indicative of a degree of plasticity within neutrophils. Recently, gene array analysis showed differential gene expression in LDGs compared to autologous SLE normal dense neutrophils (NDNs). Canonical pathways differing most significantly between LDGs and NDNs included the actin cytoskeleton and macropinocytosis [56].

When venous blood from healthy donors is separated by density gradient-based isolation techniques, immature and degranulated neutrophils are observed in the PBMC layer. Low density neutrophils have

been documented in other diseases including cancer and sepsis. However, based on phenotypic and functional analyses, these cells should be classified distinctly from SLE or psoriasis LDGs (Table I-1) [55].

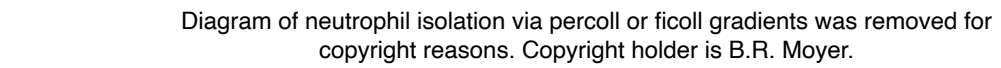


*Figures adapted from Moyer, B. R., et al. (2013). Pharmaco-Imaging in Drug and Biologics Development: Fundamentals and Applications, Springer New York.*

Table of the phenotypic and functional characteristics of low-density granulocytes from different diseases was removed for copyright reasons. Copyright holder is C. Carmona-Rivera.

**Table I-1: Phenotypic and functional characteristics of low-density neutrophils reported in different disease states.** *Reproduced from Carmona-Rivera, C. and M.J. Kaplan, Low density granulocytes: a distinct class of neutrophils in systemic autoimmunity. Seminars in immunopathology, 2013.* ***35****(4): p. 455-463.*

## 3. Cellular Mechanical Properties

The critical difference between LDGs and NDNs is their density, but prior to this thesis, other biophysical properties of LDGs had not been explored. However, the study of cellular biophysical or mechanical properties stretches back to the advent of microbiology [57]. Leeuwenhoek's earliest observations concerned the shape and size of his "animalcules" as viewed through a light microscope [58]. Early scientists discussed the concepts of cellular viscosity [59] and elasticity [60]. Viscosity was measured by centrifuging cells and analysing the time required for granules to return to their original positions [59]. Micropipette aspiration allowed for measurement of cellular and nuclear deformation in response to suction [61, 62]. Recently, powerful new techniques have been developed that expanded our capabilities to quantify these mechanical properties.

### 3.1. Tools to study cellular mechanical properties

Development of advanced technology has allowed for the quantitative assessment of cellular mechanical properties. First developed in 1986, atomic force microscopy (AFM) measures cellular elasticity by quantifying the force on the tip of a probe as it pushes into a sample, generating a topographic map of the cell's surface [63]. AFM has highlighted the mechanical nature of the cell and the interplay between structure and function of molecular motors [64, 65], the cell surface [66-68], membrane proteins [69], and other cellular components [70, 71]. Although extremely detailed and extensive information is collected, the analysis time for AFM precludes measuring kinetic processes and cells in suspension [72]. Other tools to measure cellular mechanics include contact-based magnetic bead rheology [73], contact-free optical tweezers [74] and the optical stretcher. Optical tweezers are an example of a laser trap; a single beam of light carries momentum, which is transferred to a sample as force. Sample forces can then be quantified; for example, the force of a swimming sperm [75] or the force of a molecular motor [76]. The optical stretcher is based on a double beam laser trap, and was developed to fill the gap between optical tweezers and AFM [77]. This tool allows for quantification of contact free cell deformation at speeds of one cell per second, when coupled to an automatic flow chamber [78]. Recently, high throughput mechanical phenotyping has enabled new insights into basic immunology (*e.g.* cell cycle biology and cell differentiation) as well as clinical medicine (*e.g.* malignant transformation in haematology and oncology). Cellular mechanical properties alter during processes including differentiation, motility, cell cycle and cell activation, and there is an increasing appreciation of the biomechanical changes in cells during states of disease.

### 3.2. Real-time deformability cytometry

The introduction of high throughput, microfluidics-based deformability cytometry techniques has allowed for mechanical analysis of virtually limitless cell numbers in real time. Tse *et. al.* developed deformability cytometry, which measures the deformation of cells by deceleration as they encounter an opposing flow [79, 80]. Real-time Deformability Cytometry (RT-DC) as introduced by Otto *et. al.*, deforms cells by shear stresses and pressure gradients as they fly through a microfluidic chamber (Figure I-4) [81, 82]. This technique was optimised during and is heavily relied upon in this thesis. Multi-sample deformability cytometry uses a microfluidic chamber resembling that of Otto *et. al.*, which allows for analysis of up to ten clinical samples within a single experiment [83]. Compared to the detailed topographical force map generated by AFM, less information is collected about each individual cell. However, deformability cytometry is label-free, allows for analysis of heterogeneous samples including whole blood, and measures over 1000 cells per second [80, 82, 83].

**A**

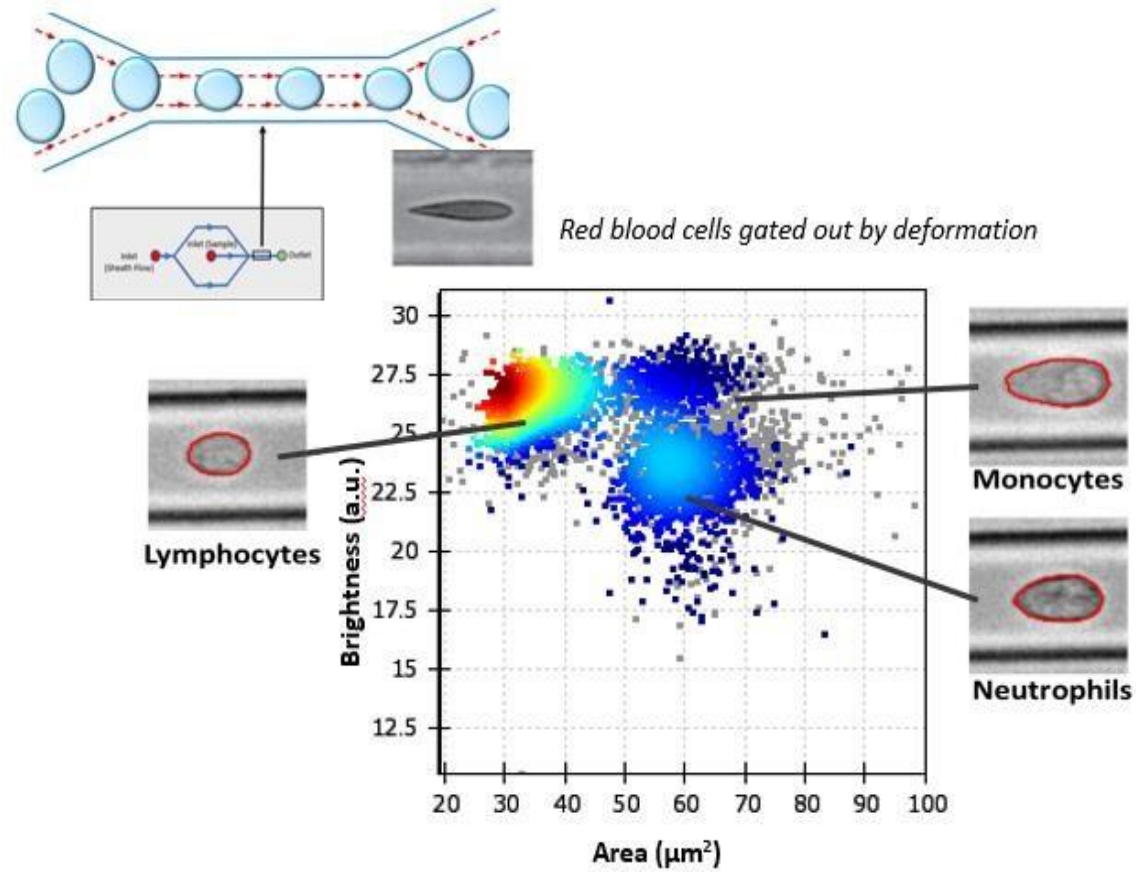

**B**

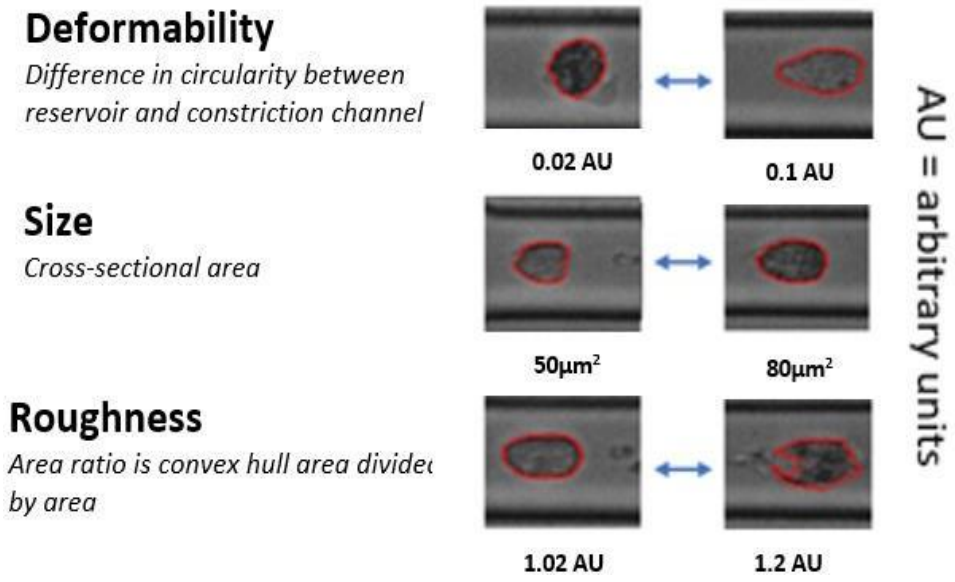


**Figure I-4: Real-time deformability cytometry, as introduced by *Otto et al.*** (A) An inverted microscope and high-speed camera capture images of individual cells moving through a narrow constriction channel within a PDMS microfluidic chip. (B) A cell tracing algorithm is applied to these images and a biomechanical profile for each cell is generated. This includes measurement of cell size (cross-sectional area), roughness (a measure of perturbations in the cell surface, quantified by dividing the convex hull area by the cross-sectional area), and deformability (1-circularity within a constriction channel). Cell populations can be identified within a mixed sample (*e.g. blood*) based on size (*i.e. cross-sectional area*) and brightness (*i.e. cell granularity*).

## 3.3. Neutrophil mechanical properties during differentiation

The differentiation of progenitor cells to mature immune cells is coupled to major changes in their mechanical properties. This is partially due to differences in intracellular organisation and composition [84-86]. Neutrophils, monocytes and macrophages develop from a common myeloid progenitor [87], however mature monocytes, macrophages, and neutrophils have been successfully distinguished from progenitors and from each other based solely on mechanical properties analysed by an optical stretcher [88]. In some instances, progenitor mechanical properties can serve as predictive biomarkers for differentiation outcomes [89].

Most cell types stiffen as they differentiate, due to an increase in cellular cytoskeletal content [84, 90], however neutrophils are an exception [91, 92]. Immature myeloid precursor cells are unable to migrate throughout the body and are relatively resistant to deformation [93]. Mature neutrophils are responsible for actively monitoring distant sites of the body for infection and other danger signals, and need the capacity to move swiftly through large blood vessels, squeeze between epithelial cells, and migrate through narrow microcapillary networks [94]. Classical descriptions of myeloid cell trafficking depend largely on biochemical mediators, specifically selectins, chemokines and cell adhesion molecules and their respective receptors [94, 95]. However, cellular remodelling and mechanical changes are also essential for motility [96]. Mature neutrophils are more deformable than progenitors [93], facilitated by microtubule dynamics, the distinctive multi-lobulated nucleus [97, 98] and the down-regulation of cytoskeletal proteins including vimentin [99]. Fitting with this, microtubules have been implicated alongside actin networks in aiding nuclear constriction during migration through narrow vessels [100]. In addition, it has been demonstrated that pharmacological stabilisation of microtubules in neutrophils interferes with deformation and remodelling, slowing motility through a 3D system [101].

## 3.4. Neutrophil mechanics during immunologic function

In addition to trafficking through microcapillaries, neutrophils are capable of a diverse range of carefully modulated effector functions. As described in section 2.3, exposure of neutrophils to pro- inflammatory cytokines or chemokines (*e.g.* tumour necrosis factor, i.e. TNF, n-formylmethionyl- leucyl-phenylalanine, *i.e.* fMLF, or granulocyte-macrophage colony-stimulating factor, *i.e.* GM-CSF) induces transition to a ‘primed’ state, characterised by increased responsiveness to agonist stimulationsand a ‘polarized’ or ‘shape-changed’ morphology [26-28]. This change in morphology may be driven by increased exocytosis of secretory vesicles [102]. There is also literature to suggest that this polarised morphology is driven by phosphatidylinositol 3,4,5-triphosphate (PIP3) and protrusive F-actin at the front of the neutrophil, with actomyosin contraction at the sides and back leading to a non-uniform shape within a primed neutrophil [103]. However, understanding of mechanisms driving mechanical changes including polarisation remains limited. With respect to size, studies of neutrophil mechanical

properties post-stimulation conflict with each other, with reports of neutrophils becoming both smaller [68, 104-106] and larger [107].

Neutrophil deformability has a marked impact on trafficking through the human body. Following neutrophil adherence to the endothelium, cells deform in a matter of seconds, appearing to expand in area by unfurling plasma membrane. This process is necessary for extravasation [108]. Mechanical changes are largely driven by cytoskeletal reorganisation and actin polymerisation [109]. The complement activation product and chemoattractant C5a reorganizes the actin cytoskeleton, increases neutrophil deformability and induces migration of neutrophils into inflammatory sites [107]. Recently, RT-DC demonstrated that chemoattractants CXCL16 and IL-8 enhance neutrophil deformation similarly to C5a, thereby facilitating transmigration through vessel walls [110].

The lung microvasculature takes the entire cardiac output and is a complex network of particularly narrow capillaries [111]. It has been established that cytoskeletal stiffening promotes the sequestration of neutrophils in the lung pulmonary microvasculature [112]. There is both *in vitro* and *in vivo* evidence to indicate if the priming stimulus is removed, primed neutrophils gradually de-prime, reverting to a quiescent state resembling un-primed neutrophils. With regards to immunologic function, this entails decreased responsiveness to agonists and with respect to morphology, the smoother, "non-polarized" shape of de-primed neutrophils leads to escape from entrapment in the microvasculature [42]. When primed neutrophils are mechanically perturbed by an optical stretcher or 'micro-circulation mimetic' [50], active depolarisation occurs two orders of magnitude faster than spontaneous de-priming [41].

To further explore this phenomenon *in vitro*, microcirculation mimetics have been employed. These mimetics are physical conduits intended to imitate the pulmonary microcirculation. When neutrophils were trafficked through the microcirculation mimetic, polarized primed neutrophils were hindered more than the smooth, un-primed cells. However, within ten minutes of their repeated compression and release by the mimetic's constrictions, primed neutrophils reverted to a round phenotype, and molecular evidence indicated they had become de-primed [41]. These results confirm the data obtained from the optical stretcher [41]. This process, in which a physical force elicits a functional response, is an example of mechano-transduction [113-115].

*In vivo* radiolabelling studies have demonstrated that primed neutrophils are retained in the lungs, while de-primed neutrophils traffic similarly to their un-primed counterparts [116]. These studies contribute to the hypothesis that repeated advection of primed neutrophils through the pulmonary microvasculature may serve to mechanically de-prime neutrophils, thus allowing for regulation of the immune system [43, 116]. This is predicted to have implications for respiratory diseases including ARDS and chronic obstructive pulmonary disease (COPD) [44].

### 3.5. Established mechanical signatures of disease

High throughput mechanical phenotyping has begun to identify the mechanical signatures present in specific disease states [117]. Increases in neutrophil size occur in trauma patients prior to organ dysfunction [118] and neutrophil deformability decreases in patients with chronic renal failure [119]. RT-DC showed that patients with ARDS and patients hospitalised with viral respiratory tract infections (RTI) have larger and more deformable neutrophils in their blood than healthy volunteers [117]. This may be due to sequestration and mechanical de-priming of stiff, shape-changed neutrophils in the pulmonary vasculature [43, 44, 116]. Monocytes are larger in both ARDS and RTI but more deformable only in patients with viral RTI. Patients infected with Epstein Barr virus exhibited more deformable circulating monocytes, but neutrophils showed less of a response [117]. Eosinophils isolated from patients with asthma are rougher than those from healthy volunteers, but do not differ in size or deformation [120]. Such phenotypic analysis, in which several types of immune cells are mechanically profiled, has been termed morpho-rheologic phenotyping, or MORE phenotyping [121]. Although a new phenomenon, with the advent of machine learning and an increase in the number of mechanical properties that can be analysed at high throughputs, scientists may, very soon, be capable of distinguishing between bacterial and viral infections, achieving more definitive diagnoses of some inflammatory diseases, and anticipating critical health developments such as septic shock.

### 3.6. Emerging ideas about the mechanics of pharmacology

In addition to understanding disease pathogenesis, mechanical phenotyping is also being used to better understand responses to treatment. For example, it has long been known that glucocorticoids induce de-margination of leukocytes from the microcirculation, increasing the white blood cell count as measured by the clinical full blood count (FBC) [122]. Historically, this phenomenon has been attributed to down-regulation of selectins and other adhesion molecules [123], though some evidence refutes this [124, 125]. Recently, it was demonstrated that glucocorticoids and catecholamines mediate granulocyte cytoskeleton remodelling and softening. As a result, granulocytes move more swiftly through capillary beds and re-enter the circulation from marginated intravascular pools. These softer cells also demarginate to a position of equilibrium closer to the vessel centre than stiffer counterparts, perhaps mitigating extravasation [126]. Thus, a potential mechanical solution sheds new insight into the mechanism of action of glucocorticoids.

Studies have already used measures of neutrophil deformability to assess drug efficacy in deactivating neutrophils and increasing cellular movement through the microcirculation [127]. Milrinone, piclamilast, urinastatin, ketamine, protein C concentrate, and nitric oxide donor FK 409 are drugs that showed promise in reducing inflammation, and mechanical phenotyping demonstrated that these drugs successfully reduced neutrophil deformability in both neonates and adults [127]. Future wide-scale

testing of the effect of various drugs on myeloid cell mechanical properties may allow for discovery of new compounds capable of mitigating inflammation or achieving other desired outcomes.

### 3.7. Future of high-throughput mechanical phenotyping

High throughput mechanical phenotyping techniques have only been available in recent years and the capabilities of cellular phenotyping for new diagnostics, bedside monitoring of critical conditions including sepsis and leucocytosis, assessing patient response to treatment, and scanning compound libraries for potential novel therapeutic options are in their infancy. High throughput mechanical phenotyping will increasingly allow research labs to compare purified cells to their pre-processed counterparts found in whole blood. It will further improve isolation techniques, allowing for experiments on myeloid cells that have not been disrupted from their *in vivo* state and allow for the characterisation of *in vivo* cell functions in health and diseases. AFM remains capable of assessing cells on a much more detailed level than deformability cytometry and, at least in the immediate future, is likely to remain the tool of choice for scientists unconcerned with heterogeneous samples, measuring mechanical kinetics over time or achieving particularly large sample sizes. However, incorporation of machine learning also promises to drastically expand the mechanical properties assessed by deformability cytometry. This is an exciting time for mechanical phenotyping. As high throughput deformability cytometers become prevalent in laboratories across the globe, numerous discoveries that will tangibly aid our basic research efforts and how we understand and treat diseases will be made.

## 4. Chapter summary and areas for further research

Neutrophils are a key immune cell whose dysregulation contributes to development of a variety of acute and chronic inflammatory conditions including SLE. Given that real-time deformability cytometry (RT-DC) has only recently been introduced, considerable optimisation work is necessary to accurately and precisely measure the biomechanical properties of neutrophils in whole blood and in isolation. Such optimisation will permit experiments to be conducted on isolated neutrophils that are biomechanically indistinct from their whole blood counterparts.

As the first responders to infection, neutrophils require highly tuned functional flexibility. The ability to change functional status in response to immune-modulators allows the neutrophil to patrol the body in a relatively quiescent state while remaining capable of sensing and then employing appropriate responses when threats arise [102]. Neutrophil priming is characterised by the generation of reactive oxygen species, and some enhanced immune functions including neutrophil extracellular trap (NET) formation and chemotaxis. This primed state enhances their response to a subsequent exposure to an activating stimulus [26, 34]. It has been established that neutrophil priming is linked to distinct biomechanical changes which may be responsible for changes in neutrophil immunologic function but reports of specific biomechanical changes vary (*e.g.* with discrepancies in neutrophils becoming smaller

[52, 85-87] or larger [88] post-priming). Analysis of the biomechanical kinetics of neutrophils as they become primed and de-primed is necessary to clarify these inconsistencies. In addition, our understanding of the impact on neutrophil immune function conferred by a change in biomechanical properties is currently largely theoretical. Further research into this area, and identification of specific impacts on trafficking regulated by cellular mechanics, will provide insight into how real-time deformability cytometry could be useful in diagnosing diseases or identifying therapeutics from compound libraries.

Finally, LDGs appear to directly contribute to SLE pathogenesis, but these cells have few distinguishing characteristics aside from their low density. Given that density is a biomechanical property, analysing additional biomechanical properties of these LDGs in comparison to their normal dense counterparts could shed new light into the nature of these cells, specifically with respect to their trafficking capabilities. The field will also benefit from proteomics and phosphoproteomic profiling of these cells, as this may uncover previously unappreciated signalling networks responsible for LDGs' seemingly more pathogenic immunologic capabilities. This thesis aims to address these issues, and the following research aims are presented in each experimental chapter.

## 4.1 Central research questions

1) How do neutrophil biomechanical properties relate to neutrophil priming and immune function in the contexts of health and SLE?
2) Do SLE LDGs more closely resemble healthy LDGs or other normal dense neutrophil subsets by biomechanical phenotyping, proteomic profiling, and trafficking assays?

## 4.2 Research aims

Chapter III

- To replicate previous work by *Otto et. al.*[82] establishing that RT-DC yields consistent and replicable results.
- To identify baseline parameters of neutrophil deformability, area, and area ratio by RT-DC.
- To determine whether neutrophil biomechanical properties vary based on age or sex.
- To assess the effect of time post-venepuncture on neutrophil biomechanical properties in the interest of optimising future experiments.
- To establish optimal protocols for neutrophil and LDG isolation yielding pure, undisrupted neutrophils.
- To affirm RT-DC can identify known biomechanical differences in immune cells in the context of disease.

Chapter IV

- To describe the biomechanical kinetics of neutrophil priming
- To ascertain whether neutrophil priming kinetics are consistent across priming agents
- To identify the mechanism regulating neutrophil expansion after priming
- To determine the density of primed neutrophils relative to un-primed counterparts
- To compare the biomechanical profiles of un-primed, primed, and de-primed neutrophils

Chapter V

- To compare immune cells from healthy individuals and patients with active or stable SLE.
- To describe the biomechanical profile of SLE LDGs.
- To determine how SLE LDGs biomechanically compare to other neutrophil subsets.
- To identify clinical or demographic characteristics which affect neutrophil biomechanical phenotype.
- To design and produce a device that mimics the pulmonary microvasculature and can be used for trafficking assays.
- To determine if SLE LDGs and other neutrophil subsets differ with respect to their trafficking through a pulmonary microvasculature mimetic.
- To decouple the molecular and biomechanical contributions to modulation of neutrophil trafficking and to determine their relative effects.

Chapter VI

- To understand neutrophil heterogeneity at the proteome and phosphoproteome levels.
- To reveal new insights into SLE LDG biology and function.
- To compare proteomes and phosphoproteomes of healthy neutrophils with SLE neutrophils.
- To identify potential mechanisms regulating the SLE LDG biomechanical phenotype.
- To reveal the effect of neutrophil priming on the proteome and phosphoproteome.

# Chapter II: Methods

## 1. Consumables and reagents

**Table II-1: Consumables and reagents**

| Consumable/Reagent | Supplier | Location |
|---|---|---|
| BSA IgG | Abcam | Massachusetts, USA |
| Endothelial growth media, Human dermal microvascular endothelial cells | AngioProteomie | Massachusetts, USA |
| U1 RNP/Sm antigen | Arotech Diagnostics ATR01-10 | Wellington, New Zealand |
| Pasteur pipettes (2ml, 5ml, 10 ml, 25 ml) | Appleton Woods<br>USA Scientific | Birmingham, UK<br>Florida, USA |
| Sterile saline (0.9%) | Baxter Healthcare | Berkshire, UK |
| Polypropylene Falcon tubes (15 ml, 50 ml), polystyrene round bottom tube (5 ml), syringes (50 ml) | BD Biosciences | Oxford, UK |
| 5ml round bottom polystyrene FACS tube | Corning | New York, USA |
| Dextran 500 | GE Healthcare | Little Chalfont, UK |
| 19-gauge Butterfly needle | Hospira | Lake Forest, UK |
| 8-well glass chamber slide, µ-slide VI 0.4 chambers | Ibidi | Wisconsin, USA |
| Sterile calcium chloride, Sterile sodium citrate | Martindale/Ethyfarm | Wooburn Green, UK |
| 24-well cover glass imaging plates | Miltenyi Biotech | Bergisch-Gladbach, Germany |
| S-Monovette citrate, EDTA, Heparin vacutainers, 24- and 96- well tissue culture plates | Sarstedt | Numbrecht, Germany |
| PBS, Ficoll, fMLF, Phorbol myristate acetate, Ethanol, SDS, LPS, DMSO, Cytochalasin D, C5a | Sigma-Aldrich | Dorset, UK<br>Missouri, USA |

| | | |
|---|---|---|
| Pipette tips (graduated, filter tip) | Starlab<br>USA Scientific | Milton Keynes, UK<br>Florida, USA |
| EasySep neutrophil isolation kit, EasySep direct neutrophil isolation kit | StemCell Technologies | Massachusetts, USA |
| BSA, 12 % NuPage Bis-Tris gels, GM-CSF, HALT protease inhibitor cocktail, High-Select™ Fe-NTA Phosphopeptide enrichment Kit, PageRuler Plus prestained protein ladder, ProLong Gold Antifade, RPMI 1640 media (phenol-free), TMT labelling kit, TEAB, TrypLE Express 1x | Thermo Fisher Scientific | Massachusetts, USA |
| PAF | Tocris Bioscience | Abingdon, UK |
| Flic20, CellCarrier | ZellMechanik | Dresden, Germany |

**Table II-2: Antibodies and stains for fluorescence microscopy or gel electrophoresis**

| Antibody | Supplier | Location |
|---|---|---|
| SiR-actin live cell actin probe | Spirochrome | Colorado, USA |
| Secondary antibodies | Jackson ImmunoResearch | Pennsylvania, USA |
| Anti-MPO | Abcam | Massachusetts, USA |
| Anti-CD86, anti-HLDR4 | StemCell Technologies | Massachusetts, USA |
| Hoechst 33342, Coomassie blue stain, Sytox green, Anti-CD41a | ThermoFisherScientific | Massachusetts, USA |
| Hoechst 33342, pHrodo Green 10,000 Dextran | ThermoFisherScientific | Warrington, UK |

## 2. Patient recruitment

All studies were approved by site-specific institutional review boards, including the Cambridge Local Research Ethics Committee (REC reference 06/Q0108/281) and NIAMS IRB (NIH 94-AR-0066). All subjects provided written informed consent. Subjects with SLE fulfilled the American

College of Rheumatology revised criteria for SLE [128]. Subjects were recruited from the University of Cambridge and the NIAMS Lupus Clinics. Healthy volunteers were recruited by advertisement. Inclusion criteria were: SLE diagnosis. Exclusion criteria was treatment with corticosteroids. Exclusion criteria were selected due to evidence for corticosteroids altering neutrophil mechanical properties [126].

## 3. Blood

At the University of Cambridge, blood was drawn into a 40 mL syringe and transferred to 50 mL Falcon polypropylene tubes (BD Biosciences, Bedford, MA, USA) with 4 mL of 3.8 per cent sodium citrate (Martindale Pharmaceuticals, Essex, UK). At the NIH Clinical Center in Bethesda MD, peripheral blood was drawn by venepuncture and collected into tubes containing 3.8 per cent sodium citrate (Sarstedt, Numbrecht, Germany) from recruited SLE and HC subjects. All subjects signed informed consent. Where indicated, subjects gave a blood donation from each arm, one hour apart.

## 4. Neutrophil isolation

A wide variety of neutrophil isolation strategies were employed during the research presented in this thesis in an attempt to optimise a strategy that yielded pure neutrophils biomechanically resembling neutrophils analysed directly in whole blood. Details for individual experiments can be found in the figure legends. Unless otherwise mentioned, low and normal dense neutrophils were isolated via a ficoll gradient followed by an EasySep neutrophil isolation kit. The process by which this isolation technique was optimised is described in Chapter III. A step by step protocol for this isolation process can be found in the appendices of this thesis.

For all experiments using isolated neutrophils, either plasma-percoll [29] (Sigma-Aldrich, Dorset, UK)) or ficoll (Sigma-Aldrich, Dorset, UK) [52] discontinuous density gradient centrifugation methods were used to separate granulocytes from peripheral blood mononuclear cells (PBMCs). Full protocols for both isolation strategies can be found in the appendices and a visual diagram of each strategy can be found in Figures I-2 and I-3.

Both the plasma-percoll and ficoll gradients allowed plasma from blood samples to be collected and serum to be generated by incubating plasma with CaCl2 (Martindale, Wooburn Green, UK) for 1 hour at 37 degrees C. CaCl2 should be added to the fresh plasma at approximately a 1:100 w/v ratio.

When using a ficoll gradient (most commonly used in this thesis), 20 mL of blood was layered on top of 20 mL of ficoll. The gradient was centrifuged for 20 minutes at 150g with the brake set at 1. After centrifugation, a plasma layer, PBMC layer, ficoll layer, and mixed erythrocyte and granulocyte layer were clearly visible. The PBMC layer was removed and resuspended with PBS in a separate tube. The bottom layer containing the mixed erythrocyte and granulocyte populations

were also placed in a separate tube. These two separated cell fractions subsequently went through a protocol to isolate the neutrophils found in both.

Following the ficoll gradient phase, normal dense neutrophils (NDNs) were separated from erythrocytes via the EasySep direct neutrophil isolation kit (StemCell Technologies, Massachusetts, USA) as per the manufacturer's instructions. LDGs were separated from PBMCs via the EasySep neutrophil isolation kit with customized antibodies targeting CD86 and HL-DR4 (StemCell Technologies, Massachusetts, USA), also as per the manufacturer's instructions. In some experiments completed in Chapter III, LDGs were separated from PBMCs via a magnet associated cell sorting (MACS) negative isolation system (Miltenyi Biotec, Maryland, USA). Following isolation, neutrophils were resuspended in PBS with calcium and magnesium ions (PBS+/+) and counted using a hemacytometer.

When using plasma-percoll gradients, 40 mL of blood was first centrifuged for 20 minutes at 300g. Plasma was removed following centrifugation, and the pellet containing white and red cells was resuspended in 1.5% dextran 500 (GE Healthcare, Little Chalfont, UK) and 0.9% warm saline (Baxter Healthcare, Berkshire, UK). The resuspended pellet was allowed to sit at room temperature for approximately 40 minutes, at which time the erythrocytes had fully sedimented and the white blood cells could be removed to a new tube. The white blood cells were subsequently pelleted by centrifugation for 5 minutes at 260g. Two percoll gradients were made using platelet-poor plasma generated from the same donor by centrifugation of the plasma and removal of the platelets. One 42% percoll gradient and one 51% percoll gradient were each generated. After the white blood cell pellet was resuspended in 2 mL of autologous platelet-poor plasma, the two percoll gradients were underlaid below the white blood cells. After centrifugation for 14 minutes at 150g, the top interface contained PBMCs while the purified normal dense neutrophils sat at the interface between the 42% and 51% percoll gradients. Any contaminating erythrocytes were found at the bottom of the gradients. The plasma-percoll gradient system was not used in conjunction with the EasySep neutrophil isolation system because the use of dextran interfered with EasySep-based system.

## 5. Recovery of isolated neutrophils

Unless otherwise noted, neutrophils were rested at a concentration of 1 million cells per mL for 35 minutes at 37 degrees C in PBS+/+ (Sigma-Aldrich, Dorset, UK) and 5% autologous serum immediately following isolation. Cells were rested in PBS, PBS+/+ or PBS+/+ with 5% autologous serum for experiments in Figure III-5. This served to recover their whole blood biomechanical phenotype, as described in Chapter III.

## 6. Neutrophil viability

Cytospin slides were prepared for each isolation and neutrophil purity was assessed by light microscopy at a magnification of 400x. Cells were stained with haematoxylin (Sigma-Aldrich,

Dorset, UK) for 3 minutes, de-stained with water for 1 minute, then stained with eosin (Sigma-Aldrich, Dorset, UK) for 1 minute and examined visually to determine the percentage of neutrophils in the sample. Numbers of neutrophils, erythrocytes, monocytes, lymphocytes and eosinophils were counted in three fields containing at least 100 cells for each preparation. Preparations were routinely >95 per cent neutrophils.

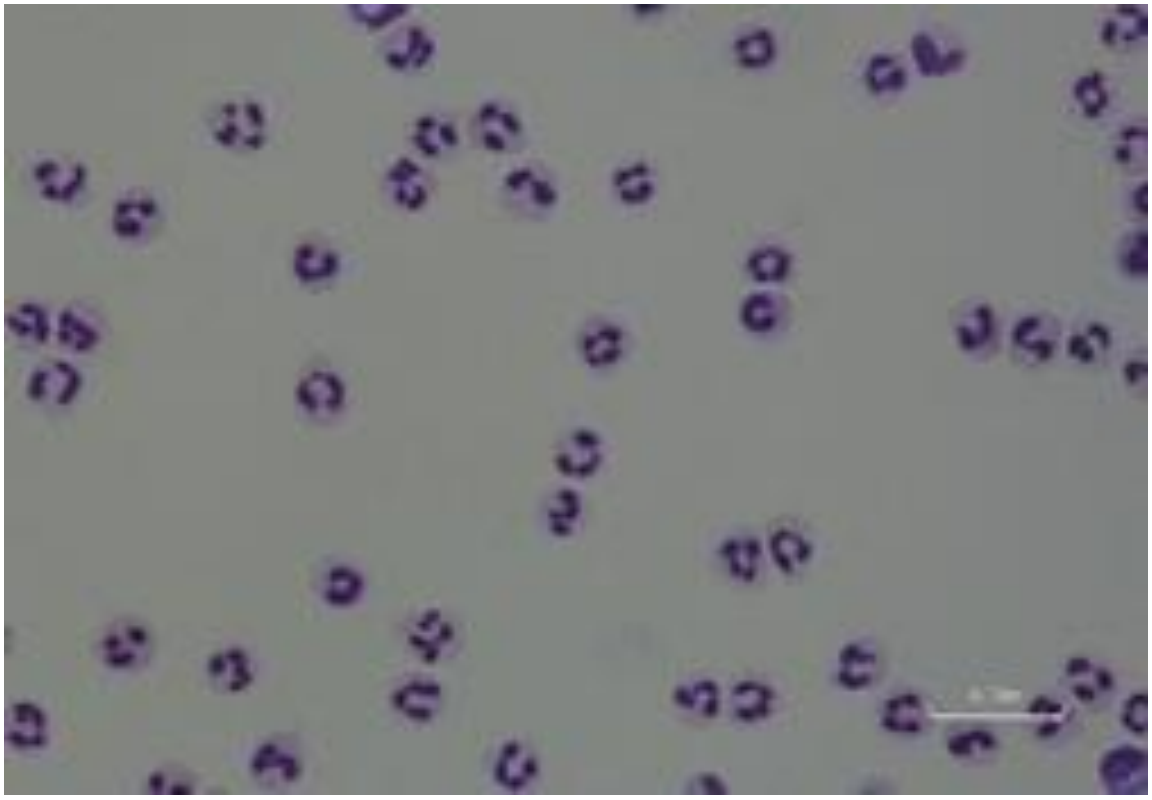

**Figure II-1: Prepared cytospin showing neutrophils with the characteristic multi-lobulated nuclei.**

## 7. Neutrophil priming and stimulation

Where indicated in the experimental legends and as required for assessing the effects of priming or stimulation in experiments completed in Chapter VI, neutrophils were exposed to the following stimuli: fMLF (0.1-1000nM for Figure VI-1, otherwise 100nM) , PAF (1 µM), LPS (1 µg/mL), C5a (0.1 µg/mL) or GM-CSF (0.1 µg/mL) (see Table II-1 for sources). Neutrophils were analysed at multiple time points over the course of an hour in Figures IV-1, IV-2, IV-3, and IV-4. For all experiments completed in Chapter VI, neutrophils were additionally exposed to dimethyl sulfoxide (DMSO) (Sigma-Aldrich, Dorset, UK) as the vehicle control.

For experiments displayed in Figure IV-4, neutrophils were pre-treated with either 10 µM amiloride (Sigma-Aldrich, Dorset, UK) or the amount of DMSO amiloride was dissolved in for 30 minutes. Pre-treatment took place at 37 degrees C in PBS+/+ with 5% autologous serum. Following pre-treatment, neutrophils were exposed to either 100nM fMLF or the equivalent volume of DMSO for 45 minutes.

For experiments completed for Figure V-8, neutrophils were stimulated with 100-2000 units/mL of recombinant human type 1 interferon (IFNα) (R&D Systems, Minneapolis, MN), 10 ng/mL Sm/RNP immune complexes [7] (Arotech Diagnostics, Wellington, NZ), or 5% serum from either patients with active SLE or healthy volunteers.

For proteomics experiments, some healthy neutrophils were stimulated with 100nM fMLF for 20 minutes.

During all instances of stimulation, neutrophil samples were kept in 2 mL tubes (Eppendorf, Stevenage, UK) at 37 degrees C with 5% CO2. In some instances, neutrophils in whole blood were analysed, always within 1 hour of venesection. The exception to this can be found in Figure V-8 where the experiment was completed within four hours of venesection due to requirements for NETosis and time-matched controls were completed.

In experiments when isolated neutrophils were analysed, cells were resuspended in PBS+/+ at 1 million cells per mL. Experiments were initiated within 1 hour of isolation for purified neutrophil experiments. DMSO or PBS+/+ served as vehicle controls.

## 8. Generation of immune complexes

SLE-relevant IgG were isolated from serum samples from patients with SLE in the NIH lupus cohort expressing high titres of anti-RNP/Sm antibodies. IgG from age/sex/race-matched control serums were also isolated and served as controls. To isolate these IgGs, the Melon Gel IgG spin purification kit (Thermo Fisher Scientific, Massachusetts, USA) was employed according to the manufacturer's instructions. The purified IgG fractions were run out on a gel via electrophoresis to assess IgG purity as described in section 19.2 of this chapter. The gel was stained with colloidal blue stain (Thermo Fisher Scientific, Massachusetts, USA) as described in section 19.3 of this chapter. This staining indicated protein bands at 150 kDa, the molecular weight for IgG, as well as at 25 kDa and 50 kDa (heavy and light chains respectively) [129].

To generate immune complexes, these purified IgG samples or commercially available bovine serum albumin (BSA) IgG (Abcam, Massachusetts, USA) were incubated with exogenous U1 RNP/Sm antigen (Arotech Diagnostics, Wellington, New Zealand) or exogenous BSA (2 mg/mL, Thermo Fisher Scientific, Massachusetts, USA) respectively at a 1:1 ratio for 30 minutes at room temperature. Normal dense neutrophils purified from the blood of healthy volunteers were seeded

onto coverslips pre-coated with poly-L-lysine (Sigma-Aldrich, Dorset, UK) and were exposed to 10 µg/mL of immune complexes or pure IgG for 4 hours at 37 degrees C to assess induction of NETosis. The isolation and use of SLE-relevant immune complexes to induce NETosis in healthy human neutrophils was previously described by Lood *et al.* [50].

## 9. Induction of NETosis

Neutrophils purified by ficoll gradient were resuspended in RPMI-1640 (Thermo Fisher Scientific, Massachusetts, USA) at a concentration of $1 \times 10^6$ neutrophils/mL. Poly-L-lysine pre-coated coverslips were placed in each well of a 24 well plate. In a total sample volume of 50 µL, 50,000 neutrophils were seeded onto each coverslip and subsequently exposed to 10 µg/mL of IgG or immune complexes, generated as described above, for 4 hours at 37 degrees C. Other neutrophil samples were exposed to 500 ng/mL PMA (Sigma-Aldrich, Missouri, USA), or no additional stimulus for 4 hours at 37 degrees C. Following the incubation, 1 mL of 4 per cent paraformaldehyde was placed over the sample and the plate was wrapped in parafilm and incubated at 4 degrees C overnight. Fluorescence microscopy was used to observe NETosis. No serum was included in these assays.

## 10. Florescence microscopy

In brief, coverslips were washed on a rocker at room temperature with 0.2 per cent gelatine in PBS for 30 minutes. After washing, coverslips were incubated for 1 hour at 37 degrees C with rabbit polyclonal anti-human MPO (1:1000 in PBS) (ab9535, Abcam, Massachusetts, USA) or mouse monoclonal anti-human CD41a (1:1000 in PBS) (Clone HIP8, StemCell Technologies, Massachusetts, USA). After incubation with the primary antibody, coverslips were washed three times for five minutes each with PBS. After washing, the coverslips were incubated for 30 minutes in the dark at 37 degrees C with secondary fluorochrome-conjugated antibodies appropriately matched to the primary antibodies (1:400 in PBS), specifically Alexa Fluor 594 AffiniPure Goat Anti-Rabbit IgG and Alexa Fluor 488 Goat Anti-Mouse IgG (Jackson ImmunoResearch, Pennsylvania, USA). After washing coverslips an additional 3 x 5 minutes using PBS, coverslips in some experiments were stained with 5 units/mL Phalloidin-iFluor 594 Reagent (ab176757, Abcam, Massachusetts, USA) for twenty minutes at room temperature, in the dark. In some experiments, coverslips were additionally/alternatively stained with Hoechst (1:1000 in PBS) (Thermo Fisher Scientific, Warrington UK) for 5 minutes in the dark at room temperature. Coverslips were mounted onto slides with a drop of ProLong Gold Antifade (Thermo Fisher Scientific, Massachusetts, USA) and three images per slide were taken with a Leica 4000B inverted light microscope (Leica Microsystems, Illinois, USA) with a x40 objective using the appropriate channels for each fluorophore present in the stained sample. This process of analysing neutrophils by florescence microscopy was previously described by [50].

## 11. Quantification of NETosis

From images of fluorescence microscopy, neutrophils undergoing NETosis were manually counted (based on MPO and DAPI co-localisation on strand-like DNA structures) and divided by the total number of neutrophils present (based on DAPI-only) under blinded conditions. Each experiment had at minimum three technical replicates and three images taken per slide. The mean value for the percentage of neutrophils undergoing NETosis on each slide was calculated.

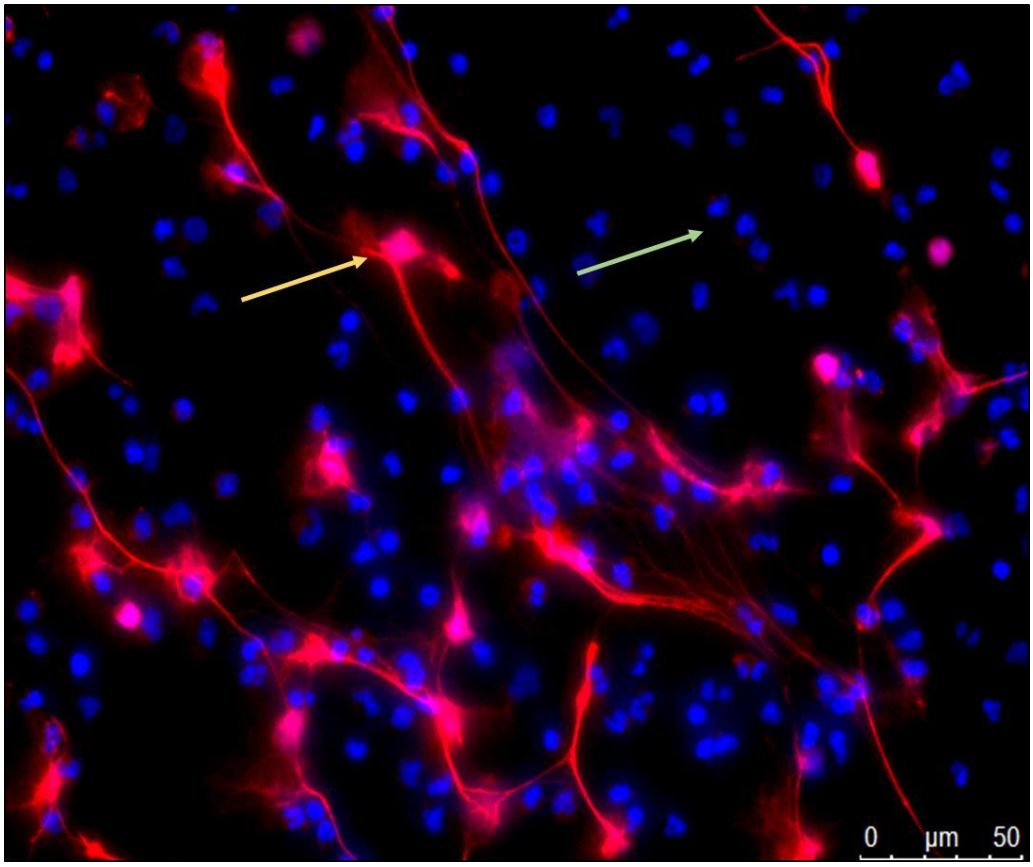


**Figure II-2: Neutrophils undergoing NETosis by florescence microscopy.** Yellow arrow indicates a neutrophil undergoing NETosis. Green arrow indicates a neutrophil not undergoing NETosis. NETosis was quantified by dividing the number of neutrophils undergoing NETosis by the total number of neutrophils.

## 12. Real-time deformability cytometry (RT-DC)

RT-DC was first developed very shortly prior to this thesis and is extensively described in the following papers: [130] [131]. All RT-DC related work was completed independently. To perform RT-DC using the AcCellerator setup at the University of Cambridge, neutrophils were resuspended by gentle mixing in CellCarrier buffer (ZellMechanik Dresden GmbH, Germany) at a concentration of $2.5 \times 10^7$ cells/mL. CellCarrier buffer is based on 1x PBS +/+ buffer containing 0.5 per cent methylcellulose. In order for the kinetic studies completed in Chapter IV to be more relevant to

expected kinetics in the blood, it was important that calcium and magnesium ions be present in the CellCarrier buffer as these ions play important roles in macropinocytosis, the mechanism regulating neutrophil priming [132]. The purpose of the methylcellulose is to slightly increase the viscosity of the sample, which allows for optimal analysis of cells moving through the microfluidic chamber. Methylcellulose at this concentration has been demonstrated to be biocompatible with all cell lines and primary cells tested by ZellMechanik Dresden to date [82].

Cell suspensions were drawn into 1 mL syringes and placed in one of the syringe pumps (neMESYS, Cetoni Gmbh, Korbussen, Germany) of the AcCellerator (ZellMechanik Dresden GmbH, Germany), which is an extension for an inverted microscope. The other syringe pump was filled with CellCarrier buffer without cells, to serve as an additional source of fluid flow. These two syringes were connected to polymer tubing, which was in turn attached to the sample inlet andthe sheath flow inlets respectively of a Flic20 PDMS microfluidic chip (ZellMechanik Dresden GmbH, Germany). The chip contains reservoirs that are connected by a square measurement channel with a 20×20 $\mu m^2$ cross-section. RT-DC measurements were collected at a cellular flow rate of 0.12 μL/s (0.03 μL/s sample flow and 0.09 μL/s sheath flow).

RT-DC employs gating strategies similar to those used in flow cytometry. For isolated cell populations, an open gating strategy was employed. For whole blood measurements, 50 μL blood was diluted into 950 μL CellCarrier buffer and a gate for cells sized 5–16 μm parallel to and 5–20 μm perpendicular to flow direction was applied. This allowed for exclusion of single erythrocytes and erythrocyte doublets. An inverted microscope in combination with a high-speed complementary metal-oxide-semiconductor (CMOS) camera (Mikrotron GmbH, Unterschleißheim, Germany) captured images of cells at a frame rate of 2000 frames per second asthey reached the end of the constriction channel. A cell tracing algorithm was applied to the framesto detect cells and perform analysis in real time. The data files necessary for single-cell MORE analysis (see below) were exported for all detected cells.

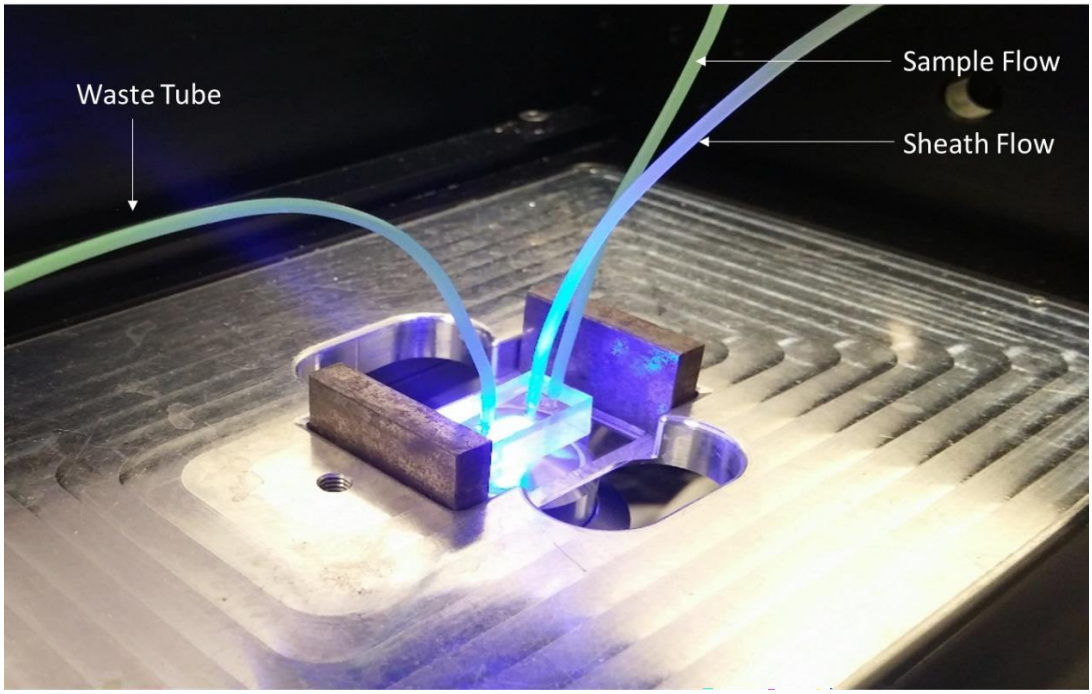


**Figure II-3: Microfluidic chip mounted on the AcCellerator, prepared for RT-DC.** Arrows indicate the inputs and outputs of the microfluidic chip. The inverted microscope can be seen below the chip.

## 13. Morpho-rheological analysis

Several reports have described methods to analyse RT-DC data files [35, 54, 55]. This thesis analyses data collected via RT-DC via these same methods. Firstly, during the data collection stage a tracing algorithm implemented in C/LabVIEW was applied to images of cells. Secondly, off-line analysis was completed using ShapeOut software and custom-written Python scripts, which allowed for generation of a neutrophil morpho-rheological or "MORE" profile.

For each cell detected, data describing a bright field image of the cell, the contour of the cell, and the cell size (as the cross-sectional area of the cell) were exported and analysed. Cell size was obtained from the area inside the convex hull, a processed contour, where all points contributing to concave curvature were removed.

Deformation is a measure of the cell's deviation from sphericity and is calculated from the convex hull of the cell: $\text{Deformation} = 1 - \frac{2\sqrt{\pi A}}{l}$, where A is the convex hull area and l is the length of the convex hull perimeter. Pre-existing shape deviations from sphericity were controlled for by analysing cells within a reservoir devoid of stresses in front of the constriction channel. In this manner, cellular deformation due to constriction stresses alone was obtained and presented.

The ratio of convex hull area to cell contour area is defined as the cellular area ratio and provides a measure of cell surface roughness. Cells with area ratios in the range of 1.0–1.05 were used to compare leukocyte deformation and size. Figure II-4A displays how cell size, deformability, and area ratio/roughness is visualised via RT-DC

The mean brightness of the cell was determined using all pixel values falling within the cell's contour. Major leukocyte sub-populations were identified based on cell size and mean brightness, as can be seen in in Figure II-4B. Erythrocytes can be easily identified due to their extremely deformable state within the constriction channel. Importantly, pixel brightness can be influenced by factors including the image focus and thickness of the microfluidic chip. This is not an issue when distinguishing between populations of cells measured at the same time, through the same microfluidic chip. For further detailed information around how these analyses were developed, see [35]. ShapeOut is available as an open source application on GitHub https://github.com/ZELLMECHANIK-DRESDEN/ShapeOut/releases. A step by step protocol for RT-DC can be found in the appendices.

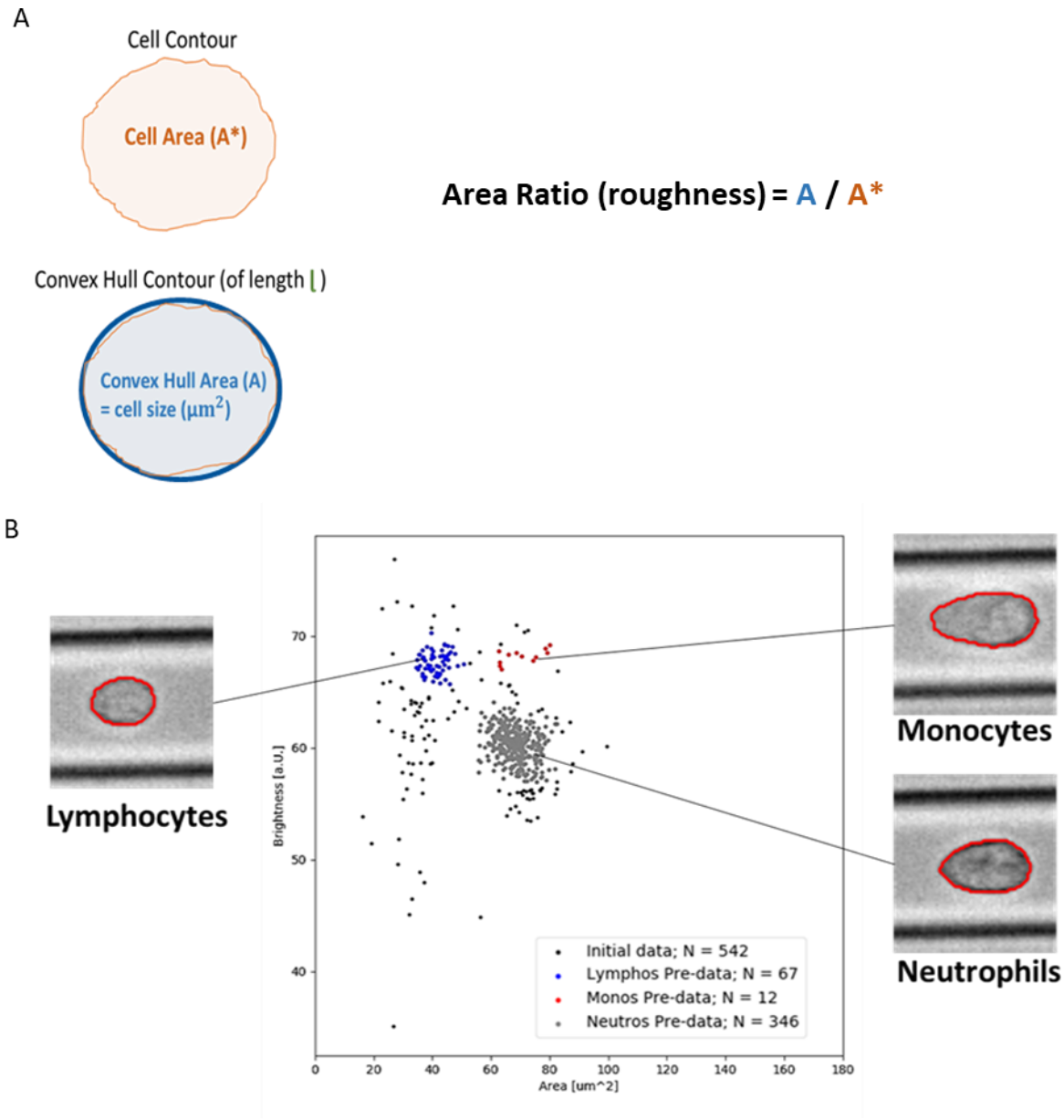


**Figure II-4: Off-line analysis of images captured by RT-DC.**

(A) Area ratio is a measure of cell roughness, essentially quantifying the amount of perturbations in the cell surface. An area ratio of one signifies a perfectly smooth cell. Most unstimulated neutrophils have an area ratio of approximately 1.032. (B) By plotting cell size by cell brightness (i.e. a measure of cell granularity), the major populations of immune cells in blood can be identified.

## 14. Confocal microscopy

Confocal microscopy was used to analyse dextran uptake by primed neutrophils. Neutrophils were prepared at 2 × $10^6$ cells per mL in Live Cell Imaging Solution (Thermo Fisher Scientific, Warrington, UK) containing 1 per cent autologous serum and plated (180 µL of the above suspension) in 12-well, poly-L-lysine-coated flat bottomed plate wells and treated with 1 µL. of amiloride or vehicle control DMSO for 30 minutes at 37 degrees C with 5 per cent $CO_2$. Cells were subsequently treated with 100 nM fMLF, or vehicle control DMSO, in the presence of 10 µg/mL of pHrodo Green 10,000 Dextran (Thermo Fisher Scientific, Warrington, UK). Cells were concomitantly stained with 0.1 per cent Hoechst 33342 (Sigma-Aldrich, Dorset, UK) and imaged using an SPE Leica® confocal microscope (Leica Microsystems, Wetzlar, Germany). Two lasers were used; the ultraviolet laser was used to excite Hoechst 33342 with 15 per cent laser power and 800 gain, and the blue laser to excite pHrodo green 10,000 Dextran with 25 per cent laser power and 850 gain. *Z*-stacks of 5–10 µm were obtained with minimum three random fields per condition.

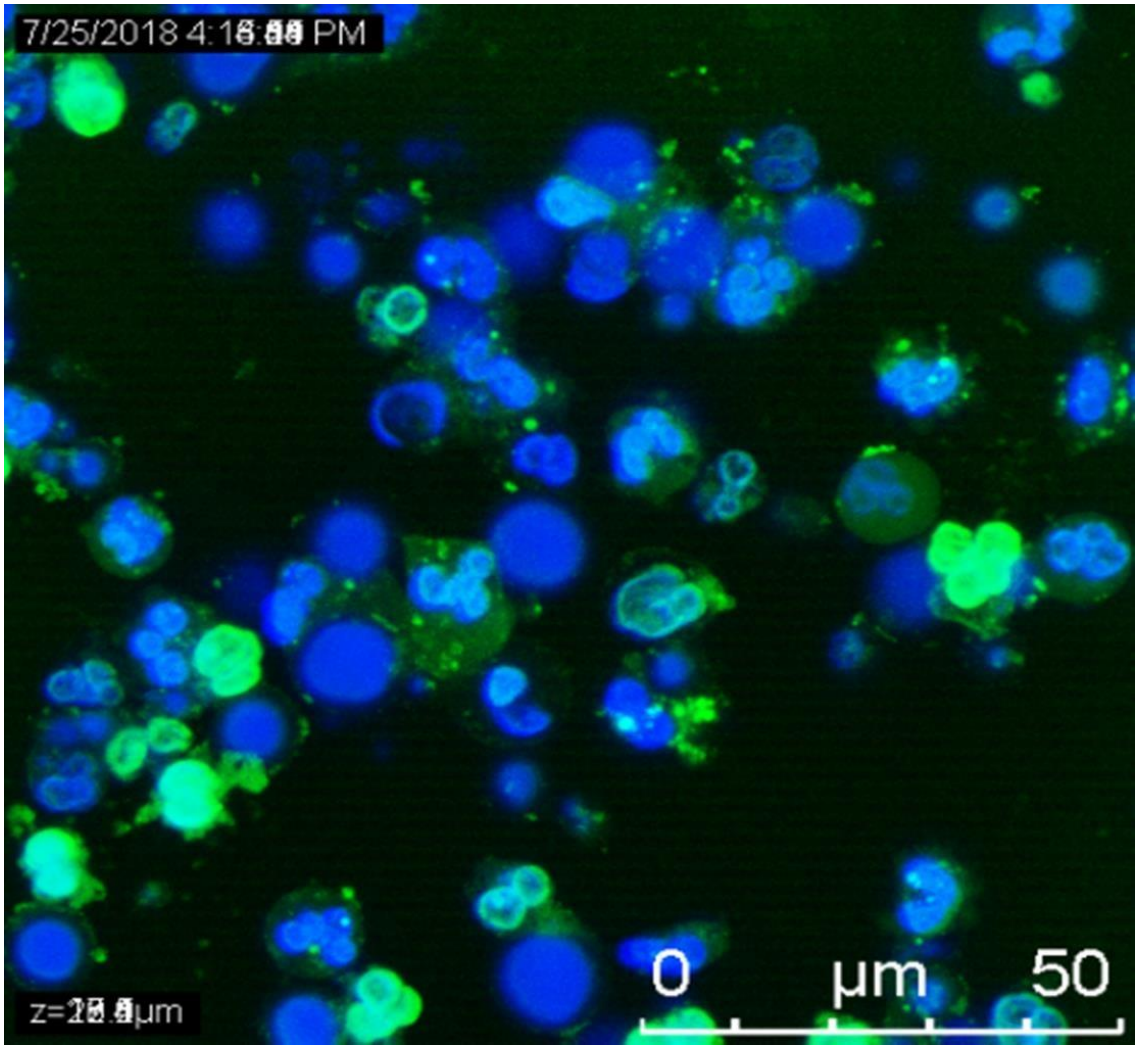


**Figure II-5: Typical image generated by confocal microscopy of neutrophils (blue) taking up pHrodo Green 10,000 Dextran.**

## 15. Scanning electron microscopy

50,000 neutrophils suspended in 50 µL of RPMI-1640 (Thermo Fisher Scientific, Massachusetts, USA) were seeded on poly-l-lysine coated glass coverslips and incubated at 37 degrees C for 20 minutes. Specimens were subsequently fixed with 4 per cent glutaraldehyde (Sigma-Aldrich, Dorset, UK) and 0.1 M calcium chloride (Sigma-Aldrich, Dorset, UK) in 0.1 M sodium cacodylate buffer, pH 7.2 (Sigma-Aldrich, Dorset, UK) for 24 hours and washed in 0.1 M cacodylate for 3 x 10 minutes, followed by post-fixation with 1 per cent OsO4 (Sigma-Aldrich, Dorset, UK) in 0.1 M cacodylate buffer for 1 hour on ice in the dark. Cells were dehydrated using washes with a graded ethanol (Sigma-Aldrich, Dorset, UK) series (30%, 50%, 70%, 85%, 95%, 100%), where each wash consisted of 10 minutes at room temperature. Specimens were dried using a Samdri-795 critical point dryer (Tousimis Research Corp, Rockville, MD) for 45 minutes. Afterwards, the samples were mounted on aluminium stubs, sputter coated with 5 nM of gold in a EMS 575-X sputter coater (Electron Microscopy Sciences, Hatfield, PA), and imaged with a Hitachi S-3400N1 scanning electron microscope at 7.5 kV (Hitachi High Technologies America, Inc., Pleasanton, CA). This technique was developed by [40] and a minimum of ten images per sample were captured.

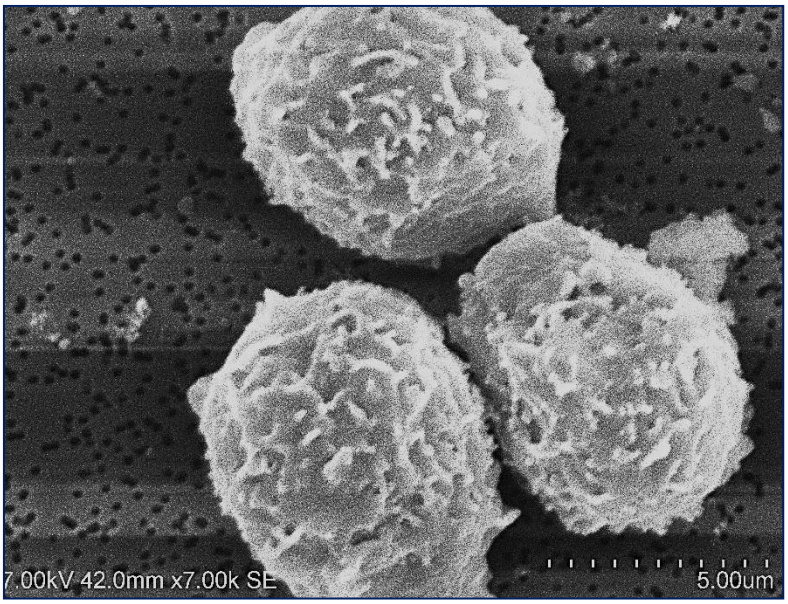


**Figure II-6: Typical image of three healthy and unstimulated neutrophils generated by electron microscopy.**

## 16. Ibidi endothelial flow assay

Human pulmonary microvascular endothelial cells (HMVEC-P) (AngioProteomie, Massachusetts, USA) were grown to 80 per cent confluence on 75 $cm^2$ flasks in endothelial cell growth MV2 medium (AngioProteomie, Massachusetts, USA) with 2 per cent foetal calf serum (FCS) (AngioProteomie, Massachusetts, USA). Endothelial cell growth MV2 medium is commercially produced and contains 10 ng/mL fibroblast growth factor (FGF), 20 ng/mL insulin-like growth factor (Long R3 IGF1), 0.5 ng/mL vascular endothelial growth factor (VEGF), 5 ng/mL epidermal growth factor (EGF), 1 µg/mL ascorbic acid, and 0.2 µg/mL hydrocortisone. The cells were lifted off the flasks using 6 mL of TrypLE (Thermo Fisher Scientific, Massachusetts, USA) for 3 minutes, neutralized with 12 mL of medium. The cells were spun at 260g for 3 minutes, and the supernatant removed, before being re-suspended in medium at 1 million/mL. 120 µL of cell suspension was transferred to Ibidi® µ-slide VI 0.4 chambers (Ibidi, Wisconsin, USA) and grown to confluence overnight at 37 degrees C in 5 per cent $CO_2$. Human neutrophils were isolated as defined above and suspended in PBS+/+ at 1 million cells per mL. Where indicated, endothelial cells were activated with 0.4 ng/mL of IFNγ (R&D Systems, Minneapolis, MN) and 0.4 ng/mL TNFα (R&D Systems, Minneapolis, MN) for 4 hours at 37 degrees C. The confluent endothelial cells were washed for 2 minutes with PBS+/+ at 0.4 mL/minute using an Ibidi pump system (Ibidi, Wisconsin, USA) mimicking the circulatory flow system. Cells were imaged using a DMI6000 inverted widefield microscope (Leica Microsystems, Illinois, USA) using an oil immersion 20X/0.8 numerical aperture objective (Leica Microsystems, Illinois, USA). During the entire experiment, cells were maintained at controlled temperature (37 degrees C) and $CO_2$ (5%). Isolated neutrophils were flowed across the slide surface with confluent endothelial cells for three minutes at 0.4 mL/minute. Time-lapse recordings were captured using a cooled Andor EM-CCD camera driven by the LAS X software (Leica Microsystems, Illinois, USA) at a rate of 56 fps to evaluate neutrophil-endothelial interaction. Images were evaluated manually to determine the percentage of total neutrophils adhering to the endothelial cells under each condition. The step-by-step protocol developed for this assay can be found in the appendices.

**Figure II-7: Frame from a typical movie file of neutrophils (white arrows) flowing across and adhering to endothelial cells.**

## 17. PDMS microvasculature mimetic

To mimic the trafficking of cells in pulmonary vasculature, the microvasculature mimetic (MM) was developed. After conceptualisation, the design was undertaken using L-Edit (Mentor Graphics) with help from the National Institute for Biomedical Imaging and Bioengineering (NIBIB) for four variants of the MM: two branched pyramidal networks without constrictions (constant width of 15 µm and 10 µm) and two single channels with periodic constrictions of 7 and 10 µm (maximum width 15 µm). A polyester photomask of the designs was printed commercially (Fineline Imaging, Colorado, USA). Using the photomask, the master moulds were fabricated by myself with support from a research assistant at NIBIB following standard photolithographic techniques. Briefly, SU-8 2015 (Kayaku Advanced Materials, Westborough, MA) was deposited on silicon wafer substrates using a spin-coater (Laurell Technologies, North Wales, PA), pre-baked, patterned using the masks and a collimated light source (OAI Instruments, Milpitas, CA), post-exposure baked, and developed. To increase durability, the master moulds were hard baked at 150 degrees C for two minutes, after which they were treated with a vapor of (tridecafluoro-1,1,2,2-tetrahydrooctyl)-1-trichlorosilane (UCT Specialties, Bristol, PA) in a vacuum desiccator for one hour. For soft lithography, PDMS (Sylgard 184, Dow Corning, Michigan, USA) was combined in a 10:1 w/w ratio of base to curing agent in a planetary mixer (THINKY, Laguna Hills, CA), then poured onto the master moulds, briefly degassed under vacuum, and baked for 45 minutes at 80 degrees C. After demoulding the cured PDMS and cutting out the device, inlet and outlet holes were punched (Acuderm, 1.5 mm punch). The PDMS devices were cleaned with tape in a HEPA filtered hood and bonded to glass cover slips using oxygen plasma (PE-100, Plasma Etch, USA).

Using one microfluidic device at a time for experiments, I connected the inlet and outlet to a microfluidic pressure control unit (Flow-EZ, Fluigent, Massachusetts, USA) using polyethylene tubing (Scientific Commodities, Lake Havasu AZ), such that less than 500 µL of cell suspension was introduced for each experiment. Cells were suspended in PBS at $3.33\times10^5$ cells/mL and flowed through the microchannels using constant driving pressures within the physiological range (25, 50, and 100 mbar). For imaging, the device was mounted on a DMI6000 inverted widefield microscope (Leica Microsystems, Illinois, USA) with a dry 10X/0.45NA (Leica Microsystems, Illinois, USA) objective for measuring the transit time through the entire device.

During the entire experiment, cells were maintained at controlled temperature (37 degrees C) and $CO_2$ (5%). Time-lapse recordings were captured using a cooled Andor EM-CCD camera driven by the LAS X software (Leica Microsystems, Illinois, USA) at a rate of 56 fps. Transit times for a minimum of 50 neutrophils per sample were extracted manually from the videos by me. Devices were developed based on previous method performed by [38]. Trypan blue was used to stain cells pre-entry to the MM and post-exit from the MM to assess cell viability. The step-by-step protocol developed for performing this assay can be found in the appendices.

For experiments conducted using the MM, both normal and low density neutrophils were isolated from either healthy volunteers or patients with SLE as described previously. Some healthy neutrophils were incubated with 100nM fMLF, 0.1 µM cytochalasin D (Sigma-Aldrich, Missouri, USA), or an equivalent volume of vehicle control DMSO for 20 minutes at 37 degrees C before being passed through the MM.

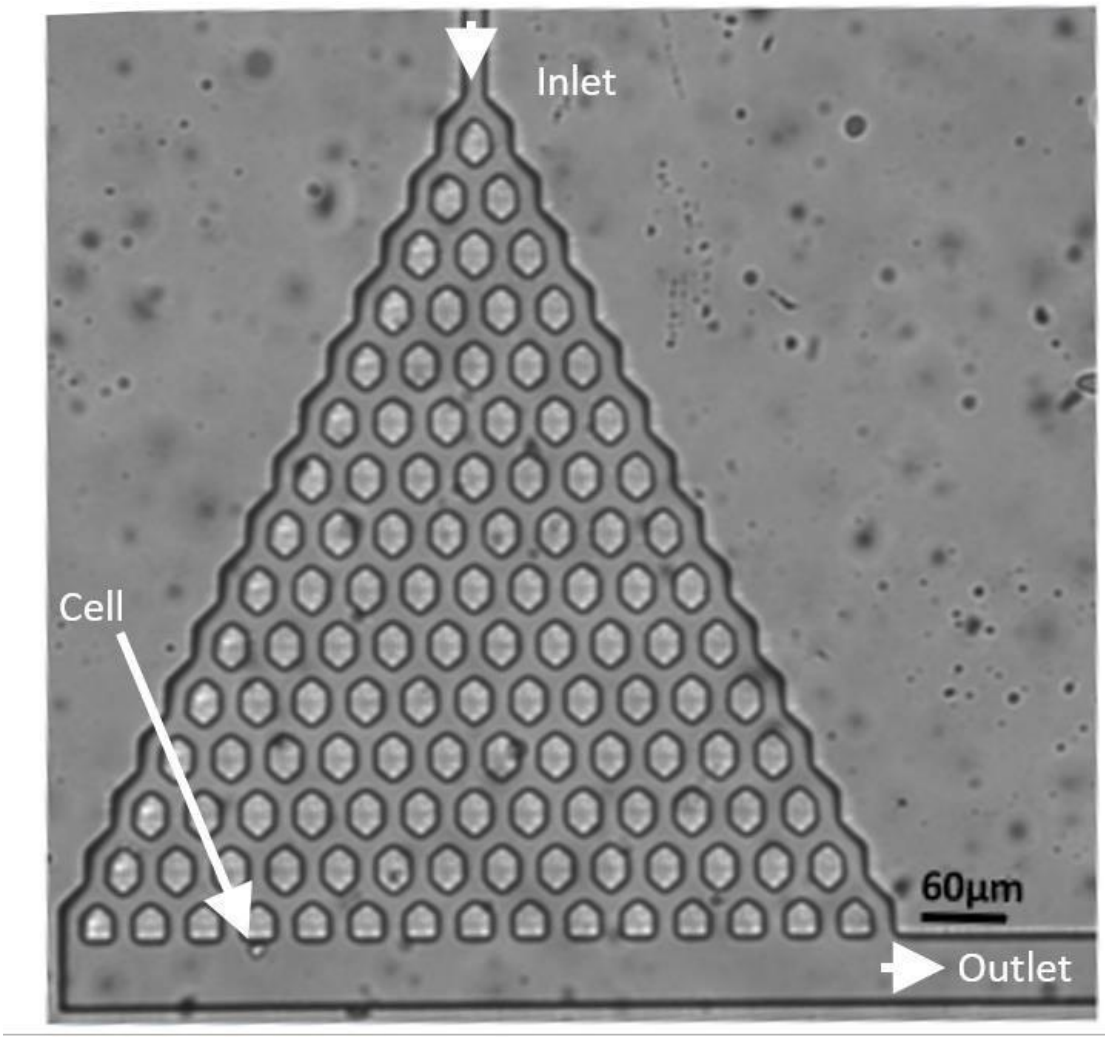


**Figure II-8: Frame from a typical movie file of the MM. White arrows signify the inlet and the outlet of the MM, as well as a neutrophil which has recently finished navigating the mimetic.**

## 18. Brightfield and lattice light-sheet fluorescence microscopy

Neutrophils were suspended in Hank's Buffered Salt Solution with 25mM N-(2-Hydroxyethyl)piperazine-N'-(2-ethanesulfonic acid) (HEPES) (Thermo Fisher Scientific, Massachusetts, USA), at a concentration of 1 million cells/mL. 200 µL of cell solution was aliquoted into an 8-well glass chamber slide (Ibidi, WI, USA). Cells were concomitantly stained with 167 nM SYTOX green (Thermo Fisher Scientific, Massachusetts, USA) and 500 nM of SiR-Actin (Spirochrome, Colorado, USA) for 30 minutes at 37 degrees C and 5 per cent $CO_2$. Brightfield and fluorescence live recordings of actin changes in response to priming with 100 nM fMLF or 25 nM PMA (Sigma-Aldrich, Missouri, USA) were acquired using a Zeiss lattice light-sheet 7 inverted

microscope equipped with a Plan-Apo 48X/1.0NA detection objective, a cooled PCO.edges CMOS camera and driven by the Zen Blue 3.1 software (Zeiss, California, USA). Brightfield images were obtained by illumination of samples with white LED light. For fluorescence acquisition, a 650 nm-waist light sheet was employed. Image volumes were acquired with a lateral translation of 0.2 µm, and the 488 nm and 640 nm laser lines were used for SYTOX green and SiR-Actin (shown in red), respectively. Time-lapse recordings were acquired in dithering mode and then deconvolved in the processing module of the Zen Blue 3.1 software applying the "Constrain Iterative" algorithm. Data were then transformed ("deskewed") to achieve a conventional x, y, z visualisation and exported as .CZI files. Finally, data were imported into IMARIS 9.5.1 software (Bitplane, Connecticut, USA) for processing. Neutrophils were visually inspected to compare morphologies.

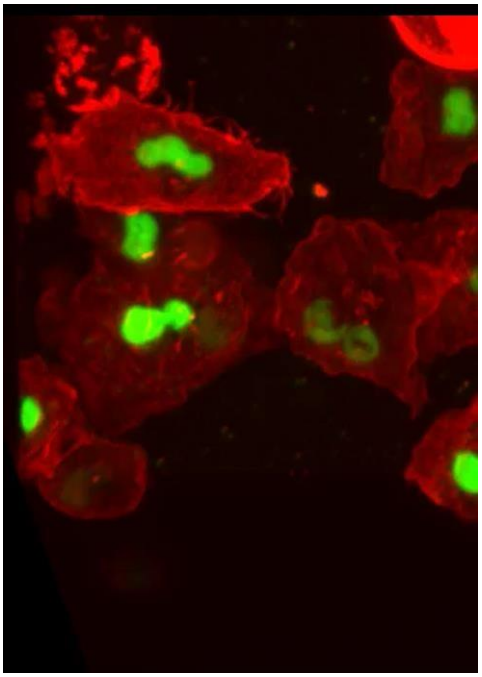

**Figure II-9: Frame from a typical movie file generated using the lattice light sheet microscope. Neutrophils are stained with SYTOX green and SiR-actin.**

## 19. Proteomic and phosphoproteomic studies

The proteomics workflow is outlined in Figure II-10.

### 19.1 Preparation of lysates for proteomics

NDNs and LDGs were isolated from patients with SLE and age/sex-matched healthy volunteers. Isolated neutrophils were resuspended at 10 million/mL in PBS and rested for 25 minutes at 37 degrees C with or without 100 nM fMLF. These four conditions (SLE NDNs, SLE LDGs, healthy

NDNs and primed healthy NDNs were the four subsets of neutrophils analysed by proteomics. In an optimal world, I would have also analysed healthy LDGs, however I needed a minimum of 40 µg of protein from each neutrophil sample. The low percentage of LDGs found in healthy volunteers meant that it would have been unethical to attempt to draw sufficient blood to obtain sufficient number of healthy LDGs for subsequent proteomics analysis. This is a caveat of this study. In place of healthy LDGs, I used primed healthy NDNs which I demonstrate in chapter IV to be another subset of healthy neutrophils that can present as low density. Ideally, I would have also completed proteomics analysis on primed SLE NDNs. However, the nature of 11-TMT labelling proteomics experiments is such that 10 samples can be directly compared to each other most easily. Completing two sets of 10 samples allowed me to directly compare the proteomes of both LDGs and NDNs from five independent donors with SLE while also directly comparing the proteomes of un-stimulated and primed healthy neutrophils from five independent healthy donors. More discussion on the benefits and caveats of this experimental design can be found in Chapters VI and VII.

Following isolation of these neutrophils, samples were centrifuged at 400g for 5 minutes at 4 degrees C, supernatants were aspirated, and cell pellets were snap frozen in liquid nitrogen. Ice cold lysis buffer with 0.5 per cent sodium dodecyl sulphate (SDS) (Sigma-Aldrich, Missouri, USA), 0.1 M tetraethylammonium bromide (TEAB) (Thermo Fisher Scientific, Massachusetts, USA), and 1X HALT protease and phospho-protease inhibitor cocktail (200 µL) (Thermo Fishes Scientific, Massachusetts, USA) was added to each cell pellet and cells were mechanically lysed for 10 minutes. Lysates were centrifuged at 20,000 g for 10 minutes at 4 degrees C, the supernatant was removed, and the protein was stored at -70 degrees C. Protein integrity was assessed by SDS-polyacrylamide gel electrophoresis (PAGE) and colloidal blue staining (Thermo Fisher Scientific, Massachusetts, USA).

## 19.2 SDS-polyacrylamide gel electrophoresis (SDS-PAGE)

Lysate protein concentration was determined by bicinchoninic acid assay (Bio-Rad, California, USA). Proteins were reduced by heating to 90 degrees C for 5 minutes in the presence of β-mercaptoethanol (βME) (Sigma-Aldrich, Missouri, USA). Protein (15 µg) or a pre-stained protein ladder (PageRuler™ Plus) (Thermo Fisher Scientific, Massachusetts, USA) was loaded into each well of a 12 per cent pre-cast SDS NuPAGE™ Bis-Tris gel (Thermo Fisher Scientific, Massachusetts, USA) and run according to the manufacturer's instructions.

## 19.3 Colloidal blue staining of SDS-PAGE gel

SDS-PAGE gels were stained with colloidal blue stain (Thermo Fisher Scientific, Massachusetts, USA) for three hours, then washed for >12 hours in deionized water. Gels were photographed to assess protein degradation.

## 19.5 11-plex TMT labelling

Alongside a staff member in the proteomics core of the National Heart, Lung, and Blood Institutes, I performed the following labelling process. Approximately, 40 µg of protein per sample and internal standard (pooled equivalent amounts of each sample) were reduced in 5 mM Tris(2-carboxyethyl)phosphine (TCEP) (Sigma-Aldrich, Missouri, USA) for one hour at 55 degrees C, which was followed by alkylation of cysteines with 18 mM iodoacetamide (Sigma-Aldrich, Missouri, USA) for 30 minutes in the dark, at room temperature. Six volumes of chilled acetone were added, and precipitation proceeded overnight. Lysates were resuspended in 0.1 M TEAB (Thermo Fisher Scientific, Massachusetts, USA) before trypsin (Thermo Fisher Scientific, Massachusetts, USA) was added at a 1:40 trypsin:protein ratio by mass. Digestion was carried out overnight at 37 degrees C. Tandem mass tag (TMT) reagents (0.4 mg) were reconstituted in 41 µL anhydrous acetonitrile and peptide samples were labelled according to the manufacturer's instructions (Thermo Fisher Scientific, Massachusetts, USA). Following incubation at room temperature for one hour, the reaction was quenched with hydroxylamine to a final concentration of 5 per cent (v/v) for 15 minutes at room temperature. The TMT-labelled samples including internal standard were pooled across the 11 samples for each TMT set (patient, healthy volunteer). Pooled TMT sample sets were concentrated and desalted using Oasis HLB 1 cc cartridge (Waters, Massachusetts, USA). The pooled samples were vacuum centrifuged to dryness and subjected to basic pH reversed-phase (bRP) fractionation.

## 19.4 Label-free proteomics

Alongside a staff member in the proteomics core of the National Heart, Lung, and Blood Institutes, I performed the following process. Approximately 100 µg of protein per sample were reduced in 5 mM Tris(2-carboxyethyl)phosphine (TCEP) (Sigma-Aldrich, Missouri, USA) for one hour at 55 degrees C, which was followed by alkylation of cysteines with 18 mM iodoacetamide (Sigma-Aldrich, Missouri, USA) for 30 minutes in the dark at room temperature. Lysates were resuspended in 0.1 M TEAB (Thermo Fisher Scientific, Massachusetts, USA) before trypsin (Thermo Fisher Scientific, Massachusetts, USA) was added at a 1:40 trypsin:protein ratio by mass. Digestion was carried out overnight at 37 degrees C. Samples were concentrated and desalted using Oasis HLB 1 cc cartridge (Waters, Massachusetts, USA). Mass spectrometry was undertaken as described in section 18.8. Raw data files were subsequently processed using Proteome Discoverer (v2.3, Thermo Fisher Scientific, Massachusetts, USA), using Sequest HT (Thermo Fisher Scientific, Massachusetts, USA) search node. All searches were performed against UniProt Knowledgebase protein database [133] with the selected taxonomy Homo sapiens. Search modifications used were as follows; (fixed) carbamidomethyl of cysteine, (variable) oxidation of methionine, deamidation (NQ) and acetyl on protein N-terminus. For MS2, the precursor and fragment ion tolerances of 10 ppm and 0.02 Da were applied, respectively. Up to two-missed tryptic cleavages were permitted. Percolator was used to calculate the false discovery rate (FDR) of peptide spectrum matches, set to

a p-value of 0.05 [134]. Relative protein quantification of the proteins identified in the three groups were performed using the precursor ion quantifier node Minora algorithm in Proteome Discoverer. Minora uses the chromatographic profiles of individual features or peaks in calculating the area under the curve label-free quantification. The intensity measurements of peptides assigned to each protein were summed and these values were normalized so that the sum of the signal for all proteins in each sample was equivalent to account for equal protein loading. Protein ratios were calculated as the median of all possible pairwise peptide ratios calculated between replicates of all connected peptides. In Microsoft EXCEL, identified proteins were aligned with the gene transcripts identified in an RNA-Seq data set, generously shared by Dr. Luis Franco of the National Institutes of Health.

## 19.6 Offline reversed-phase fractionation

For each TMT set, high pH reversed-phase liquid chromatography was performed on an offline Agilent 1200 series HPLC (Agilent, California, USA). Approximately, 0.44 mg of desalted peptides from each set were resuspended in 0.1 mL 10 mM TEAB (Thermo Fisher Scientific, Massachusetts, USA) with 2 per cent (v/v) acetonitrile (Sigma-Aldrich, Missouri, USA). Peptides were loaded onto an Xbridge $C_{18}$ HPLC column (Waters, Massachusetts, USA; 2.1 mm inner diameter x 100 mm, 5 µm particle size), and profiled with a linear gradient of 5–35 per cent bufferB (90% acetonitrile, 10 mM TEAB) over 60 minutes, at a flowrate of 0.25 mL/minute. The chromatographic performance was monitored by sampling the eluate with a diode array detector (1200 series HPLC, Agilent, California, USA) scanning between wavelengths of 200 and 400 nm.Fractions were collected at one minute intervals followed by fraction concatenation [135]. 15 per cent (v/v) of each of the 12 concatenated fractions were separated into a new tube dried and resuspended in 0.01 per cent formic acid, 2 per cent acetonitrile for full proteome analysis. Approximately 500 ng of peptide fraction mixture was loaded per liquid chromatography-mass spectrometry run. The remaining volume in each fraction was subjected to phosphopeptide enrichment.

## 19.7 Phosphoprotein enrichment

The initial 12 fractions were combined into six fractions and sequential metal oxide affinity chromatography (SMOAC) phosphopeptide enrichment was performed. Briefly, TMT labelled tryptic digest was subjected to the High-Select TiO2 Phosphopeptide Enrichment kit according to manufacturer's protocol (Thermo Fisher Scientific, Massachusetts, USA). The TiO2 eluent was saved for mass spectrometry (MS) analysis. The TiO2 flow through and wash fractions were pooled, and the phosphopeptides were enriched using the High-Select Fe-NTA Phosphopeptide Enrichment kit according to manufacturer's protocol (Thermo Fisher Scientific, Massachusetts, USA), eluent was saved for MS analysis.

## 19.8 Mass spectrometry

All fractions were analysed on an Ultimate 3000-nLC coupled to an Orbitrap Fusion Lumos Tribrid

instrument (Thermo Fisher Scientific Massachusetts, USA) equipped with a nano-electrospray source. Peptides were separated on an EASY-Spray $C_{18}$ column (75 µm x 50 cm inner diameter, 2 µm particle size and 100 Å pore size, Thermo Fisher Scientific Massachusetts, USA). Peptide fractions were placed in an autosampler and separation was achieved by 120-minute gradient from 4-32 per cent buffer B (100% ACN and 0.1% formic acid) at a flow rate of 300 nL/minute. An electrospray voltage of 1.9 kV was applied to the eluent via the EASY-Spray column electrode. The Lumos was operated in positive ion data-dependent mode, using Synchronous Precursor Selection (SPS-MS3) [136]. Full scan MS1 was performed in the Orbitrap with a precursor selection range of 375–1,275 m/z at nominal resolution of 1.2 x 105. The AGC target and maximumaccumulation time settings were set to 4 x 105 and 50 ms, respectively. The top ten precursors werethen selected for MS2/MS3 analysis. MS2 was triggered by selecting the most intense precursor ions above an intensity threshold of 5 x 104 for collision induced dissociation (CID)-MS2fragmentation with an AGC target and maximum accumulation time settings of 1 x 104 and 90 ms,respectively. Mass filtering was performed by the quadrupole with 0.7 m/z transmission window, followed by CID fragmentation in the linear ion trap with 35 per cent normalized collision energy in rapid scan mode and parallelizable time option was selected. SPS was applied to co-select 10 fragment ions for HCD-MS3 analysis. SPS ions were all selected within the 400–1,200 m/z rangeand were set to preclude selection of the precursor ion and TMTC ion series [137]. The AGC target and maximum accumulation time were set to 1 x 105 and 150 ms (respectively) and parallelizable time option was selected. Co-selected precursors for SPS-MS3 underwent HCD fragmentation with 65 per cent normalized collision energy and were analysed in the Orbitrap with nominal resolution of 5 x 104.

## 20. Proteomics Analysis

Raw data files were processed using Proteome Discoverer (v2.4, Thermo Fisher Scientific, Massachusetts, USA), with Sequest HT (Thermo Fisher Scientific, Massachusetts, USA) search node. All peak lists were searched against the UniProtKB/Swiss-Prot protein database released 2019_11 with *Homo sapiens* taxonomy (20,316 sequences) [133] and concatenated with reversed copies of all sequences. The following search parameters were set with fixed modifications: carbamidomethylation of Cys, TMT 11-plex modification of lysines and peptide N-terminus, and variable modification of methionine oxidation. For SPS-MS3 the precursor and fragment ion tolerances were set to 10 ppm and 0.6 Da, respectively. Up to two-missed tryptic cleavages were permitted. Percolator algorithm (v.3.02.1, University of Washington, Washington, USA) was used to calculate the false discovery rate (FDR) of peptide spectrum matches (PSM), set to a q-value <0.05 [134, 138-140]. These conditions were decided upon by the scientists at the proteomics core of the NHLBI who assisted me with these experiments.

Proteins were quantified by summing reporter ion counts across all matching PSMs, also as

described previously [141]. Reporter ion intensities were adjusted to correct for the isotopic impurities of the different TMT reagents according to manufacturer specifications. The signal-to-noise (S/N) measurements of peptides assigned to each protein were summed and these values were normalized so that the sum of the signal for all proteins in each channel was equivalent to account for equal protein loading. Finally, each protein abundance measurement was scaled to internal standard channels to reduce multi-batch variability [142]. The p-values were calculated for the reported quantitative ratios using ANOVA testing.

Data from the phosphopeptide enrichment were processed and quantified similarly except an additional variable modification of phosphate on serine, threonine, and tyrosine residues was included as a Sequest search parameter. Quantitative values were based at the peptide group level for site specific phosphorylation quantitation. For more detail into the proteomics method used, see [143]. Following this data analysis, I independently performed network mapping as described below.

### 20.1 Network mapping

Network mapping to GO biological processes (i.e. GO biological enrichment analysis) was undertaken using opensource software ShinyGo [144] and the online platform MetaScape [145]. Proteins upregulated with an abundance ratio of >1.5 or downregulated with an abundance ratio of <0.5 in four of the five matched samples were included in network mappings to account for individual variation. For phosphoproteomics, proteins with differential phosphorylation at a given phospho-site in at least 4/5 matched samples were included. False discovery rate (FDR) was used to rank enriched networks based on significance. Heatmaps were generated in GraphPad Prism (GraphPad Software, California, USA).

## 21. Statistical Analysis

Graphs were generated in GraphPad Prism (GraphPad Software, California, USA) and are indicative of at least three individual experiments. Mean ± SEM was plotted. Statistical tests were performed in GraphPad Prism as described in each figure legend. One, two, or three asterisks denote significance levels $p<0.05$, $p<0.01$, and $p<0.001$, respectively.

For each sample analysed by RT-DC, the median measurement of over 500 cells was plotted as an individual point. Those median values were analysed with statistical tests and the mean ± SEM of the median measurements for each condition is depicted.

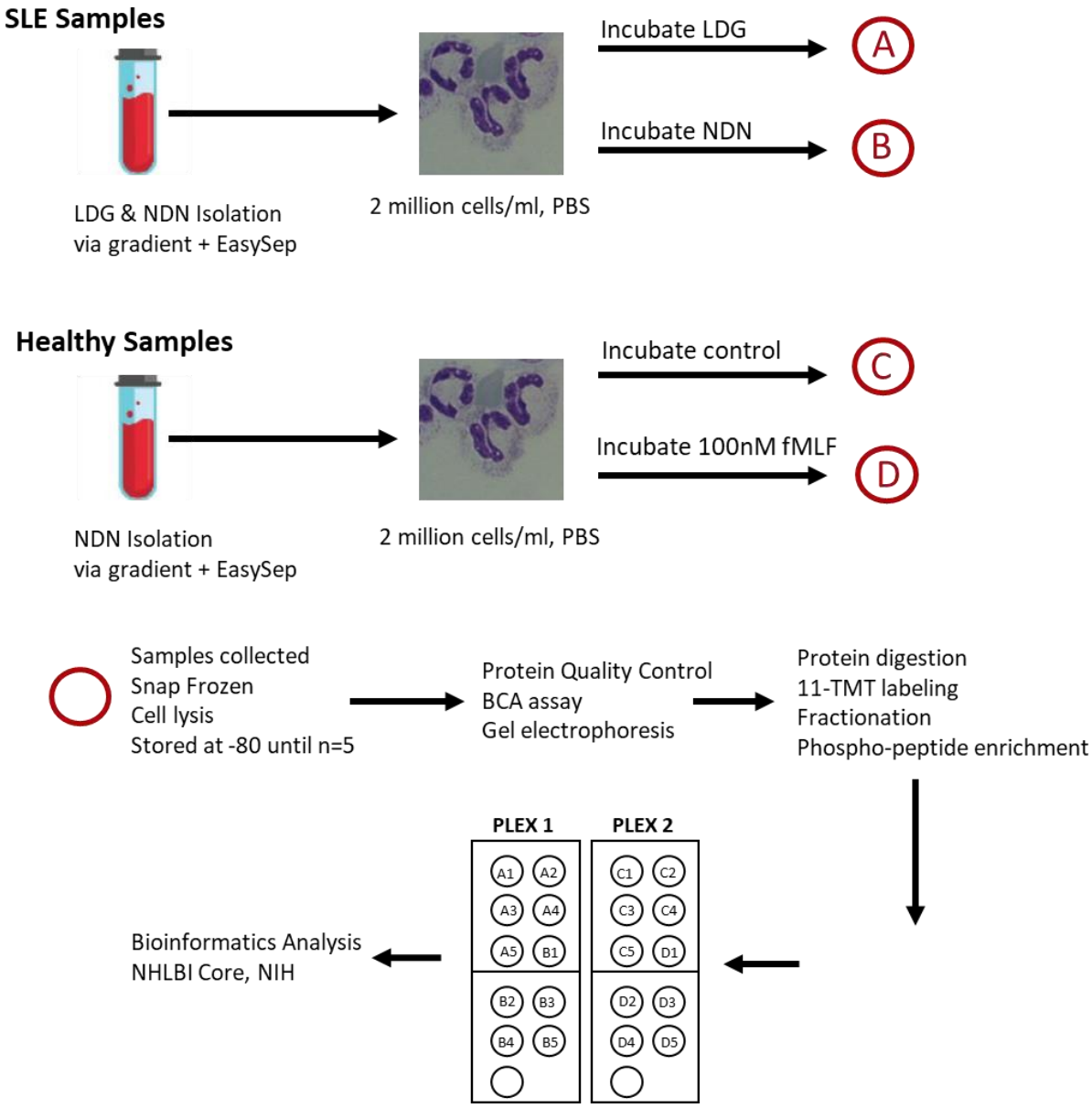


**Figure II-10: Proteomics and phosphoproteomics experimental work-flow**

# Chapter III: Optimisation of RT-DC for mechanical phenotyping of healthy neutrophils

## 1. Chapter Introduction

Given that RT-DC was introduced one year prior to the beginning of my PhD [82], optimisation experiments were required to ensure biomechanical phenotyping of neutrophils was precise and consistent. Collaborators shared with us data, unpublished at the time, demonstrating RT-DC could be used to identify major immune cell subtypes in blood based on size and intracellular brightness [121]. However, neutrophil biomechanical properties post-isolation had not yet been analysed using RT-DC.

In the literature, there is no consensus on the optimal neutrophil isolation technique for functional studies. Various isolation strategies resulting in similar neutrophils yields and purities have been described [29, 146, 147], but comparative studies report variation in the functional activity of neutrophils isolated via different methods [148, 149]. Given the sensitivity of neutrophils to isolation, it seemed that evaluating neutrophil biomechanical attributes *in vitro* could lead to difficulties in extrapolating the relevance of these biomechanical properties *in vivo*.

The work in this chapter established and validated use of RT-DC in the analysis of neutrophil mechanical properties, both in whole blood and following cell purification. Baseline biomechanical properties for a healthy neutrophil were established and it was determined that these properties do not vary significantly with age or sex. An isolation method and recovery protocol to yield purified neutrophils biomechanically indistinct from their whole blood counterparts was optimised and subsequently used in experiments detailed in the later chapters of this thesis. Finally, blood from patients with grey platelet syndrome (GPS), a condition characterised by abnormally large platelets [150], was investigated as a positive control. This allowed for early confirmation of RT-DC's ability to identify differences in immune cell biomechanical phenotypes associated with disease, prior to recruiting patients with SLE as described in Chapter V.

## 2. Hypothesis and Aims

*RT-DC can be used to consistently and accurately measure biomechanical properties of neutrophils both in whole blood and in isolated, cell purified populations.*

- To replicate previous work by *Otto et. al.*[82] establishing that RT-DC yields consistent and replicable results.
- To identify baseline parameters of neutrophil deformability, area, and area ratio by RT-DC.
- To determine whether neutrophil biomechanical properties vary based on age or sex.
- To assess the effect of time post-venepuncture on neutrophil biomechanical properties in the interest of optimising future experiments.
- To establish optimal protocols for neutrophil and LDG isolation yielding pure, undisrupted neutrophils.
- To affirm RT-DC can identify known biomechanical differences in immune cells in the context of disease.

## 3. Method Notes

Methods for optimal use of RT-DC were developed in an iterative process described in this chapter. Final methods for RT-DC and generation of the figures presented in this chapter are described in Chapter II. The full protocols for neutrophil isolation strategies are provided in the Appendices.

## 4. Results:

### 4.1 Verifying RT-DC consistency in measurements

I first attempted to replicate the work of Otto *et. al.* [82] and Toepfner *et. al.* [121] to determine whether RT-DC could precisely and consistently determine the biomechanical properties of cells. I analysed whole blood neutrophils by RT-DC to establish whether the technique was replicable and consistent. I also validated the data analysis pathway by replicating the analysis of the same data files gathered during RT-DC to ensure the off-line analysis methods were replicable and consistent. Figure III-1 showsthat consistent measurements were obtained.

## 4.2 Neutrophil mechanical properties across sex and age

Prior to my work, little mechanical phenotyping of neutrophils had been undertaken so it was important to determine whether variation existed in the healthy human population. I compared neutrophils in the whole blood of heathy males and females and determined that no differences in neutrophil biomechanical phenotype exist between sexes. I also compared neutrophils in the whole blood of subjects of different ages, and similarly did not identify any biomechanical differences (Figure III-2). Although these data suggest that age and sex-matching of samples for subsequent experiments was not required, I continued to use age and sex-matched donors whenever possible, and certainly for all studies comparing neutrophils in health and disease.

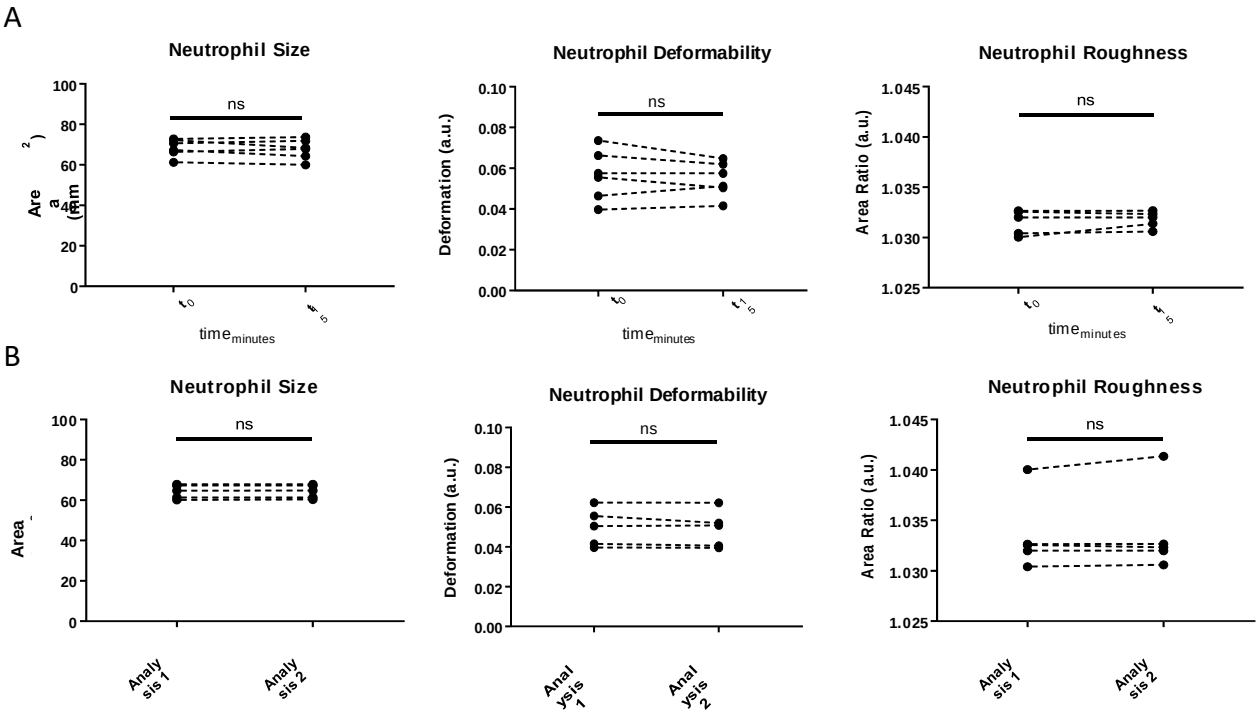


**Figure III-1: RT-DC consistently determines the biomechanical properties of neutrophils in blood.**

(A) RT-DC was performed twice on each individual blood sample (n=5), at 0 minutes and 15 minutes post-venipuncture. The median value of over 500 neutrophils was plotted for each sample measurement. Significance was tested by Mann-Whitney U tests. (B) Analysis was performed on the same RT-DC data files twice. This was repeated for n=5 data files. The median value of over 500 neutrophils was plotted for each analysis. Significance was assessed by Mann-Whitney U-test. $p>0.05$ = ns.

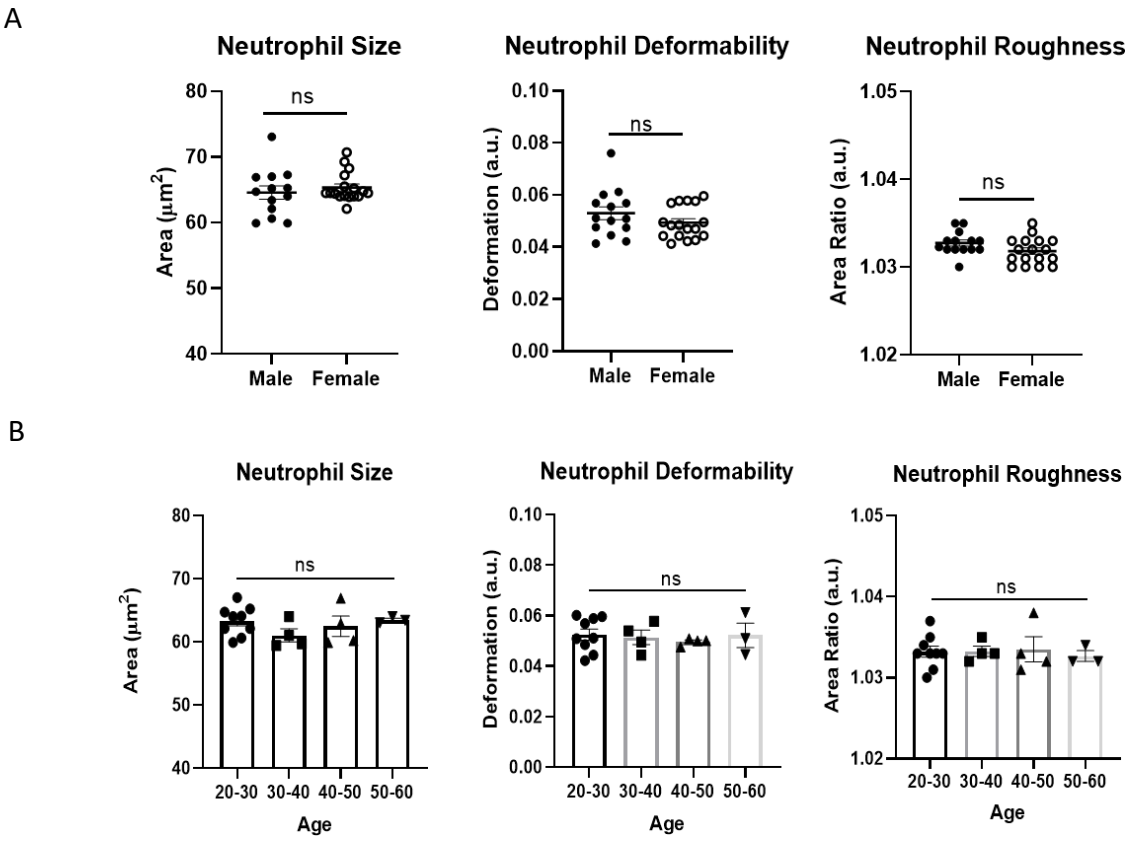


**Figure III-2: Neutrophil biomechanical phenotype does not vary with sex or age.**

(A) RT-DC was used to biomechanically phenotype whole blood neutrophils of age-matched, healthy males and females. The median value of over 500 neutrophils for each sample was plotted. (B) RT-DC was used to biomechanically phenotype neutrophils in the whole blood of healthy individuals aged 20-60 years. Each data point represents the median value of over 500 neutrophils from a single sample. Significance was assessed by Mann-U-Whitney test (A) or one-way ANOVA (B) and set at $*p<0.05$.

## 4.3 Confirmation that RT-DC identifies mechanical biomarkers: Grey Platelet Syndrome.

Grey Platelet Syndrome (GPS) or platelet alpha-granular deficiency is a rare congenital bleeding disorder occurring in approximately 60 people worldwide. This autosomal recessive disorder is caused by a mutation in NEALB2 and causes megakaryocytes to be unable to package secretory proteins into alpha-vesicles. Alpha granules in platelets are reduced, and GPS is clinically characterised by abnormally large agranular platelets in peripheral blood smears as well as thrombocytopenia [150]. Currently however, there are no automated ways to accurately quantify platelet size. Given the biomechanical phenotype associated with GPS, blood samples from these patients were analysed by RT-DC for two reasons; to determine whether any information critical to our understanding of GPS

would emerge and to confirm that RT-DC can accurately identify biophysical differences in the blood cells of patients with disease.

RT-DC was performed in a blinded manner on peripheral blood collected from patients with GPS or healthy age/sex/ethnicity matched controls to determine whether RT-DC could identify defining biomechanical characteristics of immune cells in the context of health and disease. Larger platelets were successfully identified in blood of patients with GPS, while lymphocytes (not involved in this disorder) were found to be biomechanically indistinct from healthy controls (Figure III-3), consistent with the expected biomechanical manifestations of this disease.

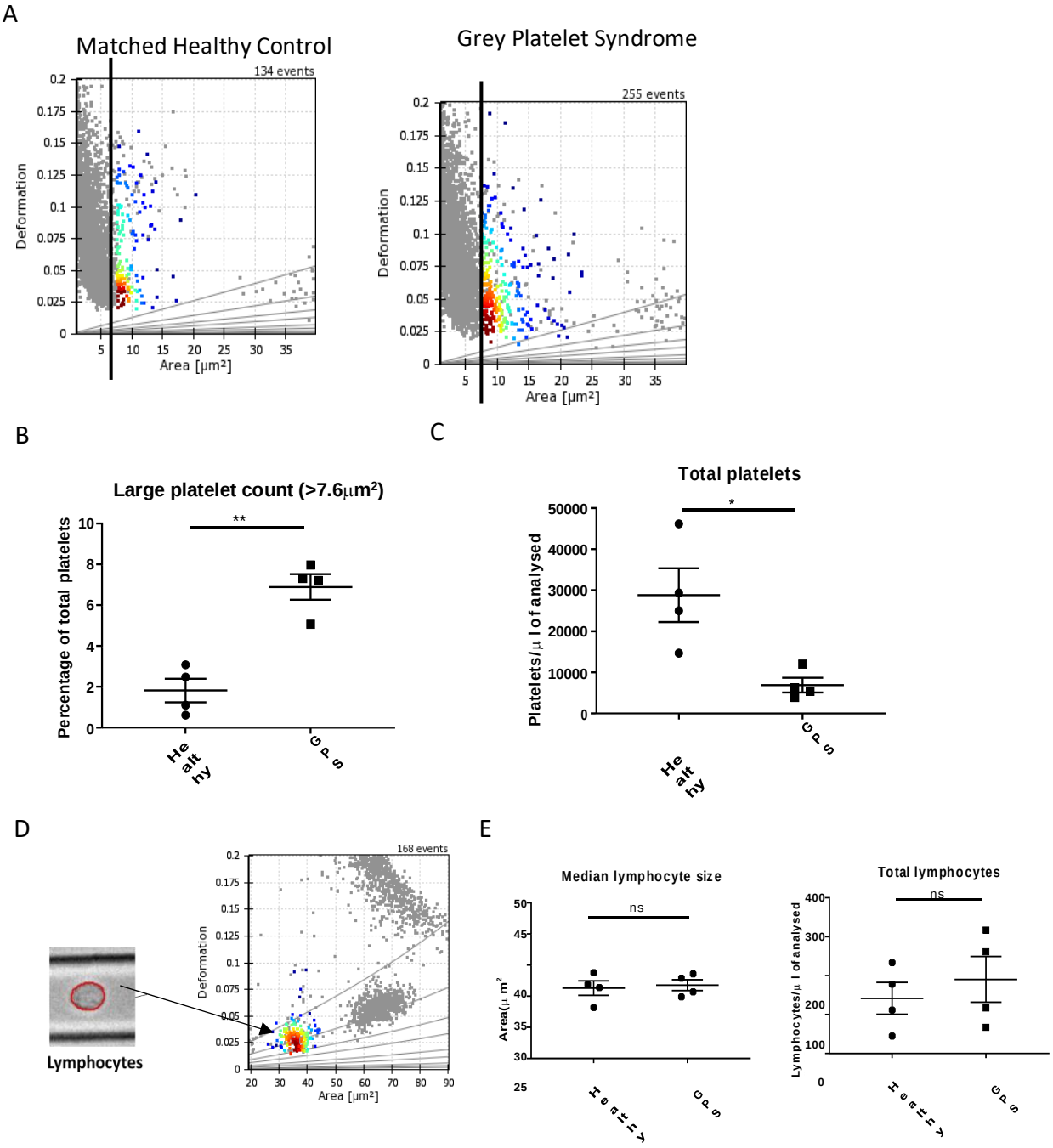


**Figure III-3: RT-DC identified large platelets in patients with GPS.**

(A) RT-DC was performed on the blood of patients with GPS or age/sex/ethnicity-matched healthy controls. Platelets larger than 7.6µm$^2$ were included in the gate for large platelets. 7.6µm$^2$ is two standard deviations larger than the size of the average healthy platelet. (B) GPS platelets have a significantly higher percentage of large platelets and (C) significantly fewer total platelets. (D & E) RT-DC does not identify any biomechanical differences in the lymphocytes of patients with GPS relative to matched healthy volunteers. Samples were compared by Mann-Whitney U-test and significance was set at *$p$<0.05, ns=not significant.

## 4.4 GPS neutrophils are smaller than healthy neutrophils.

NEALB2 is expressed in neutrophils as well as megakaryocytes and platelets [151], and so neutrophils from patients with GPS and healthy subjects were compared. GPS neutrophils were determined to be smaller than healthy neutrophils (Figure III-4C), which was confirmed by flow cytometry undertaken by a collaborator. This was interesting because prior to analysis with RT-DC, this difference between patient with GPS and the healthy population had not been identified.

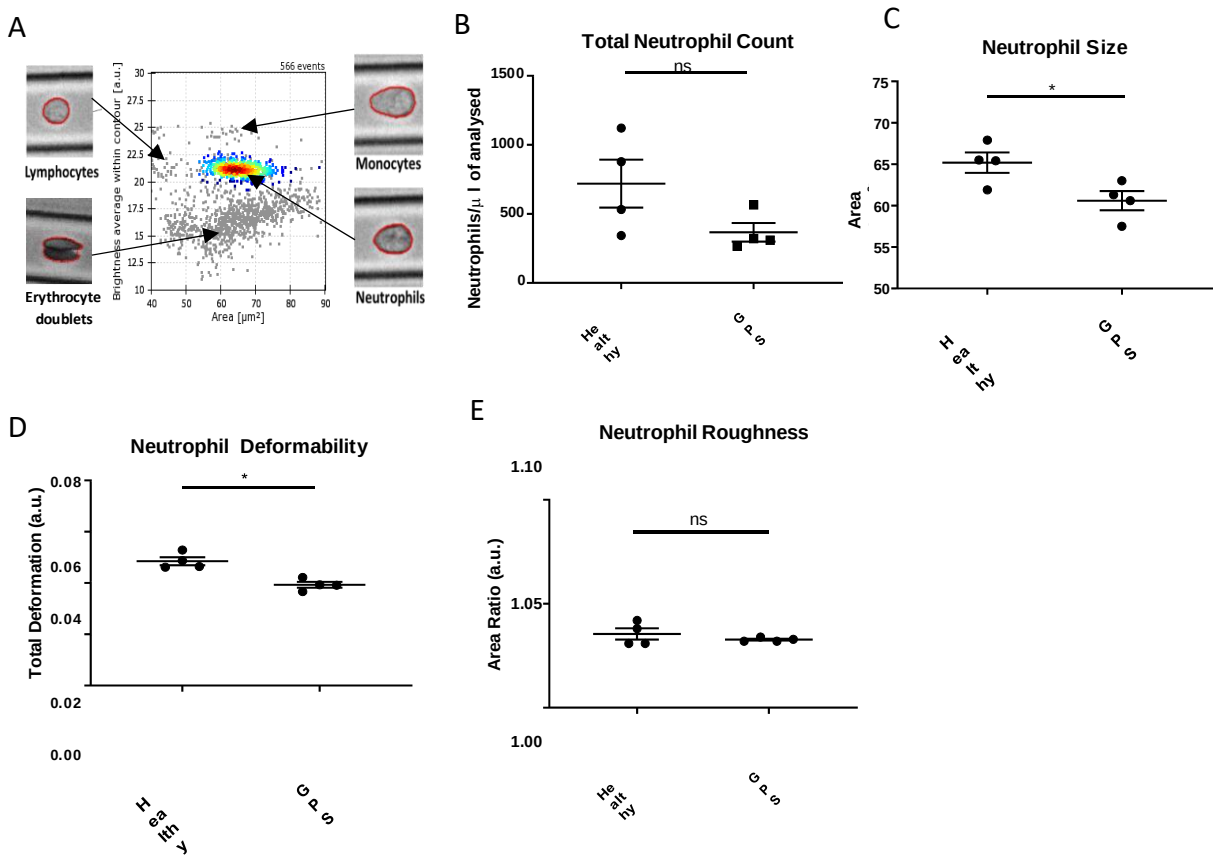


**Figure III-4: RT-DC determines neutrophils from patients with GPS are smaller and less granulated than neutrophils from matched healthy controls.**

(A) RT-DC was performed on the blood of patients with GPS or age/sex/ethnicity-matched healthy controls and neutrophils were gated on. (B) GPS patients and healthy controls do not have significantly different numbers of neutrophils per microliter of blood. GPS neutrophils are significantly (C) smaller and (D) more deformable, but not (E) rougher than healthy neutrophils. Significance was determined by Mann-Whitney U-test and set at *$p$<0.05, ns = not significant.

## 4.5 Impact of time on neutrophil biomechanical properties

Although experiments presented in this thesis were always completed as quickly after venesection as possible, I anticipated that in some instances it would be necessary to treat neutrophils with inhibitors or priming agents to determine their effects on biomechanical properties. As such, I needed to understand the stability of neutrophil biomechanical properties over time. Small aliquots of blood taken from the same donor were stored at 37 degrees C and analysed 0, 1, 2, and 3 hours after venesection. Figure III-5A shows the time from venesection to sample analysis had a significant effect on neutrophil size ($p$<0.05 by one-way ANOVA). Change in neutrophil area over time was plotted to derive an equation to correct for time-induced expansion, but future experiments relied on negative controls to correct for time-induced changes. I also established that blood could be kept for up to one hour at 37 degrees C with no alteration in neutrophil size or deformability (Figure III-3). Accordingly, I designed experiments to be started and completed within this one-hour window whenever possible.

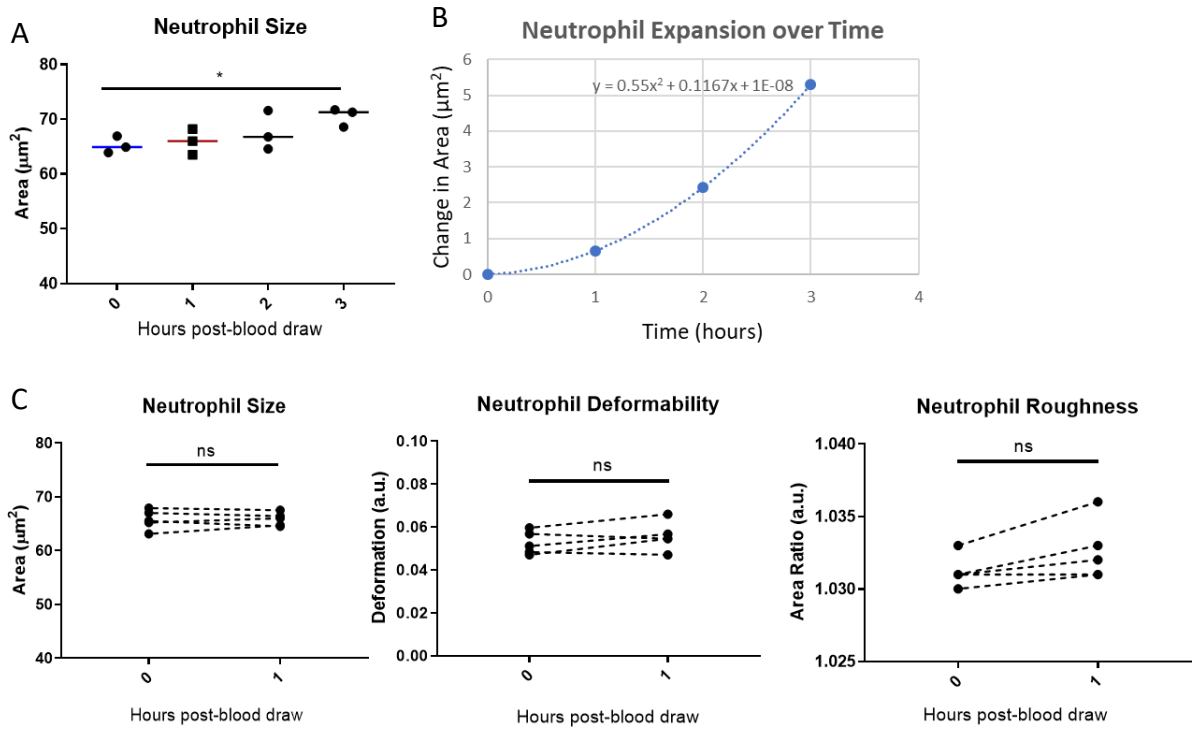


**Figure III-5: Time post-blood draw impacts neutrophil biomechanical properties.**

(A) Blood was drawn from healthy volunteers and kept at 37 degrees C until analysis by RT-DC. At the times indicated, whole blood neutrophils were biomechanically phenotyped using RT-DC. Matched samples were compared by one-way ANOVA. (B) The magnitude of neutrophil expansion over time was calculated and an equation was fitted to the data. (C) Neutrophils in blood drawn from healthy volunteers were analysed by RT-DC immediately after venesection or following an hour of incubation at 37 degrees C. Matched samples are compared by Mann Whitney U-test. Significance was set at *$p$<0.05, $p$>0.05 = ns.

## 4.6 Mechanical impact of purification techniques on neutrophils

Whenever possible, I performed biomechanical phenotyping of neutrophils in whole blood to avoid any isolation-induced alteration of the neutrophils. However, for certain experiments it was necessary to purify neutrophils. Thus, identifying an isolation strategy to minimize alterations in neutrophil biomechanical properties was critical. Whole blood neutrophils were analysed immediately after venesection and following various steps involved in standard neutrophil isolation processes including plasma-Percoll and Ficoll density gradient centrifugations, erythrocyte lysis and magnet-associated cell sorting (MACS). Erythrocyte lysis and MACS negative isolation strategies were particularly disruptive to neutrophil biomechanical properties (Figure III-6A). This finding is particularly interesting and worrisome given wide-spread use of MACS and erythrocyte lysis in neutrophil biology. Although plasma-Percoll and Ficoll density gradients did not disrupt neutrophil biomechanical properties as profoundly as erythrocyte lysis or MACS, neutrophils were less deformable immediately following isolation (Figure III-6B).

## 4.7 Recovering purified neutrophils to their whole blood mechanical phenotype

To avoid isolation-induced effects on neutrophil biomechanical properties during experiments, I identified a strategy to recover neutrophils isolated using discontinuous plasma-Percoll gradient centrifugation to their original mechanical properties. Neutrophils were biomechanically characterised in whole blood and following isolation, after resting the cells in various media (Figure III-7A). PBS with 5 per cent autologous serum partially recovered the whole blood biomechanical phenotype in isolated neutrophils. Next, I determined the optimal incubation length to be 35 minutes (Figure III-7B) and the optimal incubation temperature to be 37 degrees C (Figure III-7C).

## 4.8 Recovered neutrophils are biomechanically identical to their whole blood counterparts

Ultimately, it was established that incubation at 37 degrees C for 35 minutes in PBS containing calcium and magnesium ions (PBS+/+) with 5 per cent autologous serum successfully recovered gradient-isolated neutrophils to their whole blood mechanical phenotype (Figure III-8). Accordingly, neutrophil isolation by density gradient followed by a period of recovery incubation was employed for all subsequent experiments.

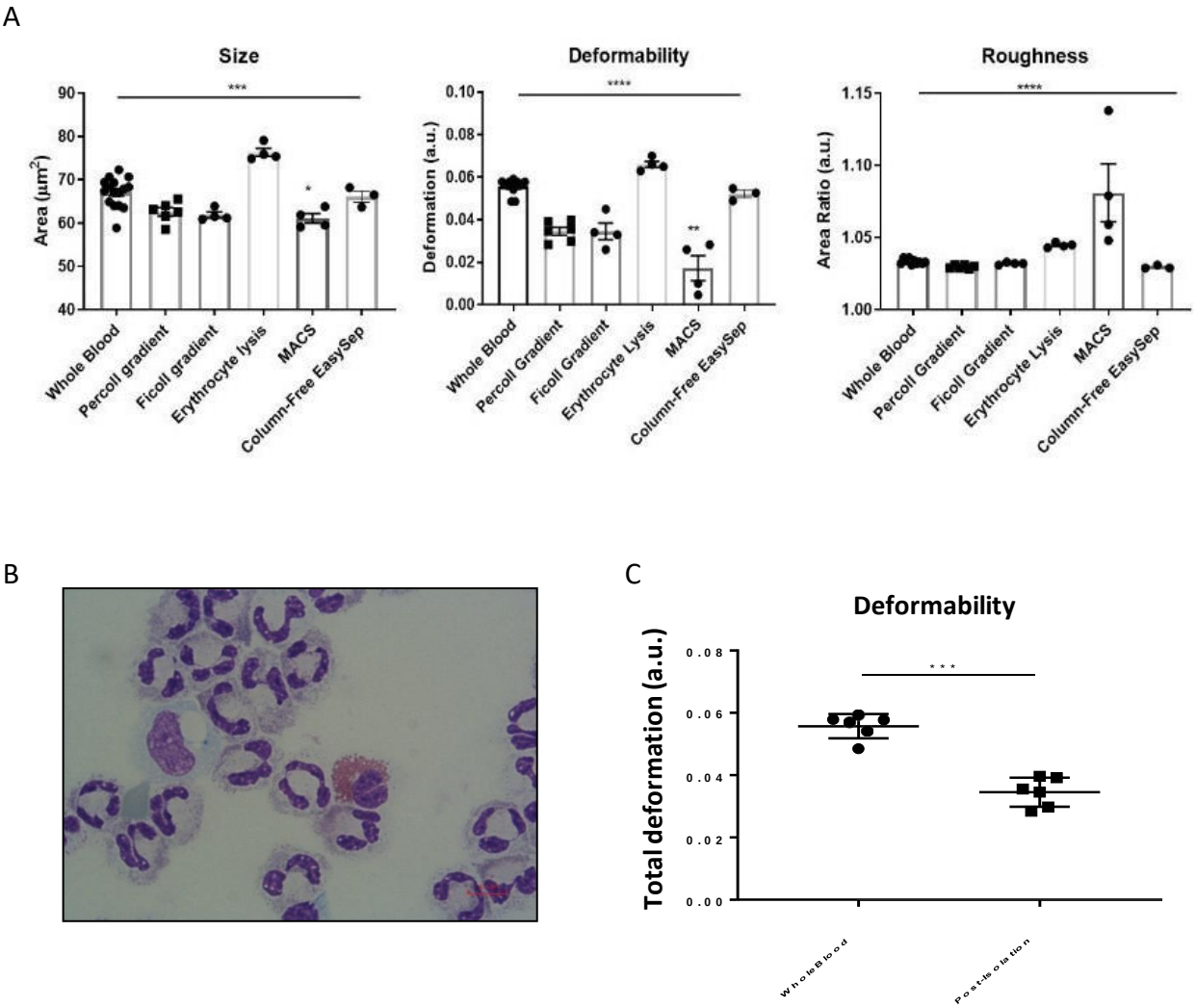


**Figure III-6: Isolation protocols considerably impact neutrophil biomechanical properties.**

(A) Neutrophils were analysed in blood drawn from healthy volunteers and again following standardly used neutrophil isolation protocols. Significance was established by Kruskal-Wallis test with a post hoc Dunn's test to compare isolated neutrophils to neutrophils in whole blood. (B) Cytospin of neutrophils following a plasma-Percoll gradient. (C) RT-DC reveals neutrophils are more deformable in blood, prior to isolation by percoll gradient. Matched samples are compared by Wilcoxon matched-pairs signed rank test with significance set at *$p$<0.05, **$p$<0.001, ***p<0.001, ****$p$<0.0001.

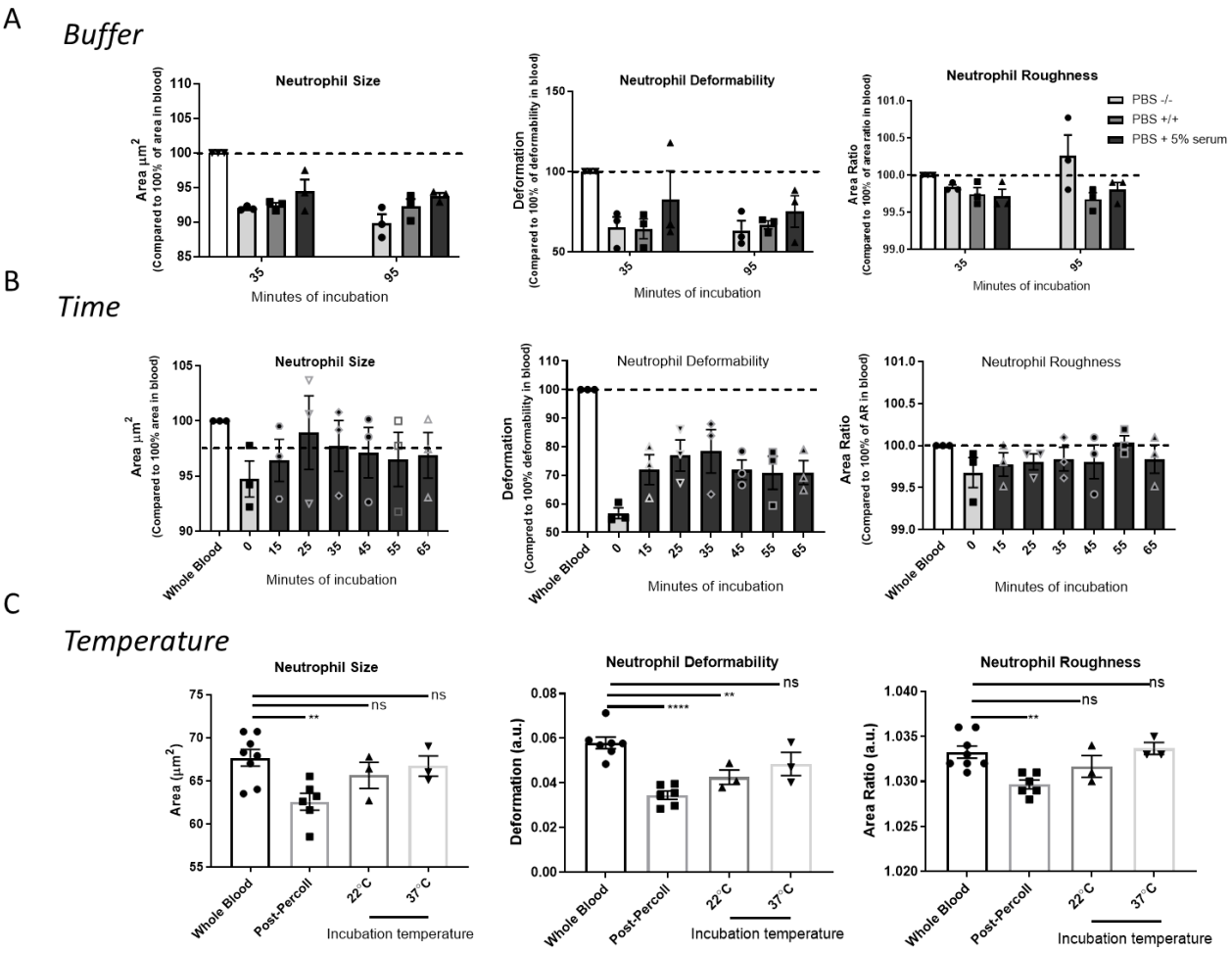


**Figure III-7: Optimisation of a protocol to return purified neutrophils to their whole blood biomechanical phenotype.**

(A) Neutrophils were analysed by RT-DC in blood drawn from healthy volunteers (open bar, which served as the reference data set), and again following isolation by percoll gradient and again following a 45 minute incubation in PBS (light grey), PBS with calcium and magnesium ions (PBS+/+) (medium grey bar), or PBS+/+ with 5 per cent autologous serum (dark grey bar). (B) Having determined PBS+/+ with 5% autologous serum to be the optimal recovery buffer, neutrophils were analysed in blood drawn from healthy volunteers (open bar, reference dataset), and again following isolation by percoll gradient with incubation in PBS+5% autologous serum for 0 minutes (light grey bar) or 10 to 60 minutes (dark grey bar). (C) Having determined 35 minutes to be the optimal recovery time, neutrophils were analysed in blood drawn from healthy volunteers, immediately following isolation by percoll gradient, and again following incubation in PBS+5% autologous serum for 35 minutes at either 22- or 37-degrees C. Neutrophils are compared to whole blood counterparts from the same individuals by Kruskal-Wallis test with post hoc Dunn's test. Significance was set at *$p$<0.05, **$p$<0.01, ****$p$<0.001, ns=not significant.

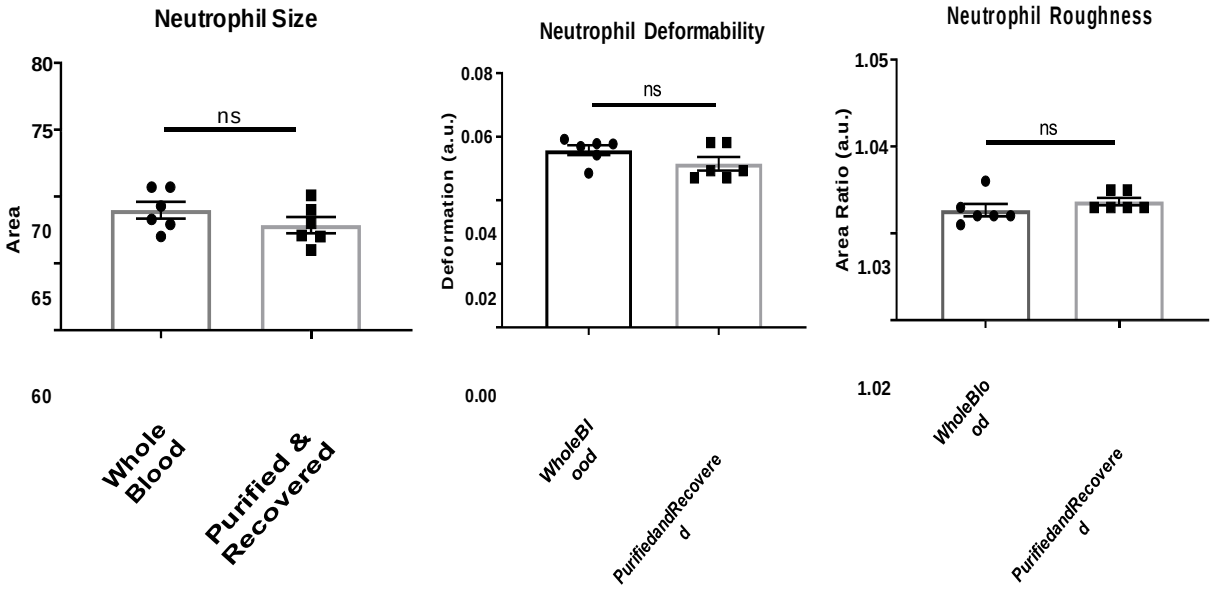


**Figure III-8: Purified neutrophils can be recovered to their whole blood biomechanical phenotype.**

Neutrophils were analysed in blood drawn from healthy volunteers and following isolation by discontinuous plasma-Percoll gradient density and incubation in PBS+5% autologous serum for 35 minutes at 37 degrees C. Matched samples were compared by Wilcoxon matched pairs test with significance set at *$p$<0.05, ns=not significant.

## 4.9 Optimising isolation of LDGs from the PBMC layer

Although density gradient centrifugation-dependent techniques effectively isolate neutrophils, low density neutrophils (LDNs) are found in the peripheral blood mononuclear cell (PBMC) fraction and require further processing to achieve a pure population of cells. LDNs are a heterogenous population of neutrophils, containing immature neutrophils, degranulated neutrophils, and a subset found in patients with inflammatory diseases (*e.g.* SLE), often referred to as low density granulocytes or LDGs [152].

The standard isolation strategy for SLE LDGs requires a density gradient followed by MACS negative isolation strategy [153]. However, I previously determined MACS substantially disrupts the biomechanical properties of neutrophils (Figure III-6). As such, it was necessary to identify a new isolation strategy that did not rely on MACS but did yield a pure population of biomechanically undisrupted LDGs.

LDGs were biomechanically analysed post-density gradient and following a column-free magnetic negative isolation strategy. Although this column-free system, called EasySep, did not biomechanically

disrupt the LDGs, the purity was very poor (Figure III-9A). A collaborator determined that the major

contaminating cell populations were CD86+ or HLDR4+, and so the producers of the EasySep kit generated custom antibodies against these cell surface markers. When the CD86 and HLDR4 antibodies were included in the EasySep kit, a pure population of LDGs were obtained based on nuclear morphology & RT-DC (Figure III-9C). This strategy (gradient followed by EasySep kit) does not disrupt neutrophil biomechanical properties (Figure III-9D) and was used to isolate both LDG and normal dense neutrophils (NDNs) for trafficking and proteomics experiments in Chapters 5 and 6 of this thesis.

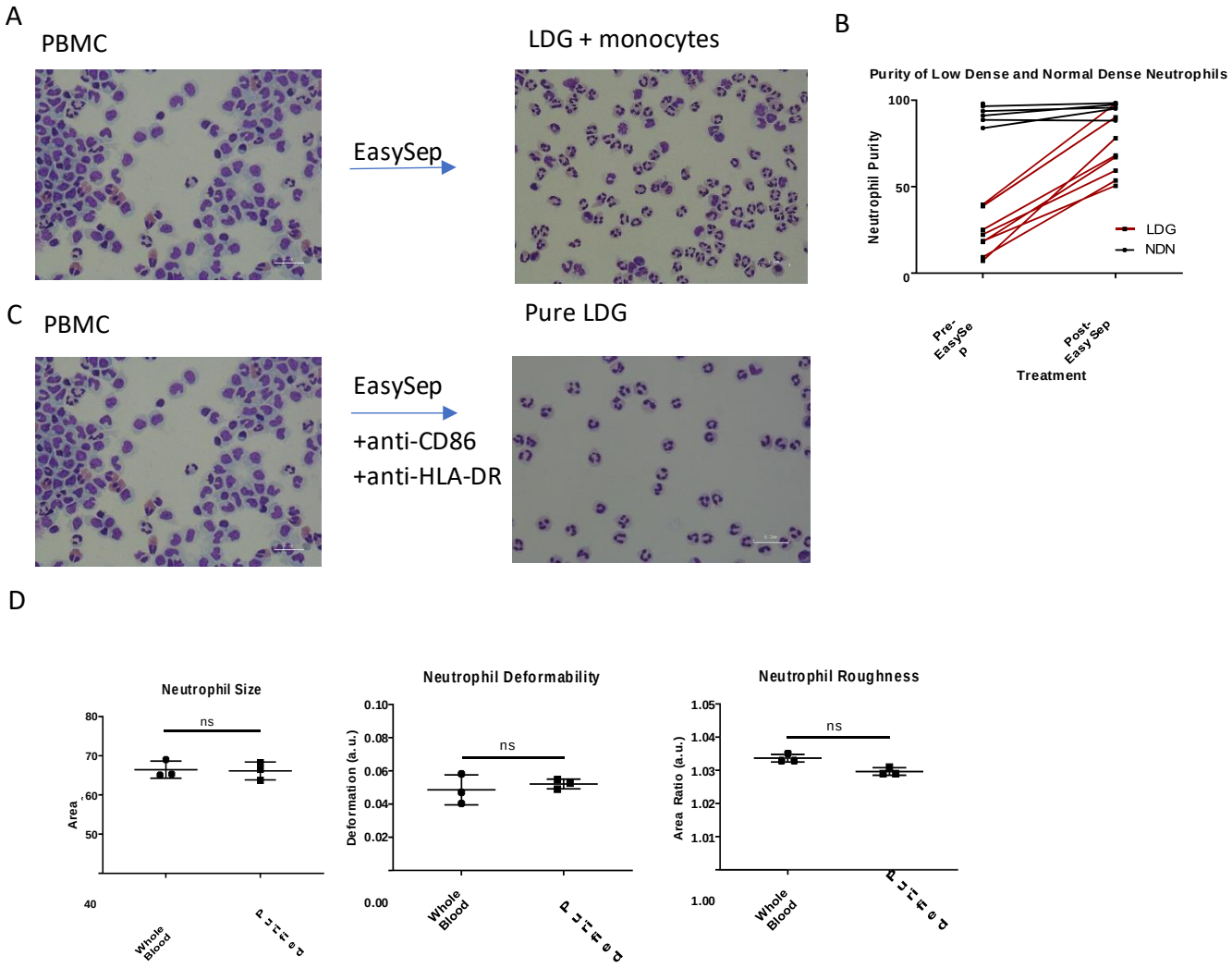


**Figure III-9: Optimisation of a protocol to isolate LDGs purely and without biomechanical disruption.**

(A) LDG purity was quantified by cytospin in mixed PBMC fraction and following EasySep kit. (B) EasySep kit alone improved LDG purity but not sufficiently. (C) LDG purity was quantified by analysing cytospins of the mixed PBMC fraction and of LDG samples purified by EasySep kit with antibodies against CD86 and HLA-DR4 spiked in. This protocol yielded sufficiently pure LDG samples. (D) Neutrophils were analysed in whole blood and following isolation by percoll gradient and EasySep kit. Matched samples are compared by Mann Whitney U-test with significance set at *$p$<0.05, ns=not significant.

## 5. Discussion

This chapter presents the initial experiments I undertook to validate the techniques that provided the foundation for my further work and, more broadly, the use of RT-DC to characterise neutrophils. RT-DC is a new technology and accordingly, quality controls and optimisation studies had to be performed to ensure that consistent and accurate results would be obtained in the rest of my work. Similar to analysing flow cytometry data, analysing RT-DC data offline involves a considerable human component in visually selecting the cells that will fall within the analysis gates. As such, technical verification of both data collection and analysis was necessary before proceeding.

After verifying RT-DC quantifies the mechanical properties of immune cells in a technically reproducible manner, I identified the baseline values of healthy neutrophil deformation (0.06 a.u.), area ratio (1.032-1.033 a.u.) and neutrophil size (65-75 $mm^2$), which match the values consistently measured by the producers of RT-DC at ZellMechanik. I observed little inter-sex or inter-age variation,confirming the observations of Otto *et al.*,[82] that little inter-donor variability in neutrophil mechanicalphenotype exists within the healthy population. Interestingly, area ratio appears to be the most stable of the mechanical parameters measured by RT-DC. All healthy volunteers analysed over the course of mywork had neutrophil area ratios of 1.031-1.034 a.u. Although I was not expecting wide variability in neutrophil mechanical properties across the general population, I was surprised at how stable the area ratio of neutrophils was from person to person. Over the course of my PhD research, my colleagues and I isolated neutrophils from a new healthy volunteer nearly four days a week for almost four years. In time, we found that when healthy volunteers donated neutrophils with area ratios over 1.034 a.u., my colleagues' experimental results acquired that day, using the same neutrophils, would look unusual. We began following up with individuals and more often than not, those individuals reported that they had come down with a cold shortly after donating, or perhaps they hadn't been feeling well in the days prior to donating. Though more research is required in this area, it appears that neutrophil area ratio may be intrinsically linked to health.

Subsequently, I assessed the change in neutrophil biomechanical properties over time. Time from blood sampling to analysis had a considerable effect on neutrophil biomechanical properties, though blood kept at 37 degrees C preserved neutrophil biomechanical properties for up to an hour. For all experiments conducted, time-matched controls were completed. Whenever possible, experiments were completed within one-hour of venesection. In instances where this was impossible, as in some experiments presented in Chapter IV, time-matched controls were used differentiate between the effect of time and the effect of the variable being assessed. This finding that neutrophil biomechanical properties change over time, with one hour following venesection being the cut-off for accurate analysis, could pose challenges for the adaptation of RT-DC to the clinic. In some instances, it may notbe feasible to perform RT-DC on a blood sample within one hour of venesection.

In addition, I established a method for analysing isolated neutrophils by RT-DC. Although neutrophils biomechanically phenotyped immediately post-isolation by gradient appear smaller and less deformable than their whole blood counterparts, the whole blood mechanical phenotype can be recovered by resting neutrophils for 35 minutes in PBS+/+ with 5 per cent autologous serum at 37 degrees C. I also established that using a density gradient followed by an EasySep negative isolation strategy successfully purifies LDGs. Currently, RT-DC is not capable of differentiating between LDGs and NDNs in whole blood, and so true comparison of LDGs in blood with isolated LDGs is not possible. However, NDNs purified by gradient followed by EasySep and optimised recovery period are biomechanically identical to their whole blood counterparts. LDGs post-gradient are also biomechanically identical to post-EasySep LDGs. As such, LDGs and NDNs appear to be sufficiently similar that isolation strategies optimised for one subset also allows the other subset to be purified without biomechanical disruption.

Identifying these isolation strategies were essential for conducting physiologically relevant experiments with isolated neutrophils, both LDGs and NDNs. This work provides further evidence to support the proposal that neutrophil isolation strategy considerably impacts physiology and function [148]. Indeed, if two cell populations are to be compared, then identical isolation strategies are necessary to avoid differential isolation-induced effects. For this thesis, the isolation strategy employing density gradients followed by a magnetic system to isolate neutrophils from the normal density and low-density bands was developed. An alternative strategy could have involved isolating all neutrophils directly from the blood via an EasySep magnet-based system, then performing a density gradient to separate the NDNs from the LDNs [54]**.** It may have been beneficial to place the density gradient second in the interest of avoiding any potential monocyte-driven activation of the LDNs within the PBMC layer during the short time between executing the density gradient and purifying the LDNs [54]**.** This is something I would like to have explored further, to determine whether the order of performing the density gradient and EasySep magnetic isolation steps have any effect on NDN and LDN biomechanical properties.

As noted, isolated neutrophils are smaller and less deformable immediately following isolation, before they are recovered to their whole blood mechanical phenotype. Deformation, a measure of how much a cell constricts within a narrow channel, is intimately related to cell size and cell stiffness. The magnitude of lowered deformability in neutrophils post-isolation suggests this decreased deformability is a product of a smaller cell size, rather than a fundamental change to cell stiffness induced via the isolation process. Young's modulus can be used to decouple the independent contributions of size and stiffness to deformability [154]. It is currently unclear why the isolation process leads to small changes in neutrophil cell size, nor is it clear how incubation with PBS+/+ and autologous serum facilitates a recovery to the neutrophils' original biomechanical phenotype. However, these experiments do lend support to the idea that consistent exposure to autologous serum throughout the neutrophil isolation

process assists with neutrophil viability and the subsequent relevance of experiments to *in vivo* systems [29].

It was clear that attempts to isolate neutrophils via MACS columns had a huge impact on neutrophil biomechanical properties (Figure III-6). Neutrophils isolated via MACS columns were much rougher and stiffer than neutrophils isolated by other methods including the EasySep column-free method which also makes use of magnets to isolate neutrophils. One of the main differences between the MACS-based system and the EasySep-based system is the 30 minute incubation on ice with magnet-tagged antibodies that is required for cells to be isolated via the MACS-based system. Given how sensitive neutrophils are to temperature changes even between 37 degrees C and room temperature (Figure III-7), I suspect that the 30 minute incubation with ice is the key driver of these biomechanical changes. This finding is concerning given the widespread use of MACS-based systems for LDN isolations in particular [50].

The experimental work in this chapter additionally included a comparison of healthy and GPS platelets, as seen in Figure III-3. Before comparing immune cells in healthy controls relative to diseased patients (as will be discussed in Chapter 5), it was necessary to affirm RT-DC can identify known, previously characterised biomechanical changes in cells. Indeed, the larger platelets known to be a hallmark of GPS are easily identifiable by RT-DC. In short, the data presented in this chapter lay a firm foundation for the research which follow. These optimised protocols for neutrophil analysis using RT-DC were employed consistently during the rest of this thesis.

# Chapter IV: RT-DC reveals sequential contraction and expansion of neutrophils during priming

## 1. Chapter Introduction

As discussed previously, neutrophils require highly tuned functional flexibility as the first responders to infection. The ability to change functional status in response to immune-modulators allows the neutrophil to patrol the body in a quiescent state while remaining capable of sensing and then employing appropriate responses when threats arise [102]. When quiescent, or un-primed neutrophils are exposed to certain pro-inflammatory cytokines or chemokines (*e.g.* TNF, fMLF, PAF, GM-CSF) they transition into a primed state, characterised by the generation of reactive oxygen species, and some enhanced immune functions including NET formation, chemotaxis, and phagocytosis [36]. This primed state enhances their response to a subsequent exposure to an activating stimulus [26, 36].

Neutrophil priming is a receptor-mediated process. For example, chemoattractant fMLF binds g-protein coupled formyl peptide receptors (FPRs), which subsequently induces a $Ca^{2+}$ response. Actin polymerisation follows, which can drive chemotaxis or phagocytosis [155]. Numerous other priming or activating agents induce similar changes to neutrophil functional capabilities but rely on varying molecular pathways including different mitogen activated protein kinases (MAPKs). For example, signalling driving priming is protein (p)38-driven in the instance of TNF, and extracellular signal-regulated kinase (ERK)-driven in the instance of GM-CSF [156]. fMLF-mediated priming relies on signalling through both the p38 and ERK MAPKs [157]. Such signalling leads to exocytosis of secretory vesicles, which drives increased expression of NADPH oxidase subunits. Thus, neutrophils are subsequently prepared to increase production of reactive oxygen species at the cell membranes. Exocytosis of secretory and gelatinase vesicles contributes to neutrophil degranulation [102].

As mentioned, fMLF-mediated priming drives elevated intracellular $Ca^{2+}$ transients [102]. $Ca^{2+}$ influx accordingly drives activation of phospholipase D, protein phosphorylation, and activation of the NADPH oxidase [158]. Phosphorylation in the context of neutrophil priming has been linked to actin cytoskeletal rearrangements driven by the p38 MAPK [159].

Indeed, in addition to functional and biochemical changes neutrophils undergoing priming or activation exhibit morpho-rheological changes to their biophysical shape. It has been reported that activated neutrophils are smaller and stiffer than their un-activated and un-primed counterparts [68, 104-106], although there exist conflicting reports of neutrophils expanding post-stimulation [107]. Travel into and through the microcapillary system is essential for neutrophil migration to sites of tissue injury. Narrow capillary diameters (5 µm) force neutrophils to deform in order to transit [41]. Hence, changes

in neutrophil shape, size and stiffness all drastically influence neutrophil passage through such capillary beds. As neutrophils become primed and subsequently activated, they take on a progressively polarized shape. Primed neutrophils have also been reported to be much stiffer than resting neutrophils [105, 106], a process that might be useful for the tethering and rolling process neutrophils undergo within blood vessels prior to extravasation into surrounding tissues in response to a stimulatory agent [112].

Of note, the lung pulmonary microvasculature, which takes the entire cardiac output approximately once per minute, consists of a particularly extensive and narrow capillary network [17]. Although the small, bi-concave, non-nucleated erythrocytes can move through the pulmonary microvasculature with ease, and seemingly also un-primed neutrophils, stiffer primed leukocytes exhibit markedly delayed transit through the human lungs [45]. This is particularly interesting in the context of lung diseases such as ARDS where high levels of neutrophil priming in the circulation leads to increased neutrophil entrapment in the pulmonary microcirculation [44, 116]. However, the trapping of these primed neutrophils in the lungs is surprisingly transient. One potential explanation for how primed neutrophils exit from the pulmonary vasculature has been the proposal that these cells can recover *i.e.* actively de-prime in the pulmonary capillaries [28, 44].

Although several mechanisms of neutrophil de-priming have been advanced, this process remains poorly understood. Firstly, neutrophils appear to spontaneously de-prime if they do not receive on-going or repeated stimulation [42, 43]. Secondly, it has been shown that neutrophils can be mechanically de-primed [41]. Thirdly glucocorticoids and catecholamines have been reported to increase neutrophil deformability and reduce pseudopod formation [160]. This leads to neutrophil release from the microcapillary networks (particularly those associated with intravascular marginated pools) and back into the freely circulating blood pool. Interestingly, TNF and IL-1β also stiffen leukocytes, possibly leading to increased margination and endothelial interactions consistent with the inflammation associated with these cytokines [119]. Given the importance of biomechanical properties to neutrophil entrapment and migration within the vasculature, it is likely that such changes also impact on leukocyte dysfunction in disease.

With the advent of RT-DC, it is possible to track and define in more detail the changes in the morphological and biomechanical properties of neutrophils during priming and de-priming. In this chapter, I report on the morphological and mechanical characteristics of neutrophil priming under whole-blood relevant conditions using RT-DC. I describe the biphasic cellular response to priming, which consists of a rapid (and previously recognized) contractile phase, but also a later volumetric expansion with neutrophils swelling by approximately 18 per cent over their original size. In addition, I present evidence that the Na+/H+ antiporter is mechanistically involved in this neutrophil expansion and speculate that this process may occur in parallel with neutrophil de-priming.

## 2. Hypothesis and Aims

*RT-DC can identify and provide a mechanistic understanding of the biomechanical kinetics of neutrophil priming*

- To describe the biomechanical kinetics of neutrophil priming
- To ascertain whether neutrophil priming kinetics are consistent across priming agents
- To identify the mechanism regulating neutrophil expansion after priming
- To determine the density of primed neutrophils relative to un-primed counterparts
- To compare the biomechanical profiles of un-primed, primed, and de-primed neutrophils

## 3. Method Notes

This chapter presents results generated using methods detailed in Chapter II and techniques optimised in Chapter III. Namely, RT-DC was performed on *ex-vivo* primed neutrophils in whole blood, immediately after venesection, and alongside a time-matched, untreated aliquot of blood from the same healthy volunteer. Figure IV-2B & 2D show datasets generated in collaboration with Dr Nicole Toepfner at Universitat Technisat Dresden, Germany. Confocal imaging of neutrophil uptake of dextran beads shown in Figure IV-3D was kindly completed by Dr. Arlette Vassallo, a fellow PhD student in the Department of Medicine.

# 4. Results

## 4.1 During fMLF priming neutrophils sequentially contract, then expand.

Neutrophils were analysed by RT-DC in whole blood immediately following blood sampling, eliminating the need for further cell purification and the challenges described in Chapter III. All experiments were carefully controlled to include comparison of neutrophils at time zero to unstimulated neutrophils that were time-matched to autologous stimulated counterparts. These data demonstrated no impact of time on unstimulated neutrophil size, deformation, or area ratio within the time frames analysed (Figure IV-1B).

First, I analysed neutrophils in whole blood following 20 minutes of incubation with various concentrations of fMLF. fMLF has a dose-dependent effect on neutrophil biomechanical properties (Figure IV-1A). 100nM fMLF is a standard concentration used to prime neutrophils [34] and this concentration indeed led to a substantial change in neutrophil deformability and size. Neutrophil roughness, *i.e.* the amount of perturbations on the cell surface, was also increased following treatment with 100nM fMLF. Although higher concentrations of fMLF (*e.g.* 1 mM) induced even greater biomechanical changes, the extremely shrunken, stiff, and rough morphology of these neutrophils was such that the cells appeared damaged.

Next, the biomechanical kinetics of neutrophils following stimulation with 100nM fMLF were assessed every 15 minutes for an hour. Fascinatingly, I found that neutrophil size contracts within seconds, only to expand after 15 minutes for over an hour. Alongside the changes in neutrophil size, neutrophils became less deformable, then more deformable. In addition to the noted changes in neutrophil size and deformability, I observed a dramatic increase in area ratio within 1 minute of stimulation with fMLF (Figure IV-1B). This increase in area ratio signifies an increase in neutrophil "roughness". This term "roughness" is used as a quantification of perturbations in the neutrophil surface, *i.e.* how far the neutrophil surface is from being perfectly smooth. Previous accounts of neutrophil priming include observations of neutrophil "polarisation" which is identified by the RT-DC as a change in area ratio *i.e.* roughness. See Figure II-4 for a visual explanation of the measure of area ratio.

## 4.2 Priming kinetics are consistent for fMLF, PAF, GMCSF, and LPS.

As discussed in Chapter III, neutrophil biomechanical properties vary little across the healthy population. However, to suppress the little variation that does exist, the data can be presented as delta values *i.e.* the absolute difference between unstimulated and primed neutrophils from the same individual. This allows for clear graphical representation of a dynamic process with consistent kinetics across healthy blood donors. (Figure IV-2). In the interest of transparency, raw data for unstimulated neutrophils over time can be seen in Figure IV-1.

The biphasic signature of neutrophil contraction followed by expansion was consistent across a variety of neutrophil priming agents, including platelet activating factor (PAF), lipopolysaccharide (LPS), and granulocyte macrophage colony stimulating factor (GM-CSF). Although the kinetics in response to different priming agents varied slightly, the distinct sequential phases of neutrophil contraction followed by expansion were consistent in all instances (Figure IV-2A). Given the similarities in neutrophil signalling [161] and the comparable neutrophil phenotypic effects induced by these agents [34, 162], it was not overly surprising to see overlap in their biomechanical responses. It was interestingto see the kinetic differences in response to different priming agents. This may point to mechanistic differences, and indeed there are known differences in neutrophil priming in the context of different stimulatory agents. For example, priming by LPS or GM-CSF have been found to expand the neutrophillife span *in vitro* while priming with PAF or fMLF have no effect [34].

The deformation of neutrophils exposed to fMLF or other stimuli was assessed by comparing time-matched, stimulated and unstimulated blood neutrophils. Deformability did not change in unstimulated neutrophils over time (Figure IV-1B). However, post stimulation deformation trends (Figure IV-2B) followed similar kinetics to the changes in neutrophil size, with neutrophils becoming less deformable, then more deformable over the 60 minutes after priming. Priming with other agents such as GM-CSF, LPS, or PAF induced similar changes in neutrophil deformability. In some instances, neutrophil deformability recovered to resemble those of unstimulated neutrophils with time (Figure IV-2B), suggesting priming may be a reversible phenomenon.

As discussed in Chapter III, both cell size and cell stiffness contribute to cellular deformation, therefore I hypothesised that that changes in neutrophil deformability might be mediated solely by changes in neutrophil size. My collaborators in Germany calculated the Young's modulus, a measure of elasticity, for each sample in this dataset to determine the measure of cell stiffness [154]. They reported that at the early (1 minute) time-point after fMLF exposure, neutrophils were significantly stiffer (in addition to being smaller and less deformable). Furthermore, neutrophils became significantly softer during the post-priming expansion phase. Taken together, these data reveal the biomechanical kinetics of neutrophil priming follow sequential phases of cellular contraction and stiffening, followed by cellular expansion and softening.

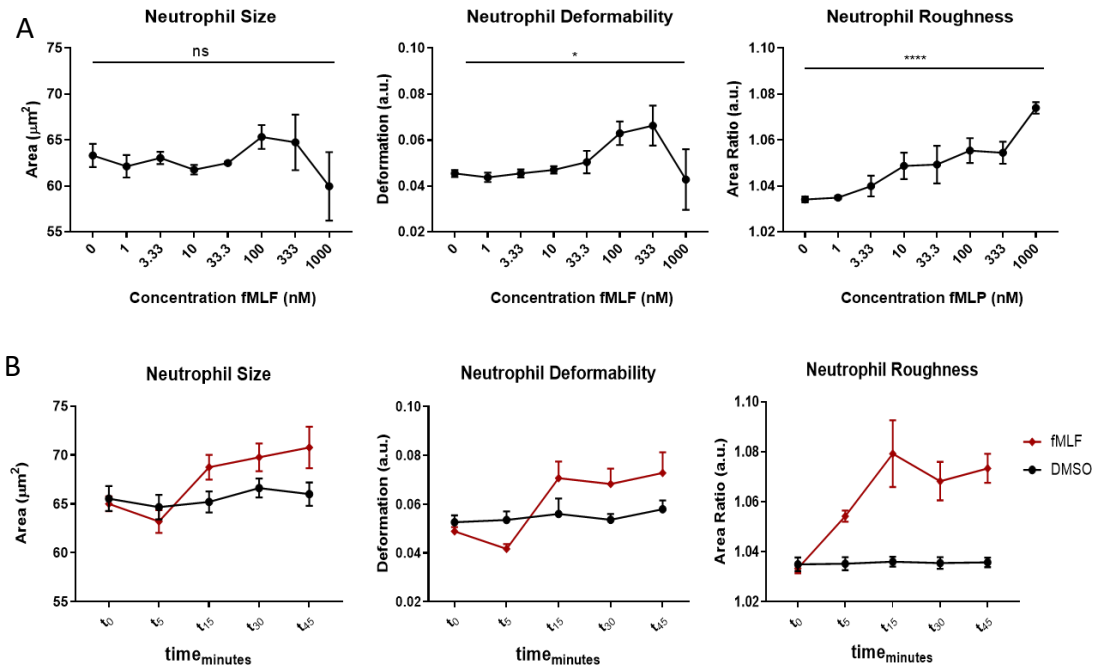


**Figure IV-1: fMLF induces neutrophil biomechanical property changes in a dose-dependent manner. Neutrophils contract and stiffen, then expand and soften.**

(A) Neutrophils within whole blood were primed with various concentrations of fMLF. After 20 minutes, cell size, deformability, and area ratio (*i.e.* roughness, *i.e.* measure of perturbations in the cell surface) was quantified by RT-DC (n=3). Significance was established by one-way ANOVA and set at *$p$<0.05, ****$p$<0.0001, ns = not significant. (B) Neutrophils within whole blood from autologous donors and treated either with 100nM fMLF or an equivalent volume of DMSO were analysed at matching time points (n=6). For each blood sample analysed by RT-DC, the median value of >500 neutrophils' size, deformability, or area ratio was plotted. The mean±SEM for each condition was also depicted. This is raw data; Figure IV-2 displays the same data presented in panel B, but normalised to the biomecanical parameters of an autologus unstimulated neutrophil at time zero.

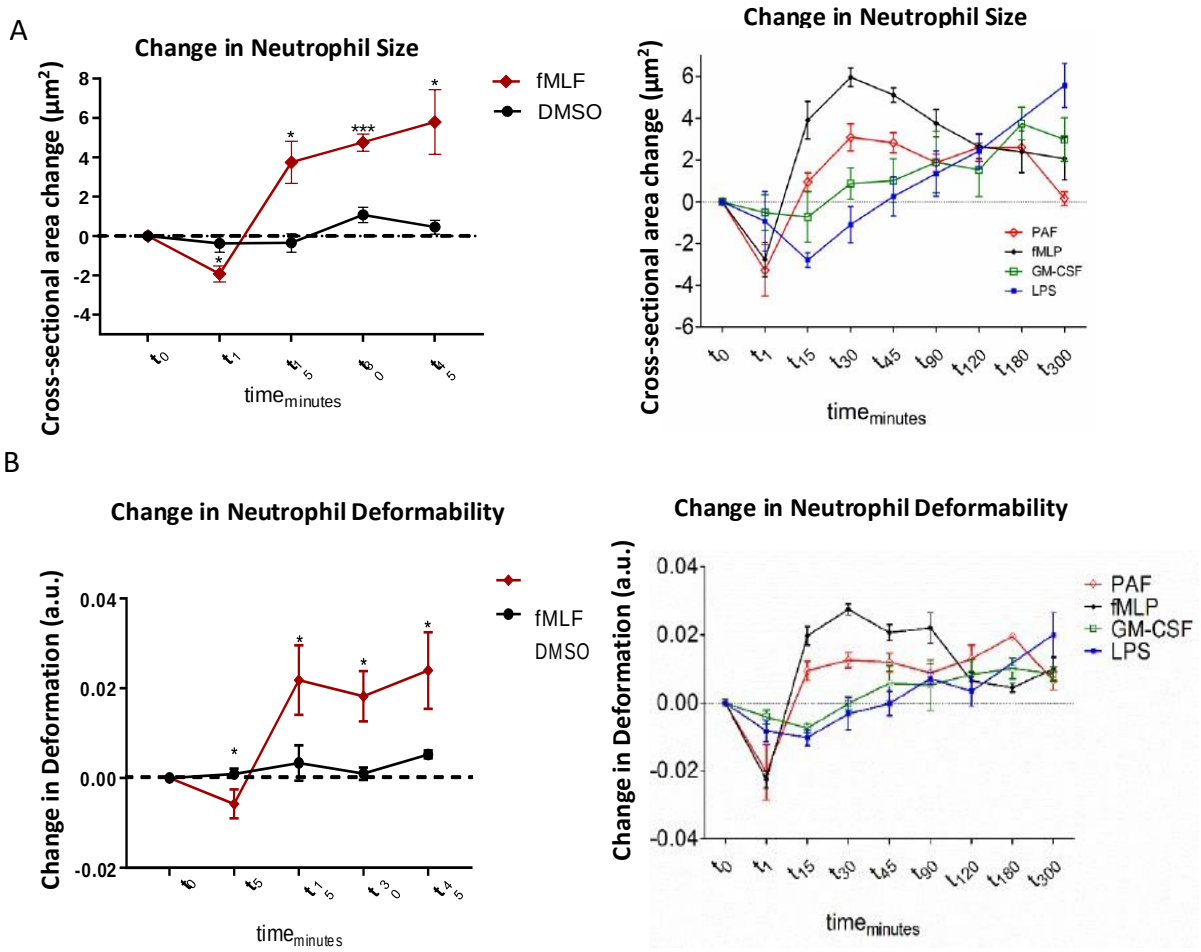


**Figure IV-2: Neutrophil priming induces a phase of neutrophil contraction and lower deformability, followed by a phase of neutrophil expansion and increased deformability.**

(A) Time courses of blood neutrophil size after stimulation of whole blood with 100nM fMLF and overview of neutrophil size kinetics after blood stimulation with different agonists fMLF (black diamond), PAF (red diamond), GM-CSF (green square) and LPS (blue square). (B) Time courses of blood neutrophil deformability after stimulation of whole blood with 100nM fMLF and overview of neutrophil deformability kinetics after blood stimulation with different agonists fMLF (black diamond), PAF (red diamond), GM-CSF (green square) and LPS (blue square). For each sample analysed by RT-DC, the median of >500 neutrophils was plotted. Mean and SEM of stimulated blood neutrophil size changes, shown in reference against unstimulated, time-matched controls. Differences between treatment and controls were identified by repeated measures ANOVA and Bonferroni post-test (t0 to t45; n = 8. t90 to t300; n=3). Significance was set at *$p$<0.05, ***$p$<0.001. Raw data is displayed in Figure IV-1.

*Panel B represents a combination of data generated in collaboration with Dr. Nicole Toepfner.*

## 4.3 Stimulation with priming agents increases neutrophil roughness.

In addition to changes in size and deformability, neutrophil priming with fMLF is accompanied by an increase in neutrophil roughness. Neutrophil polarisation was visually confirmed with cytospins (Figure IV-3A) and later in Chapter V by scanning electron microscopy and lattice light sheet microscopy (Figure V-5). See Figure II-4 for a visual explanation of the measure of area ratio i.e. neutrophil roughness.

Priming with complement factor 5a (C5a) and PAF also induced changes in neutrophil roughness. When primed with PAF, neutrophils returned to their original roughness within two hours (Figure IV- 3B). To further explore this phenomenon, neutrophils were assessed in blood and following isolation and incubation with PBS+ and 5 per cent autologous serum at 37 degrees C for two hours (Figure IV- 3C). Neutrophils were primed with PAF immediately following isolation, allowing them to de-prime over two hours during their recovery. Other neutrophils were primed with PAF at two hours and compared to neutrophils unstimulated with PAF. This allowed for comparison of un-primed, primed and de-primed neutrophils. As expected, primed neutrophils were smaller, less deformable, and rougherthan their un-primed counterparts. Likely due to time-induced effects, un-primed neutrophils were slightly biomechanically different from their whole blood counterparts. Interestingly, of all the conditions, de-primed neutrophils resembled their whole blood counterparts most closely, suggesting perfect recovery of the un-primed *in vivo* biomechanical phenotype. These data describe the kinetics of neutrophil morphology during priming and suggest the ability of neutrophils to de-prime *ex vivo.*

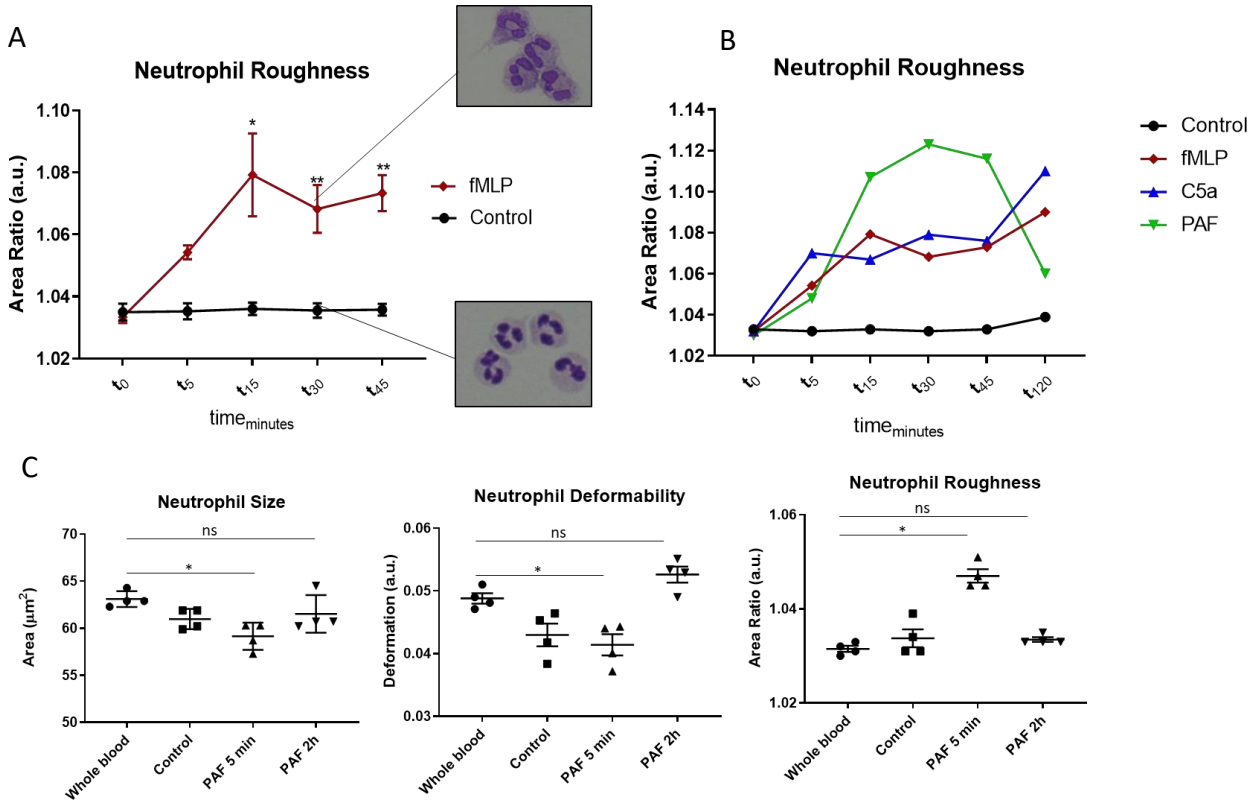


**Figure IV-3: Neutrophil priming induces a phase of neutrophil contraction and less deformability, followed by a phase of neutrophil expansion and increased deformability.**

(A) Time courses of blood neutrophil roughness after stimulation of whole blood with 100nM fMLF (n=6), with morphology shown by cytospin (n=8). The mean and SEM of roughness for indicated time points post-stimulation is shown, with comparisons to unstimulated, time-matched controls. Differences between samples and controls were identified by repeated measures ANOVA and Bonferroni post-test. (B) Overview of neutrophil roughness kinetics after blood stimulation with different agonists fMLF (red diamond), PAF (green triangle), C5a (blue triangle) and DMOS (black circle). The mean is shown (n=3). (C) Neutrophils were analysed by RT-DC in whole blood or following stimulation with DMSO or PAF for time periods indicated. Comparisons between neutrophils from autologous donors in whole blood or post-priming were made by Wilcoxon matched-pairs signed rank tests with significance set at *$p$<0.05, **$p$<0.01; n=4. For all samples analysed by RT-DC, the median of >500 neutrophils was plotted.

## 4.4 The expansion phase of neutrophil priming is mediated by macropinocytosis.

There is a limited amount of previous research which indicates neutrophils are capable of undergoing macropinocytosis [163]. Macropinocytosis is a method by which cells perform membrane ruffling to form small vesicles and take up small amounts of water and extracellular material to bring inside the cell [164]. In light of this literature and given the changes in both roughness and size which could be attributed to morphological changes induced by macropinocytosis, I decided to explore whether macropinocytosis might be responsible for the expansion phase of neutrophil priming.

To determine the mechanism modulating neutrophil expansion after exposure to priming agents, I used the macropinocytosis inhibitor amiloride. Blocking the Na+/H+ anti-porter with amiloride had no biomechanical effect on unstimulated neutrophils within the time frames assessed (Figure IV-4A), but completely impeded the post-priming expansion phase (Figure IV-4B) and significantly reduced the increase in neutrophil roughness (Figure IV-4C). The role of macropinocytosis in modulating the kinetics of neutrophil priming was also assessed by confocal microscopy. While neutrophil uptake of 10,000 MW dextran was evident even under basal unstimulated conditions, priming induced a clear increase in the uptake of dextran consistent with the timeline observed for increases in cell size. Treatment with amiloride reduced dextran uptake (Figure IV-4D). Taken together, these data suggest this expansion phase of neutrophil priming is mediated by macropinocytosis.

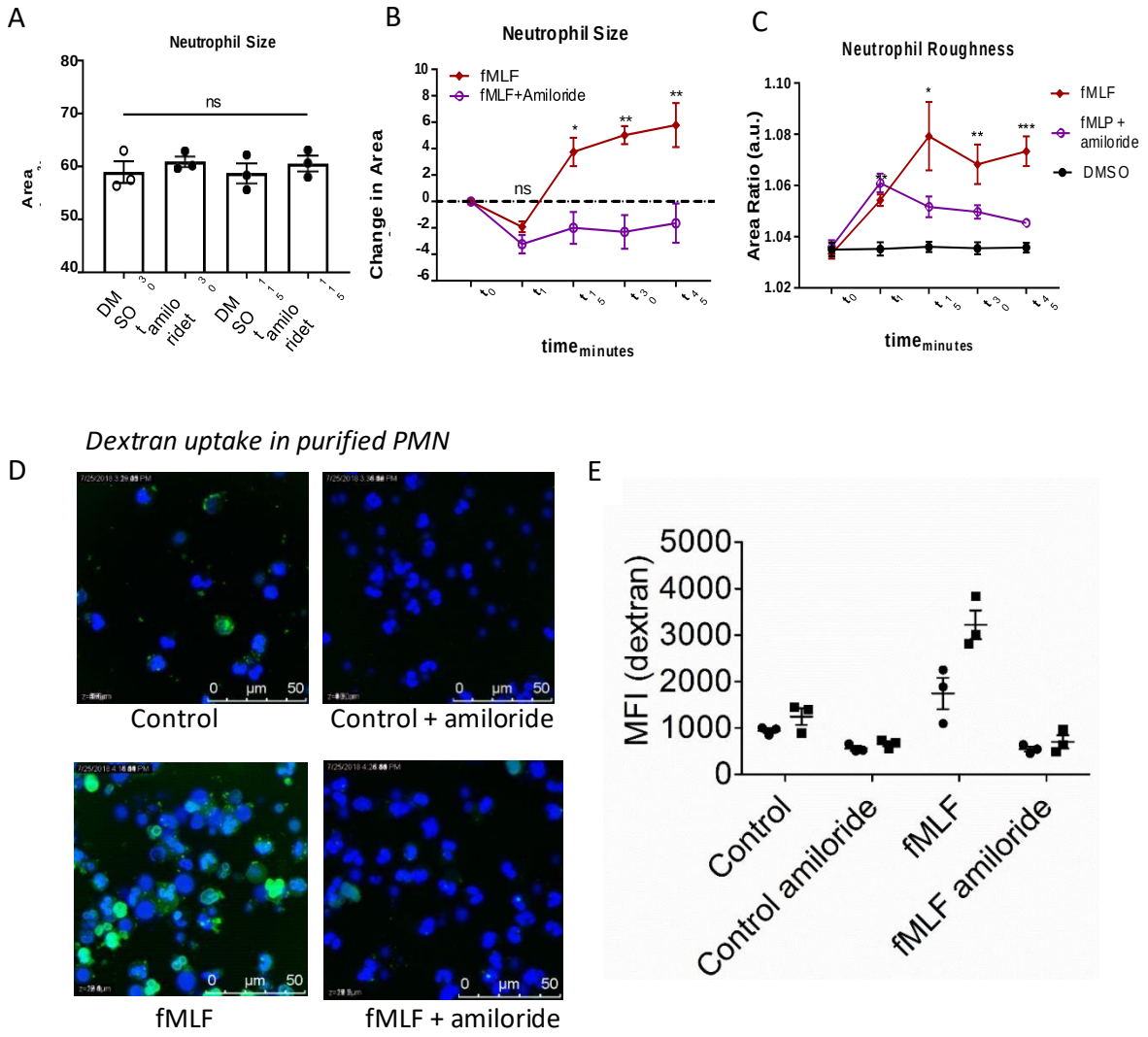


**Figure IV-4: fMLF-mediated neutrophil expansion is Na+/H+ antiport dependent.**

(A) Neutrophil size after 30 minutes (pre-treatment) and 115 minutes (post-experiment time) of exposure to amiloride or DMSO. Mean and SEM are shown (n = 3). (B) Size kinetics of fMLF stimulated purified neutrophils with and without amiloride pre-treatment, samples shown as mean and SEM, referenced against unstimulated, time-matched controls. Differences between fMLF treatment and amiloride by two-way ANOVA with significance set at *p<0.05, **p<0.01, ***p<0.001; n=3. (C) Morphological kinetics of fMLF stimulated purified neutrophils with and without amiloride pre-treatment, samples shown as mean and SEM, referenced against unstimulated, time-matched controls. Differences between treatments by two-way ANOVA with significance set at *p<0.05, **p<0.01, ***p<0.001; n=3. (D) Amiloride-mediated inhibition of dextran uptake. Exemplary confocal images of purified neutrophils 15 minutes post fMLF stimulation with and without amiloride pre-treatment. Green fluorescence indicates dextran uptake. (E) Quantification of neutrophil dextran uptake**.** Mean fluorescence intensity (MFI) of dextran in purified neutrophils 5 minutes (dots) and 15 minutes (squares) post fMLF stimulation, compared to fMLF stimulated neutrophils pretreated with amiloride. For each sample analysed by RT-DC, the median of >500 neutrophils was plotted.

*Panel D was kindly generated by Dr. Arlette Vassallo*

## 4.5 Expansion-phase neutrophils are low density.

I observed that neutrophils began to enter the expansion phase by 15 minutes after exposure to priming agents. Given previous reports of primed neutrophils being low density [152], I assessed the density of these expansion-phase neutrophils. Erythrocytes were removed from blood by dextran sedimentation. The remaining leukocytes were primed with fMLF or left unstimulated, then placed on a density gradient. Neutrophils primed for 20 minutes with fMLF were less dense than their unstimulated counterparts, with approximately 80 per cent isolating with the lymphocyte- and monocyte-rich Percoll layer compared to less than 5 per cent with unstimulated neutrophils (Figure IV-5A-C). RT-DC analysis revealed that fMLF-treated neutrophils placed on the density gradient were larger than unstimulated controls by the same magnitude observed in the previous experiments assessing the post-priming kinetics (Figure IV-5D, IV-2A). The alignment of these independent approaches supports my characterisation of post-primed, expansion phase neutrophils.

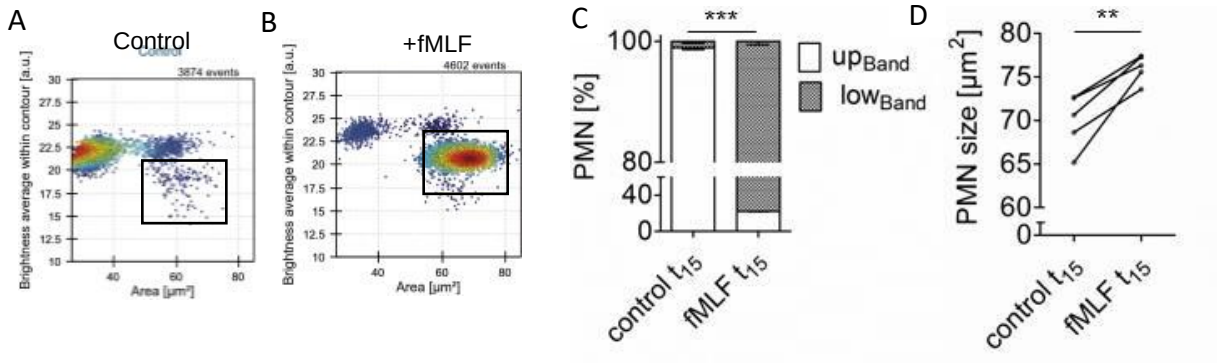


**Figure IV-5: fMLF induces changes to neutrophil density, leading to a less dense phenotype.**

(A & B) RT-DC panels depicting the PBMC layer of unstimulated blood (A) or the PBMC layer of blood stimulated with fMLF for 15 minutes (B). Box indicates neutrophils in the PBMC layer (upper band). Images representative of n = 5. (C) Change in neutrophil distribution between PBMC ($up_{Band}$) and granulocyte ($low_{Band}$) bands after 15 minutes ($t_{15}$) of fMLF stimulation (D) Size of neutrophils from autologous donors isolated with or without 15 minutes of fMLF blood stimulation. Differences between samples by Wilcoxon matched-pairs signed rank test (n = 5). For each sample analysed by RT-DC, the median of >500 neutrophils was plotted, with the mean and SEM across samples shown. Significance was set at *p<0.05, **p<0.01, ***p<0.001; n=3. Brightness levels vary from chip to chip and cannot be compared when different chips are used, as they are panels A and B.

## 5. Discussion

This chapter describes novel observations of the morphological kinetics of neutrophil priming. In doing so, this chapter demonstrates that neutrophil functional changes associated with priming (*e.g.* macropinocytosis) are intimately linked to distinct biomechanical changes (*e.g.* increase in size). Prior to this thesis it was reported that polarisation and reorganisation of the actin cytoskeleton increase with neutrophil migration, facilitating invasion at inflammatory sites and the clearance of pathogens (*i.e.* phagocytosis) [107, 165, 166]. In addition, it has been speculated that such biomechanical changes may allow for neutrophils to be freed from entrapment within microvasculature [116]. In this chapter I demonstrate that neutrophils are capable of returning to a spherical shape from their heavily polarised (*i.e.* rough), primed state, and do so with a clear increase in their overall cell size and deformation. This makes sense in the context of neutrophils' capability to circulate through capillary networks and subsequently return to bigger vessels.

RT-DC conducts analyses of neutrophil biomechanical properties in a contact-free environment. In the microvasculature, primed neutrophils are entrapped within capillaries and in direct contact with endothelial cells. However, the major advantage of RT-DC is that it allows analysis of many thousands of neutrophils within whole blood immediately after blood sampling *i.e.* with minimal sample manipulation. With RT-DC, I have been able to study in detail and in real-time the events occurring in human neutrophils following exposure to priming agents. This is not currently possible using *in vivo* techniques [41].

Each of the four priming agents I tested (GM-CSF, fMLF, PAF, and LPS) induced similar biomechanical changes to neutrophils, but kinetic differences were observed. The contraction phase was approximately 30 minutes for neutrophils primed with GM-CSF or LPS, while neutrophils primed with fMLF or PAF had a much shorter contraction phase of 15 minutes or less. While structural differences exist between these stimuli, both PAF and fMLF bind to g-protein linked receptors (GPCRs). Receptors within this family are structurally very similar in the signalling domain, and thus induce similar signalling pathways [167, 168]. Specifically, fMLF binds the GPCR formyl peptide receptor 1 (FPR1) to drive neutrophil activation at sites of infection [169]. GM-CSF does not bind a GPCR, and instead mediates priming through the JAK/STAT signalling pathway [170]. LPS promotes neutrophil priming following binding to CD14 and toll-like receptors 4 [171]. Thus, kinetic differences in response to different priming agents may be indicative of this variation between priming agents and their mechanisms of action. Differences in neutrophil function following priming by different stimulatory agents are also documented; as mentioned in the results section above, priming by LPS or GM-CSF extends the neutrophil life span *in vitro* while priming with PAF or fMLF has no effect [34].

Within the expansion phase of neutrophil priming, neutrophils are larger and more deformable. Theoretically, a smaller and more pliable neutrophil would be most effective at manoeuvring through the narrow pulmonary or systemic microvasculature. For the range of values associated with the described kinetics of post-priming, simple free energy comparisons demonstrate that a reduction in stiffness contributes most strongly to a cell's ability to pass through narrow constrictions [172]. Accordingly, in the context of neutrophil-relevant size and stiffness values, a larger, softer sphere deforms more than a smaller, stiffer sphere. Specifically, expansion phase neutrophils would be advected through a 5 μm constriction more easily because of their reduced stiffness, despite their increased diameter. The increased actinomyosin cortex occurring during the initial priming-induced contraction phase resists shape changes due to the enhanced surface tension, despite these cells' decreased size. Subsequent volume increase ameliorates the contractility of the cortex, facilitating easier shape changes to accommodate passage through small constrictions.

In addition to an expansion phase of neutrophil priming, the first 5-30 minute of neutrophil priming consistently exhibited a contraction phase where neutrophils became stiffer and smaller. Rapid neutrophil stiffening via the increased thickness and contractility of the actomyosin cortex is a hallmark of neutrophil activation. Y-27623, which does not affect neutrophil viability but specifically inhibits ROCK [173] has previously been used to successfully reduce the magnitude of cell stiffening occurring after priming with fMLF. In this instance, inhibition of ROCK partially blocked contraction in cell size, yet seemingly had no impact on later cell expansion [132], suggesting different mechanisms regulate these two biomechanical phases.

The expansion phase of neutrophil priming appears mediated by macropinocytosis. Macropinocytosis is an actin-dependent, clathrin-independent form of endocytosis, in which surface membrane ruffles non-selectively fold extracellular material into endocytic vacuoles called macropinosomes, which are subsequently engulfed into the cell [163]. Macropinocytosis is particularly important for antigen presentation by macrophages and dendritic cells [163], and although the literature around neutrophil macropinocytosis is not extensive [174, 175], the process has been linked to neutrophil migration [176]. Macropinocytosis also plays a role in tumour metastasis [177]. Amiloride inhibits the Na+/H+ antiporter, and selectively inhibits macropinocytosis without affecting other types of endocytosis [164, 178, 179]. I demonstrated that amiloride blocks post-priming neutrophil expansion completely, and further showed through dextran uptake assays [180, 181] that primed neutrophils undergo macropinocytosis on a timeline consistent with the observed kinetics of neutrophil expansion. These results indicate neutrophils are not expanding due to water uptake alone, *e.g.* as if a rough neutrophil expanded its contained volume and took on a smooth phenotype. Rather, bulk plasma membrane is added during this kinetic process through fusion of secretory vesicles. In addition, the increase in neutrophil roughness post-priming is consistent with membrane ruffling associated with macropinocytosis [182]. In addition, it has been established that treatment with choline chloride, which

also prevents function of the Na+/H+ antiporter, blocks the expansion phase of neutrophil priming [132]. This provides further support for the idea that this expansion phase is macropinocytosis driven through the Na+/H+ antiport.

In addition to non-specific extracellular uptake via macropinocytosis, antiport-mediated transport of Na+ into cells drives subsequent influx of water [183] and thus it is possible that water uptake via aquaporins, might contribute to the expansion phase of neutrophil priming. Both macropinocytosis and water influx are blocked by inhibition of Na+/H+ exchange (*i.e.* the method of action for amiloride) [179, 183]. In addition, patients with systemic inflammatory response syndrome have neutrophils with increased AQP-9 expression [184] and blocking AQP-9 has been shown to reduce neutrophil activation-induced shape changes [185]. AQP-9 is the most widely researched neutrophil aquaporin [186, 187], but unpublished data from the Chilvers research group indicates that neutrophils additionally express AQP-1 and AQP-6 in the plasma-membrane, which may play a similar role to AQP9. (Subburayalu J and Pocock J, unpublished). In addition, AQP-5 and AQP-1 have been shown to regulate neutrophil migration in the context of sepsis [188]. Given the potential importance of aquaporins to neutrophil morphology and function, further research should determine the role of the aquaporins in neutrophil priming and their contribution to the neutrophil expansion phase.

The development of sepsis is due to an over-powerful inflammatory response. In severe sepsis, impairment of neutrophil migration to infection sites leads the infected patient unable to eliminate the infection [189]. In addition, increased numbers of larger neutrophils (relative to healthy controls) circulating in the blood stream have been observed in patients with sepsis [190]. In line with these findings, a recent study demonstrated that patients with viral respiratory tract infections or acute respiratory distress syndrome have larger, more deformed neutrophils in their blood [121]. Neutrophil swelling has also been reported in the context of severe trauma [191], although activated neutrophils are canonically thought to be stiffer [68, 104-106]. I propose this apparent discrepancy may be traced back to the time course demonstrated here. Neutrophils contract immediately following priming, and yet become larger, softer, and less dense as they begin to recover from the priming process. Consequently, in patient blood, researchers or clinicians may observe only the larger, softer cells rather than the smaller, stiffer early primed cells, which are apt to get trapped in the pulmonary microcirculation. Accumulation of primed or activated neutrophils within the lung microvasculature and interstitial components is a hallmark of ARDS, and thought to be responsible for local injury associated with this disease [192]. In Chapters V and VI, the relationship between activated neutrophils in the context of disease, biomechanical properties, and trafficking capabilities is explored further and this discussion is expanded.

Interestingly, neutrophils in the expansion phase of neutrophil priming were revealed to be less dense than un-primed counterparts. This phenomenon may be driven by the increase in neutrophil size relative to its mass; perhaps the neutrophil undergoing macropinocytosis largely takes up water or other low mass extracellular matter which leads to lower total density. Thus, neutrophils in the expansion phase of priming could end up in a lower density section of a density gradient than their un-primed, smaller, counterparts. Perhaps an increase in neutrophil priming is responsible for the increase in low density neutrophil populations observed in patients with disease. To explore this phenomenon further, Chapter V explores the relationship between these expansion phase, primed neutrophils and other known subsets of low dense neutrophils, *e.g.* LDGs found in patients with SLE [193].

# Chapter V: SLE LDGs have a unique biomechanical phenotype which may impact their trafficking capabilities.

## 1. Chapter Introduction

As discussed briefly in Chapter I, systemic lupus erythematosus (SLE) is a multifaceted disease in which innate and adaptive immune dysregulation lead to autoantibody production, complement activation, and tissue damage [5]. Neutrophil dysregulation appears to play a critical role in development of SLE and its associated organ damage. More specifically, enhanced release of neutrophilextracellular traps (NETs), a phenomenon involving extrusion of chromatin containing oxidized nucleicacids and granule proteins, may play an important pro-inflammatory role in activation of the immune system. This includes type 1 interferon (IFN) pathway and inflammasome activation, as well as exacerbation of proinflammatory responses, vasculopathy and organ damage associated with this disease [9, 10, 25, 55].

A subset of proinflammatory neutrophils were previously identified in the peripheral blood mononuclear cell (PBMC) layer of patients with SLE. As discussed in Chapters I and III, these neutrophils are known as low density granulocytes, or LDGs [6], as opposed to normal density neutrophils (NDNs). SLE LDGs have a striking predisposition to form NETs in the absence of any additional *in vitro* stimulus and these NETs are more proinflammatory and vasculopathic than NETs generated by NDNs [50, 56]. In addition, SLE LDGs produce higher levels of type 1 IFNs than NDNs and induce endothelial cell apoptosis [6], thrombosis and vascular dysfunction *in vitro* and *in vivo.* Numbers of SLE LDGs are also correlated with *in vivo* levels of vascular inflammation, coronary atherosclerosis [55, 194-196], and T cell activation [197]. These data suggest LDGs play an important role in SLE pathogenesis and the associated vascular dysfunction. Thus, specifically targeting LDGs could mitigate immune dysregulation, premature atherosclerosis, and other clinical manifestations in SLE [51]. Studies to understand the origin and pathogenicity of LDGs have focused primarily on transcriptomic data [56, 193, 194, 198, 199], leading to the understanding that SLE LDGs are a heterogenous population of cells. The majority represent intermediate-mature cells with strong proinflammatory potential, enhanced type I IFN responses and the enhanced ability to form NETs and damage the endothelium. The minority of LDGs represent bona fide immature neutrophils that lack many of the canonical neutrophil functions [200]. However, the biomechanical properties of these cells, relative to autologous SLE or healthy NDNs, have not been systematically characterised and it is not known how distinctions in biomechanics may contribute to the LDG's strong proinflammatory potential.

In this chapter, I compared the biomechanical properties of SLE LDGs, SLE NDNs, and healthy NDNs by real-time deformability cytometry (RT-DC) and determined that SLE LDGs are biomechanically distinct from other neutrophil subsets. I developed a novel polydimethylsiloxane (PDMS) device to mimic trafficking through the pulmonary microvasculature and determined that biomechanical properties of SLE LDGs may profoundly affect their ability to traffic through small blood vessels, with implications for organ damage characteristic of this disease.

## 2. Hypothesis and Aims

*Diseased and healthy neutrophils are biomechanically distinct and such differences in biomechanical properties are capable of conferring differences in cell trafficking capabilities.*

- To compare immune cells from healthy individuals and patients with active or stable SLE.
- To describe the biomechanical profile of SLE LDGs.
- To determine how SLE LDGs biomechanically compare to other neutrophil subsets.
- To identify clinical or demographic characteristics which affect neutrophil biomechanical phenotype.
- To design and produce a device that mimics the pulmonary microvasculature and can be used for trafficking assays.
- To determine if SLE LDGs and other neutrophil subsets differ with respect to their trafficking through a pulmonary microvasculature mimetic.
- To decouple the molecular and biomechanical contributions to modulation of neutrophil trafficking and to determine their relative effects.

## 3. Method Notes

This chapter presents results generated using methods detailed in Chapter II and RT-DC as it was optimised in Chapter III. Neutrophils, LDGs, monocytes, and lymphocytes were analysed by RT-DC within whole blood or within the PBMC layer whenever possible. Paniz Sangsari and Dr. Nicole Morgan of the National Institute of Biomedical Imaging and Bioengineering assisted in the design and generation of the PDMS pulmonary microvasculature mimetic. Dr. Davide Randazzo of the light imaging section at the National Institute of Arthritis, Musculoskeletal, and Skin disease provided invaluable support with the lattice light-sheet microscopy.

Most of the research completed in this chapter focuses on neutrophils from patients with clinically quiescent SLE; this is due to the challenges around recruiting patients with active SLE during my time at Cambridge.

# 4. Results

## 4.1 Patients with active SLE have rougher neutrophils than stable or healthy individuals.

Neutrophil size, deformability and roughness were measured in peripheral blood obtained from healthy controls (HC) (n=11), subjects with clinically quiescent (n=11) or with clinically active SLE (n=4). Any patients on steroids were excluded from analysis given the known effects of steroids on neutrophil morphology [201].

In some experiments, fMLF was added directly to healthy peripheral blood to prime the neutrophils prior to analysis. Neutrophils from healthy and clinically quiescent SLE subjects were biomechanically identical, while peripheral blood neutrophils from active SLE subjects were larger in diameter and displayed enhanced deformability and roughness. Healthy peripheral blood neutrophils that were primed with fMLF were also larger and more deformable than neutrophils from autologous, unstimulated healthy peripheral blood. Primed healthy neutrophils were significantly rougher than any category of unstimulated neutrophils (Figure V-1). Overall, these results indicate that neutrophils from subjects with active SLE displayed altered biomechanical properties relative to healthy neutrophils. It is unclear whether these neutrophils from patients with SLE are temporarily primed in some way, or whether this is an innate difference in neutrophils from patients with SLE.

## 4.2 SLE monocytes and lymphocytes are mechanically indistinct from healthy cells.

In addition to neutrophils, lymphocytes and monocytes were also analysed in blood from healthy volunteers and patients with clinically quiescent SLE. In contrast to neutrophils, there were no significant biomechanical differences in these cell types between SLE subjects and healthy volunteers (Figure V-2).

## 4.3 RT-DC identifies an expanded population of LDGs in SLE patients.

Next, I measured the biomechanical properties of LDGs and NDNs purified from subjects with clinically quiescent SLE and compared them to purified healthy NDNs. To preserve neutrophil biomechanical properties, granulocytes and PBMCs were separated by density gradient and RT-DC was undertaken immediately, with no further processing or manipulation of the samples. All experiments involving isolated cells used optimised purification strategies to avoid disruption of biomechanical properties developed as described in Chapter III. The gating strategy used during the data analysis phase of RT-DC allowed for identification of neutrophils, monocytes, lymphocytes and eosinophils in mixed cell fractions, as described in Chapter III. Neutrophil percentages were higher in SLE PBMC fractions than healthy PBMC fractions (Figure V-3), consistent with previous reports that LDG numbers are increased in SLE [194].

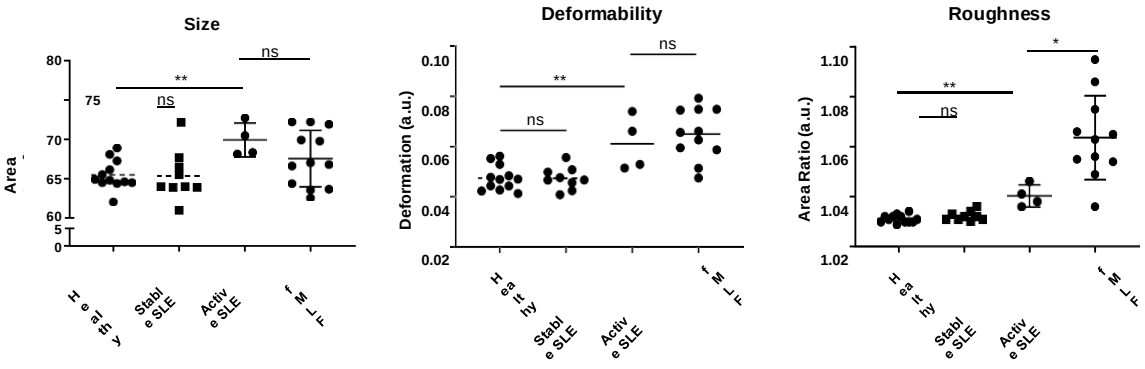


**Figure V-1: Patients with active SLE have rougher neutrophils than healthy individuals.**

Biomechanical profiling of neutrophils in blood samples obtained from healthy volunteers (n=12), clinically quiescent SLE patients (n=9), and clinically active SLE patients (n=4) by RT-DC. In some instances, 100 nM fMLF was used to prime neutrophils within the healthy blood. For each sample analysed by RT-DC, the median measurement of over 500 neutrophils is plotted and the mean ± SEM for each neutrophil subset is depicted. Autologous unstimulated/primed healthy (HC) NDNs or autologous SLE NDN/LDGs were compared and significance was established by Wilcoxon matched-pairs signed rank test. In other comparisons, significance was established by Mann-Whitney U-test. Significance was set at $*p \leq 0.05$, $**p \leq 0.01$, ns=not significant.

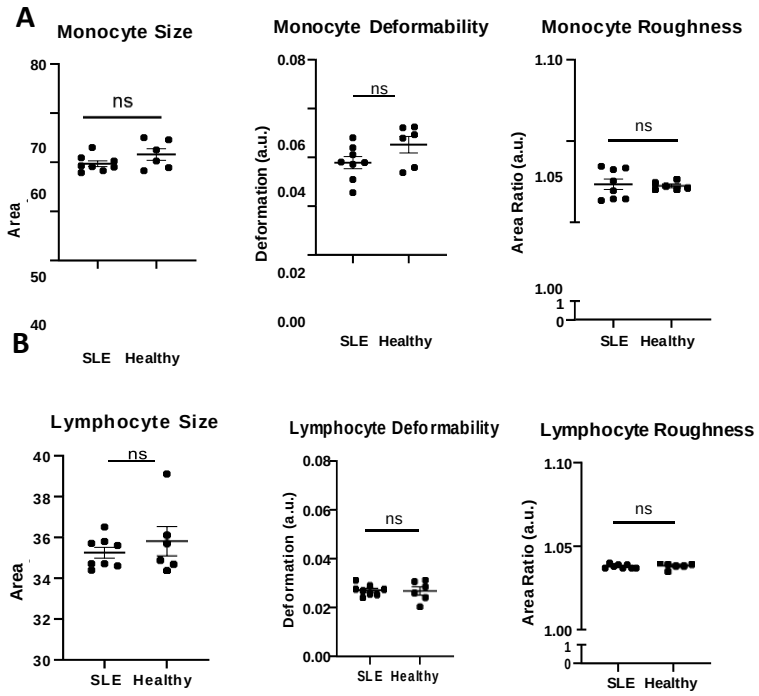


**Figure V-2: The biomechanical properties of lymphocytes and monocytes do not differ between healthy individuals and clinically quiescent SLE.**

(A) Biomechanical profiling of monocytes from SLE patients (n=8) and healthy volunteers (n=6) by RT-DC. (B) Biomechanical profiling of lymphocytes from SLE patients (n=8) and healthy volunteers (n=6) by RT-DC. For each sample analysed by RT-DC, the median measurement of over 300 lymphocytes or monocytes is plotted and the mean ± SEM for each cell subset is depicted. Significance was established by Mann-Whitney U-tests and was set at *$p$<0.05, ns=not significant.

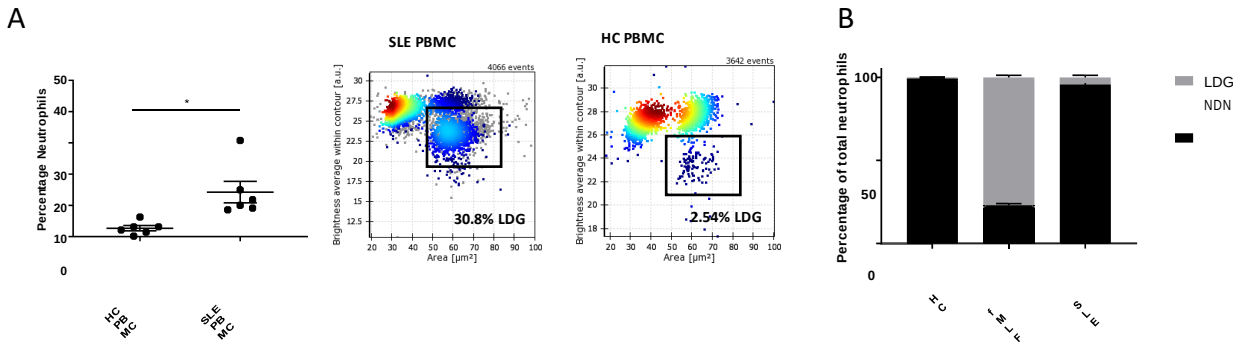


**Figure V-3: RT-DC identifies a greater percentage of LDGs in the blood of patients with SLE than are found in the blood of healthy volunteers.**

(A) Percentage of LDGs identified in SLE (n=6) and healthy control (HC) PBMCs (n=6) by RT-DC. Black boxes show the population of LDGs in the mixed PBMC layer which also includes lymphocytes and monocytes. (D) LDGs as a percentage of total neutrophils in SLE patients (n=6), HC volunteers (n=6), and fMLF-primed healthy blood (n=6). Significance was established by Mann-Whitney U-test and was set at **p*<0.05.

## 4.4 SLE LDGs are rougher than other SLE or healthy neutrophil subsets.

RT-DC showed SLE LDGs displayed distinct biomechanical features relative to other neutrophil subsets (Figure V-4). Compared to the consistently round, autologous SLE NDNs or healthy NDNs, SLE LDGs had a significantly rougher (*i.e.* more perturbed) cell surface. It has been uncertain whether LDGs are a population of neutrophils also present in very small numbers in healthy individuals but expanded in SLE [202]. Accordingly, I compared the biomechanical properties of SLE LDGs to the small population of healthy LDGs. Like their autologous healthy NDNs, and not consistent with the SLE LDG biomechanical phenotype, healthy LDGs had a consistently smooth surface. In addition, healthy LDGs were more deformable than autologous healthy NDNs (Figure V-3). These considerable differences in biomechanical properties of SLE and healthy LDGs suggest that the SLE LDG population does not merely represent expansion of an LDG population found in healthy individuals.

At this stage, it is early in the field's understanding of how a difference in deformability affects neutrophil function, and thus more research is necessary to determine why healthy LDGs are consistently more deformable than autologous healthy NDNs or indeed what meaningful impact it might have on neutrophil trafficking or function. This difference in deformability could be linked to nuclear morphology and how a multi-lobed nucleus versus a nucleus with fewer lobes responds to evenly distributed sheer pressure. Although the multi-lobed nucleus facilitates migration through small blood vessels by allowing the nucleus to stretch out and compress, in the context of RT-DC, shear pressure is evenly applied from both sides of the channel to the entire cell rather than to a section of the cell at a time. Thus, the multi-lobed nucleus could possibly lead healthy NDNs to be consistently given a slightly

stiffer read-out for deformability than their more immature, healthy LDG counterparts. However, as RT-DC is increasingly used in conjunction with studies of immune function in the future, we will develop a greater understanding of what a change in biomechanical properties actually means for a cell's ability to mount an immune response.

### 4.5 SLE LDGs morphologically differ from fMLF-stimulated NDNs.

As reported in Chapter IV, fMLF-primed neutrophils are morphologically rougher and, like LDGs, localise with the PBMCs during density gradient purification rather than with the erythrocytes and NDNs. In addition, the roughness of SLE LDGs and primed healthy NDNs were very similar. However, primed healthy NDNs were consistently larger than autologous un-primed NDNs, while SLE LDGs were similar in size to autologous SLE NDNs (Figure V-4), suggesting primed healthy NDNs and SLE LDGs are not identical cell populations at a biomechanical level.

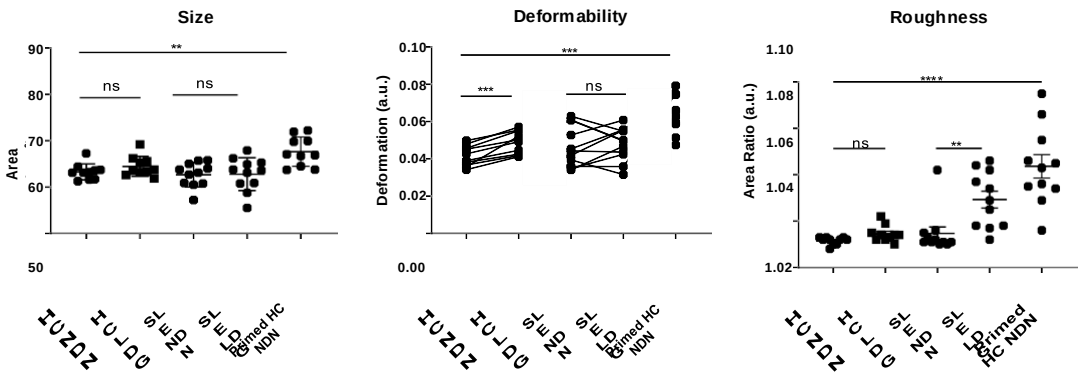


**Figure V-4: SLE LDGs are rougher than SLE NDNs or other healthy NDN subsets.**

Biomechanical profiling of isolated NDNs and LDGs from healthy (HC) volunteers (n=11) and clinically quiescent (*i.e.* stable) SLE patients (n=11) by RT-DC. Some HC NDNs were primed with fMLF prior to isolation. For each sample analysed by RT-DC, the median measurement of over 500 neutrophils is plotted and the mean ± SEM for each neutrophil subset is depicted. Autologous unstimulated/primed HC NDNs or autologous SLE NDNs/LDGs were compared and significance was established by Wilcoxon matched-pairs signed rank test. For other comparisons, significance was established by Mann-Whitney U-test. Significance was set at *$p$<0.05, **$p$<0.01, ns=not significant.

## 4.6 SLE LDG roughness is confirmed by scanning electron microscopy and lattice light-sheet microscopy.

The increase in roughness measured by RT-DC in primed healthy NDNs and SLE LDGs relative to unstimulated healthy and SLE NDNs was confirmed by light microscopy undertaken in parallel with RT-DC (Figure V-5A), as well as by scanning electron microscopy (Figure V-5B) and lattice light-sheet microscopy (Figure V-5C, D). Although RT-DC quantifications of roughness in SLE LDGs and primed healthy NDNs were similar, lattice light-sheet microscopy qualitatively indicated that these cell populations have very different shapes. The cell surface of primed healthy NDNs appeared to ruffle, with small membrane perturbations moving inwards and outwards. In contrast, the cell surface of SLE LDGs was largely smooth, except for sections of dramatic protrusion, which were irregularly shaped (Figure V-5C). Overall, these results indicate that SLE LDGs and primed healthy NDNs have different biomechanical properties compared to un-primed healthy NDNs. Furthermore, while both SLE LDGs and primed healthy NDNs displayed perturbations in their cell membranes, the morphology of these changes appears to be different between the two cell types. In addition, SLE LDGs did not morphologically resemble healthy NDNs treated with PMA to induce NETosis.

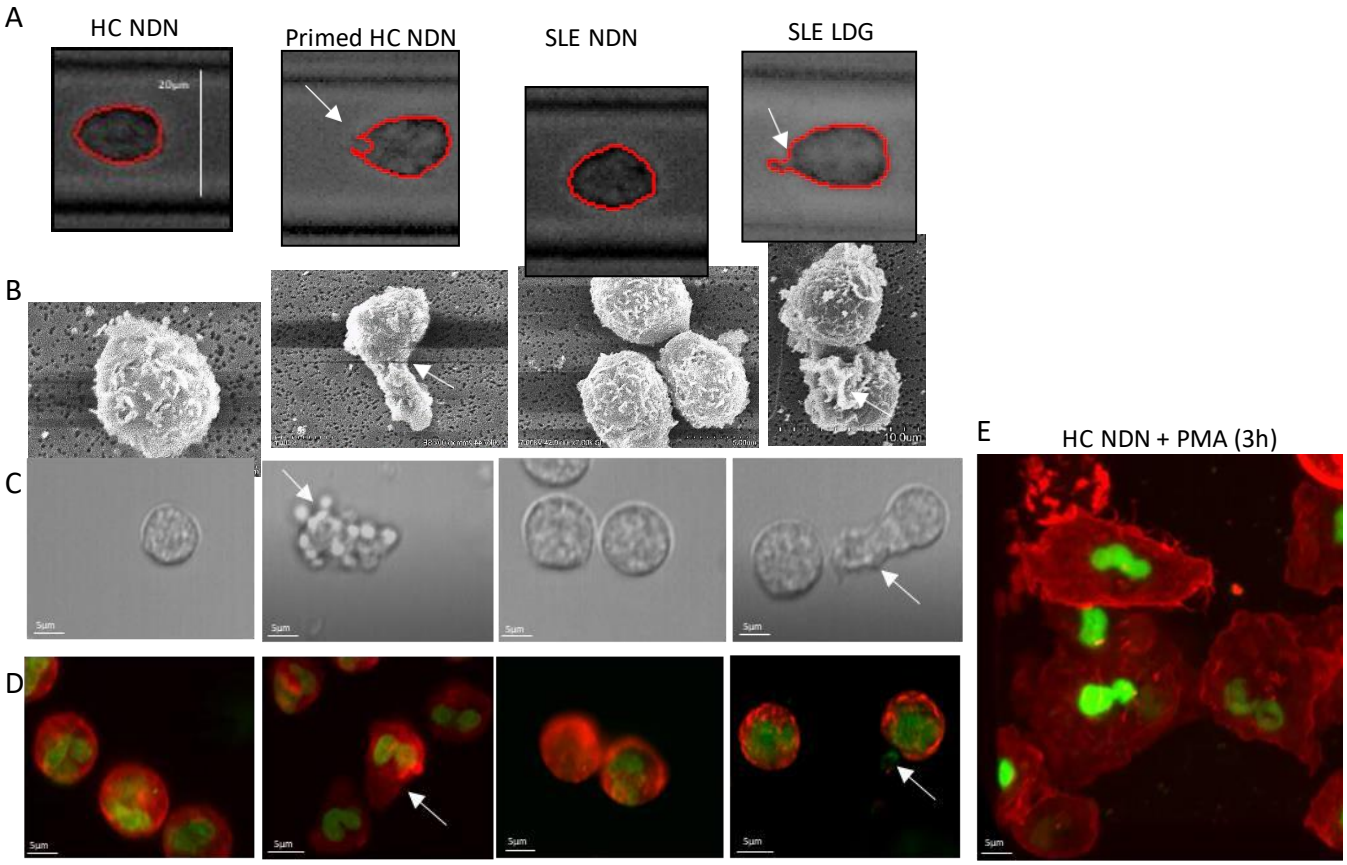


**Figure V-5: SLE LDG roughness is confirmed by lattice light-sheet microscopy and scanning electron microscopy.**

(A) Images of NDNs and LDGs captured during RT-DC, representative of >500 images of each neutrophil subset from n=11 SLE patients and n=11 HC volunteers, 10x objective. White arrows identify a concave cell surface feature common in primed healthy NDNs and an irregular protrusion in the cell surface common in SLE LDGs. (B) Neutrophils captured by scanning electron microscopy. White arrows identify a concave cell surface feature common in primed healthy NDNs and an irregular protrusion in the cell surface common in SLE LDGs. Images representative of n=5. (C) Images of NDNs and LDGs captured by the bright field of a lattice light-sheet microscope. Images representative of n=3. White arrows identify a concave cell surface feature observed in 100% of primed healthy NDNs and an irregular protrusion in the cell surface present in ~30% of SLE LDGs. (D) Neutrophils stained for actin (far red) and DNA (green) by a SiR-actin probe and sytox green and imaged by lattice light-sheet microscopy. Images representative of n=2. White arrows identify a concave cell surface feature observed in 100% of primed healthy NDNs and an irregular protrusion in the cell surface present in ~30% of SLE LDGs. (E) Healthy NDNs undergoing NETosis induced by stimulation with 25 nM PMA for three

## 4.7 SLE LDG roughness correlates with SLE patient age but not with other clinical or demographic features.

Overall, no clinical or demographic characteristics were associated with specific SLE LDG biomechanical properties, with the exception that age of the SLE subjects correlated negatively with LDG roughness (Figure V-6).

## 4.8 Neutrophil roughness is not affected by SLE-derived Sm/RNP immune complexes or type 1 interferon but is increased by heterologous serum.

To determine whether SLE-relevant immune stimuli may promote the biomechanical properties observed in SLE LDGs, I exposed healthy NDNs to 10 ng/mL Sm/RNP immune complexes isolated from SLE patient serum [50] and/or 1000-2000 units/mL recombinant human IFN-α for timepoints ranging from 45 minutes to three hours. I hypothesised that SLE LDGs might represent a neutrophil that had been primed by the unique autoinflammatory environment that it was exposed to, and thus by using immunostimulatory agents found in the blood of patients with SLE, such as type I IFN or immune complexes, I might be able to induce healthy NDNs to take on the biomechanical phenotype of the SLE LDG.

Although I established that the Sm/RNP immune complexes generated from the serum of patients with SLE induce NETosis in healthy NDNs (Figure V-7A-B), these stimuli did not lead to an increase in NDN roughness (Figure V-7C, E). In addition, I exposed healthy NDNs to serum from autologous or heterologous healthy donors, as well as serum from patients with active SLE. Interestingly, heterologous serum, whether from a healthy donor or active patient, increased NDN roughness (Figure V-7D). These results indicate that the differential biomechanical properties displayed by SLE LDGs do not appear to be related to exposure to immune complexes or type I IFNs. In addition, these results provide more support for the concept that neutrophil exposure to specifically autologous serum is critical to preserve viability during isolation.

## 4.9 Design of a novel microfluidic microvasculature mimetic.

Recent observations have demonstrated a putative role for neutrophil biomechanical properties in modulation of transit through the pulmonary microvasculature. Indeed, primed neutrophils are increasingly retained in the lungs [116], possibly due to enhanced cell stiffness and/or irregular cell shape [41]. To mimic trafficking through the pulmonary microvasculature, I developed a mimetic formed of a branched pyramidal network within a polydimethylsiloxane (PDMS) chip (Figure V-8A). Trafficking through the mimetic did not impact neutrophil viability (Figure V-8B).

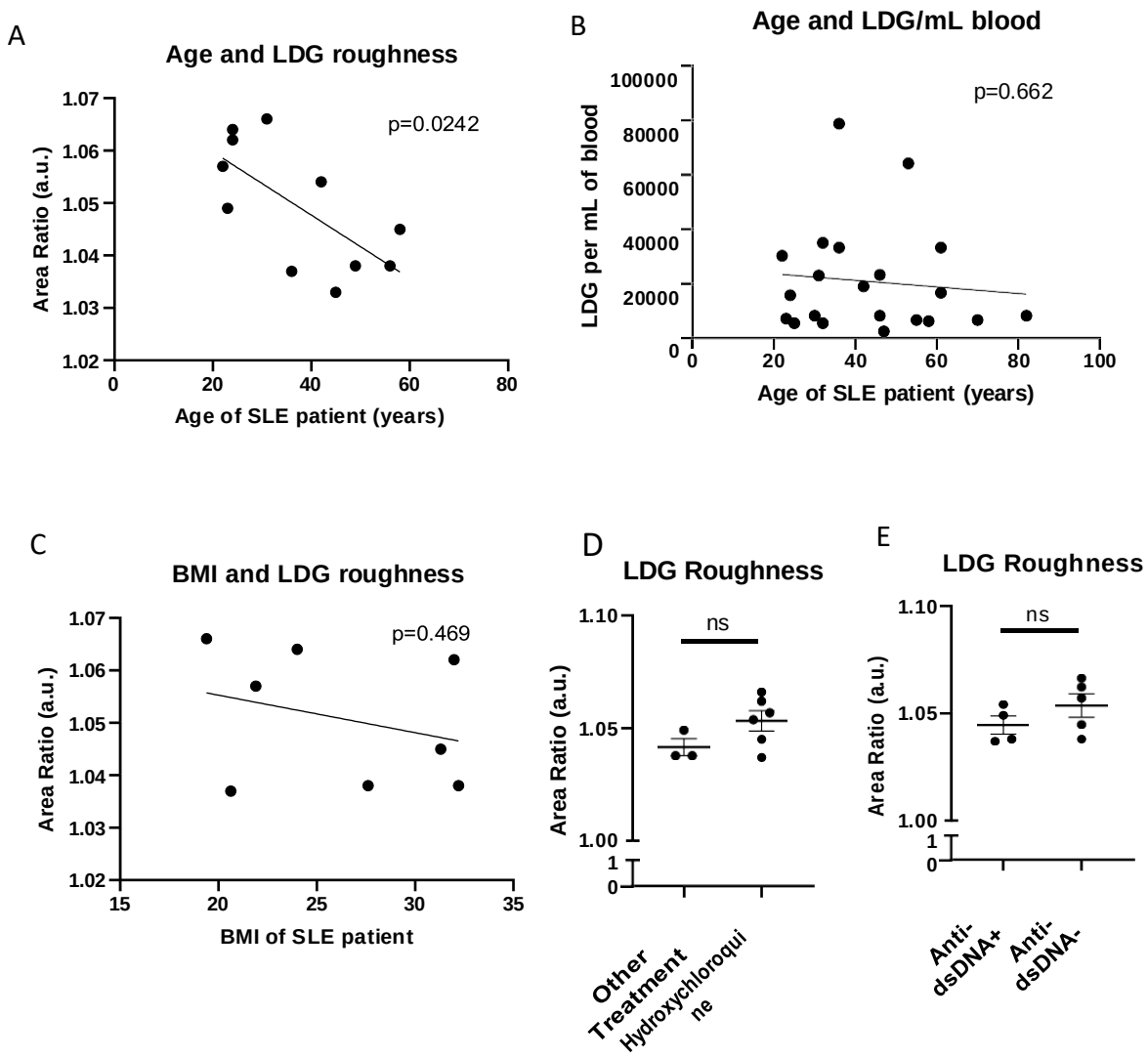


**Figure V-6: SLE LDG roughness correlates with patient age but no other clinical or demographic characteristics.**

(A) Correlation of LDG roughness with SLE patient age in SLE (n=11). (B) Correlation of LDG numbers with age of SLE patient (n=21). (C) Correlation of LDG roughness with BMI in SLE patients (n=8). For all correlations, significance was assessed by linear regression analysis and set at **p*<0.05, ns=not significant. (D) LDG roughness in SLE subjects treated with hydroxychloroquine (n=5) or other treatments (n=3). (E) LDG roughness in SLE patients positive (n=4) or negative (n=4) for serum anti-dsDNA antibodies. Roughness was determined by RT-DC. The median roughness measurement from over 500 neutrophils from each subject is plotted and the mean± SEM for each treatment or clinical category is depicted. For D and E, significance was established by Mann-Whitney U-tests and set at **p*<0.05, ns=not significant. Note that blood from patients treated with steroids were not analysed for these experiments given the known connection between steroids and changes to neutrophil morphology.

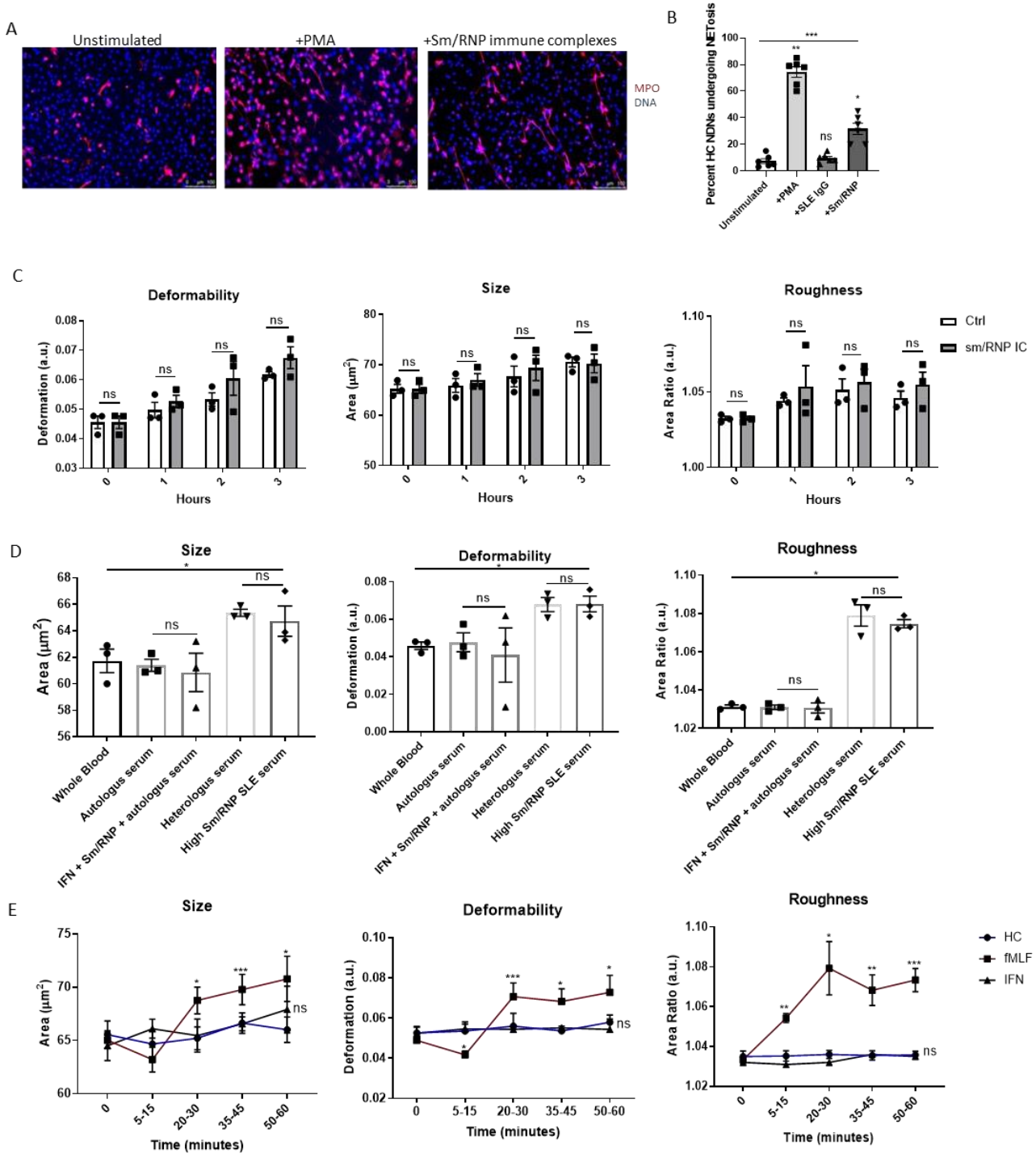
A
Unstimulated
+PMA
+Sm/RNP immune complexes
MPO
DNA
B
Percent HC NDNs undergoing NETosis
Unstimulated
+PMA
+SLE IgG
+Sm/RNP
C
Deformability
Size
Roughness
Deformation (a.u.)
Area (μm²)
Area Ratio (a.u.)
Hours
Ctrl
sm/RNP IC
D
Size
Deformability
Roughness
Area (μm²)
Deformation (a.u.)
Area Ratio (a.u.)
Whole Blood
Autologus serum
IFN + Sm/RNP + autologus serum
Heterologus serum
High Sm/RNP SLE serum
E
Size
Deformability
Roughness
Area (μm²)
Deformation (a.u.)
Area Ratio (a.u.)
Time (minutes)
HC
fMLF
IFN

**Figure V-7: Immune stimuli associated with SLE do not modulate the biomechanical properties of healthy neutrophils.**

(A, B) Sm/RNP immune complexes used for downstream RT-DC analysis induce *in vitro* NET formation in HC NDNs (n=6). Healthy NDNs were treated with 10 ng/mL of Sm/RNP immune complexes for 3 hours to induce NETosis before cells were fixed and stained by immunofluorescence. Red indicates MPO, blue indicates DNA. (C) Biomechanical profiling of HC NDNs incubated with 10ng/µl Sm/RNP immune complexes or with DMSO over three hours by RT-DC (n=3). (D) Biomechanical profiling of HC NDNs treated with autologous HC, heterologous HC, or heterologous, active SLE patient serum for 45 minutes by RT-DC. Some HC NDNs were also treated with 10ng/µl Sm/RNP immune complexes and 1000units/mL IFNα (n=3). (E) Biomechanical profiling over time of neutrophils in HC blood stimulated with DMSO, 100nM fMLF, or 1000units/mL IFNα (n=3). For each sample analysed by RT-DC, each graphical point shows the median of >500 neutrophils, and the mean±SEM of those medians for each cell subset is depicted. For C & E, unstimulated neutrophils treated with DMSO were compared to stimulated neutrophils from autologus donors at matched time points. For D, neutrophils from autologus donors treated with different serum samples were compared. Significance was established by

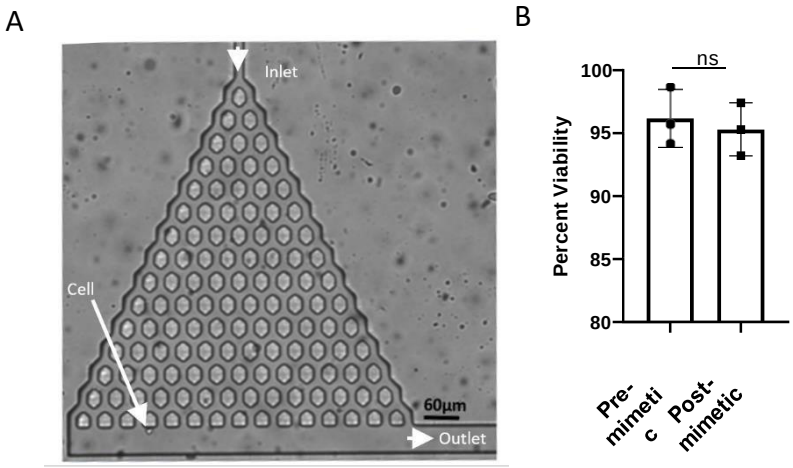


**Figure V-8: Design and production of a microvasculature mimetic.**

(A) A branching microfluidic mimetic of the pulmonary microvasculature was designed. Arrows indicate the inlet, outlet, and a cell navigating the network, 10x objective. (B) Neutrophil viability before and after transiting the microvasculature mimetic (n=3). Significance was established by Mann Whitney U-test and set at *$p$<0.05, ns=not significant.

## 4.10 A microvasculature mimetic increasingly retains SLE LDGs.

Purified SLE NDNs and autologous LDGs, as well as un-primed and primed (20 minutes, 100nM fMLF) healthy NDNs, were suspended in PBS and advected through the branched vasculature mimetic at 37 degrees C and physiologically relevant pressure. Data presented was collected at 50 mbar; that is, 51.0 $cmH_2O$, as has been used in previous vasculature mimetic studies [41].

Consistent with previous observations [41, 116], primed healthy NDNs were increasingly retained in the branched network, with over 80 per cent unable to fully navigate the mimetic (Figure V-9A). In contrast, over 80 per cent of un-primed healthy NDNs navigated the pulmonary microvasculature mimetic within three seconds. Trafficking patterns of the SLE LDGs resembled those observed in primed healthy NDNs, with over 75 per cent of SLE LDGs retained in the mimetic network compared to just over 50 per cent of autologous SLE NDNs (Figure V-9A). Of the neutrophils able to transit the entire capillary mimetic, both SLE and un-primed healthy NDNs averaged a transit time of just under 0.9 seconds, while SLE LDGs and primed healthy NDNs averaged transit times of 1.87 and 2.89 seconds respectively (Figure V-9B).

In addition, healthy NDNs were treated with 0.1 µM cytochalasin D, a molecule that disassembles filament actin and thereby decreases the deformability of neutrophils [130]. Cytochalasin D-treated neutrophils have previously been used in RT-DC studies as a control group to verify that it is a biomechanical change driving the experimental results, rather than some yet to be recognised and thus uncontrolled molecular driver [82]. Altering the biomechanical properties of healthy NDNs with cytochalasin D led to increased retention of the cells in the pulmonary microvasculature mimetic, with over 75 per cent of cytochalasin D treated healthy NDNs retained compared to under 20 per cent of healthy NDNs treated with 0.025 per cent (v/v) DMSO (Figure V9-C). Taken together, these results support a role for modulation of biomechanical properties in mediating neutrophil trafficking and suggest that, like primed healthy NDNs [116], SLE LDGs could be increasingly retained in microvasculature networks due to their differing biomechanical properties.

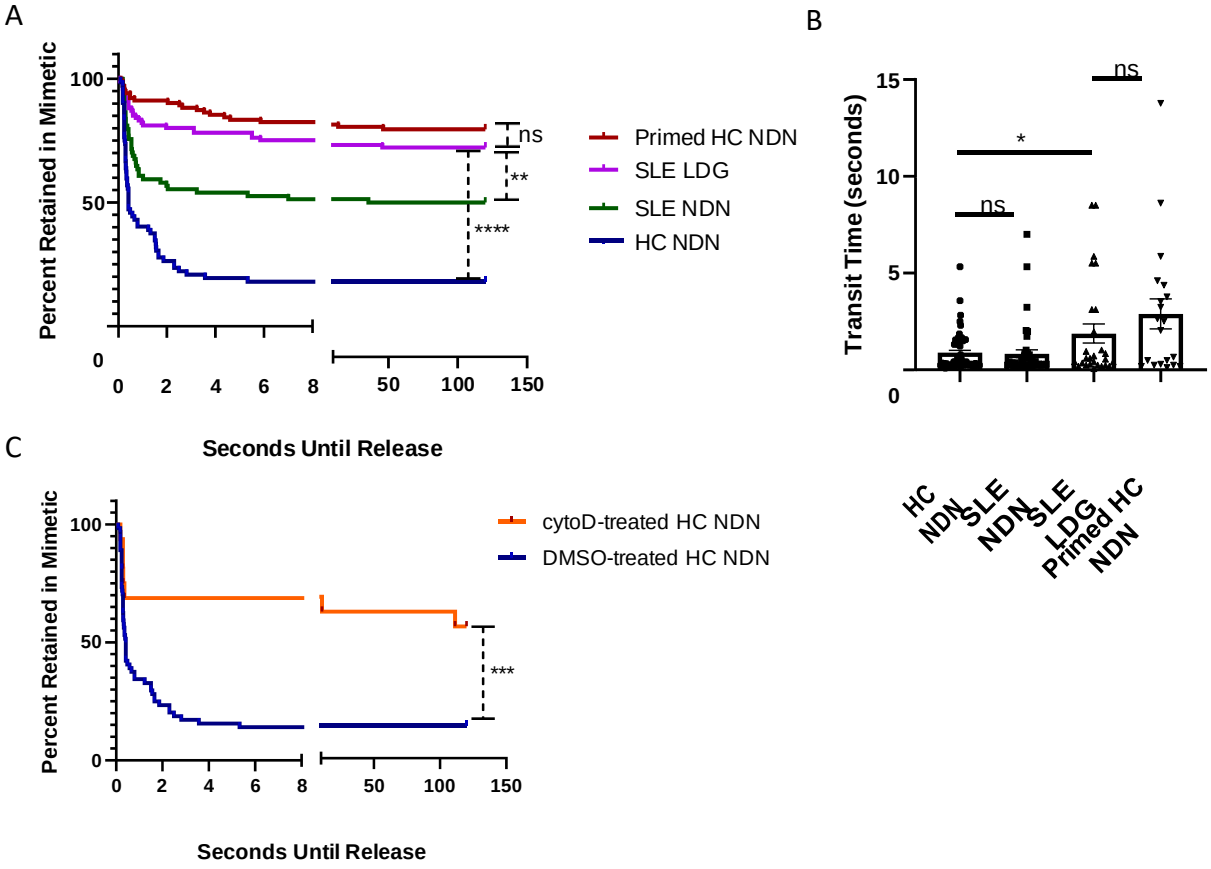


**Figure V-9: SLE LDGs are increasingly retained within a three-dimensional pulmonary microvasculature mimetic.**

(A) Retention of NDNs and LDGs in the microvasculature mimetic (n>150 neutrophils per subset from n=6 HC volunteers and n=6 SLE patients). Seconds until release refers to the amount of time each neutrophil was retained within the mimetic, measured from entry at the inlet to exit at an outlet. Seconds until release was recorded as >120 seconds if cells did not exit the mimetic within two minutes. Times were determined manually with a blinded analyser and a timer superimposed on the video during data collection. Significance was determined by log-rank test. (B) Transit times through the microvasculature mimetic for all NDNs and LDGs navigating the entire device. Significance was assessed by Mann-Whitney U-test. (C) Retention of HC NDNs treated with DMSO or 0.1 µM cytochalasin D in the microvasculature mimetic (n>50 neutrophils from n=3 HC volunteers). Significance was determined by log-rank test. All results are mean ± SEM with significance was set at *$p$<0.05, **$p$<0.01, ****$p$<0.0001, ns=not significant.

## 4.11 SLE LDGs do not increasingly bind endothelial cells under a system of flow.

The pulmonary microvasculature mimetic is a three-dimensional system that evaluated the effects of cellular biomechanical properties on trafficking but did not address the putative role of neutrophil cell surface molecules (such as integrins) and their interactions with the endothelium to modulate cell traffic. By decoupling the effects of biomechanical properties and cell-surface markers on neutrophil trafficking, I aimed to evaluate their independent contributions. Accordingly, I performed a two-dimensional assay evaluating neutrophil interactions with the microvascular endothelium under a circulatory flow system mimicking physiological conditions at 37 degrees C and flow rate of 0.4 mL/min. Confluent human lung microvascular endothelial cells were expanded in Ibidi® μ-slide VI 0.4 chambers in the presence or absence of TNF and IFNγ for 4 hours. Isolated un-primed and primed healthy NDNs, SLE LDGs and autologous SLE NDNs were flowed across the endothelial cell monolayer at a constant rate of 0.4 mL/min over a three-minute observation period (Figure V-10). The percentage of neutrophils either rolling along or adhering to endothelial cells during this observation period was quantified and the results were compared among subsets. Overall, 15 per cent of primed healthy NDNs interacted with unstimulated endothelium, compared to less than 10 per cent of healthy NDNs, SLE LDGs, and SLE NDNs ($p<0.01$) (Figure V-10A). Furthermore, 60 per cent of primed healthy NDNs interacted with activated endothelium, compared to less than 20 per cent of unstimulated healthy NDNs, SLE LDGs, and SLE NDNs ($p<0.01$) (Figure V-10B). These observations suggested a potential role for neutrophil-endothelium interactions in the retention of primed healthy NDNs in the microvasculature. In contrast, levels of SLE LDG and SLE NDN interaction with endothelium were similar ($p>0.05$), suggesting that neutrophil-endothelial interactions are unlikely to be responsible for any differences in trafficking between SLE LDGs and NDNs.

Taken together, results from the three-dimensional microvasculature mimetic and the two-dimensional endothelial flow assay suggest that the SLE LDGs may be increasingly retained in microvasculature networks relative to SLE NDNs, similar to what has been described for primed healthy NDNs relative to healthy NDNs [116]. SLE LDG retention may be driven by intrinsic changes in biomechanical properties rather than by specific interactions with the endothelium, while retention of primed healthy NDNs may be driven by a combination of their interactions with the endothelium and biomechanical properties.

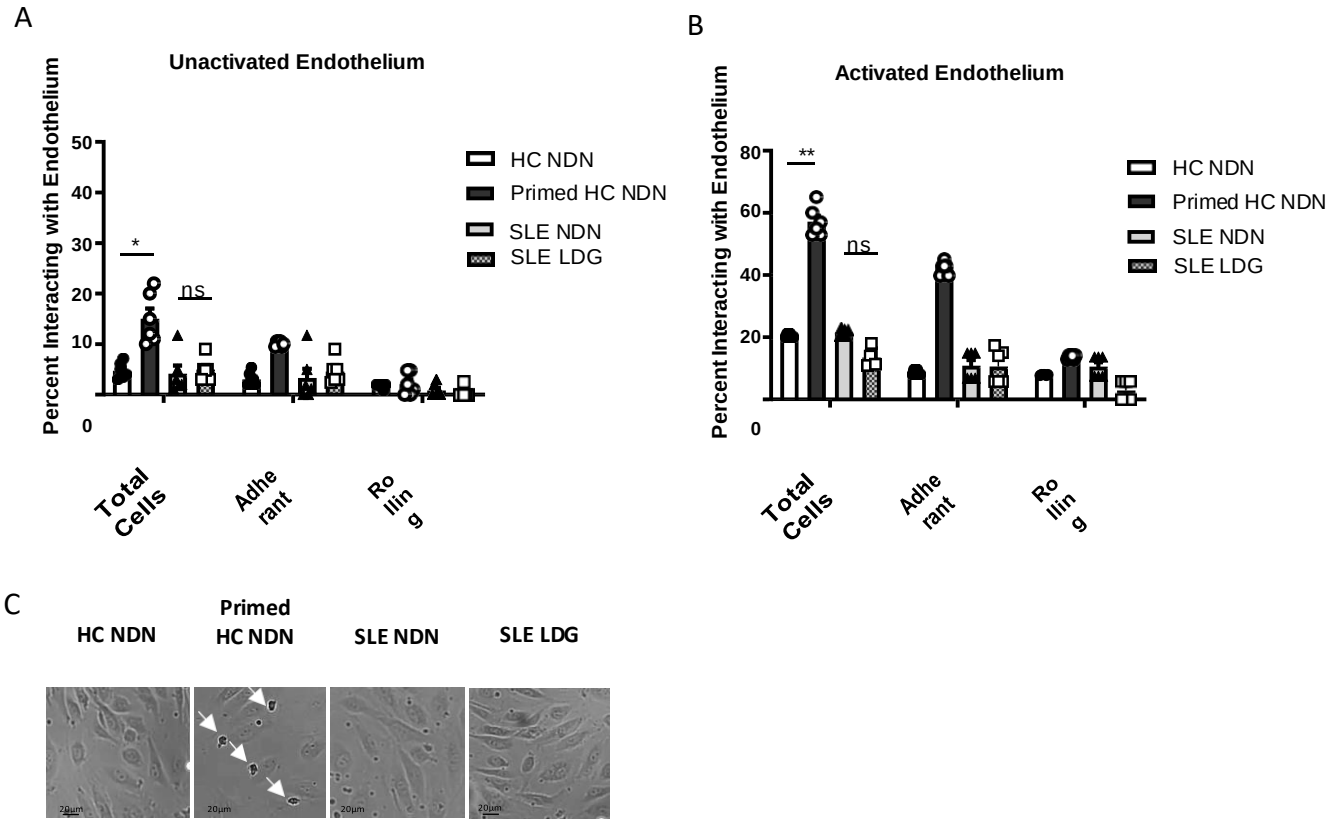


**Figure V-11: SLE LDGs do not display enhanced adherence to endothelial cells in a two-dimensional system of flow.**

(A) Percentage of neutrophils interacting with endothelium under 0.4 mL/min flow. (B) For some experiments, endothelium was activated with IFNγ and TNFα. Significance was determined by Kruskal-Wallis test with post hoc Dunn's tests for multiple comparisons. (C) Light microscopy of neutrophil binding to un-activated endothelium post-flow assay with a 20x objective. Arrows show enhanced binding of primed NDNs. Images are representative of n=4 images obtained for each neutrophil subset isolated from n=6 SLE patients or n=6 HC volunteers. All results are mean ± SEM with significance was set at *$p$<0.05, **$p$<0.01, ns=not significant.

## 5. Discussion

Previously, transcriptomic analyses identified differential expression of genes associated with the actin cytoskeleton in SLE LDGs relative to autologous SLE NDNs [200]. Consistent with this report, I found that SLE LDGs were biomechanically distinct from SLE and healthy NDNs. Specifically, SLE LDGs have a rougher cell surface than unstimulated neutrophils, with more perturbations in their cytoskeleton. This phenotype is distinct from that observed in healthy, *in vitro* primed neutrophils. Despite quantitative measurements of roughness being similar in SLE LDGs and primed neutrophils, lattice light-sheet microscopy revealed SLE LDGs have a wide, irregular protrusion from one side of the cell, while primed neutrophils have small, rounded protrusions ruffling along the entire cell membrane. As determined in Chapter IV, neutrophils primed with fMLF for 20 minutes undergo macropinocytosis, and the observed membrane protrusions are consistent with membrane ruffling associated with macropinocytosis [164].

A mechanism potentially responsible for enhanced cell surface roughness in LDGs is their enhanced ability to form NETs, as this process promotes cytoskeleton perturbations and disruptions in the integrity of the cell membrane [193, 203-205]. Although SLE LDGs do not appear to morphologically resemble healthy control neutrophils induced to undergo NET formation by PMA stimulation under lattice light-sheet microscopy, previous studies have found distinct differences in spontaneous LDG NET formation and PMA-induced NET formation regarding kinetics and intracellular pathways involved [206], induction of vasculopathy [50, 56], and possibly additional factors. The potential link between NET formation and cytoskeletal roughness in SLE LDGs could be more fully addressed with *in vitro* inhibitors of NET formation in future research studies.

Changes in neutrophil morphology have been previously associated with functional dysregulation in their ability to circulate in the microvasculature, with rougher, primed neutrophils increasingly retained in the lungs [41, 207]. The results obtained using a microvasculature mimetic suggest that SLE LDG roughness may similarly hinder the SLE LDG's ability to traffic through narrow microcapillaries and supports the hypothesis that biomechanical properties are critical in mediating neutrophil trafficking. These differences in biomechanical properties could have important implications in the context of lupus manifestations in various organs (*e.g.* lungs, kidneys), and in the development of small vessel vasculopathy. For example, the development of pulmonary arterial hypertension (PAH), vasculopathy in lung capillaries, and other types of lung vascular involvement are severe and important complications in SLE associated with blood vessel damage, and are instances in which neutrophils have been proposed to play pathogenic roles [208-210]. Indeed, circulating immune complexes, typically abundant in SLE, can induce neutrophil activation by both Fc and complement receptors. This can trigger the release of proinflammatory molecules promoting endothelial cell barrier dysfunction and increasing vascular permeability [211, 212]. As such, while the distinct biomechanical properties of SLE LDGs did not

align with preferential binding of these cells to microvascular endothelial cells, LDGs are known to have potent deleterious effects on the endothelium through NET-mediated effects independent of endothelial cell activation [50, 213, 214]. Accordingly, I propose a model in which slow transit of SLE LDGs in the microvasculature coupled to an enhanced ability to form NETs in circulation and in tissues, would promote both endothelial cell damage and vasculopathy, with important pathogenic consequences that may be further exacerbated by circulating immune complexes. Future studies should determine both the mechanism of enhanced SLE LDG roughness and the *in vivo* significance of its effect on SLE LDG trafficking.

In contrast to SLE LDGs, *in vitro* primed healthy NDNs showed enhanced ability to adhere to both activated and non-activated endothelium. Overall, these data support that SLE LDGs are distinctly different, biomechanically and in their interactions with the vasculature, to acutely primed neutrophils. To pursue this line of research further, an easy and important experiment would be to prime SLE NDNs with 100nM of fMLF to determine how their biomechanical properties or abilities to traffic through the MM change. Despite some clear differences between healthy primed NDNs and SLE LDGs with respect to biomechanical properties and interactions with the vasculature, these differences could be driven by differences in disease statues (SLE versus healthy), rather than indicating that SLE LDGs are not conventionally primed neutrophils. In addition, I treated healthy NDNs with various immunostimulatory agents present in the blood of patients with SLE (*e.g.* immune complexes, type 1 IFNs) in an attempt to induce and thus begin to understand the unique biomechanical properties of SLE LDGs. Perhaps a more fruitful line of investigation would have been to treat SLE NDNs with those various immunostimulatory agents. At this point, it is not fully clear how neutrophils from healthy volunteers and patients with stable SLE may be innately different from each other and despite their near-identical biomechanical phenotypes, there may exist unrecognised differences linked to biomechanical changes associated with priming which would be important to explore further. However, given how different primed healthy NDNs look from SLE LDGs via lattice light sheet microscopy and scanning electron microscopy, my initial hypothesis is that the biomechanical differences between SLE NDNs and SLE LDGs is driven by a different mechanism than the macropinocytosis-driven membrane ruffling and expansion seen in healthy primed NDNs.

In addition to these experiments around priming of SLE NDNs, I would have liked to complete experiments aimed at measuring trafficking of neutrophils treated with amiloride through the MM. In Chapter IV, I reported that pre-treatment of neutrophils with amiloride blocked subsequent priming-induced biomechanical changes. I could have supported this conclusion further by similarly pre-treating primed neutrophils before sending them through the MM. Amiloride-treated neutrophils do not undergo biomechanical changes to size and roughness, so I hypothesise that they would not be retained in the MM. If my hypothesis was correct, those observations would support my conclusions that 1)

biomechanical changes are linked to retention in the MM and 2) macropinocytosis drives biomechanical changes in primed healthy NDNs.

While the origin of LDGs in inflammatory diseases remains to be fully characterised [152, 215], I determined that SLE LDGs are biomechanically distinct from resting or primed healthy neutrophils, supporting that LDGs may be a distinct neutrophil subset in inflammatory diseases [152], and do not appear to be an expanded population of immature or primed neutrophils also present in healthy individuals. The variability in LDG roughness among SLE subjects supports previous observations at the transcriptomic level that these cells represent a heterogenous cell subset with some degree of plasticity [200]. Future studies will be necessary to fully elucidate the origin of LDGs and the factors that modulate their various pathogenic properties. As mentioned above, initial studies around priming of SLE NDNs may be a good place to start.

Overall, my observations indicate that SLE LDGs have specific biomechanical features that may impact ability to transit through the microvasculature. This chapter adds to our understanding of neutrophil heterogeneity in the context of blood vessel trafficking, with potentially important implications for the development of small vessel vasculopathy and clinical manifestations in specific organs in SLE such as the lungs and kidneys. The results have potential implications for the development of therapeutics that may modulate neutrophil biomechanical properties [127] and continue to support that LDGs have pleiotropic pathogenic roles in autoimmune diseases. This theme of LDG pathogenicity will be further explored and discussed in Chapter VI.

# Chapter VI: Proteomic and phosphoproteomic profiling describe SLE LDG biology and potential mechanisms modulating their unique biomechanical signature.

## 1. Chapter Introduction

As discussed in Chapter V, although it has been well documented that LDGs are a proinflammatory neutrophil subset promoting tissue and vascular damage in several inflammatory diseases [193], previous studies to understand the origin and pathogenicity of SLE LDGs have focused primarily on transcriptomic data [56, 193, 194, 198, 199]. As neutrophils are characteristically less transcriptionally active and have lower RNA content than other cell types, storing many of their proteins in granules and other intracellular compartments, I wanted to assess if differences in the neutrophil proteome and phosphoproteome contribute to some of the functional or biomechanical abnormalities described in SLE LDGs. The SLE LDG proteome and phosphoproteome relative to autologous SLE or healthy NDNs, have not been systematically characterised. It is not known how distinctions in proteomics may contribute to the SLE LDG's strong proinflammatory potential, nor whether the proteome or phosphoproteome may modulate SLE LDG biomechanical properties. In this chapter, I used proteomic and phosphoproteomic analyses to compare SLE LDGs, SLE NDNs, healthy NDNs and healthy NDNs primed with fMLF. I identified differential phosphorylation of proteins associated with cytoskeletal organisation in SLE LDGs relative to other neutrophil subsets, suggesting a potential mechanism responsible for the unique SLE LDG biomechanical phenotype. In addition, this analysis provided a substantial number of new insights pertaining to SLE LDG biology as well as neutrophil heterogeneity at the proteome and phosphoproteome levels.

## 2. Hypothesis and Aims

*The SLE LDG proteome and phosphoproteome are distinct from those of other neutrophil subsets.*

- To understand neutrophil heterogeneity at the proteome and phosphoproteome levels.
- To reveal new insights into SLE LDG biology and function.
- To compare proteomes and phosphoproteomes of healthy neutrophils with SLE neutrophils.
- To identify potential mechanisms regulating the SLE LDG biomechanical phenotype.
- To reveal the effect of neutrophil priming on the proteome and phosphoproteome.

## 3. Method Notes

The techniques discussed in this chapter have been detailed in Chapter II, specifically in sections 18 and 19.2. The proteomics and phosphoproteomics workflow is summarised in Figure II-1. All neutrophil preparations were purified using a Ficoll gradient followed by EasySep isolation of SLE LDGs from the PBMC layer and NDNs from the layer of erythrocytes and granulocytes. This protocol was optimised to minimise biomechanical disruption of cells from their unstimulated state in whole blood, as was described in Chapter III. To complete these proteomic analyses, I first assessed protein degradation in my samples and completed label-free proteomics to ensure the lysis buffer I planned to use delivered good quality results. After determining my methods were appropriate, I performed the II-TMT labelling with assistance from the proteomics core facilities at the National Heart, Lung, and Blood institute. The key results are detailed below.

# 4. Results

## 4.1 Label-free proteomics indicates successful preparation of neutrophils.

Label-free proteomics of heathy NDNs, primed healthy NDNs, and SLE NDNs (n=1) was completed to ensure good quality results would be obtained during 11-TMT labelling. Protein degradation was low (Figure VI-1A) and 1426 total proteins were identified, with some variation between neutrophil subsets (Figure VI-1B). An RNA-Seq data set generated by a collaborator, Dr. Luis Franco, was aligned with the healthy neutrophil proteome (Figure VI-C) and it was clear that the lysis buffer used for the proteomics successfully identified proteins encoded by the entire spectrum of high abundance to low abundance RNA transcripts. This suggested the lysis buffer effectively preserved proteins from degradation and would allow for deep proteomic profiling.

## 4.2 Successful 11-TMT labelling of four neutrophil subsets.

I undertook proteomics and phosphoproteomics using TMT-labelling of SLE LDGs, autologous SLE NDNs, and healthy (HC) NDNs purified from 5 subjects with SLE and 5 age/sex/race-matched healthy volunteers (Table VI-1). Although these patients with SLE were heterogenous with respect to disease presentation and medication, for the proteomics experiments it was critical to be able to age, sex, and race-match patients to healthy volunteers, and to have these individuals able to donate blood on the same day. Same-day donations were important for purposes of controlling the neutrophil isolation process. To help control for the variability in SLE patient clinical manifestations and antibody presentation, only proteins or phospho-proteins different in 4+ of the matched SLE LDG/NDN samples or 4+ patient/healthy volunteer matched pairs were included in analysis.

Some healthy NDNs were analysed following priming with 100 nM fMLF for 20 minutes. This served as the nearest possible healthy control for SLE LDGs, as priming decreases HC NDN density (as described in Chapter V) and it was unethical to draw the amount of blood from a healthy volunteer that would have been required to obtain sufficient innate healthy LDGs for proteomics.

Mass spectrometry analysis identified 4109 proteins (Figure VI-2A) in the neutrophil proteome. This was comparable to the most robust neutrophil proteomic analysis previously completed [216]. 875 proteins were identified to be phosphorylated in serine, threonine, and/or tyrosine residues in neutrophils (Figure VI-2B). Some proteins were phosphorylated at multiple sites (Table VI-2). For the purposes of technical validity, individual proteins and phosphoproteins were independently identified and quantified in all five donors; those identified in fewer than four donors were not included in subsequent analyses. However, total protein and phosphoprotein levels were very stable within neutrophils from the same conditions (*e.g.* SLE NDNs, healthy NDNs), despite ample variation in protein expression and abundance when neutrophil subsets are compared. Unsurprisingly, unstimulated and primed healthy NDN proteomes consisted of the same proteins with very little variation in protein

abundance (Figure VI-2). An exception was L-selectin; abundance was lower in primed healthy NDNs, suggesting shedding of this protein and validating *in vitro* activation [217] (Figure VI-3B).

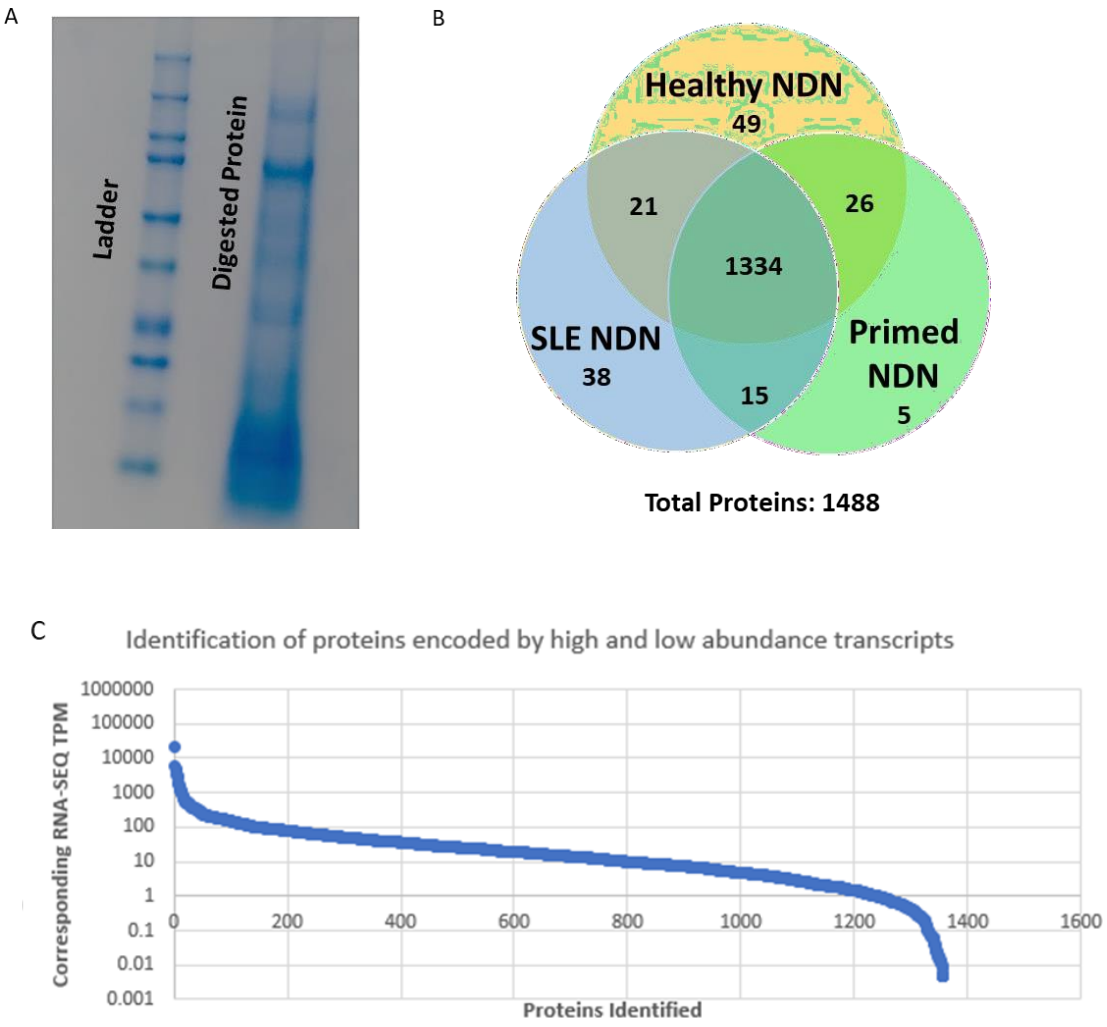


**Figure VI-1: Label-free proteomics indicates successful preparation of neutrophil lysates.**

(A) Digested protein separated by SDS-PAGE and stained with colloidal blue staining shows minimal protein degradation. (B) Distribution of 1426 total proteins identified by label-free proteomics. Heterogeneity is identified among neutrophil subsets. (C) Allignment of healthy NDN proteins identified by label-free proteomics with their corresponding RNA-SEQ transcript in transcripts per million (TPM).

Matched donors for proteomics

| SLE Donors | | Healthy Donors | |
|---|---|---|---|
| Age | Sex | Age | Sex |
| 61 | F | 64 | F |
| 36 | F | 35 | F |
| 32 | F | 31 | F |
| 53 | F | 50 | F |
| 46 | F | 45 | F |
| Avg=45.6 | | Avg=45.0 | |

SLE Demographics and SLEDAI

| LE Num | Visit Date | Gender | Age | Year of Diagnosis | Disease duration years | Ethnicity | SLEDAI TOTAL AT FIRST APPOINTMENT | SLEDAI SEIZURE | SLEDAI PSYCHOSIS | SLEDAI OBS | SLEDAI VISUAL DISTURB | SLEDAI CRANIAL NERVE | SLEDAI LUPUS HEADACHE | SLEDAI CVA | SLEDAI VASCULITIS | SLEDAI ARTHRITIS | SLEDAI MYOSITIS | SLEDAI URINARY CAST | SLEDAI HEMATURIA | SLEDAI PROTEINURIA | SLEDAI PYURIA | SLEDAI RASH | SLEDAI ALOPECIA | SLEDAI MUCOSAL ULCERS | SLEDAI PLEURISY | SLEDAI PERICARDITIS | SLEDAI LOW COMPLEMENT | SLEDAI INC DNA BIND | SLEDAI FEVER | SLEDAI THROMBOCYTOPENIA | SLEDAI LEUKOPENIA | SLEDAI TOTAL |
|---|---|---|---|---|---|---|---|---|---|---|---|---|---|---|---|---|---|---|---|---|---|---|---|---|---|---|---|---|---|---|---|---|
| LE-19-375 | 10/18/2019 | F | 61 | 2000 | 20 | African American | 2 | 0 | 0 | 0 | 0 | 0 | 0 | 0 | 0 | 0 | 0 | 0 | 0 | 0 | 0 | 0 | 0 | 0 | 0 | 0 | 0 | 2 | 0 | 0 | 0 | 2 |
| LE-19-388 | 10/24/2019 | F | 36 | 2010 | 10 | Hispanic | 12 | 0 | 0 | 0 | 0 | 0 | 0 | 0 | 0 | 0 | 4 | 0 | 0 | 0 | 0 | 2 | 2 | 0 | 0 | 2 | 2 | 0 | 0 | 0 | 0 | 8 |
| LE-19-419 | 11/18/2019 | F | 34 | 2012 | 8 | Hispanic | 4 | 0 | 0 | 0 | 0 | 0 | 0 | 0 | 0 | 0 | 0 | 0 | 0 | 0 | 0 | 0 | 2 | 0 | 0 | 0 | 0 | 2 | 0 | 0 | 0 | 4 |
| LE-19-433 | 11/25/2019 | F | 53 | 1992 | 28 | Caucasian | 0 | 0 | 0 | 0 | 0 | 0 | 0 | 0 | 0 | 0 | 0 | 0 | 0 | 0 | 0 | 0 | 0 | 0 | 0 | 0 | 0 | 0 | 0 | 0 | 0 | 0 |
| LE-19-432 | 11/25/2019 | F | 46 | 2003 | 17 | Hispanic | 8 | 0 | 0 | 0 | 0 | 0 | 0 | 0 | 0 | 4 | 0 | 0 | 0 | 0 | 0 | 0 | 0 | 0 | 0 | 0 | 2 | 2 | 0 | 0 | 0 | 8 |

Lab

| LE Num | Visit Date | Weight Kg | Height Cm | BMI | C3 | C4 | Anti-dsDNA | ANA | ENA | Anti-Sjogren's sy. A | Anti-Sjogren's sy. B | Anti-Smith(SM) | Anti-SmRNP | Date ENA |
|---|---|---|---|---|---|---|---|---|---|---|---|---|---|---|
| LE-19-375 | 10/18/2019 | 97.3 | 167.4 | 34.7 | 128 | 12.9 | 171 | 11.1 (11/25/2015 | neg | <0.2 | <0.2 | 0.2 | 0.3 | 11/25/2015 |
| LE-19-388 | 10/24/2019 | 125.2 | 155.8 | 51.6 | 84.6 | 9.7 | neg | 10.2 (7/9/2013 | >200 | <0.2 | 0.3 | >8.0 | 6.8 | 4/7/2017 |
| LE-19-419 | 11/18/2019 | 92 | 160.1 | 35.9 | 91 | 14.2 | >1000 | >12.0 (12/20/2012 | neg | neg | neg | neg | neg | 9/25/2017 |
| LE-19-433 | 11/25/2019 | 89.8 | 155.2 | 37.3 | 125.8 | 22.3 | neg | 1.3 (6/25/2015) | neg | neg | neg | neg | neg | 6/25/2015 |
| LE-19-432 | 11/25/2019 | 98.3 | 159.8 | 38.5 | 98.4 | 8.3 | 59 | >12.0 (6/8/2015) | >200 | 3.2 | <0.2 | >8.0 | 7.1 | 9/25/2017 |

Medications

| LE Num | Visit Date | HCQ [mg/day] | Prednisone [mg/day] | AZA [mg/day] | MTX [mg/week] | MMF [mg/day] | other | other | other | other | other | other |
|---|---|---|---|---|---|---|---|---|---|---|---|---|
| LE-19-375 | 10/18/2019 | 400 | 5 | 100 | No | No | Losartan/HCTZ 50 /12.5 mg PO daily | Metformin 1 gram BID | Prilosec 20mg daily | Synthroid 75 mcg daily | | |
| LE-19-388 | 10/24/2019 | 400 | 60 | No | No | No | Albuterol 90 mcg/actuation as needed | Pantoprazole 40 mg daily | Xarelto 20 mg daily | Atorvastatin 40 mg daily, | Toprol XL 25 mg daily, | Levothyroxine 150 mcg daily |
| LE-19-419 | 11/18/2019 | 400 | 10 | No | No | 2000 | Eliquis 5mg twice a day | Medroxyprogesterone 104 milligrams subcutaneous, | | | | |
| LE-19-433 | 11/25/2019 | No | 5 | No | 10 | No | Simvastatin 20mg daily | Synthroid 125mcg daily | | | | |
| LE-19-432 | 11/25/2019 | 400 | 6 | No | 25 | No | Tofacitinib 5mg BID | Acyclovir 400mg daily for prophylaxis | | | | |

**Table VI-1: Demographic and clinical characteristics for proteomics.**

Demographic and clinical characteristics of SLE patients (n=5) donating blood for proteomics analysis of LDGs and NDNs. Healthy volunteers were age and sex-matched.

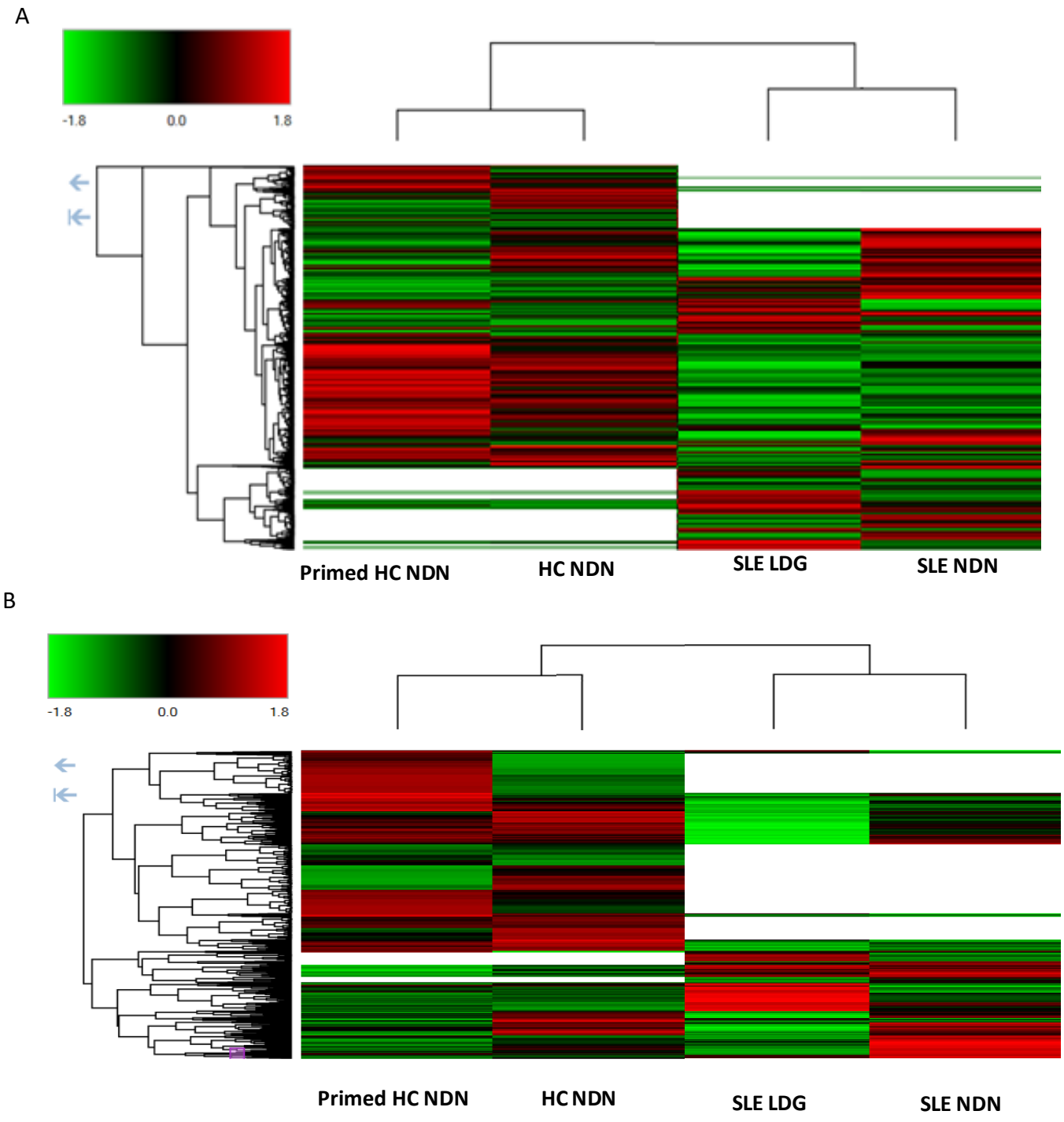


**Figure VI-2: Proteins and phosphoproteins identified in four neutrophil subsets by mass spectrometry.**

A total of 4109 proteins (A) and 875 phosphoproteins (B) were identified by mass spectrometry in LDGs and NDNs from SLE subjects (n=5) and unstimulated and primed NDNs from healthy (HC) volunteers (n=5). Open boxes in heatmaps indicate the given protein was not identified in the sample.

| Gene Name | Protein Accession | Protein Description | Phosphopeptide Sequence |
|---|---|---|---|
| PECAM1 | P16284 | Platelet endothelial cell adhesion molecule | YsRTEGSLDGT |
| ADAM22 | Q9P0K1 | Disintegrin and metalloproteinase domain-containing protein 22 | LSVVHTNtYAK |
| DOCK5 | Q9H7D0 | Dedicator of cytokinesis protein 5 | APEPDLMsPTR |
| PIEZO1 | Q92508 | Piezo-type mechanosensitive ion channel component 1 | SGsEEAVTDPGER |
| LCP1 | P13796 | Plastin-2 | GsVSDEEMMELR |
| LCP1 | P13796 | Plastin-2 | GsVSDEEMMELR |
| LCP1 | P13796 | Plastin-2 | EGEsLEDLMK |
| PAK1 | Q13153 | Serine/threonine-protein kinase PAK 1 | YMsFTDK |
| PXN | P49023 | Paxillin | TSSVSNPQDSVGsPCSR |
| ZYX | Q15942 | Zyxin | GPPAsSPAPAPK |
| ZYX | Q15942 | Zyxin | sPGAPGPLTLK |
| ARHGEF2 | Q92974 | Rho guanine nucleotide exchange factor 2 | QELGsPEER |
| ARHGEF2 | Q92974 | Rho guanine nucleotide exchange factor 2 | SEsLESPR |
| ARHGAP25 | P42331 | Rho GTPase-activating protein 25 | DIPLsPPAQK |
| ARHGAP25 | P42331 | Rho GTPase-activating protein 25 | GDTLAsPNSETGPGK |
| IQGAP2 | Q13576 | Ras GTPase-activating-like protein IQGAP2 | YGsIVDDER |
| WASF2 | Q9Y6W5 | Wiskott-Aldrich syndrome protein family member 2 | SsTIQDQK |
| CORO1A | P31146 | Coronin-1A | AAPEASGtPSSDAVSR |

**Table VI-2. Phosphosite information for phosphoproteins referenced in the thesis.** Information for all phosphoproteins identified can be found in the ProteomeXchange Consortium via the PRIDE partner repository with the dataset identifier PXD021096 and 10.6019/PXD021096. Lowercase letter indicates the site of phosphorylation.

## 4.3 Assessment of the neutrophil proteome and phosphoproteomes.

Of the 4109 proteins identified, 601 (14.6%) were present only in the proteome of healthy neutrophils, while 685 (16.6%) were identified only in the proteome of SLE neutrophils (Figure VI-3A). The same proteins were identified in both SLE LDGs and NDNs, albeit with considerable variation in protein abundance. Indeed, 11.3 per cent of proteins expressed by SLE neutrophils were differentially abundant between NDNs and LDGs, with 334 proteins more abundant and 65 proteins less abundant in SLE LDGs relative to SLE NDNs (ratio cut-off >1.5 or <0.5) (Figure VI-3C). Of the 2823 proteins common to both SLE and healthy NDNs, 307 proteins (10.9%) were differentially abundant (Figure VI-3D). Overall, a considerable number of proteins were uniquely present in either healthy or SLE neutrophils and protein abundances varied between SLE LDGs, SLE NDNs and healthy NDNs, indicating heterogeneity in the neutrophil proteome.

Of the 875 phosphoproteins identified by mass spectrometry, 48 phosphoproteins (5.4%) were only identified in healthy NDNs and 366 phosphoproteins (41.8%) were only identified in SLE neutrophils. The same phosphoproteins were identified in both healthy unstimulated and healthy primed NDNs, and one phosphoprotein was uniquely identified in SLE LDGs (round spermatid basic protein 1-like protein, pRSBN1L) (Figure VI-5A). When comparing SLE LDGs and autologous SLE NDNs, 95 phosphoproteins (11.5%) were differentially abundant, with 11 less abundant and 84 more abundant in SLE LDGs (Figure VI-5C). Of the 509 phosphoproteins expressed in both primed and unstimulated healthy NDNs, 167 phosphoproteins (32.8%) were differentially abundant (Figure VI-5B). Of the 460 phosphoproteins common to all neutrophils, 100 phosphoproteins (21.7%) were differentially abundant between healthy NDNs and SLE NDNs (Figure VI-5D). Overall, these data indicate heterogeneity in the neutrophil phosphoproteome.

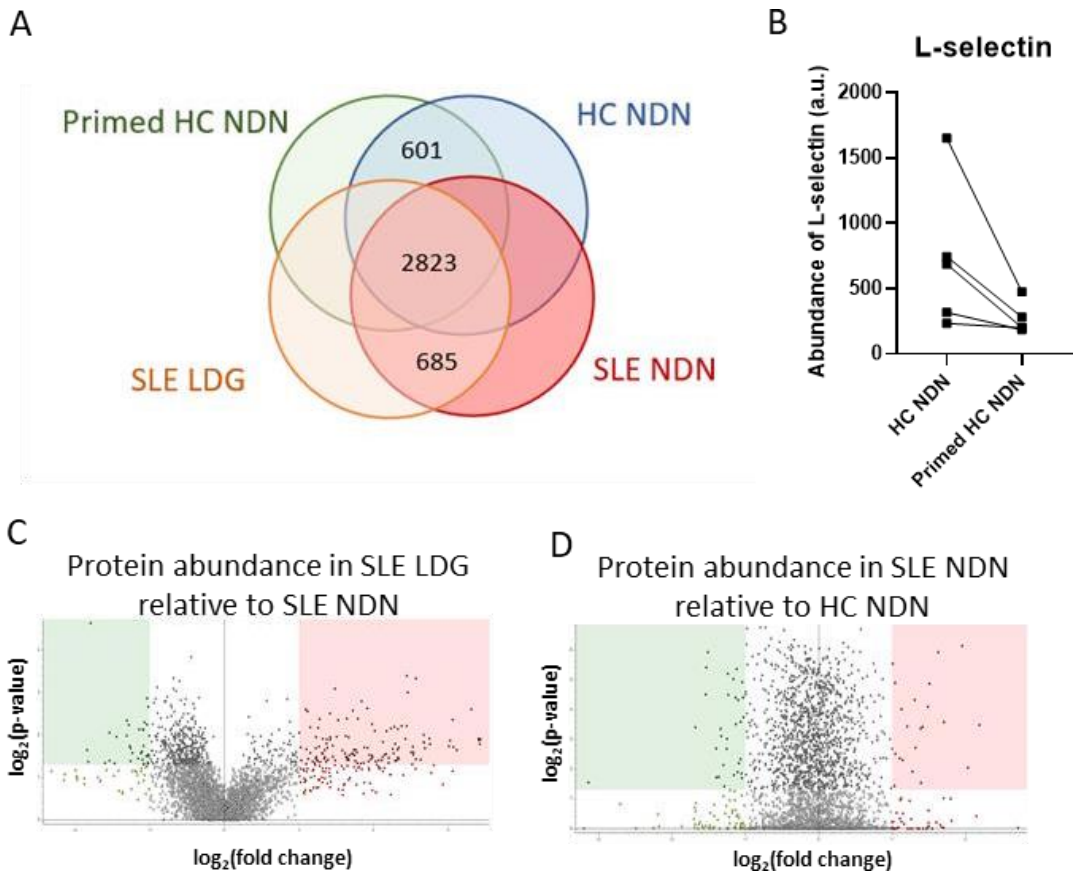


**Figure VI-3: Different neutrophil subsets show evidence of heterogeneous proteomes.**

(A) Distribution of 4109 identified proteins across all neutrophil subsets. (B) Abundance of L-selectin in arbitrary units. Results are mean ± SEM and matched samples represent un-primed/primed neutrophils from the same healthy donors. (C & D) Volcano plots depict differences between the (C) SLE NDN/SLE LDG and (D) SLE NDN/HC NDN proteomes. In panel C, the upregulated (red) and downregulated (green) proteins are from LDGs, while NDNs are the reference proteome. In panel D, the upregulated (red) and downregulated (green) proteins are from SLE NDNs, while HC NDNs are the reference proteome.

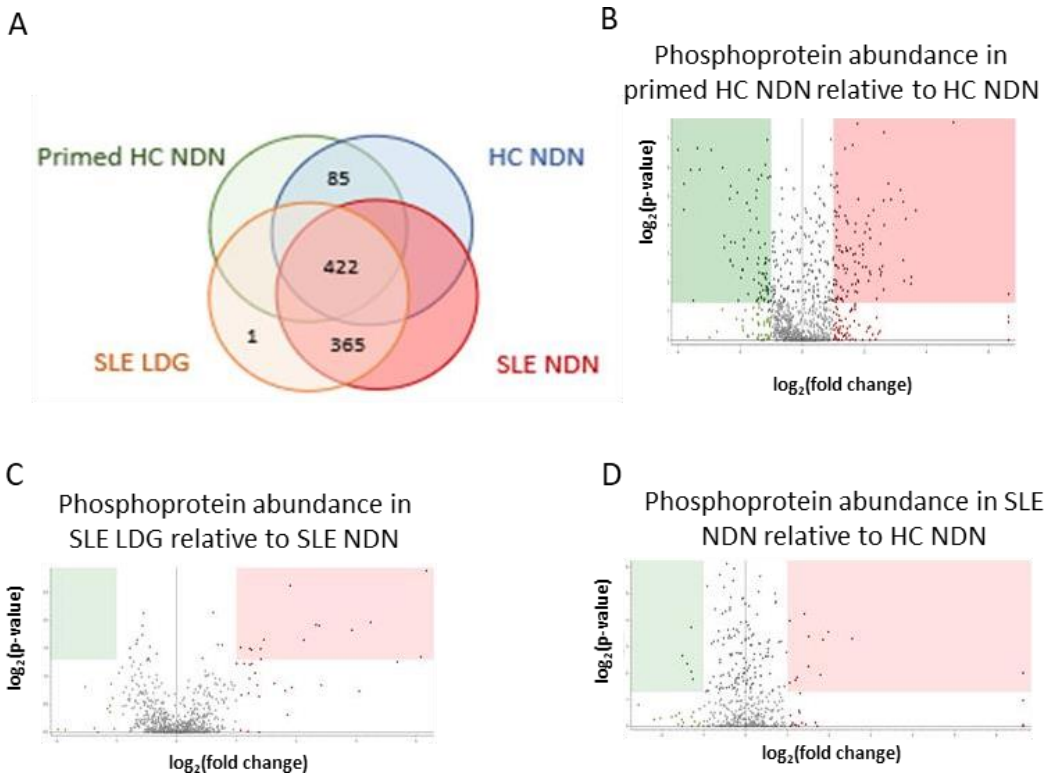


**Figure VI-4: Different neutrophil subsets show evidence of heterogeneous phosphoproteomes**

(A) Distribution of 875 identified phosphoproteins across all neutrophil subsets. (B, C, D) Volcano plots depict differences between (B) primed HC NDN/HC NDN, (C) SLE NDN/SLE LDG and (D) SLE NDN/HC NDN proteomes. In panel B, upregulated (red) and downregulated (green) proteins are from LDGs, while NDNs are the reference proteome. In panel C, the upregulated (red) and downregulated (green) proteins are from LDGs, while NDNs are the reference proteome. In panel D, the upregulated (red) and downregulated (green) proteins are from SLE NDNs, while HC NDNs are the reference proteome.

## 4.4 SLE neutrophils display evidence of activation at the proteomic level and a signature of type I IFN activation is present in SLE LDGs.

Using open source software ShinyGO [144] and MetaScape [145], I mapped proteins differentially abundant in at least 4/5 samples to known gene ontology (GO) biological processes to identify networks that may be upregulated or downregulated in different neutrophil subsets. Heatmaps were used to visualise specific proteins contributing to upregulation or downregulation of a given network.

Proteins more abundant in SLE NDNs relative to healthy NDNs mapped to neutrophil activation networks (Figure VI-5A). These networks included proteins such as CXC-motif chemokine receptor 2 (CXCR2) and pro-platelet binding protein (PPBP), which facilitate neutrophil migration to inflammatory sites and release from the bone marrow [218-220]. When comparing SLE LDGs, SLE NDNs and healthy NDNs, some proteins associated with neutrophil activation were most abundant in SLE LDGs (Figure VI-5B), including PPBP and S100A7. S100A7, also called psoriasin, is over-expressed in inflammatory diseases and has been shown to drive inflammation *in vivo* [221]. These results indicate that SLE neutrophils, and particularly SLE LDGs, have upregulation of pathways implicated in neutrophil activation and migration to inflammatory sites.

SLE subjects express elevated type 1 IFN-stimulated genes (ISGs) in various cells and organs, in association with disease severity [222], and increased ISG expression has been reported in SLE NDNs and LDGs relative to healthy NDNs [200]. While proteins encoded by ISGs were not uniformly upregulated in SLE NDNs relative to healthy NDNs, many were upregulated in SLE LDGs relative to SLE or healthy NDNs (Figure VI-5C). Although transcription of ISGs in response to type I IFNs is mediated by phosphorylation of signal transducer and activator of transcription (STAT) molecules [223], phospho-STATs were not identified by this study in any neutrophil subset. This is possibly because pTyr residues are less abundant than pSer [224] and limited LDG sample volumes prevented immunoprecipitation of pTyr residues alongside phosphopeptide enrichment. Nonetheless, collectively the SLE neutrophil proteome suggests an activated status, while the IFN-associated protein signature is distinct to SLE LDGs.

In some instances, neutrophil activation facilitates interactions with the endothelium [225]. There were no differences in adhesion proteins or integrins regulating neutrophil-endothelial interactions identified between autologous SLE LDGs and NDNs or autologous primed and unstimulated healthy NDNs (Figure VI-6A). However, proteins regulating neutrophil-endothelial interactions were increasingly phosphorylated in primed healthy NDNs relative to all other neutrophil subsets (Figure VI-6B). Despite the proteomic evidence of activation in both SLE NDNs and SLE LDGs, this suggests distinctions between SLE LDGs/NDNs and conventionally primed healthy NDNs.

Proteins with differential phosphorylation in SLE NDNs relative to healthy NDNs were associated with organelle organisation and actin cytoskeleton organisation, including phospho-coronin 1A (pCORO1A) and phospho-heat shock protein 90AA1 (pHSP90AA1) (Figure VI-7).

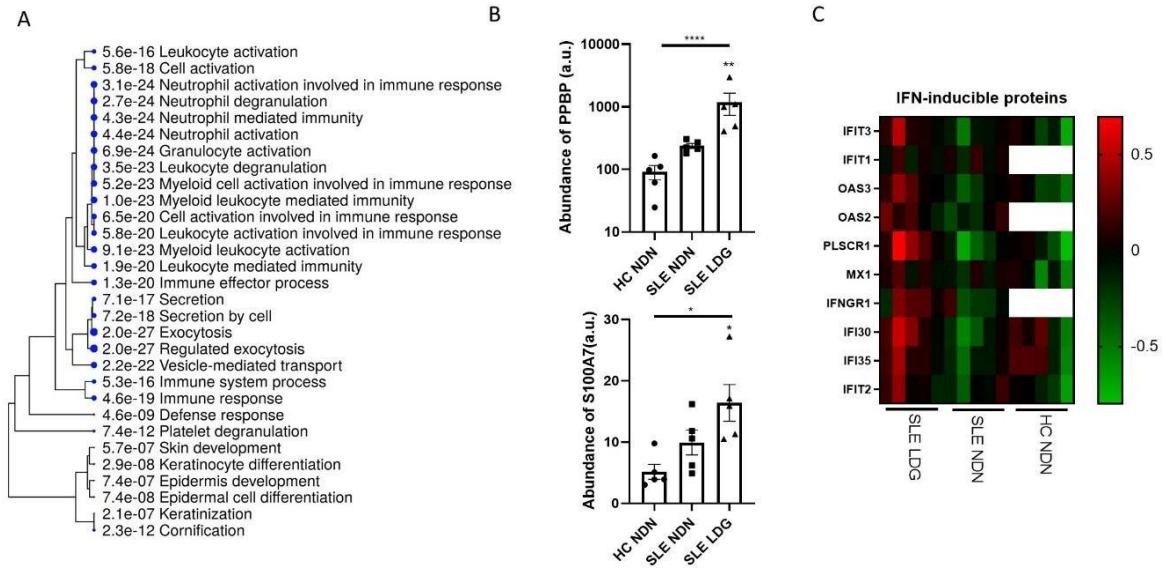


**Figure VI-5: Neutrophil activation in the SLE NDN and SLE LDG proteomes.**

(A) GO biological enrichment analysis highlights biological networks associated with proteins more abundant in SLE NDNs relative to HC NDNs. Proteins with abundance ratios greater than 1.5 in at least 4/5 SLE NDN samples relative to HC NDNs were included and significance was established by FDR. The blue circles are sized in proportion to the significance of the effect. A larger circle indicates a more significantly upregulated network. (B) PPBP and S100A7 expression in arbitrary units. Significance was established by Kruskal-Wallis test with post hoc Dunn's tests for multiple comparisons. All results are mean ± SEM and significance was set at *$p$<0.05, **$p$<0.01, ns=not significant. (C) Relative abundance of IFN inducible proteins in SLE NDNs and HC NDNs relative to SLE LDGs. SLE NDNs were compared to autologous SLE LDGs. HC NDNs were compared to the mean protein abundance in SLE LDGs. Open boxes in heatmaps indicate the given protein was not identified in the sample.

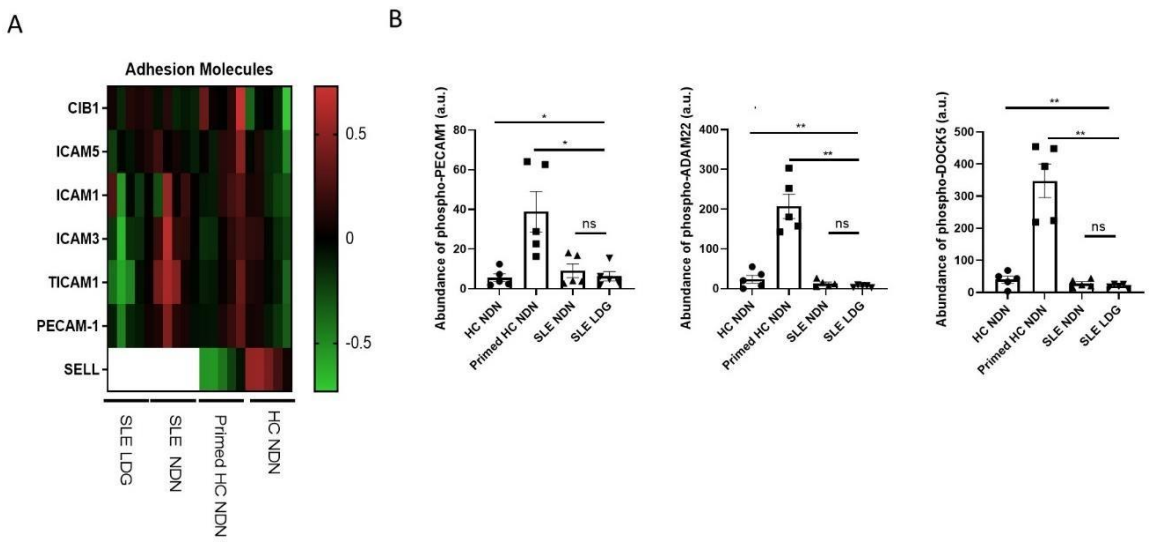


**Figure VI-6: Proteomic and phosphoproteomic regulators of neutrophil-endothelial interactions.**

(A) Abundance of cell integrins and adhesion-related proteins in SLE NDNs and HC NDNs relative to autologous SLE LDGs and autologous primed HC NDNs respectively. Open boxes in heatmaps indicate the given protein was not identified in the sample. (B) Abundance of phosphoproteins associated with regulation of neutrophil-endothelial interactions in all neutrophil subsets, in arbitrary units. Significance was established by Kruskal-Wallis test with post hoc Dunn's tests for multiple comparisons. All results are mean ± SEM and significance was set at *$p$<0.05, **$p$<0.01, ns=not significant.

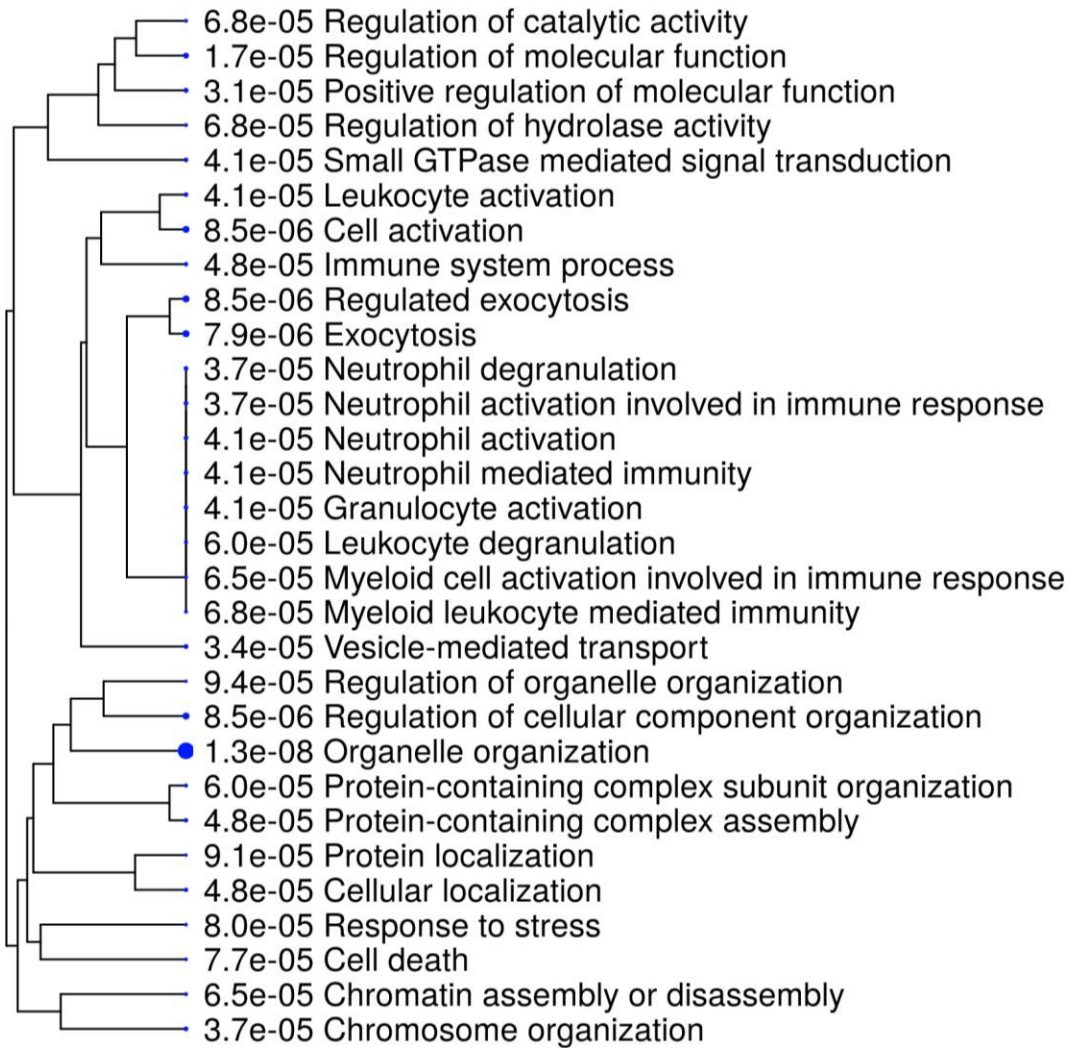


**Figure VI-7: Networks differentially regulated in the phosphoproteomes of SLE NDNs and healthy NDNs.**

GO biological enrichment analysis highlighting biological networks associated with proteins differentially phosphorylated in SLE NDNs and HC NDNs. Phosphoproteins with abundance ratios less than 0.5 or greater than 1.5 in at least 4/5 matched samples were included and significance was established by FDR. The blue circles are sized in proportion to the significance of the effect. A larger circle indicates a more significantly upregulated network.

## 4.5 The SLE LDG proteome is characterised by upregulation of networks associated with inflammatory response, translational activity, and platelets.

Some proteins less abundant in SLE LDGs relative to SLE NDNs associated with neutrophil degranulation, (Figure VI-8A), but key granule proteins including myeloperoxidase (MPO) and cathepsin-G (CTSG) were not decreased in SLE LDGs (Figure VI-8B). Rather, lower abundance of membrane proteins, particularly ficolin-1-rich granule membrane proteins, accounted for downregulated degranulation networks in SLE LDGs. As such, differences in degranulation capabilities do not explain changes in neutrophil proteomes between neutrophil subsets.

Proteins more abundant in SLE LDGs relative to SLE NDNs clustered in neutrophil activation, coagulation, platelet, and intracellular trafficking networks (Figure VI-9A). In addition, systemic lupus erythematosus (False Discovery Rate (FDR) = $10^{-11.119}$) was identified as a biological network upregulated in the SLE LDGs relative to autologous NDNs, primarily due to upregulated complement proteins (Figure VI-9B). Complement factors, immunoglobin chains, and apolipoproteins were more abundant in SLE LDGs relative to SLE or healthy NDNs and were largely responsible for enrichment of the coagulation network. Proteins differentially phosphorylated in SLE LDGs relative to SLE NDNs were also associated with neutrophil activation and intracellular trafficking (Figure VI-9C). In addition, SLE LDGs expressed higher abundances of ribosomal proteins (Figure VI-9D).

Upregulation of platelet-associated proteins was also identified in the SLE LDG proteome. Integrins (ITG)A2B and ITGB3 were more abundant in SLE LDGs than autologous or healthy NDNs, although P-selectin (SLEP) and its receptor selectin P ligand (SELPLG) were equally expressed in all neutrophil subsets (Figure VI-9E). Increased platelets were seen in SLE LDG samples by fluorescent microscopy, corroborating these findings (Figure VI-9F).

Recently, SLE LDGs were characterised as a heterogeneous population of neutrophils comprising of CD10- (more immature, less abundant) and CD10+ (intermediate-mature, most abundant) subsets. CD10, also known as common acute lymphoblastic leukaemia antigen, is expressed by mature neutrophils at their latest stage of differentiation [221]. CD10- LDGs were classified as immature based on nuclear morphology and decreased expression of transcripts for CEBPD and SPI1 relative to SLE NDNs and CD10+ LDGs [200]. The proteomic analysis performed for this thesis was completed on unfractionated SLE LDGs and SPI1 protein abundance was similar in SLE LDGs, SLE NDNs and healthy NDNs. CEBPD was not identified in healthy NDNs but it was similarly abundant in SLE LDGs and NDNs (Figure IV-10A). In addition, the majority of SLE LDGs had multi-lobulated nuclei (Figure VI-10B), suggesting the SLE LDGs analysed were predominantly intermediate-mature LDGs characterised as CD10+, consistent with previous observations that these cells represent the most abundant LDG subset in patients with SLE [200]. Overall, these results indicate distinct differences in

the proteome of SLE LDGs relative to SLE or healthy NDNs, characterised by increased levels of IFN-regulated proteins and coagulation-associated pathways.

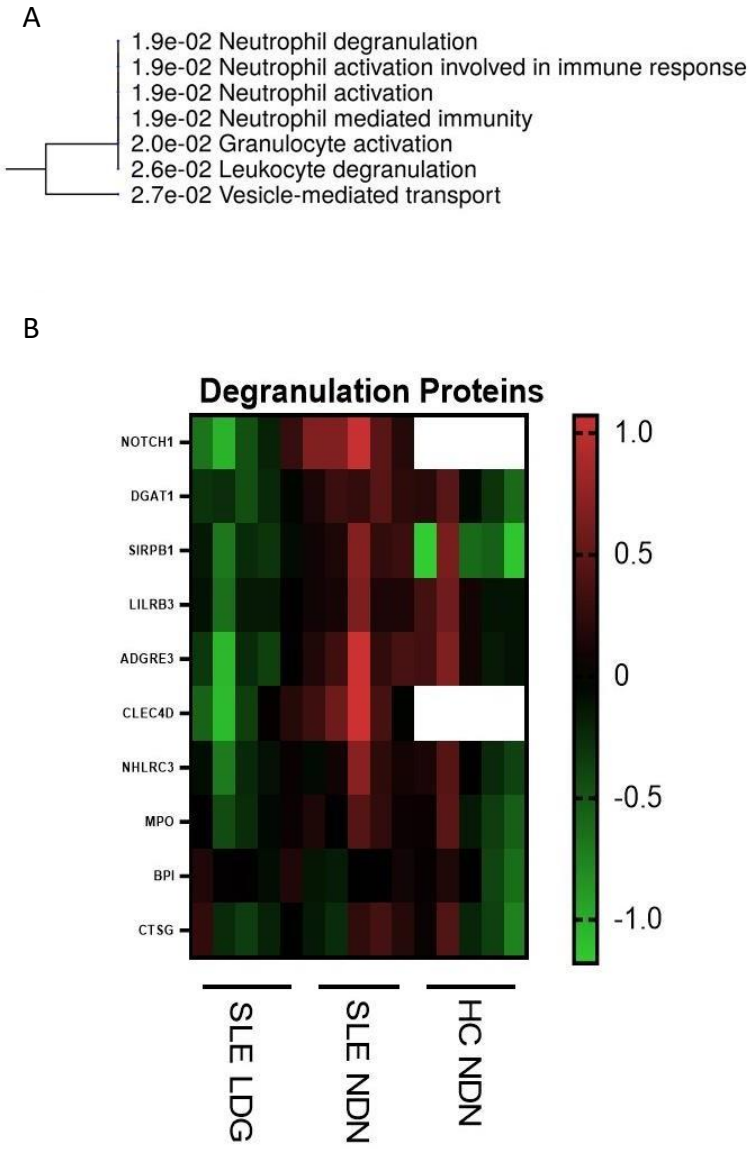


**Figure VI-8: Proteins downregulated in SLE LDGs relative to SLE NDNs are associated with neutrophil degranulation networks.**

(A) GO biological enrichment analysis highlighting biological networks associated with proteins less abundant in SLE LDGs (n=5) relative to SLE NDNs (n=5). Proteins with abundance ratios less than 0.5 in at least 4/5 matched samples were included and significance was established by FDR. (B) Relative abundance of degranulation network-associated proteins in SLE NDNs and HC NDNs relative to SLE LDGs. SLE NDNs were compared to autologous SLE LDGs. HC NDNs were compared to the mean protein abundance in SLE LDGs. Open boxes in heatmaps indicate the given protein was not identified in the sample.

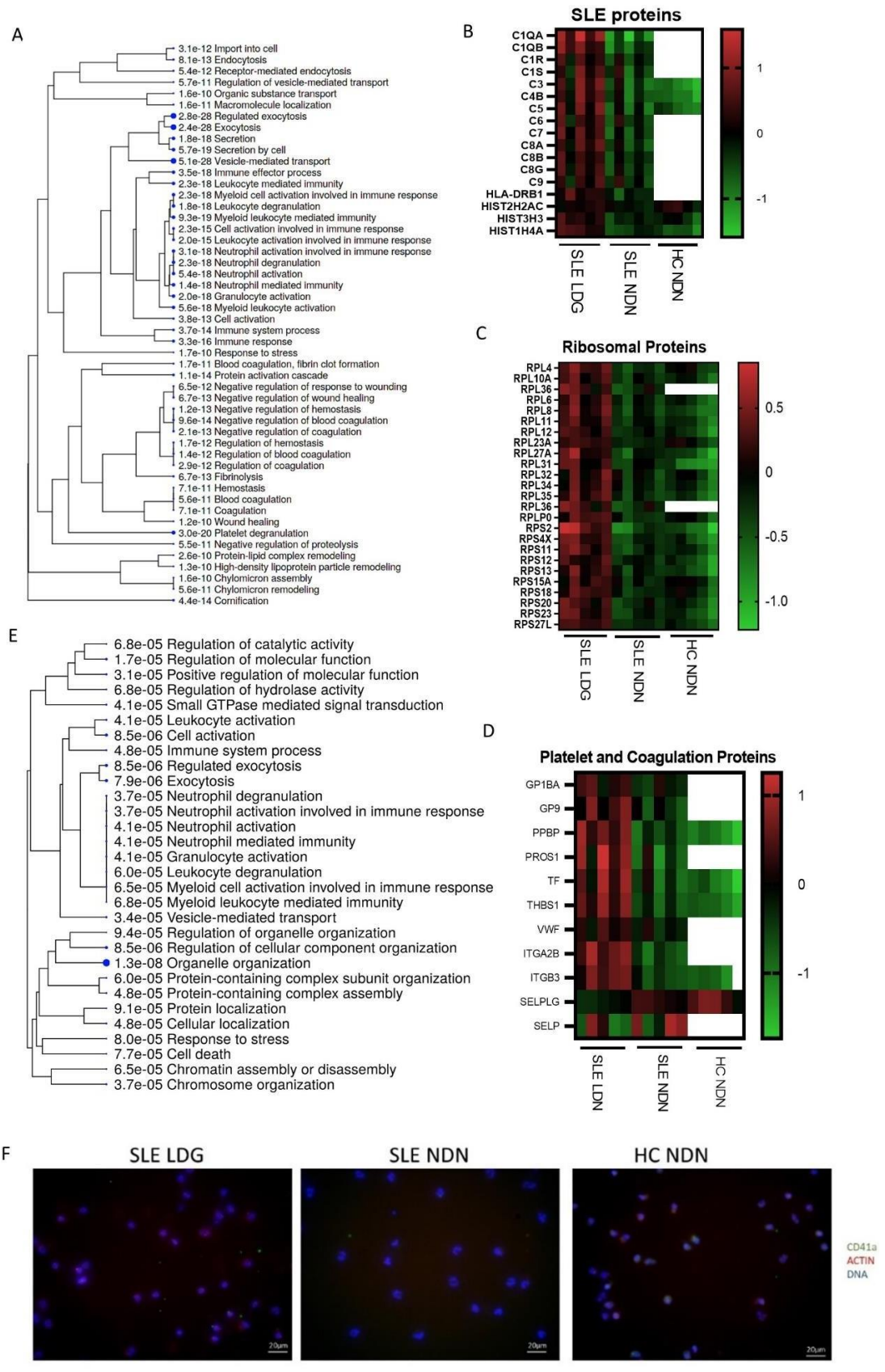
A
3.1e-12 Import into cell
8.1e-13 Endocytosis
5.4e-12 Receptor-mediated endocytosis
5.7e-11 Regulation of vesicle-mediated transport
1.6e-10 Organic substance transport
1.6e-11 Macromolecule localization
2.8e-28 Regulated exocytosis
2.4e-28 Exocytosis
1.8e-18 Secretion
5.7e-19 Secretion by cell
5.1e-28 Vesicle-mediated transport
3.5e-18 Immune effector process
2.3e-18 Leukocyte mediated immunity
2.3e-18 Myeloid cell activation involved in immune response
1.8e-18 Leukocyte degranulation
9.3e-19 Myeloid leukocyte mediated immunity
2.3e-15 Cell activation involved in immune response
2.0e-15 Leukocyte activation involved in immune response
3.1e-18 Neutrophil activation involved in immune response
2.3e-18 Neutrophil degranulation
5.4e-18 Neutrophil activation
1.4e-18 Neutrophil mediated immunity
2.0e-18 Granulocyte activation
5.6e-18 Myeloid leukocyte activation
3.8e-13 Cell activation
3.7e-14 Immune system process
3.3e-16 Immune response
1.7e-10 Response to stress
1.7e-11 Blood coagulation, fibrin clot formation
1.1e-14 Protein activation cascade
6.5e-12 Negative regulation of response to wounding
6.7e-13 Negative regulation of wound healing
1.2e-13 Negative regulation of hemostasis
9.6e-14 Negative regulation of blood coagulation
2.1e-13 Negative regulation of coagulation
1.7e-12 Regulation of hemostasis
1.4e-12 Regulation of blood coagulation
2.9e-12 Regulation of coagulation
6.7e-13 Fibrinolysis
7.1e-11 Hemostasis
5.6e-11 Blood coagulation
7.1e-11 Coagulation
1.2e-10 Wound healing
3.0e-20 Platelet degranulation
5.5e-11 Negative regulation of proteolysis
2.6e-10 Protein-lipid complex remodeling
1.3e-10 High-density lipoprotein particle remodeling
1.6e-10 Chylomicron assembly
5.6e-11 Chylomicron remodeling
4.4e-14 Cornification
B
SLE proteins
C1QA
C1QB
C1R
C1S
C3
C4B
C5
C6
C7
C8A
C8B
C8G
C9
HLA-DRB1
HIST2H2AC
HIST3H3
HIST1H4A
1
0
-1
SLE LDG
SLE NDN
HC NDN
C
Ribosomal Proteins
RPL4
RPL10A
RPL36
RPL6
RPL8
RPL11
RPL12
RPL23A
RPL27A
RPL31
RPL32
RPL34
RPL35
RPL36
RPLP0
RPS2
RPS4X
RPS11
RPS12
RPS13
RPS15A
RPS18
RPS20
RPS23
RPS27L
0.5
0
-0.5
-1.0
SLE LDG
SLE NDN
HC NDN
D
Platelet and Coagulation Proteins
GP1BA
GP9
PPBP
PROS1
TF
THBS1
VWF
ITGA2B
ITGB3
SELPLG
SELP
1
0
-1
SLE LDN
SLE NDN
HC NDN
E
6.8e-05 Regulation of catalytic activity
1.7e-05 Regulation of molecular function
3.1e-05 Positive regulation of molecular function
6.8e-05 Regulation of hydrolase activity
4.1e-05 Small GTPase mediated signal transduction
4.1e-05 Leukocyte activation
8.5e-06 Cell activation
4.8e-05 Immune system process
8.5e-06 Regulated exocytosis
7.9e-06 Exocytosis
3.7e-05 Neutrophil degranulation
3.7e-05 Neutrophil activation involved in immune response
4.1e-05 Neutrophil activation
4.1e-05 Neutrophil mediated immunity
4.1e-05 Granulocyte activation
6.0e-05 Leukocyte degranulation
6.5e-05 Myeloid cell activation involved in immune response
6.8e-05 Myeloid leukocyte mediated immunity
3.4e-05 Vesicle-mediated transport
9.4e-05 Regulation of organelle organization
8.5e-06 Regulation of cellular component organization
1.3e-08 Organelle organization
6.0e-05 Protein-containing complex subunit organization
4.8e-05 Protein-containing complex assembly
9.1e-05 Protein localization
4.8e-05 Cellular localization
8.0e-05 Response to stress
7.7e-05 Cell death
6.5e-05 Chromatin assembly or disassembly
3.7e-05 Chromosome organization
F
SLE LDG
SLE NDN
HC NDN
20μm
CD41a
ACTIN
DNA

**Figure VI-9: The SLE LDG proteome is characterised by upregulation of networks associated with inflammatory response, translational activity, and platelets.**

(A) GO biological enrichment analysis highlighting biological networks associated with proteins more abundant in SLE LDGs relative to SLE NDNs. Proteins with abundance ratios greater than 1.5 in at least 4/5 matched samples were included and significance was established by FDR. The blue circles are sized in proportion to the significance of the effect. A larger circle indicates a more significantly upregulated network. (B) Relative abundance of SLE network-associated proteins in SLE NDNs and HC NDNs relative to SLE LDGs. (C) GO biological process analysis highlighting biological networks associated with phosphoproteins differentially abundant in SLE LDGs and NDNs. Phosphoproteins with abundance ratios less than 0.5 or greater than 1.5 in at least 4/5 matched samples were included and significance was established by FDR. The blue circles are sized in proportion to the significance of the effect. A larger circle indicates a more significantly upregulated network. (D) Relative abundance of ribosomal proteins in SLE NDNs and HC NDNs relative to SLE LDGs. (E) Relative abundance of coagulation and platelet-associated proteins in SLE NDNs and HC NDNs relative to SLE LDGs. For all heatmaps, SLE NDNs were compared to autologous SLE LDGs. HC NDNs were compared to the mean protein abundance in SLE LDGs and open boxes in heatmaps indicate the given protein was not identified in the sample. (F) Neutrophil preparations did not show considerable platelet contamination, as assessed by staining for platelet marker CD41a, but increased platelets in samples of SLE LDGs could be observed (images representatively of n=6).

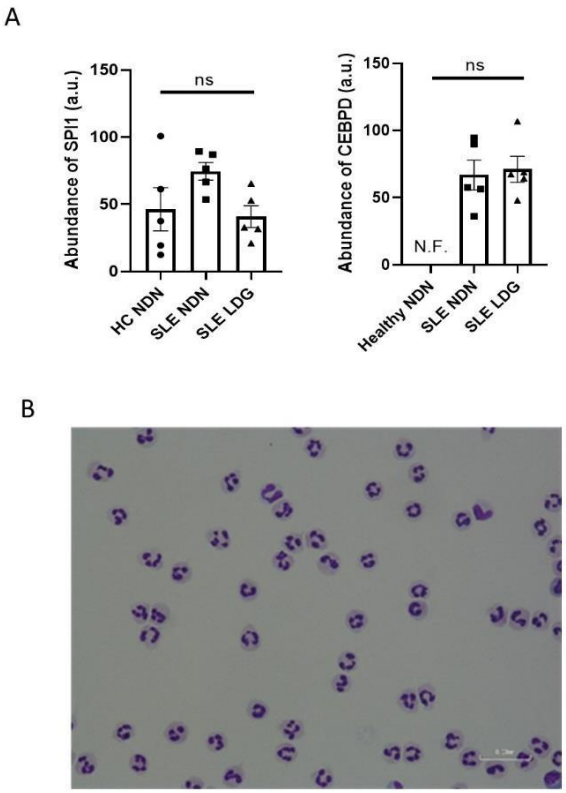


**Figure VI-10: Assessment of SLE LDG maturity by transcription factor expression and nuclear morphology.**

(A) Abundance of transcription factors CEBPD and SPI1 in arbitrary units. CEBPD was not identified in HC NDNs. Results are mean ± SEM. Significance was established by Kruskal-Wallis test with post hoc Dunn's tests for multiple comparisons and set at *$p<0.05$, ns=not significant. N.F. = not found. (B) Cytospin of isolated SLE LDGs.

### 4.6. Proteomic and phosphoproteomic analyses indicate differential expression of proteins associated with cytoskeleton function between SLE NDNs and LDGs.

Previous studies analysing neutrophil transcriptomics demonstrated that cytoskeleton-associated networks were upregulated in SLE LDGs relative to SLE NDNs [56]. Similarly, I found that cytoskeleton-associated networks were upregulated at the protein level in SLE LDGs relative to SLE NDNs (Figure VI-11A). Many of the proteins identified in the enrichment of cytoskeleton-related networks in SLE LDGs regulate intracellular trafficking. In addition, histidine rich glycoprotein (HRG) and profilin 1 (PFN1) were overabundant in SLE LDGs relative to SLE NDNs (Figure VI-11B). HRG has been reported to induce neutrophil morphologic changes [207], while PFN1 is a dual regulator of actin and microtubule dynamics [226]. Expression of these proteins did not differ in primed neutrophils relative to un-primed neutrophils (Figure VI-12), nor have I found any literature linking PFN1 or HRG to neutrophil priming. However, HRG was very recently found to contribute to the prevention of sepsis, by maintaining neutrophil morphology and phagocytosis capabilities in the presence of *E. coli and S. aureus* [227]. As such, links between neutrophil priming and HRG may exist but be undiscovered to date.

Furthermore, cytoskeleton-associated proteins were de-phosphorylated in SLE LDGs relative to SLE NDNs, including actin-bundling protein L-plastin (LCP1), actin-regulatory protein CORO1A, and cytoskeleton-associated protein Rho-Rac guanine nucleotide exchange factor 2 (ARHGEF2) (Figure VI-11C). Phosphorylation of these proteins modulates organisation of the cytoskeleton [228-230]. These data suggest differences in cytoskeleton regulation between SLE LDGs and SLE NDNs.

### 4.7 Phosphoproteomic analyses indicate differential expression of proteins associated with cytoskeleton function as well as cell adhesion, between primed and unstimulated healthy neutrophils.

To understand the changes conferred by neutrophil activation to proteins associated with the cytoskeleton, I assessed the effect of fMLF stimulation on the healthy NDN phosphoproteome. Neutrophil morphological changes in response to fMLF stimulation are well documented [104, 105, 132] (see chapter IV of this thesis) and many of the proteins differentially phosphorylated in primed healthy NDNs relative to healthy NDNs mapped to biological networks associated with cytoskeletal organisation (Figure VI-12A). Proteins modulating cytoskeletal properties, including LCP1, CORO1A, and ARHGEF, were increasingly phosphorylated in fMLF-primed relative to un-primed healthy NDNs (Figure VI-12B). These same proteins were differentially de-phosphorylated in SLE LDGs relative to SLE NDNs (Figure VI-11, Figure VI-12). Mapping of differentially abundant phosphoproteins to GO biological pathways indicated an increase in phosphorylation of proteins associated with enhanced cell adhesion (*e.g.* PECAM1 [231], a disintegrin and metalloproteinase 22 (ADAM22) [232], dedicator of cytokinesis 5 (DOCK5) [233], and piezo type mechanosensitive ion channel component 1 (PIEZO1) [234] in primed healthy NDNs relative to other neutrophil subsets, including SLE LDGs.

Findings of upregulated cytoskeleton-associated proteins in the SLE LDG proteome, alongside findings in the phosphoproteome suggestive of differential cytoskeletal reorganisation in primed healthy NDNs/SLE LDGs relative to their unstimulated NDN counterparts, was particularly interesting when considered in tandem with my previous discovery, that SLE LDGs have a distinct biomechanical phenotype.

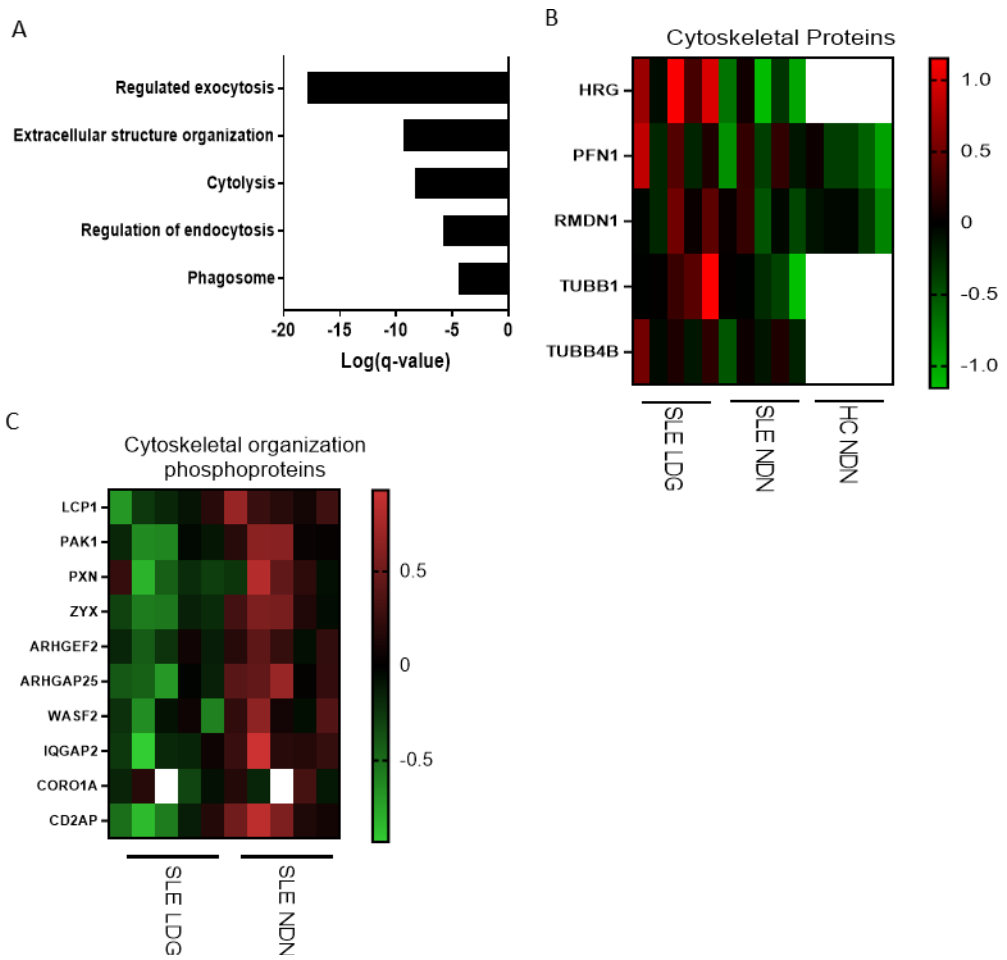


**Figure VI-11: Proteomic and phosphoproteomic analyses indicate differential expression of proteins associated with cytoskeleton function between SLE NDNs and LDGs.**

(A) GO biological process analysis highlighting biological networks related to the cytoskeleton and associated with proteins more abundant in SLE LDGs relative to SLE NDNs in at least 4/5 matched samples. Proteins with abundance ratios greater than 1.5 were included and significance was established by FDR. (B) Abundance of cytoskeleton-associated proteins in SLE NDNs and HC NDNs relative to SLE LDGs. SLE NDNs were compared to autologous SLE LDGs. HC NDNs were compared to the mean protein abundance in SLE LDGs. (C) Abundance of cytoskeleton network-associated phosphoproteins in SLE LDGs relative to abundance in autologous SLE NDNs. Open boxes in heatmaps indicate the given protein was not identified in one of the two autologous samples being compared.

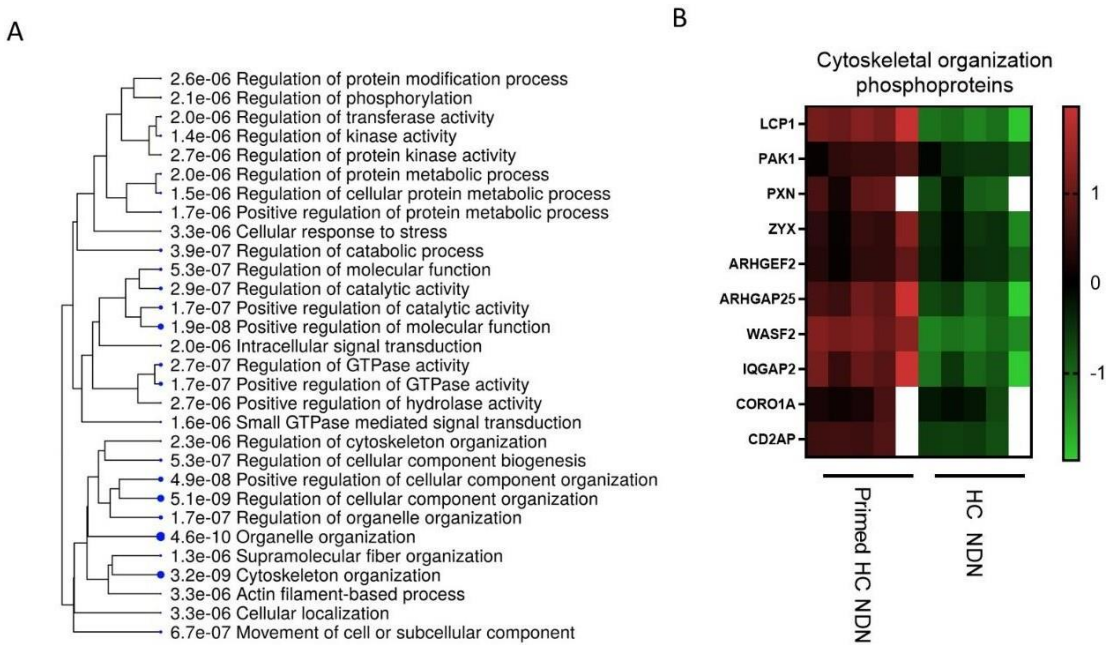


**Figure VI-12: Proteomic and phosphoproteomic analyses indicate differential expression of proteins associated with cytoskeleton function between primed and unstimulated healthy NDNs.**

(A) GO biological enrichement analysis highlighting biological networks associated with phosphoproteins differentially abundant in primed HC NDNs (n=5) and unstimulated HC NDNs (n=5). Proteins with abundance ratios greater than 1.5 or less than 0.5 in at least 4/5 were included and significance was established by FDR. (B) Abundance of phosphoproteins associated with regulation of the cytoskeleton in primed HC NDNs relative to autologous HC NDNs. Open boxes in heatmaps indicate the given protein was not identified in one of the two autologous samples being compared. The blue circles are sized in proportion to the significance of the effect. A larger circle indicates a more significantly upregulated network.

## 5. Discussion

Although the putative mechanisms promoting the increased SLE LDG cytoskeletal roughness described in Chapter V remain to be fully elucidated, the proteomic and phosphoproteomic analyses described in this chapter suggest potential mechanisms for future investigations. Firstly, the upregulation of proteins associated with GO-biological processes including exocytosis, cytolysis, and formation of phagosomes in SLE LDGs relative to normal dense neutrophils fits with the observations of a cell with a "rougher" surface. Processes like exocytosis or cytolysis are both likely to induce membrane protrusions, and thus increase read-outs of cell roughness by RT-DC. It would be interesting to assess vesicle formation in SLE LDGs to see if these cells undergo increased exocytosis relative to autologous normal dense counterparts. In addition, there were several proteins associated with cytoskeletal organisation (*e.g.* PFN1, HRG) which were upregulated in SLE LDGs relative to SLE NDNs or healthy NDNs, as well as relative to primed healthy NDNs given that un-primed and primed NDNs did not differ substantially with respect to their proteomes. Other proteins associated with cytoskeletal organisation were de-phosphorylated in SLE LDGs relative to autologous or healthy NDNs. Interestingly, those same proteins were increasingly phosphorylated in primed healthy NDNs. Overall, the proteomics data supports the biomechanical data, indicating a physical difference between SLE LDGs and other neutrophil subsets.

With respect to the mechanism underlying the difference in roughness between SLE LDGs and autologous NDNs, differential abundance of proteins associated with extracellular structure organisation and cytolysis may be implicated; for example, PFN1 and HRG are more abundant in the SLE LDG proteome relative to SLE and healthy NDNs. PFN1 regulates actin and microtubule dynamics [226, 235], and could be responsible for increased actin polymerisation [236], driving protrusions in the SLE LDG cytoskeleton, while HRG induces neutrophil morphologic changes [207] implicated in the regulation of neutrophil retention in microvasculature [207, 237]. Although previous studies indicate that HRG facilitates a smoother neutrophil phenotype, HRG may modulate morphology of NDNs and LDGs differently, or HRG levels in LDGs may be reflective of an immuno-regulatory mechanism that reduces cytoskeletal protrusions in LDGs, rather than being responsible for them. In addition, key actin-regulatory proteins are de-phosphorylated in LDGs which could induce biomechanical changes.

Expression of HRG and PFN1 did not differ in primed neutrophils relative to un-primed neutrophils, nor have I found any previous literature which links PFN1 or HRG to neutrophil priming or activation. However, as mentioned in the results section, HRG was very recently found to contribute to sepsis prevention by maintaining neutrophil morphology and phagocytosis capabilities in the presence of *E. coli and S. aureus* [227]. As such, links between neutrophil priming and HRG may exist but be undiscovered to date. This would be an exciting area of future research.

Beyond HRG and PFN1, the phosphoproteomic data may hint at an additional or alternative mechanism regulating neutrophil roughness. There is very little previous research that has been completed on the neutrophil phosphoproteome, in large part because until recently it was extremely challenging to perform proteomics experiments with neutrophils due to the large amounts of proteases and phospho-proteases stored in their granules which often led to protein degradation prior to completing the analyses. Thus, although proteins including actin-bundling protein L-plastin (LCP1), actin-regulatory protein CORO1A, and cytoskeleton-associated protein Rho-Rac guanine nucleotide exchange factor 2 (ARHGEF2) have been linked to the GO-biological process "cytoskeleton organisation", little is known about phosphorylation of these proteins in the context of neutrophils. Phosphorylation of these proteins in other cell types has been established to modulate organisation of the cytoskeleton, so it is not unrealistic that they might play similar roles in regulating the cytoskeleton in neutrophils. This is especially true given that both primed NDNs and SLE LDGs, two neutrophil subsets with biomechanical properties differing from un-primed, healthy NDNs, also differ from un-primed, healthy NDNs with respect to the level of phosphorylation in these specific proteins.

For example, LCP1 is a protein found in leukocytes known to cross-link actin filaments into tight bundles, which increases the stability of structures such as lamellipodia and podosomes [238]. Increased stability of such protrusions would certainly be expected to affect RT-DC measurements of cell roughness. Specifically, phosphorylation of LCP1 increases its actin bundling capabilities and increases breast cancer cell invasiveness, likely in part by degradation of the extracellular matrix [239]. These findings suggest that phosphorylation of LCP1 might impact on the biomechanical properties of neutrophils, resulting in changes to neutrophil roughness and possibly deformability, due to degradation of the extracellular matrix.

Perhaps increased phosphorylation of proteins including LCP1, as per primed healthy NDNs, triggers a change to the actin cytoskeleton. The protrusions caused by the membrane ruffling associated with macropinocytosis are stabilised and thus an increase in roughness is measured by RT-DC. In addition, decreased phosphorylation of proteins such as LCP1, as per SLE LDGs, might also trigger a change to the actin cytoskeleton. Phosphorylation of LCP1 to levels below those seen in un-primed NDNs might be linked to destabilisation of membrane protrusions, leading to an SLE LDG morphology in line with that observed by lattice light sheet microscopy, when part of the neutrophil membrane appeared unstable and wiggly. This less rigid membrane morphology might be quite different than that observed in primed NDNs, and yet may still be measured by RT-DC as an increase in roughness.

The pronounced differences in phosphorylation of proteins associated with the actin cytoskeleton in SLE LDGs relative to primed NDNs aligns with the images of these cells obtained by SEM and lattice light sheet microscopy. SLE LDGs and primed healthy NDNs have very different styles of membrane

protrusions, despite being categorised as similarly "rough" by RT-DC. It would be fascinating to link neutrophil proteomics and phosphoproteomics to neutrophil biomechanical properties in a more defined manner, and as neutrophil proteomics becomes increasingly common, I expect our understanding in this area to improve.

As discussed in Chapter V, primed healthy NDNs, but not SLE LDGs, showed an enhanced ability to adhere to both activated and non-activated endothelium. In this chapter, phosphoproteomic analyses demonstrated proteins associated with enhanced cell adhesion (*e.g.* PECAM1 [231], a disintegrin and metalloproteinase 22 (ADAM22) [232], dedicator of cytokinesis 5 (DOCK5) [233], and piezo type mechanosensitive ion channel component 1 (PIEZO1) [234]), are increasingly phosphorylated in primed healthy NDNs relative to other neutrophil subsets, including SLE LDGs. These phosphoproteomic findings support my conclusion that primed NDNs adhere to the endothelium in greater numbers relative to other neutrophil subsets including SLE LDGs. It also lends further support to my hypothesis that the SLE LDGs and primed NDNs, while both technically low-density neutrophils, are in fact quite distinct. These two cell types were observed to interact differently with the vasculature, and additionally have the distinct phospho-proteomic profiles which align with their respective rates of vasculature interaction. As mentioned above, there is little previous phosphoproteomic research into neutrophils that can be drawn upon to understand the mechanism behind these observations. However, phosphorylation of PECAM1 is one of the initial, critical steps in the signal transduction pathway mediating leukocyte adhesion to endothelial cells. Leukocyte PECAM was shown to become phosphorylated on two tyrosine residues of its cytoplasmic tail, and subsequent RNAi-rescue experiments demonstrated such phosphorylation is critical for migration between endothelial cells. Overall, engagement of leukocyte PECAM was shown to induce its transient phosphorylation and subsequent downstream signalling to drive adherence to endothelial cells and transmigration out of the blood stream [240]. Thus, the increased abundance of phospho-protein PECAM1 in primed NDNs relative to all other subsets of neutrophils analysed aligns with my previous finding that primed NDNs adhere to endothelial cells at higher rates than other subsets of neutrophils.

In addition, it was interesting to see the increased rates of phosphorylation in primed neutrophils relative to unprimed neutrophils. This aligns with previously demonstrated links between neutrophil priming and phosphorylation of tyrosine residues which drive exocytosis and actin cytoskeleton reorganisation [158, 159].

The type I IFN pathway is linked to SLE pathogenesis and neutrophils responding to these cytokines exhibit proinflammatory responses [25]. I found that ISG-encoded proteins are overexpressed in SLE LDGs relative to other neutrophil subsets, consistent with transcriptome reports [200]. The reasons why SLE LDGs express higher levels of ISG-encoded proteins than autologous SLE NDNs, exposed to

similar levels of cytokines *in vivo*, remains to be investigated. The answer could be related to differences in JAK-STAT activity or other signalling pathways in LDGs or to the activation status of different neutrophil subsets [200]. Future studies should address how this enhanced sensitivity to type I IFNs contributes to differences in the function and pathogenic potential of LDGs. For example, it has been reported that mature NDNs from patients with SLE release NETs following *in vivo* priming by type I IFNs and secondary exposure to SLE-derived RNP immune complexes [25]. In addition, phagocytosis of NETs by macrophages leads to translocation of the NETs to the cytosol where the NET DNA backbone activates cyclic GMP-AMP synthase (cGAS), an innate immune sensor [241], which in turn triggers type I IFN production. [242]. This suggests a positive feedback loop between NETs and type I IFN production, which is interesting given the SLE LDG's links to both NETosis and type 1 IFN.

Perhaps SLE LDGs are increasingly sensitive to type I IFN priming or indeed are already primed with type 1 IFNs in some manner. This could be linked to their predisposition to form NETs. However, SLE LDGs treated with type 1 IFNs for 0.5-3 hours did not undergo any biomechanical changes that were indicative of the priming observed in Chapter IV. This indicates differences between priming mediated by agents like fMLF or PAF which bind GPCRs and priming mediated by type 1 IFN, which binds the interferon-α/β receptor (IFNAR) [243]. The IFNAR is structurally distinct from the receptors engaged by fMLF, PAF, GM-CSF, or LPS, so it is possible that priming via different mechanisms might induce different biomechanical kinetics (or indeed a lack of biomechanical changes) during the priming process.

The SLE LDG proteome also contained higher levels of circulating acute phase response proteins than any other neutrophil subset. Although it has not been determined if these proteins are increasingly bound to SLE LDGs *in vivo*, and this is an important experiment for future investigation, many of these proteins are associated with complement and coagulation-associated biological networks and known topromote NET formation [244], a key function of SLE LDGs [50].

In addition, proteins associated with platelet biology (*e.g.* glycoprotein (GP)1BA, GP9) were more abundant in SLE LDGs relative to other neutrophil subsets, similar to transcriptomic descriptions of psoriasis LDGs [245]. This was confirmed by fluorescence microscopy (Figure VI-9F) which despite showing minimal platelet adherence to the isolated neutrophils, did suggest slightly more bound platelets to SLE LDGs relative to SLE NDNs. This also suggests commonalities in the proteome of neutrophils across inflammatory diseases associated with enhanced vascular damage. Platelet-neutrophil interactions can drive inflammation and thrombosis [246]; thus, increased platelet presence in LDG samples may contribute to their upregulation of coagulation and some neutrophil activation-associated proteins relative to NDNs. Ultimately, it is possible that LDG-platelet interactions play a

distinct pathophysiologic role in the development of vasculopathy and this phenomenon should be studied further.

Overall, my observations indicate that SLE LDGs are a proinflammatory neutrophil subset with a distinct proteomic signature that may modulate biomechanical properties and accordingly impact transit ability through the microvasculature. This work adds to our understanding of SLE LDG biology and neutrophil heterogeneity and identifies several potential avenues for future investigations to determine the mechanism behind the unique SLE LDG biomechanical phenotype identified in Chapter V.

# Chapter VII: Conclusion and Future directions

## 1. Summary of findings

### 1.1 Answering the key research questions

The core story of this thesis revolves around the relationships between biomechanical properties, trafficking capabilities, and proteomic makeup of four different neutrophil subsets. Neutrophils are key immune cells which mediate inflammatory responses by relying on functional plasticity and the ability to migrate rapidly through the vasculature and microvasculature [41]. However, neutrophil dysfunction drives a component of clinical manifestations associated with SLE. In particular, the SLE LDG, a neutrophil with unusually low density, contributes to vasculopathy [193]. Although our understanding of the relationship between neutrophil biomechanical properties (*e.g.* density) and neutrophil function is in its infancy, technical advancements in high-throughput techniques, including RT-DC, have led to rapid advancement in this field.

The first question posed at the beginning of this thesis was how do neutrophil biomechanical properties relate to neutrophil priming and immune function in the contexts of health and SLE? This thesis has enhanced our understanding of how neutrophil biomechanical properties change during *ex-vivo* priming or *in vivo* during development of SLE, and subsequently how these changes affect neutrophil trafficking capabilities. This was achieved by both optimising RT-DC as a research tool to measure the biomechanical properties of neutrophils and by developing a new pulmonary microvasculature mimetic. Primed neutrophils are substantially rougher than their un-primed counterparts. I demonstrated that this rougher neutrophil phenotype leads to retention of neutrophils in a microvasculature mimetic. In addition, I described the biphasic biomechanical kinetics that accompany neutrophil priming and identified macropinocytosis as a regulatory mechanism underpinning the second phase of cell expansion and softening. In short, neutrophil priming is associated with complex biomechanical changes including an increase in cell roughness, which may drive entrapment of primed neutrophils in the pulmonary microvasculature.

The second question posed at the beginning of this thesis was do SLE LDGs more closely resemble healthy LDGs or other normal dense neutrophil subsets by biomechanical phenotyping, proteomic profiling, and trafficking assays? Using RT-DC and the pulmonary microvasculature mimetic, I demonstrated that SLE LDGs are rougher than autologous SLE NDNs or healthy NDNs. In line with the findings of rough neutrophils becoming increasingly retained in the microvascular mimetic, SLE LDGs were also more likely to become entrapped than autologous SLE NDNs. This has important implications for LDG trafficking through microvascular beds in the context of SLE; perhaps these cells are increasingly retained in tissues, driving increased inflammation. In addition, I performed proteomics

and phosphoproteomics on four subsets of neutrophils, including SLE LDGs and primed neutrophils. These analyses provided new insights into neutrophil heterogeneity and SLE neutrophil biology, while also identifying mechanisms which potentially regulate this unique SLE LDG biomechanical phenotype and should be explored further.

Thus, in answer to that second research question, the SLE LDG is biomechanically distinct from other neutrophil subsets assessed in this study and, due to these biomechanical properties, SLE LDGs were increasingly retained in a microvasculature mimetic. Proteomic and phosphoproteomic studies have suggested future areas for investigation to determine the mechanism driving the SLE LDG biomechanical phenotype, which was beyond the scope of this thesis. These potential mechanisms should be fully explored in future investigations in order to potentially identify targets for therapeutics regulating cellular biomechanics, as well as to shed new light into cellular drivers of clinical manifestations associated with disease.

## 1.2 Summary of key findings

The major aims of Chapter III were 1) To identify baseline parameters of neutrophil deformability, area, and area ratio by RT-DC, and 2) To establish optimal protocols for neutrophil and LDG isolation yielding pure, undisrupted neutrophils. This thesis was the first instance in which RT-DC was used to analyse immune cells in the blood, in the context of inflammatory disease. Previously, the tools to study neutrophil biomechanical properties in a high-throughput manner were not available. Thus, this thesis lays foundational work for future use of RT-DC, while also making initial forays into linking neutrophil biomechanical properties with their immune function and to their proteomic makeup. It is fully expected that future research projects will use RT-DC to build on this thesis and establish a strong framework linking cellular biomechanical properties and immunologic function, with an eye to understanding disease development and aiming to therapeutically target these links.

I optimised the use of RT-DC for the study of immune cells in whole blood, as well as neutrophils following *ex vivo* isolation. I established the baseline biomechanical parameters of un-primed neutrophils by RT-DC and developed protocols appropriate for analysing the biomechanical properties of primary blood cells. A key finding was that neutrophil roughness is a remarkably sensitive biomechanical parameter. Indeed, the successfulness of purifying un-primed neutrophils from a healthy individual can be verified by RT-DC. Given the sensitivity of neutrophils to priming and the subsequent impact of neutrophil priming on neutrophil immune function, I found RT-DC to be a quick and effective method of verifying that neutrophils were un-primed before proceeding with my experiments.

RT-DC is not without its limitations and it is important to note that diseased or healthy neutrophils actively undergoing NET formation or other extreme morphological changes may be excluded from

RT-DC analysis. To be analysed, cells must pass through a series of narrowly set posts to enter the constriction channel to prevent clogging within the channel [130]. To account for this technical challenge, I suggest that 1) samples analysed by RT-DC are loaded at a consistent concentration ($2.5*10^7$ cells/mL), 2) data collection is visually monitored to ensure stable flow rates, and 3) total cell numbers or flow rates are determined during offline analysis. Even with this fail-safes, small numbers of morphologically warped cells may still not be identified. Despite this limitation, RT-DC analyses cells in whole blood, allows for measurement of biomechanical kinetics over time and analyses many hundreds of cells every second; accordingly, RT-DC is a powerful tool for scientists interested in understanding cellular biomechanical properties and how these properties may be probed to better understand development of clinical disease or how diseased immune cells might respond to various treatments.

Beyond my work to optimise RT-DC-associated protocols for use in the field of immunology and medicine, I developed a microvasculature mimetic from PDMS which successfully allowed for analysis of neutrophil trafficking *ex vivo.* This and similar tools are valuable resources for scientists aimed at decoupling the relative contributions of biomechanical and molecular characteristics to modulation of cell trafficking.

The key aims of Chapter IV were 1) to describe the biomechanical kinetics of neutrophil priming and 2) to identify the mechanism regulating neutrophil expansion after priming. By using RT-DC, I was able to measure the kinetics of neutrophil priming. I found that neutrophils go through sequential phases of stiffening and contracting, followed by softening and expanding; this kinetics is consistent among a range of stimuli. However, kinetic differences due to priming with different stimuli were also observed. For example, PAF and fMLF trigger contraction phases of approximately 5-15 minutes, while the contraction phase of neutrophils primed with LPS or GM-CSF lasts up to thirty minutes. This aligns with known differences in neutrophil priming; for example, stimulation with LPS or GM-CSF expands the neutrophil life span *in vitro* while priming with PAF or fMLF have no effect [34].

Simultaneous to these phases of stiffening and contracting, primed neutrophils become morphologically rougher. Neutrophil roughening alongside expansion was shown to be driven by macropinocytosis, which was later corroborated by scanning electron microscopy and lattice light-sheet microscopy. High resolution microscopy showed membrane protrusions over the entire surface of the primed neutrophil, resembling the membrane ruffling characteristic of macropinocytosis [40].

Proteomics demonstrated my primed neutrophils exhibited lower levels of L-selectin relative to unstimulated neutrophils. This indicates successful neutrophil priming, as neutrophils shed L-selectin quickly following exposure to a priming agent. Aside from differences in L-selectin, unstimulated and

primed neutrophil were very similar. This is unsurprising given neutrophils were primed for twenty minutes, and more time would be required to measure the effects of stimulation on protein transcription and translation. Instead, differences were observed at the level of post-translational modification, which can occur more quickly in response to a stimulus. These proteins differentially phosphorylated between primed and unstimulated neutrophils mapped to networks associated with the cytoskeleton, cellular organisation, and molecular activity, also unsurprising given the biomechanical phenotypic differences identified by RT-DC and confirmed by microscopy.

The major aims for Chapter V were 1) to compare immune cells from healthy individuals and patients with active or stable SLE, 2) to determine how SLE LDGs biomechanically compare to other neutrophil subsets, and 3) to determine the effect of biomechanical properties on modulation of neutrophil trafficking. I used RT-DC and microscopy to show that the SLE LDG has a biomechanical phenotype distinct from other neutrophil subsets, including primed healthy neutrophils. Prior to this thesis, LDGs and NDNs had been determined to be distinct based on density, with no other differentiating structural or molecular (*e.g.* cell surface marker) identifier [193]. This thesis reveals density is not the only biophysical characteristic distinguishing SLE LDGs and SLE NDNs; SLE LDGs are also morphologically rougher than other healthy unstimulated neutrophils.

A core aim of Chapter VI was to identify potential mechanisms regulating the SLE LDG biomechanical phenotype. Although the putative mechanisms promoting enhanced SLE LDG cytoskeletal roughness remain to be fully elucidated and are beyond the scope of this thesis, the proteomics and phosphoproteomics analyses identified potential mechanisms related to specific proteins and phosphoproteins that could be pursued further to identify specific strategies for modulating SLE LDG morphology and subsequent trafficking patterns. Specifically, PFN1 and HRG are more abundant in the SLE LDG proteome relative to SLE and healthy NDNs. PFN1 regulates actin and microtubule dynamics [226, 235], and could be responsible for increased actin polymerisation [236], driving protrusions in the SLE LDG cytoskeleton, while HRG induces neutrophil morphologic changes [207] implicated in the regulation of neutrophil retention in microvasculature [207, 237]. In addition to, or alternatively, phosphoproteomic differences between SLE LDGs and other neutrophil subsets could be responsible for their distinct biomechanical profile. For example, LCP1 cross-links actin filaments into tight bundles, increasing the stability of structures such as lamellipodia and podosomes [238]. Phosphorylation of LCP1 increases its actin bundling capabilities [239], and thus the decrease in LCP1 phosphorylation observed in SLE LDGs could contribute the rougher, yet seemingly more unstructured neutrophil phenotype observed by RT-DC and microscopy.

There is evidence of cellular biomechanical properties impacting cellular trafficking through narrow microcapillaries [116, 207]. Proteomics, RT-DC, and microscopy each demonstrated that SLE LDGs

and primed NDNs are rougher than unstimulated, autologous NDNs, and indeed these rougher neutrophil subsets were increasingly entrapped within a mimetic of the pulmonary microvasculature. These findings suggest a model by which the SLE LDG could contribute to SLE-associated lung vasculopathy. In combination with the SLE LDG's predisposition towards NETosis in circulation and in tissues [50], slow transit of SLE LDGs in the microvasculature could promote endothelial cell damage and vasculopathy with pathogenic consequences for patients.

In addition to the morphology-driven retention within the microvasculature, primed neutrophils increasingly adhere to endothelial cells relative to other neutrophil subsets including SLE LDGs. This finding aligns with the phosphoproteomics, which showed increased expression of phosphoproteins associated with neutrophil-endothelial interactions (e.g. PECAM1) in primed neutrophils relative to other neutrophil subsets including SLE LDGs. This suggests a model in which the macropinocytosis-driven morphology of primed neutrophils mediates slow trafficking through the microvasculature and is regulated by changes at the phosphoproteomic level. These phosphoproteomic-driven changes regulate both biomechanical changes and increased adherence to endothelial cells.

Accumulation of primed or activated neutrophils within the lung microvasculature and interstitial components is a hallmark of ARDS, and thought to be responsible for local injury associated with this disease [192]. Studies have already used measures of neutrophil deformability to assess drug efficacy in deactivating neutrophils and increasing cellular movement through the microcirculation [127]. Milrinone, piclamilast, urinastatin, ketamine, protein C concentrate, and nitric oxide donor FK 409 are drugs that have shown promise in reducing inflammation; mechanical phenotyping demonstrates that these drugs also successfully reduce neutrophil deformability in both neonates and adults [127]. Perhaps other therapeutics could be aimed at neutrophil morphology; returning rougher neutrophils to a smoother phenotype could mediate pathology associated with ARDS and diseases including SLE, driven by neutrophil dysfunction and vasculopathy-associated complications.

Additional core aims associated with Chapter VI included 1) to reveal new insights into SLE biology and function and 2) to understand neutrophil heterogeneity at the proteome and phosphoproteome levels. The numbers of proteins and phosphoproteins identified in my proteomic analyses are in line with or higher than the deepest published neutrophil proteomes [247, 248]. A search of the ProteomeXchange database using the keywords "neutrophil" and "lupus" shows two proteomic analyses of neutrophil extracellular traps [249, 250], but no phosphoproteomic, or indeed proteomic, profiling of SLE NDNs or LDGs. To my knowledge, this is the first proteomics or phosphoproteomics analysis of SLE neutrophils to be completed, and it informs our understandings of both neutrophil heterogeneity and neutrophil function in SLE. SLE NDNs show evidence of activation at the proteome level relative to healthy neutrophils, supporting the apparent role for neutrophils in development of SLE

pathogenesis [251]. In addition, the type I IFN pathway has been associated with SLE pathogenesis and neutrophils responding to these cytokines exhibit proinflammatory responses [31]. My work corroborated these findings, demonstrating that ISG-encoded proteins are higher in SLE LDGs than other neutrophil subsets, consistent with previous transcriptomic reports [13] and supporting an SLE LDG sensitivity to type I IFNs which may contribute to its function and pathogenic capabilities.

This proteomics analysis also revealed higher abundances of acute phase response proteins, platelet proteins, and ribosomal proteins in SLE LDGs relative to other neutrophils subsets. Many circulating acute phase response proteins are associated with complement and coagulation networks and may also play a role in NET formation [244], consistent with the SLE LDG predisposition towards NETosis [193]. It has not been determined if these proteins are increasingly bound to SLE LDGs *in vivo* and this will be discussed further in Section 2.2. Increased abundance of platelet proteins corroborate previous reports of psoriasis LDG transcriptomics [245], and were confirmed by fluorescence microscopy (Figure VI-9). These observations suggest commonalities in LDGs present in various inflammatory diseases associated with vascular damage and suggest LDG-platelet interactions may play a pathophysiologic role in the development of vasculopathy.

Finally, the finding of increased ribosomal proteins in SLE LDGs relative to other neutrophils was striking, with over twenty ribosomal proteins upregulated in SLE LDGs relative to other neutrophil subsets. I have not found previous reports in the literature of increased ribosomal proteins or higher levels of translation in LDGs, but this finding could have considerable implications for protein translation in SLE LDGs and should be explored further. Indeed, given these new findings into SLE biology and with consideration of how early this thesis is likely to fall in the timeline of scientists' appreciation of and understanding of cellular biomechanical properties, several exciting new lines of research investigation could follow from this thesis.

## 2. Avenues for further investigation

### 2.1 Understand the relationships between different types of neutrophil priming and link those relationships to proteomic and biomechanical phenotypes.

Neutrophils primed by a variety of stimuli moved through the same biomechanical kinetics, with a phase of shrinking and contraction, followed by a phase of expansion and softening. This suggests overlap between mechanisms of different types of neutrophil priming. While beyond the scope of my dissertation, I would like to verify whether the mechanisms driving the biphasic kinetics are conserved among multiple priming agents. Specifically, I am interested to know whether the contraction phase of neutrophil priming is mediated by ROCK in all forms of neutrophil priming, or just fMLF-mediated priming [132], and whether the expansion phase is mediated by macropinocytosis for all forms of neutrophil priming as well. The role of macropinocytosis is not well documented in neutrophils, and thus this investigation could shed light on a previously under-recognised neutrophil immune function. Given the differences in kinetics between neutrophil priming mediated by GM-CSF or LPS and priming mediated by PAF or fMLF, especially in the context of known differences between these different priming agents (*e.g.* stimulation with LPS or GM-CSF expands the neutrophil life span *in vitro* while priming with PAF or fMLF has no effect [34]), additional differences between priming in the context of different stimuli could become clear.

It would be interesting to compare the phosphoproteomic profiles of healthy neutrophils that were primed with LPS, GM-CSF, fMLF, or PAF at different time points following stimulation to determine how the phosphoproteome changes in line with the biphasic biomechanical kinetics. By tracking the changes of post-translational modifications in line with the drastic biomechanical changes occurring at the same time points, I could identify the critical phosphorylation sites driving these biomechanical changes, and in turn dig deeper into the mechanisms regulating neutrophil priming by a variety of agents. Studies like these at the intersection of cellular proteomics, biomechanical properties, and immunologic function need to be completed so that high throughput biomechanical analyses though techniques like RT-DC can be better employed in scientific investigations as well as clinical settings. At the moment, a biomechanical change in a cell is not correlated or associated with known differences on an immunologic or proteomic level, but with more large-scale studies aligning all three of these phenomena, future scientists and clinicians will be able to increasingly use biomechanical properties as a screening tool to generate hypotheses for further exploration.

In addition to these larger scale experiments, I would like to determine the role of aquaporins in neutrophil priming and their contribution to the neutrophil expansion phase. As discussed in Chapter IV, I showed that macropinocytosis plays a role in mediating the expansion phase of neutrophil priming, but water influx may also play a role. Water influx through aquaporins is blocked by inhibition of Na+/H+ exchange, the method of action by which amiloride inhibits macropinocytosis [179, 183]. In

addition, neutrophils from patients with systemic inflammatory response syndrome express increased AQP-9 [184] and blocking AQP-9 has been shown to reduce neutrophil activation-induced shape changes [185]. AQP-9 is the most widely researched neutrophil aquaporin [186, 187], but unpublished data from my research group indicate that neutrophils additionally express AQP-1 and AQP-6 in the plasma-membrane, which may play a similar role to AQP9. (Subburayalu J and Pocock J, unpublished). To pursue this line of investigation further, I could treat neutrophils with AQP-1, AQP-6 and/or AQP-9 blockers, which are all commercially available. Then, I would prime the treated neutrophils with fMLF and use RT-DC to determine whether blocking aquaporins ameliorates the expansion phase of neutrophil post-priming kinetics.

### 2.2 Confirm the results of the proteomics by western blot or cell-based assays.

Firstly, I would like to determine whether SLE LDGs are bound with acute phase response proteins *in vivo*. SLE LDGs had much higher abundances of acute phase response proteins relative to SLE NDNs, and these proteins were largely responsible for upregulation of coagulation-associated networks. Although neutrophil subsets prepared for proteomics were isolated using the same methods, I cannot fully exclude that certain technical requirements of the isolation process could have modified the proteomic/phosphoproteomic findings. For example, although neutrophil preparations were washed extensively prior to preparation of the lysates for proteomics, LDGs were exposed to the plasma layer *ex vivo* for slightly longer due to the nature of the density gradient. As such, it is not clear whether this finding is an artefact of the isolation process or whether SLE LDGs do indeed increasingly bind or take up plasma proteins *in vivo*. Given that the SLE LDGs and NDNs were obtained from the same blood samples and given that SLE LDGs were exposed to plasma for only twenty minutes longer than NDNs, I expect the second possibility is more likely. However, I would like to follow up on these results by isolating SLE LDGs and SLE NDNs separately, incubating them both with autologous plasma for thirty minutes, washing all neutrophils extensively and measuring common plasma proteins by in-cell ELISA, western blotting, or proteomics in both samples. This would support or disprove my hypothesis that the higher abundance of plasma proteins in the SLE LDG proteome was not an artefact of the cell isolation strategy. If higher abundances of plasma proteins are increasingly bound to SLE LDGs *in vivo*, then perhaps this is a method by which SLE LDGs drive increased inflammation [252]. Understanding the mechanism by which SLE LDGs might increasingly bind acute phase response proteins and finding a method to block that mechanism could be useful in mitigating pathology associated with SLE.

In addition, findings from the proteomics and phosphoproteomics analyses completed in this thesis should be validated. Firstly, I could use western blotting to measure the amount of ribosomal proteins in SLE LDGs relative to SLE NDNs. If SLE LDGs do have more ribosomal proteins than SLE NDNs, I would be interested to measure the relative rates of translation by both cells, to determine if SLE LDGs produce more proteins. Association of mRNAs with ribosomes has previously been used to estimate translation rates, given that initiation is typically the rate-limiting step in protein translation. TRAP-

Seq, ribo-Seq, and proximity-specific-Seq are all next-generation sequencing-based strategies [253] that could be used to quantify and identify the mRNAs bound to ribosomes in different neutrophil subsets. In-cell ELISAs to quantify and compare abundances of specific proteins or phosphoproteins of interest in different neutrophil subsets should also be used to verify the proteomics and phosphoproteomics datasets.

### 2.3 Understand how the SLE LDG is related to normal dense neutrophils.

Although lattice light-sheet microscopy suggested that SLE LDGs did not resemble healthy NDNs undergoing NETosis, the potential link between NET formation and cytoskeletal roughness in SLE LDGs could be more fully addressed using *in vitro* inhibitors of NET formation. SLE LDGs could be treated immediately post-isolation with vanilloids [254] or peptidylarginine deiminase (PAD) inhibitors (e.g. chloraminidine) [255], both of which inhibit NETosis. Staining for MPO and DNA followed by immunofluorescence microscopy would allow for verification of inhibitor efficacy at preventing NETosis. Then, RT-DC could be performed on SLE LDGs treated with or without inhibitors of NET formation to determine whether this recovered the morphologically rougher SLE LDG biomechanical phenotype into a smooth phenotype resembling NDNs. I would perform the same experiment on autologous SLE NDNs as a control.

The SLE LDGs also did not resemble healthy de-primed NDNs by RT-DC. However, the same actin-associated proteins that were dephosphorylated in SLE LDGs were increasingly phosphorylated in healthy primed NDNs, with unstimulated SLE and healthy NDNs sitting at a middle level of phosphorylation for these proteins. An important follow-up experiment should revolve around priming SLE NDNs. If SLE NDNs are primed by fMLF or indeed SLE-specific immune stimuli such as type 1 IFN or Sm/RNP immune complexes, do they biomechanically and proteomically resemble primed healthy NDNs? Or do innate differences between SLE and healthy NDNs exist and thus might the SLE LDG be identical to a primed SLE NDN? It would be relatively straight forward to answer this question by RT-DC.

It is important to note the proteomic overlap between SLE NDNs and healthy NDNs was much wider than the overlap between SLE LDGs and SLE NDNs. In addition, the biomechanical kinetics associated with neutrophil priming by a variety of agents were conserved but did not align with the SLE LDGs' biomechanical profile. Thus, my hypothesis is that the SLE LDG is not merely a primed SLE NDN. However, it could be a de-primed SLE NDN. Ideally, I would like to prime, then attempt to de-prime SLE NDNs using a variety of agents; PAF, fMLF, and type 1 IFN with Sm/FNP immune complexes. De-priming could be performed by allowing the neutrophils to rest for a set amount of time, or perhaps by mechanical de-priming through use of an optical stretcher [41]. I could perform RT-DC on these neutrophils at the various stages of being un-primed, primed, and de-primed, as well as complete either

phospho-proteomics or a western blot for a few of the key phosphoproteins (*e.g.* LCP1). I could also run these primed or de-primed SLE NDNs through the microvasculature mimetic to assess their trafficking capabilities. Comparing the biomechanical phenotype and phosphoproteome of the SLE LDGs to those of the SLE NDNs at the stages of being un-primed, primed, and de-primed could give scientists a much clearer understanding of how the SLE LDG is related-or not related- to a primed neutrophil. By better understanding the SLE LDG, scientists will better understand its role in SLE pathology, as well as mechanisms to target it therapeutically.

As suggested by the lattice light-sheet microscopy results, increased SLE LDG roughness appears unconnected to NETosis. As discussed in Chapter VI, the proteomics and phosphoproteomics analyses suggested some potential mechanisms that could be pursued further. Specifically, PFN1 regulates actin and microtubule dynamics [226, 235], potentially driving actin polymerisation [236] and protrusions in the SLE LDG cytoskeleton. HRG has been shown to induce neutrophil morphologic changes *in vitro* [207] and thereby reduce neutrophil retention in the lungs of mice [207, 237]. Both PFN1 and HRG are differentially expressed in SLE LDGs relative to SLE NDNs. Thus, it would be interesting to treat isolated SLE LDGs with exogenous HRG and perform RT-DC to determine the effect of HRG on SLE LDG biomechanical properties. It would be more challenging to study the effect of PFN1 on neutrophil biomechanical properties; previous studies have used genetic engineering to silence PFN1 in cell lines [256, 257], but other feasible methods for inducing PFN1 inhibition in SLE LDGs have yet to be identified. The phosphoproteome could also be explored more deeply; I would like to use in cell ELISAs to confirm the decreased abundance of phosphoproteins regulating the actin cytoskeleton like pCORO1A or pLCP1 in SLE LDGs relative to NDNs. Depending on the phosphoprotein of interest, NDNs could be treated with a drug that inhibits the kinase responsible for phosphorylating that protein. An in-cell ELISA could be used to confirm the subsequent decrease in phosphorylation within NDNs. If this decrease in phosphoprotein abundance leads the NDNs to take on the same morphology as the SLE LDGs by RT-DC, this would indicate the lack of phosphorylation on those actin-associated proteins are responsible for the distinct SLE LDG morphology. If the mechanism of enhanced SLE LDG roughness was identified, the biomechanical phenotype could be modified *ex vivo* to specifically demonstrate the SLE LDG biomechanical phenotype is responsible for its retention in the microvasculature mimetic.

### 2.4 Determine the *in vivo* significance of a change in cellular biomechanical properties on immune function.

It has been demonstrated *in vivo* that PAF or GMCSF-primed neutrophils, which are morphologically rougher than unstimulated neutrophils, are increasingly retained in the lung microvasculature [116]. To accomplish this, neutrophils were isolated, radiolabelled and primed *ex-vivo*, then reinjected into the autologous donor and imaged by γ scintigraphy [116]. It would be interesting to perform similar

experiments with SLE LDGs, which could be isolated from donors, radiolabelled, then reinjected and tracked. Trafficking of SLE NDNs could also be analysed in a similar manner for comparison. If like primed neutrophils, SLE LDGs are retained in the lungs to a greater degree than SLE NDNs, this would make a compelling case for the *in vivo* significance of SLE LDG roughness with respect to trafficking. In addition, it has been proposed that retention in the lung microvasculature applies mechanical pressure to shape-changed, primed neutrophils. This is proposed to mechanically and functionally transform the neutrophils, which leave the lung "de-primed" [41]. It would be interesting to see whether SLE LDGs exposed to similar mechanical pressures by a microvasculature mimetic or an optical stretcher also achieve a "de-primed" functionality alongside a smoother phenotype.

In addition, I would like to measure the percentage of SLE LDGs and their biomechanical phenotype in arterial blood as compared to venous blood. Perhaps arterial blood, leaving the pulmonary microvasculature, has a lower percentage of SLE LDGs and/or SLE LDGs with a biomechanically smoother phenotype. This could shed light into the nature of SLE LDGs' functional status relative to primed or un-primed neutrophils and provide insight into the *in vivo* significance of SLE LDG roughness on trafficking. These studies, in parallel with the study described in section 2.3 of this chapter, could open the door to development of new therapeutics targeting cellular morphology to mediate immune dysfunction.

Ultimately, these types of experiments linking biomechanics to *in vivo* cellular functions will allow RT-DC to be used by scientists as a hypothesis discovery-driven platform. To achieve this platform, it is critical to build up sufficient previous research linking biomechanical properties to changes that affect the immune function and clinical pathology. It would be interesting to use neutrophils from a mouse model like Catchup, which has been genetically modified on the neutrophil-specific locus Ly6G with an allele expressing Cre recombinase and the fluorescent protein tdTomato. Neutrophils from this mouse can be visualised *in vivo* based on their expression of this fluorescent protein; if these neutrophils were isolated from mouse blood, treated with or without cytoskeleton modifying agents such as cytochalasin D which have known effects on neutrophil biomechanical properties (and could be verified by RT-DC), and then re-injected into a Catchup mouse, I could visualise any changes to neutrophil trafficking or neutrophil retention in the microvasculature driven by a change in biomechanical properties. By using different types of cytoskeleton modifying agents, I could look at the effects of a change in neutrophil size, deformability, or roughness. This would be one large-scale, important experiment which would allow scientists to use RT-DC and our understanding of biomechanical properties to a greater potential.

## 2.5 Develop RT-DC into a platform that can be used effectively in a clinical setting

It would be exciting to compare the RT-DC biomechanical phenotypes of immune cells, including neutrophils, monocytes, lymphocytes, red blood cells, and eosinophils, in the blood of patients with a range of diseases. This could provide a new tool to help diagnose diseases; given the stark differences in cellular biomechanical properties displayed by patients with active SLE and healthy volunteers, perhaps patients with bacterial infections have blood cell phenotypes that differ from patients with viral infections. Alternatively, perhaps patients with autoimmune diseases have blood cell phenotypes differing from patients suffering from an infectious disease. Biomechanical properties could provide an additional parameter that would allow for a more specific disease diagnosis to be made more quickly. The cost of performing RT-DC is not prohibitive after the initial setup of the instrument and its use in a clinical setting would not require a particularly specialised operator. Development of reusable microfluidic chips could contribute to allowing this technique to be performed cost-effectively at scale. Thus, a greater understanding of if and how divergent cellular biomechanical phenotypes contribute to disease could allow RT-DC to be used to diagnose diseases and determine appropriate treatment options most quickly.

Even without this additional study, some potential uses for RT-DC in a clinical setting already exist. The use of automated patient monitoring systems to improve identification of sepsis in critically ill patients has been proposed [258]; perhaps RT-DC could be used to continuously monitor the shapes of immune cells in blood. In this instance, sudden changes in cellular deformability might alert doctors that a patient is undergoing septic shock [259]. Alternatively, RT-DC is currently capable of being supported by up to three lasers which allows the RT-DC to perform many similar functions to a flow cytometer. Flow cytometry is already utilised for disease diagnostics [260, 261]; as scientists and clinicians better understand the implications of a change in cellular biomechanics for development of disease, cytometers able to detect fluorescent markers as well as biomechanical abnormalities could become invaluable.

## 3. Closing

This thesis demonstrated the use of RT-DC in the context of immunological research, established a series of critical protocols and described the biophysical kinetics of neutrophil priming while also identifying such kinetics' underlying mechanism. In addition, this thesis demonstrates the capability of a change in immune cell biomechanical properties to lead to entrapment in the microvascular and potentially contribute to an inflammatory disease such as SLE. Extensive proteomics and phosphoproteomics corroborate each of these findings, while opening up important opportunities for further understanding their underlying mechanisms. Indeed, as with all research, this thesis has raised new questions. Theory and practice will be greatly enhanced when understandings from the intersection of biophysics and immunology can be leveraged into effective immunotherapeutic strategies for patients suffering from inflammatory dysfunction.

# Appendices

## 1. Neutrophil isolation from venous blood: discontinuous plasma-Percoll gradients

*As described by Haslett, C., et al., Modulation of multiple neutrophil functions by preparative methods or trace concentrations of bacterial lipopolysaccharide. The American Journal of Pathology, 1985. 119(1): p. 101-110.*

### 1.1 Materials

- Place following into warmer bath at 37 degrees C
    - 6% dextran
    - 0.9% saline - also keep one Falcon tube of saline at 4°C for diluting Percoll
    - PBS +/+ (with $Ca^{2+}$/$Mg^{2+}$)
    - PBS -/- (without $Ca^{2+}$/$Mg^{2+}$)
- Prepare anticoagulated Falcon tubes
- Set up 50 mL BD Falcon polypropylene tubes- 40 mL blood per Falcon tube
- Put 3.8% sodium citrate (vials in fridge) into Falcon tubes
    - Use 1 mL citrate/10mL blood = 4 mL citrate/40 mL blood
- Prepare bleach solution
    - 2 bleach tablets + water

### 1.2 Procedure

- Collect blood with 19G butterfly and 50 mL syringes (40 mL per syringe)
- Add 40mL blood down the side of each Falcon tube; invert gently to mix
- Remember to spray each item before placing in hood
- 1st spin program 1 (20 min, 300 x g)- separates into:
    - Supernatant (S/N) = platelet rich plasma (PRP)
    - Pellet = white and red cells
- Remove (pipette/Pasteur) S/N (PRP) into fresh 50 mL Falcon tubes
- Use to make platelet poor plasma (PPP) and autologous serum
- Sediment remaining cells
- Add 6% dextran down sides of tubes- add 2.5 mL dextran /10 mL cell pellet
- Then add warm saline to make up volume to 50 mL
- Mix by gently rolling tubes several times to re-suspend cells
    - Leave with caps loosely on (to let air in) for 25-40 min at room temp
- Upper layer - white cells, bottom layer = red cells
- Prepare Percoll gradients whilst waiting for sedimentation
- Once Percoll is prepared, place in fridge whilst remainder of sedimentation occurs.
- Add 10 mL PRP into sterile glass vial
- Then add 220 µL of 10 mM CaCl2 (do not add CaCl2 first) => vortex

- Place in CO2 incubator, leave for 30-60 min with lid of vial loose
    - Then store at 4°C or freeze
- Use remaining PRP- 2nd spin program 2 (20 min, 1400 x g) - separates into:
    - S/N = PPP
    - Pellet = platelets
- Remove (pipette/Pasteur) S/N (PPP) into fresh 50 mL Falcon tubes; discard pellet (platelets)
- Sedimented cells: upper layer - white cells, bottom layer = red cells
- Remove (pipette/Pasteur) upper layer (white cells) into fresh Falcon tubes
- Discard bottom layer (red cells)
- Upper layer (white cells): 3rd spin program 3 (5 min, 260 x g)
- (Discard S/N, use cell pellet for below)
- Make one set of gradients for each individual tube
- Make 90% Percoll
    - 4.5 mL Percoll + 0.5 mL Cold 0.9% saline => Vortex to mix
- Make gradients - add Percoll and PPP => Vortex

| | |
|---|---|
| 42%: | [0.8 mL + 40 µL] of 90% Percoll<br>[1.0 mL + 160 µL] of PPP |
| 51%: | [1.0 mL + 20 Ml] of 90% Percoll<br>[0.9 mL + 80 µL] of PPP |

- Get white cells after 3rd spin
    - Discard (pour carefully) S/N into waste container with bleach
- Resuspend remaining pellet by tapping tube gently
- Pool maximum of 2 tubes of cell pellets together into 15 mL Falcon tube (use glass or plastic Pasteur not Gilson)
- Add PPP to make up volume to 2 mL per tube of cells ("wash" old tube with required PPP then pipette into small tube)
- Underlay Percoll gradients: 42% first, then 51%
    - Use glass Pasteur with Pipette boy
    - Take Percoll up a glass Pasteur - avoid air bubbles
    - Slide Pasteur down the side of the cell tube to the bottom of tube, then slowly release Percoll- avoid air bubbles
- Transfer tube carefully to centrifuge
- 4th spin program 4 (14 min, 150 x g, 1/ \0) - layers:
    - Top (PPP/42%) interface: mononuclear cells (PBMCs)
    - Next (42%/51%) interface: polymorphonuclear cells (PMNs)

- Collect PBMCs. Count or analyse LDGs within the PBMC layer or purify further with EasySep.
- Collect PMNs
    - Remove PPP, mononuclear cells and 42% with P1000 Gilson/Pasteur - discard
    - Collect PMNs with fresh Pasteur- put into fresh 50 mL Falcon tube
    - Discard 51% and red cell pellet
- Add remaining PPP to PMN, mix and discard S/N
    - Resuspend cells then make up volume to 50 mL with PBS -/-
    - Use these cells in PBS -/- for cytospin and hemacytometer
- From this point onwards use Cell Saver (wide bore) pipette tips
- Breathe onto hemacytometer to moisten
- Slide cover slip over until Newton's refraction (rainbow-like) rings appear
- Fill each of the two chambers with 10 µL of cells suspend in PBS -/-
- Calculate total number of cells
- Counting area of 5 x 5 large squares with total area = 1mm2
- Depth of chamber = 0.1 mm
- Number of cells per mL = Hemacytometer count x 10000
- Total number of cells in 50 mL - Hemacytometer count x 10000 x 50
- Calculate volume of PBS +/+ required to make concentration of 5 million cells

| Dimensions | Area | Volume at 0.1 mm depth |
|---|---|---|
| 1 x 1 mm | 1 $mm^2$ | 100 nL |
| 0.25 x 0.25 mm | 0.0625 $mm^2$ | 6.25 nL |
| 0.25 x 0.20 mm | 0.05 $mm^2$ | 5 nL |
| 0.20 x 0.20 mm | 0.04 $mm^2$ | 4 nL |
| 0.05 x 0.05 mm | 0.0025 $mm^2$ | 0.25 nL |

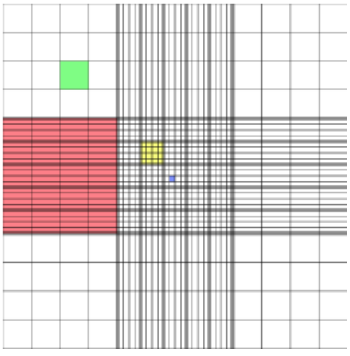

- Label slides with pencil
- Set up into clip (bottom to top): slide, filter paper smooth side facing down towards slide, funnel
- Add 100 µL of cells suspended in PBS -/- into funnel (use Cell Saver tips)

- Spin in Cytospin3 machine: program 1 (300 x rpm, 3 min, high acceleration)
- Remove slides and air dry for 10-15 min
- Stain slides;
    - 4 min in methanol => 1 min in orange stain => 3 min in blue stain
    - Rinse with water then air dry
    - When dry, mount with 1 drop of DPX then add cover slip
    - Count cells under microscope for differential count
    - Count 200 cells- count neutrophils, eosinophils, PBMCs, erythrocytes
- Cells in PBS -/-: 5th spin program 5 (5 min, 256 x g)
    - Discard S/N
- Resuspend cells then make up volume to 50 mL with PBS +/+
- Cells now in PBS +/+: 5th spin program 5 (5 min, 256 x g)
    - Discard S/N
- Resuspend cells
- Add volume of PBS +/+ required to make up a concentration of 5 million cells / mL
    - Cells are now ready

## 2. Neutrophil isolation from venous blood: Ficoll gradient + EasySep

*Protocols from Kaplan lab and StemCell Technologies, adapted by Kathleen Bashant & Liam O'Neil May 2019.*

### 2.1 Materials

- Place following into warmer bath at 37°C
    - PBS +/+ (with $Ca^{2+}$/$Mg^{2+}$)
- Set up 50 mL BD Falcon polypropylene conical tubes- 20 mL ficoll per Falcon tube, 3 tubes for 60mLs blood
- Prepare EasySep media: PBS + 2% FBS + 1mM EDTA
- Also need EasySep Human Neutrophil Isolation kit and EasySep Direct Human Neutrophil Isolation with customized antibodies against CD86 and HLA-DR4 (all from StemCell Technologies).
- 50mL BD Falcon polypropylene conical tubes for PBMC collection
- 5mL tubes for EasySep isolation

### 2.2 Procedure

- **Note before starting:** LDGs are most stable 1 hour or less after drawing blood. This protocol should be completed as quickly as possible in order to preserve the properties of the LDG

- Carefully layer 20 ml of whole blood from green top tubes over the Ficoll so you don't disturb the Ficoll layer
- Centrifuge the tubes of blood and Ficoll and the red top serum tube for 20 mins at 1440 rpm (150x g) with the brake set at 1 and the accelerator set at 1
- While the tubes are spinning, label two 1.5 ml Eppendorf tube with the patient's ID number, the date and the word "serum."
- Label another two 1.5 ml Eppendorf tubes with the patient's ID number, the date and the word "plasma."
- After the tubes finish spinning, transfer 1 ml of serum from the red top tube to each of the Eppendorf tubes labelled "serum" and transfer 1 ml of plasma from the very top of one of the conicals of Ficoll and blood to each of the Eppendorf tubes labelled "plasma."
- Do not throw out the red top after taking off the serum to bank. It may be used later for other experiments requiring autologous serum
- Using a plastic transfer pipet, lower the pipet through the plasma layer to the top of the interface where the cloudy layer is. Slowly pull up the cells as you move the pipet in circles around the cloudy layer. Deposit the cells into an empty conical. Repeat until all PBMCs from all Ficoll tubes have been transferred to the empty conical
- Note: the plasma layer will not be drawn off before the PBMCs are collected, so when the cells are deposited into a new conical, there should mostly be plasma in the tube
- Fill the conical the rest of the way up with EasySep Media (PBS with 2% FBS and 1mM of EDTA)
- Count the PBMCs on a hemacytometer after pooling
- Spin the pooled PBMCs at 1600 rpm for 7 mins with both the brake and accelerator set at 9
- While the PBMCs are spinning, remove the remaining Ficoll from one of the conicals so there is as little Ficoll over the erythrocyte layer as possible
- Mix the erythrocyte layer by swirling the tube and set aside
- After the PBMCs have finished spinning, suck off the supernatant and resuspend the cells in Easy Sep media so the concentration is 50 million PBMC/mL
- Note: The remaining steps for LDG isolation using the Human Neutrophil Isolation Kit and the NDN isolation using the Human Direct Neutrophil Isolation Kit will be done simultaneously to complete the protocol in the shortest amount of time even though the two isolation protocols are written separately.

**LDG Isolation using the Human Neutrophil Isolation Kit**

- Place up to 2 mL of the 50 million PBMC/ml solution into a 5 ml polystyrene round bottom tube. If the volume of this solution exceeds 2 mL, split the solution into as many tubes as necessary so that all tubes have the same volume and no tube exceeds a volume of 2 mL Take note of the volume in each tube
- Calculate the amount of Isolation cocktail necessary to add to each tube using the equation below:
- 50 µL/mL multiplied by volume of cell suspension=volume in µL of isolation cocktail
- Add the volume of isolation cocktail calculated above to each of the tubes of cell suspension
- Add the HLA-DR antibodies to the cell suspension using the same volume as the isolation cocktail if this antibody is not already included in the cocktail
- Add the CD86 antibodies to the cell suspension using the same volume as the isolation cocktail if this antibody is not already included in the cocktail
- Pipet up and down to mix each tube and incubate at room temperature for 5 minutes.
- While the cells are incubating, calculate the volume of Rapid Spheres to add to each tube using the equation below:
    - 40 µL/mL multiplied by volume of cell suspension=volume in µL of Rapid Spheres
- Vortex the Rapid Spheres for 30 seconds, then add the volume calculated above to each of the tubes of cell suspension
- Pipet up and down to mix each tube and incubate at room temperature for 3 mins
- Add EasySep media to each tube so that the total volume in each tube is 2.5 mL
- Mix each tube by pipetting up and down
- Place the tube on the magnet and incubate at room temperature for 5 min
- After incubating, carefully pipet out the transparent part of the solution and deposit it into a new polystyrene tube. Do not touch the sides or the bottom of the tube, as this is where the cells have stuck to the magnet and it will contaminate your solution
- Place the new tube on the magnet and incubate at room temperature for 5 min
- Pipet only the clear fraction out of the tube and place into a new polystyrene tube or conical; LDGs are now purified

**NDN Isolation Using the Human Direct Neutrophil Isolation Kit**

- For 1 mL of erythrocyte pellet in a 5 mL polystyrene tube:
- Add 1 mL of the erythrocyte layer from the Ficoll tube to a 5 ml polystyrene round bottom tube

- Dilute the erythrocyte layer by adding 1 mL of the Easy Sep media to the round bottom tube. Pipet up and down to mix until the solution is homogenized
- Vortex the vial of brown Rapid Spheres for 30 seconds
- Add 100 ul of the isolation cocktail and 100 µL of the Rapid Spheres to the diluted erythrocyte layer
- Pipet up and down to mix the solution and incubate at room temperature for 5 mins
- Add Easy Sep media so the total volume in the tube is 4 mL. Pipet up and down to mix
- Place the tube into the magnet and incubate at room temperature for 10 mins
- After incubating, carefully pipet out the transparent part of the solution and deposit it into a new polystyrene tube. Do not touch the sides or the bottom of the tube, as this is where the erythrocytes have stuck to the magnet and it will contaminate your solution.
- Vortex the Rapid Spheres again and add 100 µL to the transparent solution in the new tube
- Mix the tube by pipetting and incubate for 5 mins at room temperature.
- Place the incubated tube onto the magnet and incubate for 5 mins at room temperature.
- Add Easy Sep media so the total volume in the tube is 4 ml. Pipet up and down to mix.
- Carefully pipet the transparent fraction out of the old tube and into a new polystyrene round bottom tube. Be careful not to touch the sides or bottom of the tube with your pipet, as it will contaminate your solution
- Place the new tube with the clear fraction into the magnet for a 3rd separation. Incubate 5 mins.
- Pipet only the clear fraction out of the tube and place into a new polystyrene tube or conical; NDNs are now purified

**Neutrophils direct from whole blood (no Ficoll gradient, mix of LDGs and NDNs)**

- For 2.5 mL erythrocyte pellet in a 14 mL polystyrene tube:
- Add 2.5 ml of the erythrocyte layer from the Ficoll tube to a 14 ml polystyrene tube
- Dilute the erythrocyte layer by adding 2.5 mL of the Easy Sep media to the tube. Pipet up and down to mix until the solution is homogenized
- Vortex the vial of brown Rapid Spheres for 30 seconds
- Add 250 ul of the isolation cocktail and 250 µL of the Rapid Spheres to the diluted erythrocyte layer
- Pipet up and down to mix the solution and incubate at room temperature for 5 mins
- Add Easy Sep media so the total volume in the tube is 12 mL, pipet up and down to mix
- Place the tube into the magnet and incubate at room temperature for 10 mins

- After incubating, carefully pipet out the transparent part of the solution and deposit it into a new polystyrene tube. Do not touch the sides or the bottom of the tube, as this is where the erythrocytes have stuck to the magnet and it will contaminate your solution
- Vortex the Rapid Spheres again and add 250 µL to the transparent solution in the new tube
- Mix the tube by pipetting and incubate for 5 mins at room temperature
- Add Easy Sep media so the total volume in the tube is 12 mL. Pipet up and down to mix
- Place the incubated tube onto the magnet and incubate for 5 mins at room temperature
- Carefully pipet the transparent fraction out of the old tube and into a new polystyrene round bottom tube. Be careful not to touch the sides or bottom of the tube with your pipet, as it will contaminate your solution
- Place the new tube with the clear fraction into the magnet for a 3rd separation. Incubate 5 mins
- Pipet only the clear fraction out of the tube and place into a new polystyrene tube or conical. Neutrophils are now purified.

## 3. Real-time Deformability Cytometry

*Author: Kathleen Bashant. Last revised: January 2018.*

### 3.1 Materials

- CellCarrier buffer (PBS + 0.5% methylcellulose)
- RT-DC instrument (AcCellerator)
- 2x 1mL syringe, 3x tubing (sheath, sample, and exit)
- Flic20 PDMS microchannel devices (ZellMechanik Dresden)
- 2mL Eppendorf tubes for samples and waste

### 3.2 Procedure

**Turn on the RT-DC Instrument**

- Start computer – button on the computer and the screen; password: Cambridge
- Turn on microscope power supply and the RTDC machine (2 boxes below the syringe holder)
- Turn on microscope
- Turn on box behind syringe pump by pressing the orange switch. Use the dials on the box to adjust the voltage to 8V. Must not be above 8V before you plug the cables in.
- Plug in cables (red in red, black in black)
- Open QmixElements
    - Top right button looking like a plug: Connect to Device
    - Right click in field with syringe, “Reference move.” Click Okay.
    - This will move syringes on the machine and on the screen
    - Close Qmix
- Open “syringe pump” program
    - Initialize pump
    - Click the boxes by “no syringes”, placing a black check in each.
    - Click “Reference move” in the top right-hand corner.
- Choose folder for saving
    - New exp folder: copy/paste and rename
    - Open “new Tracking” (ShapeIn)
    - Sometimes (very rarely) may need to restart the computer
    - Go through project folder and click the folder you want to save in, don’t open it.
    - Click start, then stop to refresh (top left black arrow is start, red stop sign is stop)

- For isolated neutrophil measurements, gates should be 5, 80, 80
- For immune cells in blood, gates should be 5, 16, 20
    - Sheath tubing can stay the same for a few months. Use a different type of sample tubing for each condition
- Push dH2O through the waste tube at the beginning to ensure no blockages, then ensure you start the process with an empty waste tube, remove cap of the waste tubing
- Additional Notes:
    - If the image from the microscope is black or if the lighting seems wrong: Complete Koehler illumination method before using microscope:
        - Ensure that the light box is pushed all the way back on the microscope
        - Use the top dial to close the microscope field slightly, to see the black octagon. Ensure that the octagon is in the centre of the field of vision
        - If it's not in the centre, use the silver knobs by that top dial to adjust the octagon so it's in the centre of the field of vision
        - Focus the octagon so there is crisp contrast between the black and the light field of vision. Better to be over than under-focused
- For some experiments, you may need to note temperature when taking RTDC measurements: temperature influences viscosity, which influences shear forces.

**Preparation before RT-DC Measurements**

- Prepare sheath and sample tubing: Flush with 3x 10mL dH20 water and dry by pushing air through 1-2x 10 mL times
- Attach a blunt needle to a 1ml syringe. Draw CellCarrier buffer into the sheath flow syringe. Sheath flow level should be at 1000µL (or as high as you can get it). Tap to get rid of air bubbles. Remove needle from syringe and dispose of needle in yellow container. Attach syringe to sheath flow tubing. Repeat with the syringe for the sample & attach to sample flow tubing.
- Place syringes on RT-DC machines horizontally (syringe handles are perpendicular to machine). See picture in phone/lab notebook for details.
- In the Syringe Pump program, set the level of the syringe to the volume of liquid in each syringe. Press the green play button to prepare the machine. Unclick "no syringe".
- Set the sheath (and later sample) flow rates to 3µL/sec and press the green play button. Flush the air out of the tubes into a blue conical cap with paper (use a new cap/paper

for each sample). As soon as all the air has been flushed, decrease the flow rate to 0.1ul/s (and press “play”).

**RTDC Measurements:**

- For BLOOD
- Requires different sets of tubing between patients or good tube cleaning
- CellCarrier buffer goes into sample and sheath tubes.
- Settings are 5, 16, 20 for PMN measurement in whole blood (allows for avoidance of most erythrocytes)
- 950 µL CellCarrier buffer + 50 µL blood for dilution
- Expel blood just above tube bottom in a circular motion, up through the top of the volume.
- Mix slowly and for a while: gently by rolling and a little inversion
- Don’t activate by flicking the tube!
- Draw mixed blood dilution up flushed sample tube by the Syringe Pump program. Un-check (click) the “no syringe” box & set flow rate to 0.09ul/second for placement in microfluidic chip.

- For ISOLATED CELLS
- Requires different sets of tubing per condition or good tube cleaning. Methylcellulose buffer goes into sample and sheath tubes.
- Prepare 3 Eppendorf tube: 1x waste, 1x sample refill, 1x sheath refill. Refill tubes both get MC++ buffer inside. Use different aliquots of buffer when re-filling sample and sheath tubes to avoid contamination.
- Spin cells at 1.3rpm or 0.2g for 3 minutes at room temperature (use round bottom tubes if possible)
- Remove samples from centrifuge. Pull off supernatant using 1000ul pipette (pull it ALL off).
- Resuspend pellet in methylcellulose buffer (200 µL for 5 million cells) by gentle rolling and tapping. Be careful not to activate PMN by vigorous pipetting!
- Take the sample syringe tubing (which has been flushed with MC++ buffer) and, keeping it running at 0.09ul/sec, place the end inside the sample tube. Stop the flow rate. Adjust the syringe level to 80-150ul above the current sample syringe volume and press play

- By pressing play, 150 µL of sample will be pulled into the sample tubing. Avoid air bubbles.
- After checking for air bubbles, set the sample flow rate at 0.09 µL/sec again and press play. Only then may you remove the sample tubing from the tube that initially contained PMNs.

- START RTDC measurements:
- When a small droplet has formed on the end of the sheath and sample tubes place both tubes firmly but gently into the holes of 20 µm RTDC chips.
- Place first the sample tub into the middle hole of the cell chip. Place the sheath tub into the far-right hole (closest to the middle hole) of the cell chip. Connect the waste tube to the final far left hole.
- Use magnets to place cell chip in the RT-DC machine. Watch the chip's channel flood with sample on the microscope (Click "Get Overview" to view microscope field).
- Check for air bubbles in cell channels. Use a sheath flow rate of 0.09µl/s to eliminate bubbles. When you see sample begin to flow (cells appear), lower the sample flow to 0.03µl/s using the SyringePump program. Hit start to adjust the flow rate. You can verify the flow rate on the ShapeIn program. When there are no air bubbles and the sample appears to be flowing in a nodule pattern between the reservoir and the channel, you are ready to take measurements.
- Ensure sheath flow rate is 0.09 µL/s. Hit start. Usually wait for 30-60 sec to stabilize flow prior to measurements.
- Focus microscope on the end of the small channel where the cells will be leaving (to the far left). Adjust so that there is contrast between the black channel/cell outlines and white background. This contrast is what the machine will read. Click "start measurement"
- While sample run: Get background images every time you touch the desk/computer or if the white dots show up and don't go away (watch the "after thresholding" image). Pay attention to the microscope image as well – are the cells running through the channel smoothly and consistently or are they bouncing around? Bouncing or changes to flow rate may indicate a clog. Green dot indicates the machine is running.
- After 5000 events (or experimental preference) stop sample by pressing stop sign button.
- Click "get overview" and scan channel using microscope to check for clogs in the channel. Only accept measurements for analysis without clogging, as this will affect mechanical properties measured.

- Change “Channel” to “reservoir” and focus the microscope on the “reservoir.” Use the bottom edge as a reference to focus. Acquire image (5000 events) as a negative control, for the deformation of cells without any constriction pressures placed.
- Every RTDC analysis requires sample measurement in both channel and reservoir if you are interested in deformation
- Different conditions for different types of cells. For PMNS:
- Sheath flow: 0.09 µL/s
- Sample flow: 0.03 µL/s
- Collect not less than 5000 events and ideally 10,000 events.
- Make notes for every measurement: at minimum indicate the measurement number, the number of events, average area/deformation, the flow rate, and whether you checked for clogs.

**Shut down RTDC:**

- If you have more than an hour to wait, turn off the RT-DC machine. If the computer goes to sleep, you will need to restart the system. Otherwise, lower the flow rate to 0.01µL/second and wait for the next sample to be ready.
- Turn off sheath and sample flow. Remove chip and tubes from the instrument.
- Chips, needles and blood covered tips go into the sharps bin. Syringes (even with blood in them) go into S2 autoclave waste (make sure there is enough paper tissue to absorb the liquid)
- Run water through the sheath tubing and through the waste tubing to clean out methylcellulose. Follow with air. Let tubing sit out overnight to dry.
- Protocol changes may be necessary if large quantities of blood are used.
- Run water through the sample tubing 3-5 times. Follow with air. Leave out overnight to dry further
- Wipe down RT-DC machine with water and paper towel to eliminate methylcellulose debris
- Click out of the ShapeIn program without saving changes. If the program prompts you to save changes, it’s because you changed the program accidentally. Your samples are automatically saved in your folder.
- Quit Syringe pump program before closing out the program
- Shut the machine down in the same order you turned it on.
- First, unplug the wires from the power source. Make sure to grip the wires close to the base of the box!
- Turn off the power source behind the microscope.

- Turn off the microscope
- Turn off the RT-DC and microscope power boxes
- Turn off the computer.

**General Notes:**

- ShapeIn is RTDC measurement software and ShapeOut is the analysis software
- Need to use a hard drive to store, transfer, and backup data as these are massive data files.
- Important to run technical triplicates until you are confident in your abilities – it takes a little while to get a handle on adjusting the microscope consistently. Mistakes/variation are normal at first.
- Perform experiments with biological replicates.
- Both sheath and sample flow tubes MUST be air-free before connecting to the cell chip.
- During breaks stop the sample flow and reduce the sheath flow to 0.01 µL/sec. Increase sheath flow back to 0.09 µL/s before loading a new sample (refer to 2.5). You can adjust the flow rates to eliminate air bubble in the chip more quickly, or to try to clear a clog but you NEVER want a higher sheath than sample flow. This is likely to lead to severe clogging.
- If you use a lot of pressure to clear a clog, give the flow rate enough time to stabilize before taking measurements again – if pressures change the channel shape, you must use new chip

## 4. Ibidi Flow assay

*Original by Arlette Vassallo (Summers Laboratory). Last revised January 2020 by Kathleen Bashant.*

### 4.1 Materials

- Isolated neutrophils from whole blood
- Warmed PBS +/+ (with $Ca^{2+}$/$Mg^{2+}$)
- Ibidi Flow pump system & inverted microscope with temperature control box set at 37 degrees C with 5% $CO_2$
- Endothelial cells: grow to 80% confluence on 75 $cm^2$ flasks in endothelial cell growth MV2 medium with 2% foetal calf serum (FCS)
    - Lift cells off the flasks using 6 mL of TrypLE for 3 minutes
    - Neutralize with 12 mL of medium
    - Spin cells at 260 g for 3 minutes
    - Remove S/N and re-suspend in MV2 medium at 1 million/mL
    - Transfer 120 µL of cell suspension to Ibidi® µ-slide VI 0.4 chambers
    - Grow to confluence overnight at 37 degrees C in 5% $CO_2$

### 4.2 Procedure

- Suspend isolated neutrophils in PBS+/+ at a concentration of 1 million/mL
- Wash the confluent endothelial cells for 2 minutes with PBS+/+ at 0.4 mL/minute
- Flow neutrophils across the endothelial surface for 4 minutes at 0.4 mL/minute
- Using the 10x lens, record a 3-minute video during this time.
- Wash with PBS+/+ for 2 minutes of wash
- Using the 20x lens, image five randomly selected sites, acquiring 6 frames, 4 seconds apart.

# 5. Pulmonary microvasculature mimetic

*Author: Kathleen Bashant. Last revised: January 2020.*

## 5.1 Materials

- Isolated neutrophils from whole blood
- Warmed PBS +/+ (with $Ca^{2+}$/$Mg^{2+}$)
- Fluigent constant pressure pump system and appropriately sized tubing
- Inverted microscope with a temperature control box set at 37 degrees C with 5% CO2
- PDMS microvasculature mimetic device, flushed with water

## 5.2 Procedure

- Using the pump system, flush the device with PBS.
- Ensure channels are free from air bubbles
- Suspend isolated neutrophils in PBS+/+ at a concentration of 0.33 million/mL
- Place cells into the pump and set the pump at 20mbar to flush tubing
- As tubing is flushed, allow a small bubble to extrude from one end
- Place the end of the tubing with the bubble into the device and immediately place the device on the microscope.
- Set the pump to 50mbar (or pressure of interest)
- Using the 10x lens, watch the PBS and cells move through the entire device and begin flowing smoothly
- Using the 10x lens, record a 3-minute video of cells transiting the device
- When finished, save the videos as MP4 files with clock and scale bar
- Export MP4 files
- Manually record the amount of time each cell takes to transit the mimetic, from entry to exit of the vasculature mimetic portion of the device
- Cells retained in the mimetic for over 120 seconds are recorded as retained

# 6. Publications and presentations arising from this thesis

## 6.1 Publications

**Bashant KR**, Aponte AM, Randazzo D, Sangsari PR, Wood AJT, Bibby JA, West, EE, Vassallo A, Manna A, Playford MP, Jordan N, Hasni S, Gucek M, Kemper C, Conway Morris, A, Morgan NY, Toepfner N, Guck J, Mehta NM, Chilvers ER, Summers C, Kaplan MJ. Proteomic, biomechanical, and functional analyses define neutrophil heterogeneity in the context of systemic autoimmunity. Annals of Rheumatic Disease, Published Online First: 28 September 2020. doi: 10.1136/annrheumdis-2020-218338. [262]

**Bashant KR,** Toepfner N, Day CJ, Mehta NN, Kaplan MJ, Summers C, Guck J, Chilvers ER. The mechanics of myeloid cells. Biology of the Cell, 2020. 112: 103-112. doi:10.1111/boc.201900084. [263]

**Bashant KR**, Vassallo A, Herold C, Berner R, Menschner L, Subburayalu J, Kaplan MJ, Guck J, Chilvers E, Toepfner N. Real-time deformability cytometry reveals sequential contraction and expansion during neutrophil priming. Journal of Leukocyte Biology, 2019. 105(6): p. 1143-1153. [132]

Porter L, Toepfner N, **Bashant KR**, Guck J, Ascroft M, Farahi N, Chilvers ER. Metabolic profiling of human eosinophils. Frontiers Immunology, 2018. 9(1404). [120]

Jing C, Mathews R, Ferdinand J, Lok L, Loudon K, Richoz N, Banham G, Castro-Dopico T, Fitzpatrick S, **Bashant K**, Siegal R, Kaplan MJ, Johnson R, Murphy M, Clatworthy M. Macrophage Metabolic Reprogramming Presents a Novel Therapeutic Target in Lupus Nephritis. Proceedings of the National Academy of Sciences of the United States of America, 2020 Jun;117(26):15160-15171. DOI: 10.1073/pnas.2000943117. [264]

## 6.2 Conference presentations

**2020** Proteomic, biomechanical, and functional analyses define neutrophil heterogeneity in the context of systemic autoimmunity (oral presentation). Annual NIH Global Doctoral Partnerships Research Workshop, Maryland, USA.

**2020** Proteomic, biomechanical, and functional analyses define neutrophil heterogeneity in the context of systemic autoimmunity (oral presentation). National Institute for Arthritis and Musculoskeletal and Skin Diseases Intramural Retreat, Maryland, USA.

**2019** Applying real-time deformability cytometry (RT-DC) to the intersection of neutrophil biophysical properties and immunologic function (poster). NIH Graduate Student Research Conference, Maryland, USA.

**2019** Real-time deformability cytometry reveals the biophysical kinetics of neutrophil immune function, particularly in the context of lupus (poster). Annual NIH Global Doctoral Partnerships Research Workshop, Oxford, UK.

**2019** Real-time deformability cytometry reveals the biophysical kinetics of neutrophil immune function, particularly in the context of lupus (poster, session prize). National Institute for Arthritis and Musculoskeletal and Skin Diseases Intramural Retreat, Maryland, USA.

**2018** Real-time deformability cytometry reveals sequential contraction and expansion during neutrophil priming (poster). Annual NIH Global Doctoral Partnerships Research Workshop, Cambridge, UK.

**2018** Real-time deformability cytometry reveals sequential contraction and expansion during neutrophil priming (poster). Neutrophil 2018, Quebec City, Canada.

**2017** Real-time deformability cytometry reveals sequential contraction and expansion during neutrophil priming (poster). Cambridge University Department of Medicine Research Day, Cambridge, UK.

**2017** Using real-time deformability cytometry (RT-DC) to define the relationship between genetics, mechanical properties, and function of neutrophils in health and inflammation (poster). Annual NIH Global Doctoral Partnerships Research Workshop, Maryland, USA.

**2017** Using real-time deformability cytometry (RT-DC) to define the relationship between genetics, mechanical properties, and function of neutrophils in health and inflammation (poster). National Institute for Arthritis and Musculoskeletal and Skin Diseases Intramural Retreat, Maryland, USA.

# References


1. Wang, L., F.-S. Wang, and M.E. Gershwin, *Human autoimmune diseases: a comprehensive update*. Journal of Internal Medicine, 2015. **278**(4): p. 369-395.
2. Fairweather, D. and N.R. Rose, *Women and autoimmune diseases.* Emerging infectious diseases, 2004. **10**(11): p. 2005-2011.
3. Gupta, S., et al., *Sex differences in neutrophil biology modulate response to type I interferons and immunometabolism.* Proceedings of the National Academy of Sciences, 2020. **117**(28): p. 16481-16491.
4. de Jesus, G.R., et al., *Understanding and Managing Pregnancy in Patients with Lupus.* Autoimmune diseases, 2015. **2015**: p. 943490-943490.
5. Cusick, M.F., J.E. Libbey, and R.S. Fujinami, *Molecular mimicry as a mechanism of autoimmune disease.* Clinical reviews in allergy & immunology, 2012. **42**(1): p. 102-111.
6. Kaplan, M.J., *Neutrophils in the pathogenesis and manifestations of SLE.* Nature reviews. Rheumatology, 2011. **7**(12): p. 691-699.
7. Kaul, A., et al., *Systemic lupus erythematosus.* 2016. **2**: p. 16039.
8. James, J.A., *Clinical perspectives on lupus genetics: advances and opportunities.* Rheumatic diseases clinics of North America, 2014. **40**(3): p. 413-vii.
9. Obermoser, G. and V. Pascual, *The interferon-α signature of systemic lupus erythematosus.* Lupus, 2010. **19**(9): p. 1012-1019.
10. Dema, B. and N. Charles, *Advances in mechanisms of systemic lupus erythematosus.* Discov Med, 2014. **17**(95): p. 247-55.
11. Bardoel, Bart W., et al., *The Balancing Act of Neutrophils.* Cell Host & Microbe, 2014. **15**(5): p. 526-536.
12. Borregaard, N., *Neutrophils, from Marrow to Microbes.* Immunity, 2010. **33**(5): p. 657-670.
13. Eash, K.J., et al., *CXCR2 and CXCR4 antagonistically regulate neutrophil trafficking from murine bone marrow*. The Journal of Clinical Investigation, 2010. **120**(7): p. 2423-2431.
14. Hu, Y., *Isolation of Human and Mouse Neutrophils Ex Vivo and In Vitro*, in *Leucocytes: Methods and Protocols*, R.B. Ashman, Editor. 2012, Humana Press: Totowa, NJ. p. 101-113.
15. Lahoz-Beneytez, J., et al., *Human neutrophil kinetics: modeling of stable isotope labeling data supports short blood neutrophil half-lives.* Blood, 2016. **127**(26): p. 3431-3438.
16. Kolaczkowska, E., et al., *Molecular mechanisms of NET formation and degradation revealed by intravital imaging in the liver vasculature*. Nature Communications, 2015. **6**: p. 6673.
17. Wang, S., et al., *S100A8/A9 in Inflammation.* Front Immunol, 2018. **9**: p. 1298.
18. Tydén, H., et al., *Pro-inflammatory S100 proteins are associated with glomerulonephritis and anti-dsDNA antibodies in systemic lupus erythematosus*. Lupus, 2017. **26**(2): p. 139-149.
19. Mócsai, A., *Diverse novel functions of neutrophils in immunity, inflammation, and beyond.* The Journal of Experimental Medicine, 2013. **210**(7): p. 1283-1299.
20. Yipp, B.G. and P. Kubes, *NETosis: how vital is it?* Blood, 2013. **122**(16): p. 2784-2794.
21. Brinkmann, V., et al., *Neutrophil Extracellular Traps Kill Bacteria*. Science, 2004. **303**(5663): p. 1532-1535.
22. Gupta, S. and M.J. Kaplan, *The role of neutrophils and NETosis in autoimmune and renal diseases*. Nat Rev Nephrol, 2016. **12**(7): p. 402-413.
23. Salemme, R., et al., *The Role of NETosis in Systemic Lupus Erythematosus.* J Cell Immunol, 2019. **1**(2): p. 33-42.
24. Apel, F., et al., *The cytosolic DNA sensor cGAS recognizes neutrophil extracellular traps.* Sci Signal, 2021. **14**(673).
25. Garcia-Romo, G.S., et al., *Netting neutrophils are major inducers of type I IFN production in pediatric systemic lupus erythematosus*. Science translational medicine, 2011. **3**(73): p. 73ra20-73ra20.
26. Condliffe, A.M., E. Kitchen, and E.R. Chilvers, *Neutrophil Priming: Pathophysiological Consequences and Underlying Mechanisms*. Clinical Science, 1998. **94**(5): p. 461.

27. Hallett, M.B. and D. Lloyds, *Neutrophil priming: the cellular signals that say 'amber' but not 'green'.* Immunology Today, 1995. **16**(6): p. 264-268.
28. Sapey, E. and R.A. Stockley, *Red, amber and green: the role of the lung in de-priming active systemic neutrophils.* Thorax, 2014. **69**(7): p. 606.
29. Haslett, C., et al., *Modulation of multiple neutrophil functions by preparative methods or trace concentrations of bacterial lipopolysaccharide.* The American Journal of Pathology, 1985. **119**(1): p. 101-110.
30. Bass, D.A., et al., *Subpopulations of neutrophils with increased oxidative product formation in blood of patients with infection.* The Journal of Immunology, 1986. **136**(3): p. 860.
31. Cowburn, A.S., et al., *GM-CSF CAUSES A PARADOXICAL INCREASE IN THE BH3-ONLY PRO-APOPTOTIC PROTEIN BIM IN HUMAN NEUTROPHILS.* American journal of respiratory cell and molecular biology, 2011. **44**(6): p. 879-887.
32. Khreiss, T., et al., *Activation of extracellular signal-regulated kinase couples platelet-activating factor-induced adhesion and delayed apoptosis of human neutrophils.* Cellular Signalling, 2004. **16**(7): p. 801-810.
33. Cowburn, A.S., et al., *Role of PI3-kinase–dependent Bad phosphorylation and altered transcription in cytokine-mediated neutrophil survival.* Blood, 2002. **100**(7): p. 2607.
34. Miralda, I., S.M. Uriarte, and K.R. McLeish, *Multiple Phenotypic Changes Define Neutrophil Priming.* Frontiers in cellular and infection microbiology, 2017. **7**: p. 217-217.
35. van der Linden, M. and L. Meyaard, *Fine-tuning neutrophil activation: Strategies and consequences.* Immunology Letters, 2016. **178**: p. 3-9.
36. Miralda, I., S.M. Uriarte, and K.R. McLeish, *Multiple Phenotypic Changes Define Neutrophil Priming.* Frontiers in Cellular and Infection Microbiology, 2017. **7**(217).
*37.* Pillay, J., et al., *In vivo labeling with 2H2O reveals a human neutrophil lifespan of 5.4 days.* Blood, 2010. **116**(4): p. 625-627.
38. Colotta, F., et al., *Modulation of granulocyte survival and programmed cell death by cytokines and bacterial products.* Blood, 1992. **80**(8): p. 2012-20.
*39.* Wang, J., et al., *Visualizing the function and fate of neutrophils in sterile injury and repair.* Science, 2017. **358**(6359): p. 111-116.
40. Liew, P.X. and P. Kubes, *The Neutrophil's Role During Health and Disease.* Physiological Reviews, 2019. **99**(2): p. 1223-1248.
*41.* Ekpenyong, A.E., et al., *Mechanical deformation induces depolarization of neutrophils.* Science Advances, 2017. **3**(6).
42. Kitchen, E., et al., *Demonstration of reversible priming of human neutrophils using platelet-activating factor.* Blood, 1996. **88**(11): p. 4330.
43. Summers, C., E.R. Chilvers, and A.M. Peters, *Mathematical modeling supports the presence of neutrophil depriming in vivo.* Physiological Reports, 2014. **2**(3): p. e00241.
44. Singh, N.R.P., et al., *Acute lung injury results from failure of neutrophil de-priming: a new hypothesis.* European Journal of Clinical Investigation, 2012. **42**(12): p. 1342-1349.
45. Hogg, J.C. and C.M. Doerschuk, *Leukocyte Traffic in the Lung.* Annual Review of Physiology, 1995. **57**(1): p. 97-114.
46. Kovach, M.A. and T.J. Standiford, *The function of neutrophils in sepsis.* Current Opinion in Infectious Diseases, 2012. **25**(3): p. 321-327.
*47.* Gray, R.D., et al., *Delayed neutrophil apoptosis enhances NET formation in cystic fibrosis.* Thorax, 2018. **73**(2): p. 134-144.
48. Dieker, J., et al., *Circulating Apoptotic Microparticles in Systemic Lupus Erythematosus Patients Drive the Activation of Dendritic Cell Subsets and Prime Neutrophils for NETosis.* Arthritis Rheumatol, 2016. **68**(2): p. 462-72.
49. Cochrane, C.G., E.R. Unanue, and F.J. Dixon, *A ROLE OF POLYMORPHONUCLEAR LEUKOCYTES AND COMPLEMENT IN NEPHROTOXIC NEPHRITIS.* J Exp Med, 1965. **122**: p. 99-116.
50. Lood, C., et al., *Neutrophil extracellular traps enriched in oxidized mitochondrial DNA are interferogenic and contribute to lupus-like disease.* Nature medicine, 2016. **22**(2): p. 146-153.
51. Abou-Raya, A. and S. Abou-Raya, *Inflammation: A pivotal link between autoimmune diseases and atherosclerosis.* Autoimmunity Reviews, 2006. **5**(5): p. 331-337.

52. Clark, R.A. and W.M. Nauseef, *Isolation and Functional Analysis of Neutrophils.* Current Protocols in Immunology, 1996. **19**(1): p. 7.23.1-7.23.17.
53. Lin, A.M., et al., *Mast Cells and Neutrophils Release IL-17 through Extracellular Trap Formation in Psoriasis.* The Journal of Immunology, 2011. **187**(1): p. 490-500.
54. Hardisty, G.R., et al., *Ultra-pure isolation of low density neutrophils casts doubt on their exceptionality in health and disease.* bioRxiv, 2020: p. 2020.06.17.156588.
55. Carmona-Rivera, C., et al., *Neutrophil extracellular traps induce endothelial dysfunction in systemic lupus erythematosus through the activation of matrix metalloproteinase-2.* Annals of the rheumatic diseases, 2015. **74**(7): p. 1417-1424.
56. Villanueva, E., et al., *Netting neutrophils induce endothelial damage, infiltrate tissues and expose immunostimulatory molecules in systemic lupus erythematosus.* Journal of immunology (Baltimore, Md. : 1950), 2011. **187**(1): p. 538-552.
57. Pelling, A.E. and M.A. Horton, *An historical perspective on cell mechanics.* Pflügers Archiv - European Journal of Physiology, 2008. **456**(1): p. 3-12.
58. Egerton, F.N., *A History of the Ecological Sciences, Part 19: Leeuwenhoek's Microscopic Natural History.* Bulletin of the Ecological Society of America, 2006. **87**(1): p. 47-58.
59. Heilbrunn, L.V., *The Viscosity of Protoplasm.* The Quarterly Review of Biology, 1927. **2**(2): p. 230-248.
60. Treitel, O., *Elasticity of Plant Tissues.* Transactions of the Kansas Academy of Science (1903-), 1944. **47**(2): p. 219-239.
61. Evans, E.A. and R.M. Hochmuth, *Membrane viscoelasticity.* Biophysical Journal, 1976. **16**(1): p. 1-11.
62. Hochmuth, R.M., *Micropipette aspiration of living cells.* Journal of Biomechanics, 2000. **33**(1): p. 15-22.
63. Binnig, G., C.F. Quate, and C. Gerber, *Atomic Force Microscope.* Physical Review Letters, 1986. **56**(9): p. 930-933.
64. Taniguchi, M., et al., *MgATP-induced conformational changes in a single myosin molecule observed by atomic force microscopy: Periodicity of substructures in myosin rods.* Scanning, 2003. **25**(5): p. 223-229.
65. Kodera, N., et al. *High-Resolution Imaging of Myosin Motor in Action by a High-Speed Atomic Force Microscope.* in *Molecular and Cellular Aspects of Muscle Contraction*. 2003. Boston, MA: Springer US.
66. Pelling, A.E., et al., *Local Nanomechanical Motion of the Cell Wall of Saccharomyces cerevisiae</em&gt.* Science, 2004. **305**(5687): p. 1147.
67. Roduit, C., et al., *Measuring Cytoskeleton and Cellular Membrane Mechanical Properties by Atomic Force Microscopy*, in *Methods in Membrane Lipids*, D.M. Owen, Editor. 2015, Springer New York: New York, NY. p. 153-159.
68. Roca-Cusachs, P., et al., *Rheology of Passive and Adhesion-Activated Neutrophils Probed by Atomic Force Microscopy.* Biophysical Journal, 2006. **91**(9): p. 3508-3518.
69. Horton, M., G. Charras, and P. Lehenkari, *ANALYSIS OF LIGAND–RECEPTOR INTERACTIONS IN CELLS BY ATOMIC FORCE MICROSCOPY.* Journal of Receptors and Signal Transduction, 2002. **22**(1-4): p. 169-190.
70. Sattin, B.D. and M.C. Goh, *Direct Observation of the Assembly of RecA/DNA Complexes by Atomic Force Microscopy.* Biophysical Journal, 2004. **87**(5): p. 3430-3436.
71. Kasas, S., et al., *Superficial and deep changes of cellular mechanical properties following cytoskeleton disassembly.* Cell Motility, 2005. **62**(2): p. 124-132.
72. Müller, D.J. and Y.F. Dufrêne, *Atomic force microscopy: a nanoscopic window on the cell surface.* Trends in Cell Biology, 2011. **21**(8): p. 461-469.
73. Wang, N., J.P. Butler, and D.E. Ingber, *Mechanotransduction across the cell surface and through the cytoskeleton.* Science, 1993. **260**(5111): p. 1124.
74. Sleep, J., et al., *Elasticity of the Red Cell Membrane and Its Relation to Hemolytic Disorders: An Optical Tweezers Study.* Biophysical Journal, 1999. **77**(6): p. 3085-3095.
*75.* Tadir, Y., et al., *Force generated by human sperm correlated to velocity and determined using a laser generated optical trap**Supported by grant RR 01192 from the National*

*Institutes of Health, Bethesda, Maryland; and by grant SDI 084-88-C- 0025 from the Department of Defense, Washington, D.C.* Fertility and Sterility, 1990. **53**(5): p. 944-947.
76. Block, S.M., L.S.B. Goldstein, and B.J. Schnapp, *Bead movement by single kinesin molecules studied with optical tweezers.* Nature, 1990. **348**(6299): p. 348-352.
*77.* Guck, J., et al., *The Optical Stretcher: A Novel Laser Tool to Micromanipulate Cells.* Biophysical Journal, 2001. **81**(2): p. 767-784.
78. Guck, J., et al., *Optical Deformability as an Inherent Cell Marker for Testing Malignant Transformation and Metastatic Competence.* Biophysical Journal, 2005. **88**(5): p. 3689-3698.
79. Gossett, D.R., et al., *Hydrodynamic stretching of single cells for large population mechanical phenotyping.* Proceedings of the National Academy of Sciences, 2012. **109**(20): p. 7630.
80. Tse, H.T.K., et al., *Quantitative Diagnosis of Malignant Pleural Effusions by Single-Cell Mechanophenotyping.* Science Translational Medicine, 2013. **5**(212): p. 212ra163.
81. Otto, O., et al. *Real-time deformability cytometry as a label-free indicator of cell function.* in *2015 37th Annual International Conference of the IEEE Engineering in Medicine and Biology Society (EMBC)*. 2015.
*82.* Otto, O., et al., *Real-time deformability cytometry: on-the-fly cell mechanical phenotyping.* Nat Meth, 2015. **12**(3): p. 199-202.
83. Ahmmed, S.M., et al., *Multi-sample deformability cytometry of cancer cells.* APL Bioengineering, 2018. **2**(3): p. 032002.
84. Darling, E.M., et al., *Viscoelastic properties of human mesenchymally-derived stem cells and primary osteoblasts, chondrocytes, and adipocytes.* Journal of Biomechanics, 2008. **41**(2): p. 454-464.
85. Yourek, G., M.A. Hussain, and J.J. Mao, *Cytoskeletal changes of mesenchymal stem cells during differentiation.* ASAIO journal (American Society for Artificial Internal Organs : 1992), 2007. **53**(2): p. 219-228.
86. Lin, J., et al., *High-throughput physical phenotyping of cell differentiation.* Microsystems & nanoengineering, 2017. **3**: p. 17013-17013.
*87.* Weiskopf, K., et al., *Myeloid Cell Origins, Differentiation, and Clinical Implications.* Microbiology spectrum, 2016. **4**(5): p. 10.1128/microbiolspec.MCHD-0031-2016.
88. Ekpenyong, A.E., et al., *Viscoelastic properties of differentiating blood cells are fate- and function-dependent.* PloS one, 2012. **7**(9): p. e45237-e45237.
89. González-Cruz, R.D., V.C. Fonseca, and E.M. Darling, *Cellular mechanical properties reflect the differentiation potential of adipose-derived mesenchymal stem cells.* Proceedings of the National Academy of Sciences of the United States of America, 2012. **109**(24): p. E1523-E1529.
90. Yu, H., et al., *Mechanical behavior of human mesenchymal stem cells during adipogenic and osteogenic differentiation.* Biochemical and Biophysical Research Communications, 2010. **393**(1): p. 150-155.
91. Lautenschläger, F., et al., *The regulatory role of cell mechanics for migration of differentiating myeloid cells.* Proceedings of the National Academy of Sciences, 2009. **106**(37): p. 15696.
92. Tsai, M.A., R.E. Waugh, and P.C. Keng, *Changes in HL-60 cell deformability during differentiation induced by DMSO.* Biorheology, 1996. **33**(1): p. 1-15.
*93.* Lichtman, M.A. and E. Kearney, *Cellular Deformability during Maturation of the Myeloblast.* New England Journal of Medicine, 1970. **283**(18): p. 943-948.
94. Schmid, M.C. and J.A. Varner, *Myeloid cell trafficking and tumor angiogenesis.* Cancer Letters, 2007. **250**(1): p. 1-8.
95. Schmid, M.C. and J.A. Varner, *Myeloid cells in tumor inflammation.* Vascular Cell, 2012. **4**(1): p. 14.
96. Suresh, S., *Biomechanics and biophysics of cancer cells.* Acta Biomaterialia, 2007. **3**(4): p. 413-438.
97. Olins, A.L., et al., *The human granulocyte nucleus: Unusual nuclear envelope and heterochromatin composition.* European Journal of Cell Biology, 2008. **87**(5): p. 279-290.
98. Lammerding, J., *Mechanics of the nucleus.* Comprehensive Physiology, 2011. **1**(2): p. 783-807.

99. Olins, A.L., et al., *The LINC-less granulocyte nucleus.* European journal of cell biology, 2009. **88**(4): p. 203-214.
100. Manley, H.R., M.C. Keightley, and G.J. Lieschke, *The Neutrophil Nucleus: An Important Influence on Neutrophil Migration and Function.* Frontiers in immunology, 2018. **9**: p. 2867-2867.
101. Lautenschläger, F., et al., *The regulatory role of cell mechanics for migration of differentiating myeloid cells.* Proceedings of the National Academy of Sciences of the United States of America, 2009. **106**(37): p. 15696-15701.
*102*. Vogt, K.L., et al., *Priming and de-priming of neutrophil responses in vitro and in vivo.* European Journal of Clinical Investigation, 2018. **0**(0): p. e12967.
103. Wong, K., et al., *Neutrophil polarization: Spatiotemporal dynamics of RhoA activity support a self-organizing mechanism.* Proceedings of the National Academy of Sciences of the United States of America, 2006. **103**(10): p. 3639-3644.
104. Pai, A., P. Sundd, and D.F.J. Tees, *In situ Microrheological Determination of Neutrophil Stiffening Following Adhesion in a Model Capillary.* Annals of Biomedical Engineering, 2008. **36**(4): p. 596-603.
105. Worthen, G.S., et al., *Mechanics of stimulated neutrophils: cell stiffening induces retention in capillaries*. Science, 1989. **245**(4914): p. 183.
106. Hiramatsu, Y., et al., *Nafamostat Preserves Neutrophil Deformability and Reduces Microaggregate Formation During Simulated Extracorporeal Circulation.* The Annals of Thoracic Surgery, 2005. **79**(4): p. 1326-1332.
107. Denk, S., et al., *Complement C5a-Induced Changes in Neutrophil Morphology During Inflammation.* Scandinavian Journal of Immunology, 2017. **86**(3): p. 143-155.
108. Dewitt, S., R.J. Francis, and M.B. Hallett, *Ca<sup>2+</sup> and calpain control membrane expansion during the rapid cell spreading of neutrophils*. Journal of Cell Science, 2013. **126**(20): p. 4627-4635.
109. Renkawitz, J. and M. Sixt, *Mechanisms of force generation and force transmission during interstitial leukocyte migration.* EMBO reports, 2010. **11**(10): p. 744-750.
110. Steffen, S., et al., *Toll-Like Receptor-Mediated Upregulation of CXCL16 in Psoriasis Orchestrates Neutrophil Activation.* Journal of Investigative Dermatology, 2018. **138**(2): p. 344-354.
111. Hogg, J.C. and C.M. Doerschuk, *LEUKOCYTE TRAFFIC IN THE LUNG.* Annual Review of Physiology, 1995. **57**: p. 97-114.
112. Yoshida, K., et al., *Neutrophil Cytoskeletal Rearrangements during Capillary Sequestration in Bacterial Pneumonia in Rats*. American Journal of Respiratory and Critical Care Medicine, 2006. **174**(6): p. 689-698.
113. Ekpenyong, A.E., et al., *Mechanotransduction in neutrophil activation and deactivation.* Biochimica et Biophysica Acta (BBA) - Molecular Cell Research, 2015. **1853**(11, Part B): p. 3105-3116.
114. Mennens, S.F.B., K. van den Dries, and A. Cambi, *Role for Mechanotransduction in Macrophage and Dendritic Cell Immunobiology*, in *Macrophages: Origin, Functions and Biointervention*, M. Kloc, Editor. 2017, Springer International Publishing: Cham. p. 209-242.
115. Novikova, O.A., P.P. Laktionov, and A.A. Karpenko, *The roles of mechanotransduction, vascular wall cells, and blood cells in atheroma induction.* Vascular, 2018. **27**(1): p. 98-109.
116. Summers, C., et al., *Pulmonary retention of primed neutrophils: a novel protective host response, which is impaired in the acute respiratory distress syndrome.* Thorax, 2014. **69**(7): p. 623.
117. Toepfner, N., et al., *Detection Of Human Disease Conditions By Single-Cell Morpho-Rheological Phenotyping Of Whole Blood.* bioRxiv, 2017.
118. Hesselink, L., et al., *A Rise in Neutrophil Cell Size Precedes Organ Dysfunction After Trauma.* Shock, 2019. **51**(4): p. 439-446.
119. Skoutelis, A.T., et al., *Polymorphonuclear leukocyte rigidity is defective in patients with chronic renal failure.* Nephrology Dialysis Transplantation, 2000. **15**(11): p. 1788-1793.
120. Porter, L., et al., *Metabolic Profiling of Human Eosinophils*. Frontiers in Immunology, 2018. **9**(1404).

121. Toepfner, N., et al., *Detection of human disease conditions by single-cell morpho-rheological phenotyping of blood.* eLife, 2018. **7**: p. e29213.
122. Nakagawa, M., et al., *Glucocorticoid-Induced Granulocytosis.* Circulation, 1998. **98**(21): p. 2307-2313.
123. Weber, P.S.D., et al., *Mechanisms of glucocorticoid-induced down-regulation of neutrophil L-selectin in cattle: evidence for effects at the gene-expression level and primarily on blood neutrophils*. Journal of Leukocyte Biology, 2004. **75**(5): p. 815-827.
*124.* Jilma, B. and P. Stohlawetz, *Dexamethasone Downregulates l-Selectin In Vitro and In Vivo.* Circulation, 1998. **97**(22): p. 2279a-2281.
125. Doyle, N.A., et al., *Neutrophil margination, sequestration, and emigration in the lungs of L-selectin-deficient mice.* The Journal of clinical investigation, 1997. **99**(3): p. 526-533.
126. Fay, M.E., et al., *Cellular softening mediates leukocyte demargination and trafficking, thereby increasing clinical blood counts.* Proceedings of the National Academy of Sciences, 2016. **113**(8): p. 1987.
127. Craciun, E.M., et al., *Anti-inflammatory effects of selected drugs on activated neonatal and adult neutrophils.* Scandinavian Journal of Clinical and Laboratory Investigation, 2013. **73**(5): p. 407-413.
128. Aringer, M., et al., *2019 European League Against Rheumatism/American College of Rheumatology Classification Criteria for Systemic Lupus Erythematosus*. Arthritis & Rheumatology, 2019. **71**(9): p. 1400-1412.
129. Kirley, T.L. and A.B. Norman, *Unfolding of IgG domains detected by non-reducing SDS-PAGE.* Biochemical and biophysical research communications, 2018. **503**(2): p. 944-949.
*130.* Otto, O., et al., *Real-time deformability cytometry: on-the-fly cell mechanical phenotyping.* Nature Methods, 2015. **12**: p. 199.
131. Herbig, M., et al., *Real-Time Deformability Cytometry: Label-Free Functional Characterization of Cells*, in *Flow Cytometry Protocols*, T.S. Hawley and R.G. Hawley, Editors. 2018, Springer New York: New York, NY. p. 347-369.
132. Bashant, K.R., et al., *Real-time deformability cytometry reveals sequential contraction and expansion during neutrophil priming.* Journal of Leukocyte Biology, 2019. **105**(6): p. 1143-1153.
133. UniProt Consortium, T., *UniProt: the universal protein knowledgebase*. Nucleic Acids Research, 2018. **46**(5): p. 2699-2699.
134. Käll, L., et al., *Semi-supervised learning for peptide identification from shotgun proteomics datasets*. Nature Methods, 2007. **4**(11): p. 923-925.
135. Yang, F., et al., *High-pH reversed-phase chromatography with fraction concatenation for 2D proteomic analysis.* Expert review of proteomics, 2012. **9**(2): p. 129-134.
136. Ting, L., et al., *MS3 eliminates ratio distortion in isobaric multiplexed quantitative proteomics.* Nature Methods, 2011. **8**(11): p. 937-940.
137. Wühr, M., et al., *Accurate multiplexed proteomics at the MS2 level using the complement reporter ion cluster*. Analytical chemistry, 2012. **84**(21): p. 9214-9221.
138. Kall, L., et al., *Posterior error probabilities and false discovery rates: two sides of the same coin.* J Proteome Res, 2008. **7**(1): p. 40-4.
139. Brosch, M., et al., *Accurate and sensitive peptide identification with Mascot Percolator.* J Proteome Res, 2009. **8**(6): p. 3176-81.
140. Spivak, M., et al., *Improvements to the percolator algorithm for Peptide identification from shotgun proteomics data sets.* J Proteome Res, 2009. **8**(7): p. 3737-45.
141. McAlister, G.C., et al., *Increasing the multiplexing capacity of TMTs using reporter ion isotopologues with isobaric masses.* Anal Chem, 2012. **84**(17): p. 7469-78.
142. Cominetti, O., et al., *Proteomic Biomarker Discovery in 1000 Human Plasma Samples with Mass Spectrometry*. J Proteome Res, 2016. **15**(2): p. 389-99.
143. Wood, A.J.T., et al., *Complement C5a impairs phagosomal maturation in the neutrophil through phosphoproteomic remodelling.* bioRxiv, 2020: p. 2020.01.17.907618.
144. Ge, S.X., D. Jung, and R. Yao, *ShinyGO: a graphical gene-set enrichment tool for animals and plants*. Bioinformatics, 2019.

145. Zhou, Y., et al., *Metascape provides a biologist-oriented resource for the analysis of systems-level datasets*. Nature Communications, 2019. **10**(1): p. 1523.
146. Oh, H., B. Siano, and S. Diamond, *Neutrophil isolation protocol.* Journal of visualized experiments : JoVE, 2008(17): p. 745.
147. Kuhns, D.B., et al., *Isolation and Functional Analysis of Human Neutrophils.* Current protocols in immunology, 2015. **111**: p. 7.23.1-7.23.16.
148. Mosca, T. and W.C.N. Forte, *Comparative Efficiency and Impact on the Activity of Blood Neutrophils Isolated by Percoll, Ficoll and Spontaneous Sedimentation Methods*. Immunological Investigations, 2016. **45**(1): p. 29-37.
149. Venaille, T.J., et al., *Effects of different density gradient separation techniques on neutrophil function.* Scandinavian Journal of Clinical and Laboratory Investigation, 1994. **54**(5): p. 385-391.
150. Gunay-Aygun, M., et al., *Gray platelet syndrome: natural history of a large patient cohort and locus assignment to chromosome 3p.* Blood, 2010. **116**(23): p. 4990-5001.
*151.* Chedani, H., et al., *Neutrophil secretory defect in the gray platelet syndrome: a new case.* Platelets, 2006. **17**(1): p. 14-9.
152. Hassani, M., et al., *On the origin of low-density neutrophils.* Journal of Leukocyte Biology, 2020. **107**(5): p. 809-818.
153. Denny, M.F., et al., *A Distinct Subset of Proinflammatory Neutrophils Isolated from Patients with Systemic Lupus Erythematosus Induces Vascular Damage and Synthesizes Type I IFNs.* The Journal of Immunology, 2010. **184**(6): p. 3284-3297.
154. Herbig, M., et al., *Statistics for real-time deformability cytometry: Clustering, dimensionality reduction, and significance testing.* Biomicrofluidics, 2018. **12**(4): p. 042214.
155. Wen, X., et al., *G-protein-coupled formyl peptide receptors play a dual role in neutrophil chemotaxis and bacterial phagocytosis.* Molecular biology of the cell, 2019. **30**(3): p. 346-356.
156. Dang, P.M., et al., *A specific p47phox -serine phosphorylated by convergent MAPKs mediates neutrophil NADPH oxidase priming at inflammatory sites.* J Clin Invest, 2006. **116**(7): p. 2033-43.
157. Ward, R.A., M. Nakamura, and K.R. McLeish, *Priming of the neutrophil respiratory burst involves p38 mitogen-activated protein kinase-dependent exocytosis of flavocytochrome b558-containing granules*. J Biol Chem, 2000. **275**(47): p. 36713-9.
158. Watson, F. and S.W. Edwards, *Stimulation of primed neutrophils by soluble immune complexes: priming leads to enhanced intracellular Ca2+ elevations, activation of phospholipase D, and activation of the NADPH oxidase.* Biochem Biophys Res Commun, 1998. **247**(3): p. 819-26.
159. McLeish, K.R., et al., *Frontline Science: Tumor necrosis factor-α stimulation and priming of human neutrophil granule exocytosis.* J Leukoc Biol, 2017. **102**(1): p. 19-29.
160. Fay, M.E., et al., *Cellular softening mediates leukocyte demargination and trafficking, thereby increasing clinical blood counts.* Proceedings of the National Academy of Sciences, 2016. **113**(8): p. 1987-1992.
161. Zhao, T. and G.M. Bokoch, *Critical role of proline-rich tyrosine kinase 2 in reversion of the adhesion-mediated suppression of reactive oxygen species generation by human neutrophils.* J Immunol, 2005. **174**(12): p. 8049-55.
162. McClenahan, D., et al., *Role of inflammatory mediators in priming, activation, and deformability of bovine neutrophils*. Am J Vet Res, 2000. **61**(5): p. 492-8.
163. Lim, J.P. and P.A. Gleeson, *Macropinocytosis: an endocytic pathway for internalising large gulps*. Immunology And Cell Biology, 2011. **89**: p. 836.
164. Kerr, M.C. and R.D. Teasdale, *Defining Macropinocytosis.* Traffic, 2009. **10**(4): p. 364-371.
165. Smith, C.W., et al., *Motility and Adhesiveness in Human Neutrophils: EFFECTS OF CHEMOTACTIC FACTORS.* Journal of Clinical Investigation, 1979. **63**(2): p. 221-229.
166. *Activation of human neutrophils by C3a and C5A Comparison of the effects on shape changes, chemotaxis, secretion, and respiratory burst.* FEBS Letters, 1994. **346**(2-3): p. 181-184.

167. Fu, H., et al., *The mechanism for activation of the neutrophil NADPH-oxidase by the peptides formyl-Met-Leu-Phe and Trp-Lys-Tyr-Met-Val-Met differs from that for interleukin-8.* Immunology, 2004. **112**(2): p. 201-10.
168. Mócsai, A., B. Walzog, and C.A. Lowell, *Intracellular signalling during neutrophil recruitment.* Cardiovasc Res, 2015. **107**(3): p. 373-85.
169. Leoni, G., et al., *Human neutrophil formyl peptide receptor phosphorylation and the mucosal inflammatory response.* J Leukoc Biol, 2015. **97**(1): p. 87-101.
170. Shi, Y., et al., *Granulocyte-macrophage colony-stimulating factor (GM-CSF) and T-cell responses: what we do and don't know*. Cell Research, 2006. **16**(2): p. 126-133.
171. Gomes, N.E., et al., *Lipopolysaccharide-induced expression of cell surface receptors and cell activation of neutrophils and monocytes in whole human blood.* Braz J Med Biol Res, 2010. **43**(9): p. 853-8.
172. Mietke, A., et al., *Extracting Cell Stiffness from Real-Time Deformability Cytometry: Theory and Experiment.* Biophysical journal, 2015. **109**(10): p. 2023-2036.
173. Alblas, J., et al., *Activation of Rhoa and ROCK are essential for detachment of migrating leukocytes.* Molecular biology of the cell, 2001. **12**(7): p. 2137-2145.
174. Zhao, H., et al., *A Potential Mechanism for ADC-Induced Neutropenia: Role of Neutrophils in Their Own Demise*. Molecular Cancer Therapeutics, 2017. **16**(9): p. 1866-1876.
175. Tigran, K.D., A.A. Samvel, and S.H. Gagik, *Neutrophil F-actin Dynamics in Familial Mediterranean Fever: The Unequal Effect of Colchicine on Activated Neutrophils.* Anti-Inflammatory & Anti-Allergy Agents in Medicinal Chemistry, 2013. **12**(2): p. 165-172.
176. Carpentier, J.L., et al., *Internalization pathway of C3b receptors in human neutrophils and its transmodulation by chemoattractant receptors stimulation.* Cell Regulation, 1991. **2**(1): p. 41-55.
177. Nishimura, S., et al., *Combinatorial Targeting of the Macropinocytotic Pathway in Leukemia and Lymphoma Cells.* The Journal of Biological Chemistry, 2008. **283**(17): p. 11752-11762.
178. *Distinct endocytotic pathways in epidermal growth factor-stimulated human carcinoma A431 cells [published erratum appears in J Cell Biol 1990 Mar;110(3):859].* The Journal of Cell Biology, 1989. **109**(6): p. 2731-2739.
179. Koivusalo, M., et al., *Amiloride inhibits macropinocytosis by lowering submembranous pH and preventing Rac1 and Cdc42 signaling.* The Journal of Cell Biology, 2010. **188**(4): p. 547-563.
180. Wang, J.T.H., R.D. Teasdale, and D. Liebl, *Macropinosome quantitation assay*. MethodsX, 2014. **1**: p. 36-41.
181. Wang, J.T.H., et al., *The SNX-PX-BAR Family in Macropinocytosis: The Regulation of Macropinosome Formation by SNX-PX-BAR Proteins*. PLoS ONE, 2010. **5**(10): p. e13763.
182. Doodnauth, S.A., S. Grinstein, and M.E. Maxson, *Constitutive and stimulated macropinocytosis in macrophages: roles in immunity and in the pathogenesis of atherosclerosis*. Philos Trans R Soc Lond B Biol Sci, 2019. **374**(1765): p. 20180147.
183. Gurney, M.A., et al., *Pathophysiology of Intestinal Na(+)/H(+) Exchange*. Cellular and Molecular Gastroenterology and Hepatology, 2017. **3**(1): p. 27-40.
184. Matsushima, A., et al., *Enhanced Expression of Aquaporin 9 in Activated Polymorphonuclear Leukocytes in Patients With Systemic Inflammatory Response Syndrome.* Shock, 2014. **42**(4): p. 322-326.
185. Loitto, V.-M., et al., *Neutrophil leukocyte motility requires directed water influx.* Journal of Leukocyte Biology, 2002. **71**(2): p. 212-222.
186. Moniaga, C.S., et al., *Aquaporin-9-expressing neutrophils are required for the establishment of contact hypersensitivity.* Scientific Reports, 2015. **5**: p. 15319.
187. Karlsson, T., et al., *Aquaporin 9 phosphorylation mediates membrane localization and neutrophil polarization.* Journal of Leukocyte Biology, 2011. **90**(5): p. 963-973.
188. Rump, K. and M. Adamzik, *Function of aquaporins in sepsis: a systematic review.* Cell Biosci, 2018. **8**: p. 10.
*189.* Sônego, F., et al., *Paradoxical Roles of the Neutrophil in Sepsis: Protective and Deleterious.* Front Immunol, 2016. **7**: p. 155.

190. Zonneveld, R., G. Molema, and F.B. Plötz, *Analyzing Neutrophil Morphology, Mechanics, and Motility in Sepsis: Options and Challenges for Novel Bedside Technologies.* Crit Care Med, 2016. **44**(1): p. 218-28.
191. Hesselink, L., et al., *A Rise in Neutrophil Cell Size Precedes Organ Dysfunction After Trauma.* Shock, 9000. **Publish Ahead of Print**.
192. Juss, J.K., et al., *Acute Respiratory Distress Syndrome Neutrophils Have a Distinct Phenotype and Are Resistant to Phosphoinositide 3-Kinase Inhibition.* American Journal of Respiratory and Critical Care Medicine, 2016. **194**(8): p. 961-973.
193. Carmona-Rivera, C. and M.J. Kaplan, *Low density granulocytes: a distinct class of neutrophils in systemic autoimmunity.* Seminars in immunopathology, 2013. **35**(4): p. 455-463.
194. Denny, M.F., et al., *A distinct subset of proinflammatory neutrophils isolated from patients with systemic lupus erythematosus induces vascular damage and synthesizes type I IFNs.* J Immunol, 2010. **184**(6): p. 3284-97.
195. Carlucci, P.M., et al., *Neutrophil subsets and their gene signature associate with vascular inflammation and coronary atherosclerosis in lupus.* JCI Insight, 2018. **3**(8).
196. Denny, M.F., et al., *Interferon-alpha promotes abnormal vasculogenesis in lupus: a potential pathway for premature atherosclerosis.* Blood, 2007. **110**(8): p. 2907-2915.
197. Rahman, S., et al., *Low-density granulocytes activate T cells and demonstrate a non-suppressive role in systemic lupus erythematosus.* Ann Rheum Dis, 2019. **78**(7): p. 957-966.
198. Mistry, P., et al., *Dysregulated neutrophil responses and neutrophil extracellular trap formation and degradation in PAPA syndrome.* Ann Rheum Dis, 2018. **77**(12): p. 1825-1833.
199. Wright, H.L., et al., *Low-density granulocytes: functionally distinct, immature neutrophils in rheumatoid arthritis with altered properties and defective TNF signalling.* J Leukoc Biol, 2017. **101**(2): p. 599-611.
200. Mistry, P., et al., *Transcriptomic, epigenetic, and functional analyses implicate neutrophil diversity in the pathogenesis of systemic lupus erythematosus.* Proceedings of the National Academy of Sciences, 2019. **116**(50): p. 25222-25228.
201. Lee, S., P. Khankhanian, and J.O. Mascarenhas, *Corticosteroid-induced morphological changes in cells of the myeloid lineage.* American Journal of Hematology, 2015. **90**(7): p. 679-680.
202. Kegerreis, B.J., et al., *Genomic Identification of Low-Density Granulocytes and Analysis of Their Role in the Pathogenesis of Systemic Lupus Erythematosus.* The Journal of Immunology, 2019. **202**(11): p. 3309-3317.
203. Thiam, H.R., et al., *NETosis proceeds by cytoskeleton and endomembrane disassembly and PAD4-mediated chromatin decondensation and nuclear envelope rupture.* Proceedings of the National Academy of Sciences, 2020. **117**(13): p. 7326.
204. Metzler, K.D., et al., *A myeloperoxidase-containing complex regulates neutrophil elastase release and actin dynamics during NETosis.* Cell Rep, 2014. **8**(3): p. 883-96.
205. Neubert, E., et al., *Chromatin swelling drives neutrophil extracellular trap release.* Nature Communications, 2018. **9**(1): p. 3767.
206. Gupta, S., et al., *A High-Throughput Real-Time Imaging Technique To Quantify NETosis and Distinguish Mechanisms of Cell Death in Human Neutrophils.* J Immunol, 2018. **200**(2): p. 869-879.
207. Nishibori, M., et al., *Histidine-rich glycoprotein prevents septic lethality through neutrophil regulation.* Critical Care, 2014. **18**(Suppl 2): p. P23-P23.
*208.* Shahane, A., *Pulmonary hypertension in rheumatic diseases: epidemiology and pathogenesis.* Rheumatol Int, 2013. **33**(7): p. 1655-67.
209. Carreira, P.E., *Pulmonary hypertension in autoimmune rheumatic diseases.* Autoimmunity Reviews, 2004. **3**(4): p. 313-320.
210. Keane, M.P. and J.P. Lynch, *Pleuropulmonary manifestations of systemic lupus erythematosus.* Thorax, 2000. **55**(2): p. 159.
211. Xia, Y., et al., *Deficiency of fibroblast growth factor-inducible 14 (Fn14) preserves the filtration barrier and ameliorates lupus nephritis.* Journal of the American Society of Nephrology : JASN, 2015. **26**(5): p. 1053-1070.

212. Burg, N., et al., *Sphingosine 1-Phosphate Receptor 1 Signaling Maintains Endothelial Cell Barrier Function and Protects Against Immune Complex-Induced Vascular Injury*. Arthritis Rheumatol, 2018. **70**(11): p. 1879-1889.
*213.* King, K.R., et al., *IRF3 and type I interferons fuel a fatal response to myocardial infarction.* Nature Medicine, 2017. **23**(12): p. 1481-1487.
214. Knight, J.S., et al., *Peptidylarginine deiminase inhibition reduces vascular damage and modulates innate immune responses in murine models of atherosclerosis*. Circulation research, 2014. **114**(6): p. 947-956.
215. Singh, N., et al., *Genomic alterations in abnormal neutrophils isolated from adult patients with systemic lupus erythematosus.* Arthritis Res Ther, 2014. **16**(4): p. R165.
216. Wood, A.J.T., et al., *C5a impairs phagosomal maturation in the neutrophil through phosphoproteomic remodeling.* JCI Insight, 2020. **5**(15).
217. Amulic, B., et al., *Neutrophil Function: From Mechanisms to Disease.* Annual Review of Immunology, 2012. **30**(1): p. 459-489.
218. Reutershan, J., et al., *Critical role of endothelial CXCR2 in LPS-induced neutrophil migration into the lung.* The Journal of clinical investigation, 2006. **116**(3): p. 695-702.
219. Stillie, R., et al., *The functional significance behind expressing two IL–8 receptor types on PMN*. Journal of Leukocyte Biology, 2009. **86**(3): p. 529-543.
220. Smith, N.L.D., et al., *Elevated Levels of the Neutrophil Chemoattractant Pro–Platelet Basic Protein in Macrophages From Individuals With Chronic and Allergic Aspergillosis.* The Journal of Infectious Diseases, 2014. **211**(4): p. 651-660.
221. Marini, O., et al., *Mature CD10+ and immature CD10− neutrophils present in G-CSF–treated donors display opposite effects on T cells*. Blood, 2017. **129**(10): p. 1343-1356.
222. Tucci, M., et al., *Glomerular accumulation of plasmacytoid dendritic cells in active lupus nephritis: Role of interleukin-18.* Arthritis & Rheumatism, 2008. **58**(1): p. 251-262.
223. Leonard, W.J. and J.J. O'Shea, *JAKS AND STATS: Biological Implications*. Annual Review of Immunology, 1998. **16**(1): p. 293-322.
224. Lombardi, B., et al., *Evaluation of phosphopeptide enrichment strategies for quantitative TMT analysis of complex network dynamics in cancer-associated cell signalling.* EuPA Open Proteomics, 2015. **6**: p. 10-15.
225. Akk, A., et al., *Complement activation on neutrophils initiates endothelial adhesion and extravasation.* Mol Immunol, 2019. **114**: p. 629-642.
226. Pinto-Costa, R. and M.M. Sousa, *Profilin as a dual regulator of actin and microtubule dynamics*. Cytoskeleton, 2020. **77**(3-4): p. 76-83.
227. Takahashi, Y., et al., *Histidine-Rich Glycoprotein Stimulates Human Neutrophil Phagocytosis and Prolongs Survival through CLEC1A.* J Immunol, 2021. **206**(4): p. 737-750.
228. Schenk, L.K., et al., *Angiotensin II regulates phosphorylation of actin-associated proteins in human podocytes*. The FASEB Journal, 2017. **31**(11): p. 5019-5035.
229. Föger, N., et al., *Differential regulation of mast cell degranulation versus cytokine secretion by the actin regulatory proteins Coronin1a and Coronin1b.* The Journal of experimental medicine, 2011. **208**(9): p. 1777-1787.
230. Sandí, M.-J., et al., *MARK3-mediated phosphorylation of ARHGEF2 couples microtubules to the actin cytoskeleton to establish cell polarity*. Science Signaling, 2017. **10**(503): p. eaan3286.
231. Lertkiatmongkol, P., et al., *Endothelial functions of platelet/endothelial cell adhesion molecule-1 (CD31).* Current opinion in hematology, 2016. **23**(3): p. 253-259.
232. Zhu, P., et al., *ADAM22 plays an important role in cell adhesion and spreading with the assistance of 14-3-3.* Biochemical and Biophysical Research Communications, 2005. **331**(4): p. 938-946.
233. Frank, S.R., et al., *The focal adhesion-associated proteins DOCK5 and GIT2 comprise a rheostat in control of epithelial invasion.* Oncogene, 2017. **36**(13): p. 1816-1828.
234. Albarran-Juarez, J., et al., *Piezo1 and Gq/G11 promote endothelial inflammation depending on flow pattern and integrin activation.* J Exp Med, 2018. **215**(10): p. 2655-2672.
235. Nejedla, M., et al., *Profilin connects actin assembly with microtubule dynamics.* Mol Biol Cell, 2016. **27**(15): p. 2381-93.

236. Alkam, D., et al., *Profilin1 biology and its mutation, actin(g) in disease.* Cell Mol Life Sci, 2017. **74**(6): p. 967-981.
237. Terao, K., et al., *Histidine-Rich Glycoprotein Suppresses Hyperinflammatory Responses of Lung in a Severe Acute Pancreatitis Mouse Model.* Pancreas, 2018. **47**(9): p. 1156-1164.
238. Morley, S.C., *The actin-bundling protein L-plastin: a critical regulator of immune cell function.* International journal of cell biology, 2012. **2012**: p. 935173-935173.
239. Machado, R.A.C., et al., *L-plastin Ser5 phosphorylation is modulated by the PI3K/SGK pathway and promotes breast cancer cell invasiveness.* Cell Communication and Signaling, 2021. **19**(1): p. 22.
240. Florey, O., J. Durgan, and W. Muller, *Phosphorylation of leukocyte PECAM and its association with detergent-resistant membranes regulate transendothelial migration.* Journal of immunology (Baltimore, Md. : 1950), 2010. **185**(3): p. 1878-1886.
*241.* Apel, F., et al., *The cytosolic DNA sensor cGAS recognizes neutrophil extracellular traps.* Science Signaling, 2021. **14**(673): p. eaax7942.
242. Ma, F., et al., *Positive feedback regulation of type I IFN production by the IFN-inducible DNA sensor cGAS.* J Immunol, 2015. **194**(4): p. 1545-54.
243. McNab, F., et al., *Type I interferons in infectious disease.* Nature Reviews Immunology, 2015. **15**(2): p. 87-103.
244. de Bont, C.M., W.C. Boelens, and G.J.M. Pruijn, *NETosis, complement, and coagulation: a triangular relationship.* Cellular & Molecular Immunology, 2019. **16**(1): p. 19-27.
245. Teague, H.L., et al., *Neutrophil Subsets, Platelets, and Vascular Disease in Psoriasis.* JACC: Basic to Translational Science, 2019. **4**(1): p. 1.
246. Lisman, T., *Platelet-neutrophil interactions as drivers of inflammatory and thrombotic disease.* Cell and tissue research, 2018. **371**(3): p. 567-576.
247. Grabowski, P., et al., *Proteome Analysis of Human Neutrophil Granulocytes From Patients With Monogenic Disease Using Data-independent Acquisition.* Mol Cell Proteomics, 2019. **18**(4): p. 760-772.
248. Tak, T., et al., *Human CD62Ldim neutrophils identified as a separate subset by proteome profiling and in vivo pulse-chase labeling.* Blood, 2017. **129**(26): p. 3476-3485.
249. Chapman, E.A., et al., *Caught in a Trap? Proteomic Analysis of Neutrophil Extracellular Traps in Rheumatoid Arthritis and Systemic Lupus Erythematosus.* Front Immunol, 2019. **10**: p. 423.
250. Bruschi, M., et al., *Neutrophil Extracellular Traps protein composition is specific for patients with Lupus nephritis and includes methyl-oxidized αenolase (methionine sulfoxide 93).* Sci Rep, 2019. **9**(1): p. 7934.
251. Tsai, C.Y., et al., *What's wrong with neutrophils in lupus?* Clin Exp Rheumatol, 2019. **37**(4): p. 684-693.
252. Gabay, C. and I. Kushner, *Acute-phase proteins and other systemic responses to inflammation.* N Engl J Med, 1999. **340**(6): p. 448-54.
253. Dermit, M., M. Dodel, and F.K. Mardakheh, *Methods for monitoring and measurement of protein translation in time and space.* Molecular bioSystems, 2017. **13**(12): p. 2477-2488.
254. Sondo, E., et al., *High-Content Screening Identifies Vanilloids as a Novel Class of Inhibitors of NET Formation.* Frontiers in Immunology, 2019. **10**(963).
255. Tatsiy, O. and P.P. McDonald, *Physiological Stimuli Induce PAD4-Dependent, ROS-Independent NETosis, With Early and Late Events Controlled by Discrete Signaling Pathways.* Frontiers in Immunology, 2018. **9**(2036).
256. Cheng, Y.J., et al., *Silencing profilin-1 inhibits gastric cancer progression via integrin β1/focal adhesion kinase pathway modulation.* World J Gastroenterol, 2015. **21**(8): p. 2323-35.
257. Ding, Z., et al., *Silencing profilin-1 inhibits endothelial cell proliferation, migration and cord morphogenesis.* Journal of Cell Science, 2006. **119**(19): p. 4127-4137.
258. Gale, B.M. and K.K. Hall, *The Use of Patient Monitoring Systems to Improve Sepsis Recognition and Outcomes: A Systematic Review.* J Patient Saf, 2020. **16**(3S Suppl 1): p. S8-s11.

259. Shen, X., et al., *Targeting Neutrophils in Sepsis: From Mechanism to Translation.* Front Pharmacol, 2021. **12**: p. 644270.
260. Soh, K.T., J.D. Tario, Jr., and P.K. Wallace, *Diagnosis of Plasma Cell Dyscrasias and Monitoring of Minimal Residual Disease by Multiparametric Flow Cytometry.* Clinics in laboratory medicine, 2017. **37**(4): p. 821-853.
261. Abraham, R.S. and G. Aubert, *Flow Cytometry, a Versatile Tool for Diagnosis and Monitoring of Primary Immunodeficiencies.* Clinical and vaccine immunology : CVI, 2016. **23**(4): p. 254-271.
262. Bashant, K.R., et al., *Proteomic, biomechanical and functional analyses define neutrophil heterogeneity in systemic lupus erythematosus.* Annals of the Rheumatic Diseases, 2020: p. annrheumdis-2020-218338.
263. Bashant, K.R., et al., *The mechanics of myeloid cells.* Biology of the Cell, 2020. **112**(4): p. 103-112.
264. Jing, C., et al., *Macrophage metabolic reprogramming presents a therapeutic target in lupus nephritis.* Proceedings of the National Academy of Sciences of the United States of America, 2020. **117**(26): p. 15160-15171.